Ligand-to-Metal Charge Transfer Photocatalysis using Cerium and Iron Complexes with Defined Ligands

Dissertation

Zur Erlangung des Doktorgrades der Naturwissenschaften

(Dr. rer. nat.)

an der Fakultät für Chemie und Pharmazie

der Universität Regensburg

Vorgelegt von

Jessica Stahl

Aus Straubing

2024

The experimental work was carried out in the Institute of Organic Chemistry at the University of Regensburg under the supervision of Prof. Dr. Burkhard König between September 2019 and March 2024.

Date of submission: 17.04.2024

Date of colloquium: 17.05.2024

Board of examiners:

Chair: Apl. Prof. Dr. Rainer Müller

1st Referee: Prof. Dr. Burkhard König

2nd Referee: Prof. Dr. Ruth Gschwind

Examiner: Prof. Dr. Patrick Nürnberger

„Like any great love, it keeps you guessing,

Like any real love, it's ever-changing,

Like any true love, it drives you crazy,

But you know you wouldn't change anything, anything, anything…"

Taylor Swift

Table of Contents

1   A Survey of the Iron Ligand-to-Metal Charge Transfer in Water

"Fully hydrated" - **The Iron Ligand-to-Metal Charge Transfer in Water - Photocatalysis tests the waters**

Jessica Stahl wrote the manuscript, Burkhard König supervised the project.

CHAPTER 1

This chapter was published in:

Abstract

Iron, mostly as Fe^{2+} or Fe^{3+} bound in oxides, is the second most common element in the earth's crust after aluminium. Salts of the d-block metal are cheap and commercially available and have already been used in organic chemistry in many preparative examples for the C-H functionalisation of different classes of starting materials. The literature revealed that likewise copper or cerium, and iron can undergo ligand-to-metal charge transfer processes. Different (anionic) ligands of various sizes can be added in various stoichiometries to commercial Fe(II)/Fe(III) salts leading to a unique orientation of the ligands around the metal centre. The resulting complexes are often coloured and can be excited by UV or visible light initiating a metal-ligand bond homolysis in which the metal part gets reduced, and the ligand loses one electron to form highly reactive radical species that can abstract hydrogen atoms or in the case of halide radicals add to double or triple bonds in a suitable substrate. In most of the literature-known procedures, the photoreaction proceeds in organic (polar protic/aprotic) solvents and the reaction medium hardly competes against the ligands (such as alcoholates or halides) for free coordination sites on the metal centre. However, in pure water, unlike other solvents (polar-protic or polar-aprotic), the iron cations get fully solvated and result in aquo-complexes due to the exclusive attachment of water molecules to a metal species, such as in sulphate, nitrate, and perchlorate salts. They possess a general stoichiometry of $[M(H_2O)_n]^{z+}$ and have been known for a long time in inorganic and environmental chemistry showing unique and useful characteristics that will be exemplified in this review.

1.1   Introduction

Water is the most crucial medium on earth as it is presumed to be the basis of life – the evolutional development started in water bearing billions of diverse micro-organisms such as bacteria that were allowed to evolve further, compete for their biological niche existence, and result in the biodiversity our planet shows today on land and in water.

Liquid water shows numerous interesting characteristics as the ability to form strong hydrogen bonds. This interaction gives rise to extensive associated clusters resulting in the unique surface tension of the solvent, an outstanding polarity and a high dielectric constant.[1-6] Another peculiarity of water is the tendency to orient water molecules along their axis of dipole around inorganic cations, anions or organic compounds, respectively leading to the so-called hydration shells that stabilises the species in the liquid environment. Depending on the size of the ion or the molecule the radius of the hydration cloud and the overall number of water molecules varies drastically and an overall decrease in entropy and Gibbs free energy is achieved.[7-9] The striking advantage of running radical reactions in water is the very high bond-dissociation energy of O-H bonds in water molecules that exceeds the respective energy values for frequently used C-H precursors in organic molecules and therefore water as solvent does not play a role as competitive hydrogen atom transfer (HAT) source.[10-12]

In contrast to laboratory working scales where photo-setups are designed in a way that the penetration depth of the light coming from an artificial light source reaches the sample in the most efficient way leading to homogenous irradiation and reaction processes, natural "beakers" such as oceans, seas and lakes are not lit homogenously. Here, solar light shows impressive characteristic towards the penetration depth of waters as even in a 50-70 m distance to the surface level of the water 10% of the surface UV A irradiation (at 360 nm) can be detected. This ensures the successful chemical and biochemical transformation that proceed in the aqueous environment of oceans.[13]
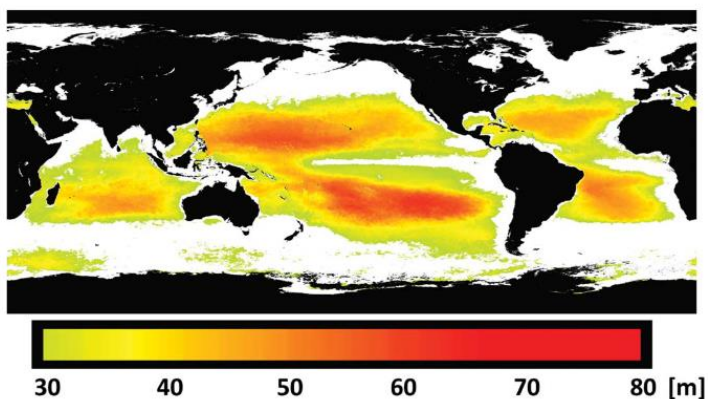
Figure 1.1. Penetration depth of solar irradiance (sun in zenith) measured at 360 nm in the global oceans, as gauged by 10% of the surface light ($Z(360)_{10\%}$)) Black areas: land and ice, white areas: waters with $K_D(412) > 0.05$ 1/cm.[13] Reproduced from ref. [13] with permission from John Wiley and Sons, copyright 2013.

In the following survey the characteristics of iron complexes in water related to their reactivity upon irradiation and the structure classes will be discussed in detail. Scheme 1.1 provides an overall summary of the most import details.
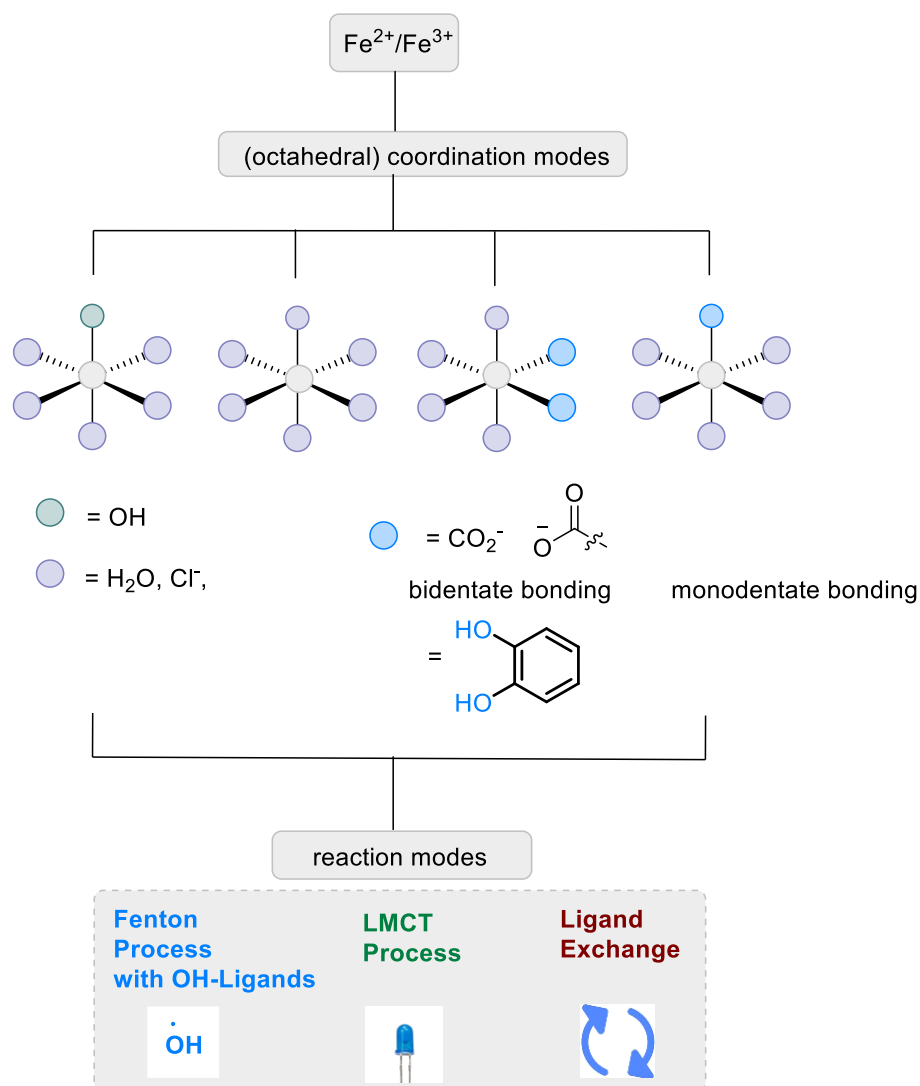
Scheme 1.1. Summary on Fe^{2+}/Fe^{3+} complexes, their constitution and reactivity in water.

1.2   Photophysical Principles of Ligand-to-Metal Charge Transfer

To compare LMCT from more widely applied (polar-protic) organic solvent systems with aqueous media we first describe in general the photophysical principle of ligand-to-metal charge transfer chemistry. Scheme 1.2 summarises the most important features of the light-induced bond homolysis event.

principle concepts of LMCT (visible) light induced **L-M** bond homolysis

ground state   LMCT excited state   ligand-metal bond homolyis
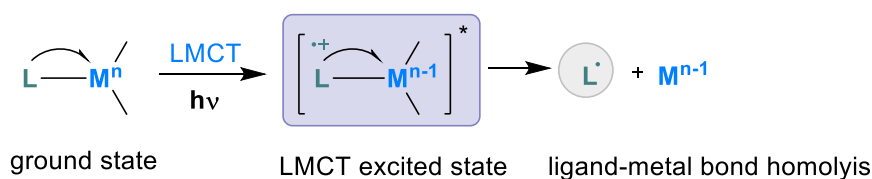
M = high-valent metal centre
Ce^{4+}, Fe^{3+}, Cu^{2+}, Bi^{3+}, Ni^{3+}, Co^{3+}, Ti^{4+}
L = σ or σ+π donor
halogen, OR, CO_2R, N_3, H_2O, alkyl..

Scheme 1.2. Concept of LMCT.

LMCT reactions can be described as a single electron transition from a filled-orbital mainly located on a ligand to an empty metal-centred orbital.[14, 15] For a successful transition, the empty d^* orbital of the metal has to be low in energy and this is the case for highly electrophilic high-valent metals such as Ce^{4+}, Fe^{3+}, or Bi^{3+} among many other candidates.[16-18] Suitable ligands for the light-induced bond homolysis are nucleophilic σ- or σ + π – donors such as halides, alcohols, carboxylic acids or azides (Scheme 1.2).[17, 19-24] In this review we discuss water ligands, that, located in the middle region of the spectrochemical row, also favour LMCT transitions. During an LMCT event, the electron density within the coordination complexes changes as the population of the anti-bonding orbital (d*, $d\sigma^*$) increases at the expense of electron density of a ligand (p/π) or a metal-ligand (dσ) bond. Hence, the bond order of the M-L bond decreases and the respective ligands become kinetically labile and easy to cleave upon irradiation. The bond dissociation is characterised being a non-irradiative deactivation.[25, 26] LMCT states cannot be detected *via* fluorescence or phosphorescence spectroscopy as their transitions show the characteristics of being short-lived and possess rather low emission quantum yields. A suitable method for investigation is ultrafast transient absorption (TA) spectroscopy that allows for tracking and imaging the generation of highly reactive radicals after the light-induced bond-homolysis event. [27, 28] In general, ligand-to-metal charge transfer states, as inverse transitions to metal-to-ligand charge transfer processes represent a valuable platform for useful (preparative) organic transformations using (visible) light as cheap and traceless reagent allowing for the formation of highly reactive and potent open-shell species.

1.3 General Aspects of Iron Photochemistry in Water

1.3.1 The Iron Aqua Complex

Metal ions in water usually exist as their hydrate form showing formulas of $[M(H_2O)_n]^{z+}$ and in most cases $n = 6$ for a metal 2+ or 3+ species. In the hydration process water molecules bind to the metal centre *via* ion-dipole bonds and are therefore mainly described by their electrostatic character.[9] Depending on the electronic configuration of the metal ions in their combined d and p orbitals the colours of the complexes differ enormously, $[Fe(H_2O)_6]^{3+}$ is pale violet while $[[Fe(H_2O)_6]^{2+}$ possesses a pale blue-green shade. The two most prominent oxidation states of iron, Fe(II) and Fe(III) are stable over a wide range of environmental conditions. In surface waters that are in contact with atmospheric oxygen, mainly Fe(III) can be detected as predominant species and in aqueous systems with low concentration of organic matter iron hydroxides are the most important metal species.[29] Iron(III) such as in $FeCl_3$ or $Fe(ClO_4)_3$ shows a large tendency to hydrolyse in water in a wide range of different pH conditions leading mainly to the (monomeric) octahedral species $[Fe(H_2O)_6]^{3+}$, $[Fe(OH)(H_2O)_5]^{2+}$ or $[Fe(OH)_2(H_2O)_4]^+$ with the possibility of a *cis* or *trans* orientation of the hydroxy ligands in the latter case. Under acidic conditions also dimeric iron cluster are known.[29]

Iron(III) is known to smoothly undergo so-called ligand-to-metal charge transfer bond homolysis events with different ligands once being irradiated with light. In literature so far, the main focus was the synthetic application of chlorine radicals that were produced upon the light-induced bond cleavage of Fe-chloride bonds or the formation of oxygen-centred radicals after iron LMCT when alcohols were provided as ligands.[24, 30-32] However, anionic or neutral aqua ligands being bound to iron metals are also able to undergo radical transformation (either thermal or photochemical) in aqueous media known as the Fenton and the Fe(III) photolysis process (Scheme 1.3, **R1** and **R2**).[33]
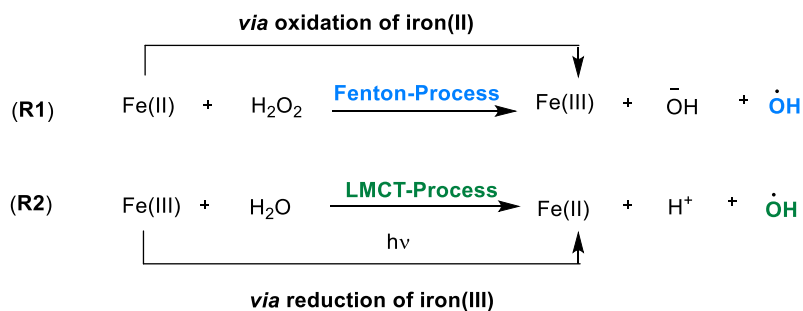
Scheme 1.3. (**R1**): Fenton-Process for the formation of hydroxy radicals upon oxidation of Fe(III); (**R2**): (visible)-light induced ligand-to-metal charge transfer event leading to the generation of hydroxy radicals with subsequent Fe(III) reduction.[33]
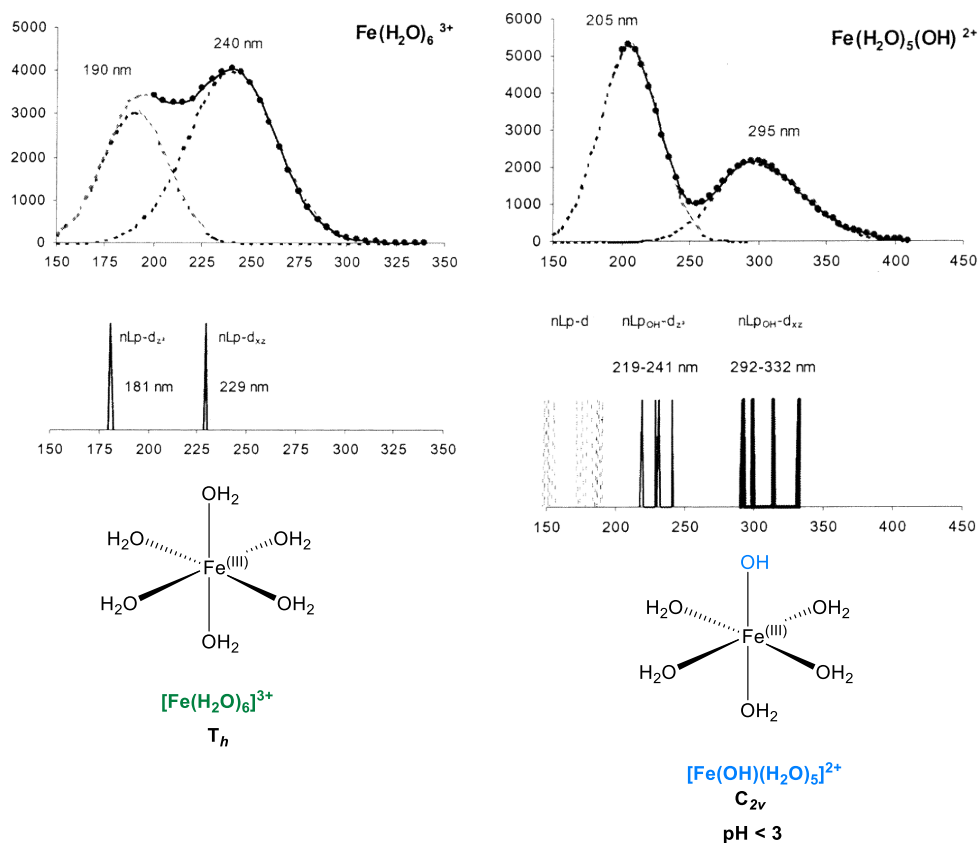
Spectrum 1.1. Comparison of the UV/Vis spectra of $Fe(H_2O)_5(OH)^{2+}$ and $Fe(H_2O)_6^{3+}$ fitted with a Gaussian decomposition (top), x-axis refers to the wavelength in nano meter (nm), the y-axis shows the absorbance in arbitrary units (AU), computed transitions from semiempirical calculations (middle) and their geometry and structure (bottom).[34, 35] Reproduced from ref. [34] with permission from American Chemical Society, copyright 2002.

$[Fe(OH)(H_2O)_5]^{2+}$ as photoactive complex shows two prominent absorption bands at 205 and at 295 nm and the latter one can be assigned as LMCT transition from the non-bonding p-orbitals of the OH⁻ ligand to the d-orbitals of the metal centre ($nLp_{OH} \rightarrow d_{Fe(III)}$). This transition is responsible for the light-triggered formation of hydroxy radicals. As the release of the hydroxy radical causes less conformational change than in $Fe(H_2O)_6^{3+}$ the quantum yield for the hydroxy radical formation after the LMCT step is higher for $[Fe(OH)(H_2O)_5]^{2+}$.[34]

1.3.2 Transformations Initiated by Hydroxy Radicals generated by Fe-OH LMCT

Hydroxy radicals are highly reactive and strong oxidants that non-selectively react with a wide range of organic molecules, nearly exclusively diffusion-controlled, leading to the oxidation of organic substances.[36] As the presence of hydroxy radicals awards aqueous systems a highly efficient oxidation power this process is investigated in detail in this review (Scheme 1.2, (R2)).[33, 37-39] Among the different Fe(III) hydroxy complexes $Fe(OH)^{2+}$, also named $[Fe(OH)(H_2O)_5]^{2+}$ that is the predominant species at pH ~ 3, shows the highest reactivity towards the formation of hydroxy radicals.[40] The mechanism for this transformation is shown in Scheme 1.3. This complex is able to undergo LMCT excitation by irradiation with UV light from the sun ($\lambda_{max} \sim 300$ nm, $\varepsilon_{max} \sim 2 \times 10^{-3}$), followed by an inner-sphere electron transfer to form Fe(II) and the hydroxy radical species.[41] This concept has been used for preparative purposes by the group of Malato in 2002 for the photodegradation of diethyl phthalate under UV light irradiation. The hydroxylated products could be monitored in HPLC using a UV/Vis detector (Scheme 1.4).[42, 43] The photodegradation of 3-(3-chlor-4-methylphenyl)-1,1-dimethylurea (chlortoluron) was achieved by sensitisation from the same iron(III)-aqua complex one year later by the group of Bolte. The urea derivative was stable in the dark in aqueous solution and even the irradiation of the compound with solar light did not lead to decomposition. In ground state a mixture of the slightly soluble organic compound and the iron complex did not show any chemical or physical interaction but upon irradiation of the mixture at 365 nm (wavelength given by the technical parameters of the high-pressure mercury lamp in the apparatus) in aqueous medium highly reactive hydroxy radicals were formed that led to the

transformation of chlortoluron into the structures highlighted in Scheme 1.4. In presence of oxygen the reaction rate increased and 2-propanol served as hydroxy radical scavenger as evidence for the oxygen-centred radical species being formed during the process.[44]
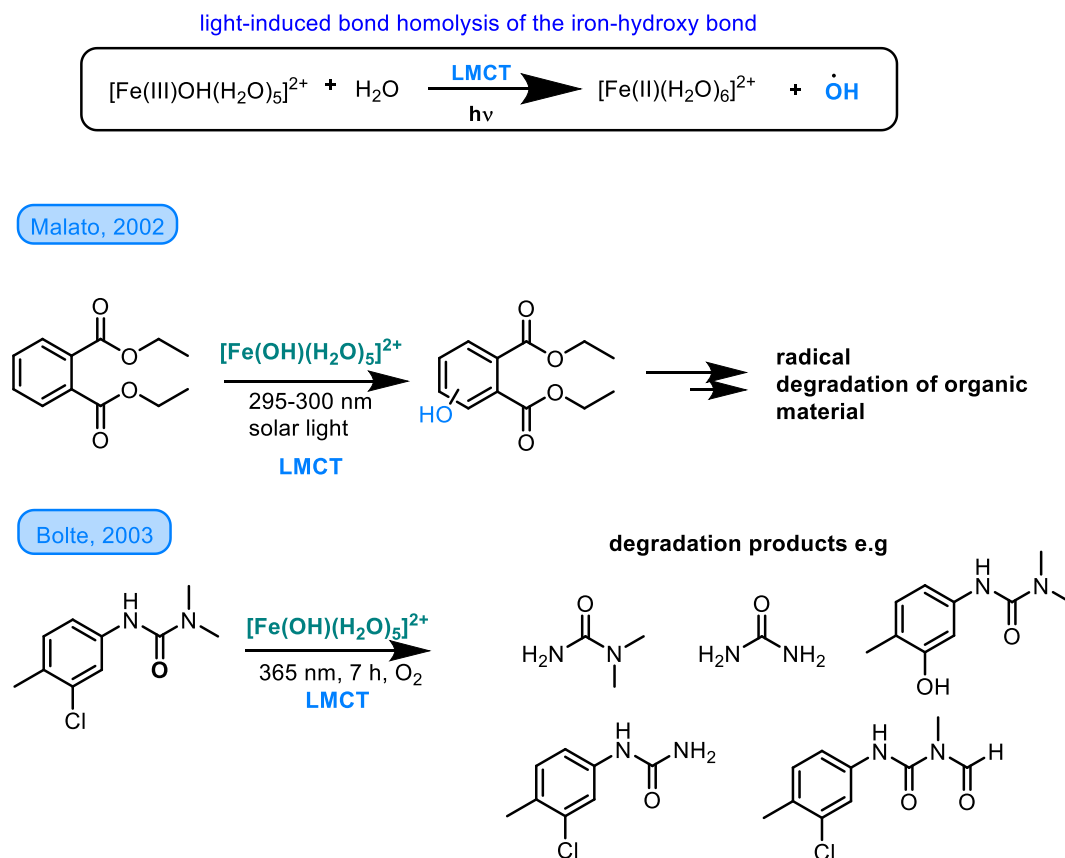
Scheme 1.4. Principle of $[Fe(OH)_2]^{2+}$ photolysis for the formation of hydroxy radicals and application in the photodegradation of diethyl phthalate or 3-(3-chlor-4-methylphenyl)-1,1-dimethylurea, respectively.[42, 44]

Once being formed by solar light induced light-to-metal charge transfer, the resulting electrophilic hydroxy radicals have a strong tendency to abstract a hydrogen atom from a suitable C-H precursor with the formation of one molecule of water as driving force (E^0 (OH·/OH⁻) = 1.9 V).[39] In 1999 the group of Bolte investigated the iron-catalysed photodegradation of tributyltin chloride in water.[45] Upon irradiation at $\lambda > 300$ nm, the initial $[Fe(OH)_2]^{2+}$ was transformed to Fe(II) as well as highly reactive hydroxy radicals that

\#

abstracted a hydrogen atom in the starting material and after trapping with oxygen and subsequent radical steps the respective alcohol or ketones of tributyltin chloride could be observed (Scheme 1.5).

In a similar fashion, hydroxy radicals were used by Carey *et. al.* in 1975 for the α-hydroxy HAT on simple alcohols and formic acid that served as scavenger for the reactive radical species. Under their diluted conditions the quantum yield for the light-induced bond homolysis was rather high and the reaction was performed efficiently as the abstraction reaction initiated by hydroxy radicals led to almost quantitative formation of the respective ketone from an alcohol starting material (Scheme 1.5). The reaction worked successfully with substrates possessing an α-hydroxy hydrogen atom and the authors state that there is supposed to be no change in the coordination spere of the iron(III) aqua complex as no ligand exchange between hydroxy and alcohol ligands was observed.[46]
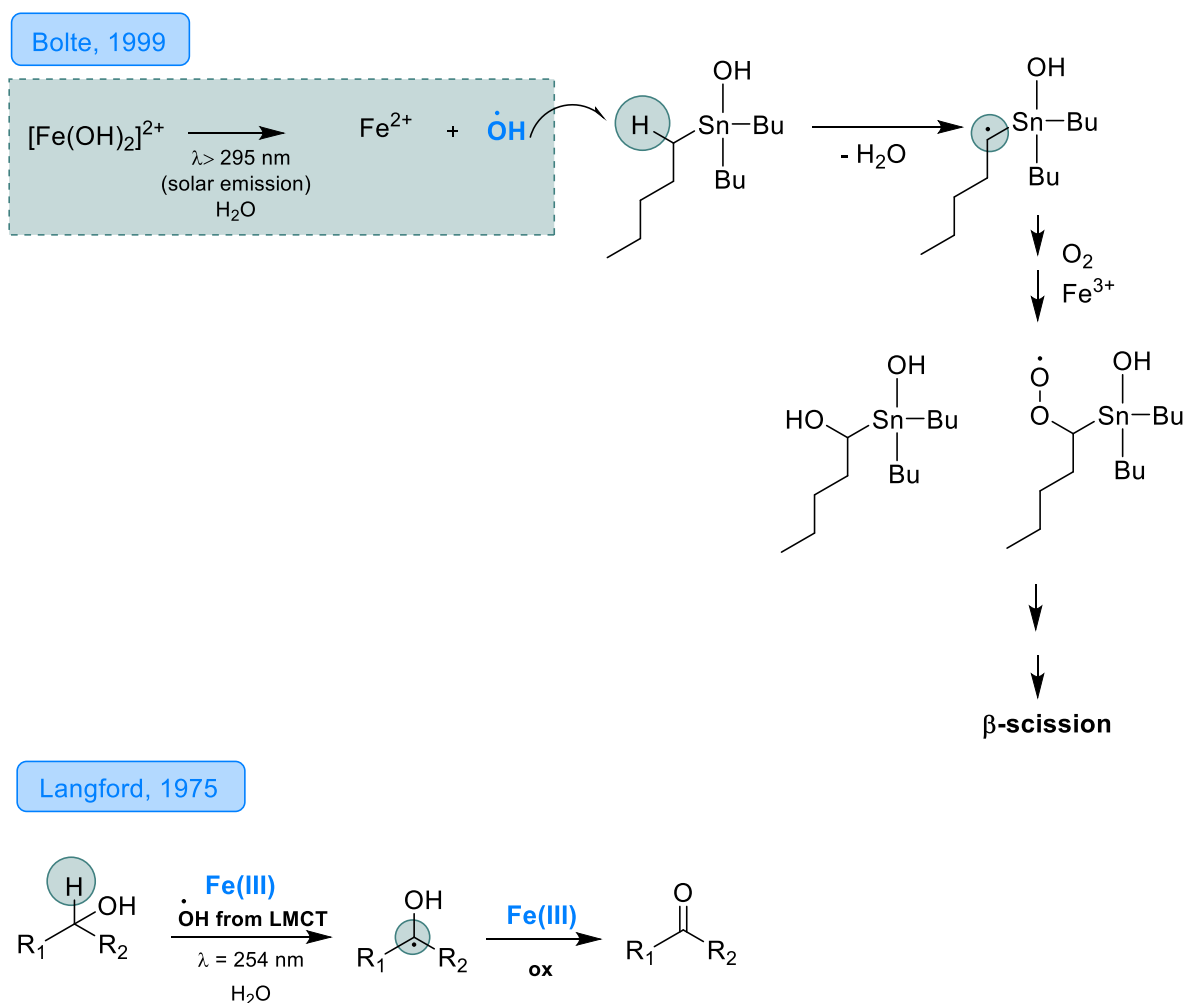
Scheme 1.5. Hydroxy radicals as strong hydrogen atom abstractors.[45, 46]

1.4 Behaviour of Iron(III) Salts in Aqueous Environment

Iron aqua complexes are not commercially available and are *in-situ* generated upon the addition of iron(III) salts to water. Possessing other substituents before, ligand exchanges on the metal centre with unique kinetics take place.[47]

1.4.1 FeCl₃

FeCl$_3$ (anhydrous or as hydrate form) or ferric chloride is an important commercially available chemical that is produced in large-scale by industry. It is generated as an aqueous solution from the reaction of ferrous chloride (FeCl$_2$) with chlorine and the primary use of this compound is industrial waste-water treatment application as it is able to remove impurities from water by agglomeration.[48] In a recent publication from 2018, the group of Ingmar Persson could differentiate by EXAFS, a methodology related to X-ray absorption spectroscopy, the bond length deviations in [Fe(H$_2$O)$_6$]$^{3+}$, [FeCl$_6$]$^{3-}$ and [Fe(Cl$_2$)$_2$(H$_2$O)$_4$]Cl·2H$_2$O that all exist as octahedral complexes in water or solid state, respectively.[49] Additionally, he showed that the dominant species in concentrated aqueous solutions is ferric chloride (FeCl$_3$) and in mixtures with an excess of chloride anions (1 mol/L), *trans*-[FeCl$_2$(H$_2$O)$_4$]$^+$ can be considered as prominent species. In diluted systems with FeCl$_3$ < 1 mol/L mostly [Fe(H$_2$O)$_6$]$^{3+}$ and non-bond chloride anions can were detected.[49] As the Fe-Cl bond length in [FeCl$_2$(H$_2$O)$_4$]Cl·2H$_2$O is shorter than in [FeCl$_6$]$^{3-}$ (2.278 Å/2.292 Å) while the Fe-O bond length is longer for the hydrated iron(III) complex (2.057 Å/2.070 Å) the chloride ions in the hydration complex are much tighter bound than in [FeCl$_6$]$^{3-}$.[49]

An interesting application for photochemical and photosensitised transformation of FeCl$_3$ in aqueous medium was published by the group of Al-Abadleh in 2011 (Scheme 1.6). They investigated the photodegradation of gallic acid (3,4,5-trihydroxybenzoic acid), an important representative and the simplest version of humic-like substances within a multi-layer film containing FeCl$_3$ as photosensitiser. The water uptake by the layer, being formed by deposition method from a diethyl ether containing FeCl$_3$ · 6H$_2$O and GA (gallic acid) solution, and the qualification of the resulting degradation products were executed by a quartz crystal microbalance.[50] After formation of a gallic acid-iron(III) complex they propose several light-induced LMCT bond homolysis events that lead to the formation of chlorinated and hydroxylated products as well as volatile chlorinated organic compounds (Scheme 1.6).

Gallic acid   **Gallic acid iron(III) complex**   film on top of bulk water

plausible reaction mechanisms

i) ... $Fe(III)Cl_3$ ... **LMCT** Xe-lamp water $\lambda > 300$ nm ... $Fe^{3+}-Cl$ ... *o*-quinone + **Fe(II)** + H^+

$Fe(III)$ Cl^-, O_2

C1-C4 volatile chlorinated compounds

ii) ... CO_2, H^+, H_2O ... + ... ring opening and formation of oxygenated products

iii) ... + $Cl^{\bullet}$ $-{\bullet}$ Cl_2 ... CO_2, H^+, H_2O ... Cl ... Cl ... ring opening and formation of chlorinated compounds
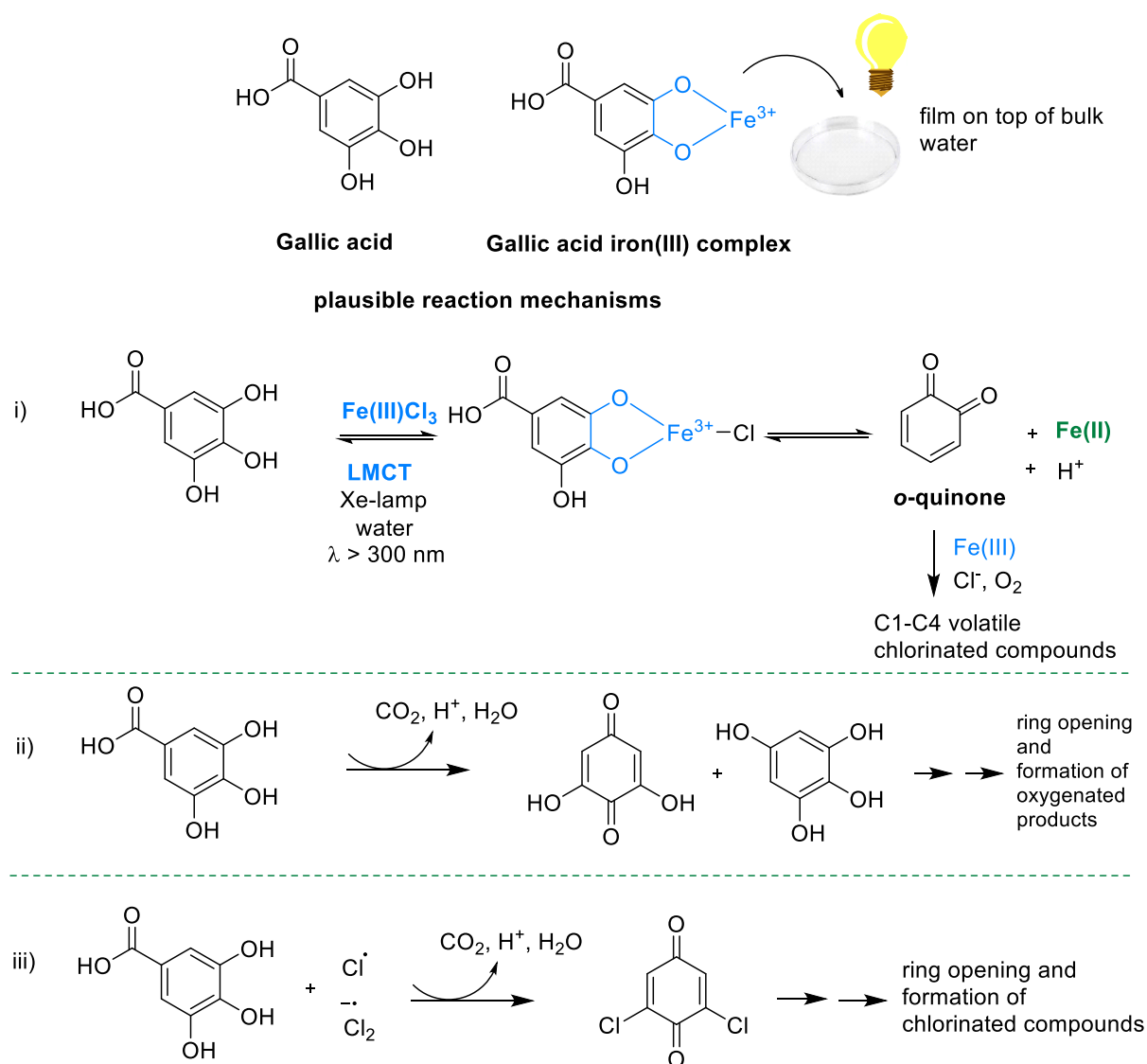
Scheme 1.6. Photodegradation of gallic acid integrated in a thin-layer film with $FeCl_3$ on bulk water. Several reaction mechanisms for the light-induced transformation are summarised; i)[51], pathway ii)[52], mechanism variant iii).[53]

1.4.2   Fe(ClO$_4$)$_3$

Similar to FeCl$_3$, Fe(ClO$_4$)$_3$ undergoes fast hydrolysis being surrounded by water molecules at low pH and aqua complexes are formed.[54] Likewise FeCl$_3$, Fe(ClO$_4$)$_3$ is able to bind to different ligands such as phenols and upon irradiation with (UV) light a ligand-to-metal charge transfer takes place. Oxygen-centred radicals on phenol are formed and the organic substrate is decomposed oxidatively.[54]

As the stability constant for anion ligands being attached to an iron(III) centre is lower for ClO$_4^-$ compared to Cl$^-$, the kinetic for the respective ligand exchange with competing water molecules is supposed to be faster for the perchlorate anion.[55]

In contrast to FeCl$_3$, Fe(ClO$_4$)$_3$ is not soluble in most organic solvents and therefore, the group of Kozlov extended their investigations based on aerobic oxidations of hydrocarbons by Fe(III)Cl$_3$ in organic solvents *via* LMCT to the perchlorate salt's reactivity in water or mixed water/acetonitrile/acetone solutions.[56] In acetonitrile the UV light induced bond homolysis of the Fe-Cl bond led to the formation of chlorine radicals that were able to abstract hydrogen atoms from simple alkanes such as *n*-pentane with a certain selectivity towards C$_2$ and/or C$_3$. After radical trapping with molecular oxygen, they received alcohol and ketone products after decomposition of the respective peroxide radical. Performing the reaction in water with addition of acetone or acetonitrile increased the solubility of the alkane and they observed the formation of the ketone as major product with only traces of the alcohol. They state that in the case of Fe(ClO$_4$)$_3$ hydroxyl radicals are responsible for hydrogen atom abstraction and the selectivity towards the carbon-centre changes upon addition of organic solvents. Shul' pin and co-workers stated that the aerobic oxidation takes places in a region close to the interface of the two phases and the selectivity is given by the ability of organic solvents to interrupt hydrogen-bonding networks in aqueous solutions (Scheme 1.7).[56]
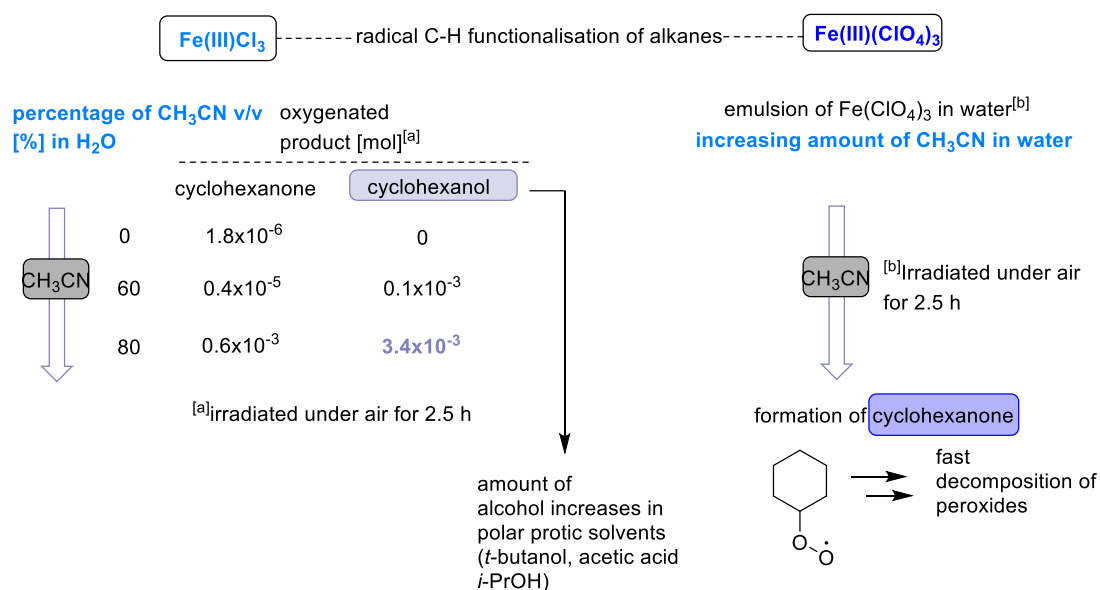
Scheme 1.7. Selectivity of hydrogen atom abstraction on alkanes for the photolysis of FeCl$_3$ and Fe(ClO$_4$)$_3$ in acetonitrile/water mixtures.[57]

1.5 Preparative Applications of Iron LMCT in Water

1.5.1 Decarboxylation Reactions

The complex formation between aliphatic and aromatic carboxylic acids and metals can be reversible and is therefore often exploited for interesting applications.[58, 59] Carboxylic acids as neutral form or as charged ligand are known to interact with Fe^{2+} or Fe^{3+} in water leading to the formation of chelate complexes with both alkyl- and aryl carboxylates.[60-65] In natural environments, such as lakes or seas, mainly short (keto)carboxylic acids as glyoxylic and pyruvic acids, as well as citric acid, acetic acid and lactic acid can be found.[66, 67] After formation of the oxygen-iron bond the complex shows characteristic colours, can be excited by UV or visible light leading to a LMCT transitions, whereat the carboxylic acid ligand gets oxidised to the respective radical generating Fe(II) at the same time. The driving force for product formation is the elimination of CO$_2$ that increases the entropy of the system and ends in the formation of highly reactive carbon-centred radicals that build the platform for numerous further synthetic transformations (Scheme 1.8).[61]

16
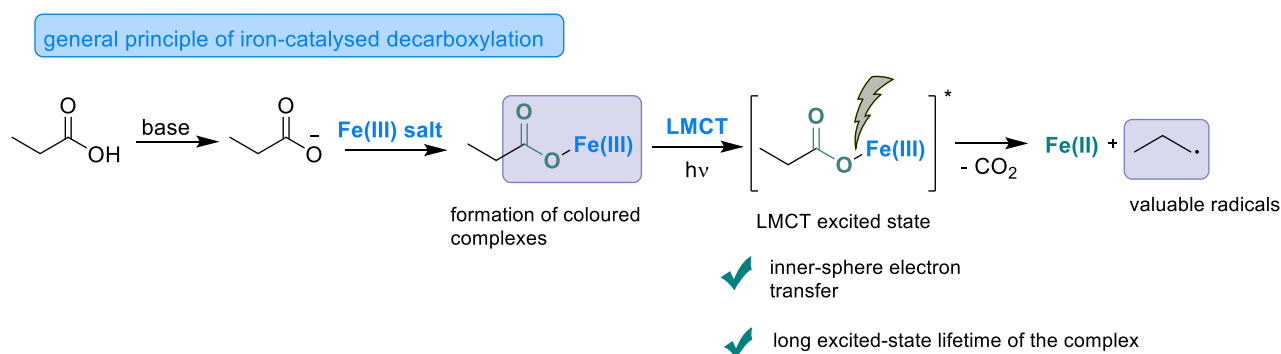
Scheme 1.8. Basic principle of LMCT reactions in iron(III) carboxylic acid complexes.

Several examples from literature depicting the usefulness of the methodology are summarised in Scheme 1.9. In 1995 the group of Hoffmann investigated heterogenous catalysis using iron(III)oxyhydroxides, such as γ-Fe_2O_3, $Fe_2O_3 \cdot 3H_2O$, α-FeOOH or α-Fe_2O_3 to realise the photo-transformation of halogenated acetic acids. They observed that the photoreduction of the iron cation in the oxides to the respective Fe^{2+} is most efficient for $Fe_2O_3 \cdot 3H_2O$ in combination with FCH_2COOH with decreasing relative reactivity for $ClCH_2COOH$, $BrCH_2COOH$ and ICH_2COOH. Halide ions and glycolic acids are formed during this photo-transformation whose key mechanistic step involves hydrogen atom abstraction by surface-bound hydroxyl radicals (Scheme 1.9, I)). Fully halogenated halo-acetic acids show Kolbe-type reactivity and reacting those substrates with iron oxides led to the formation of CO_2 and simple halogenated acid (Scheme 1.9, II)).[60, 68, 69]
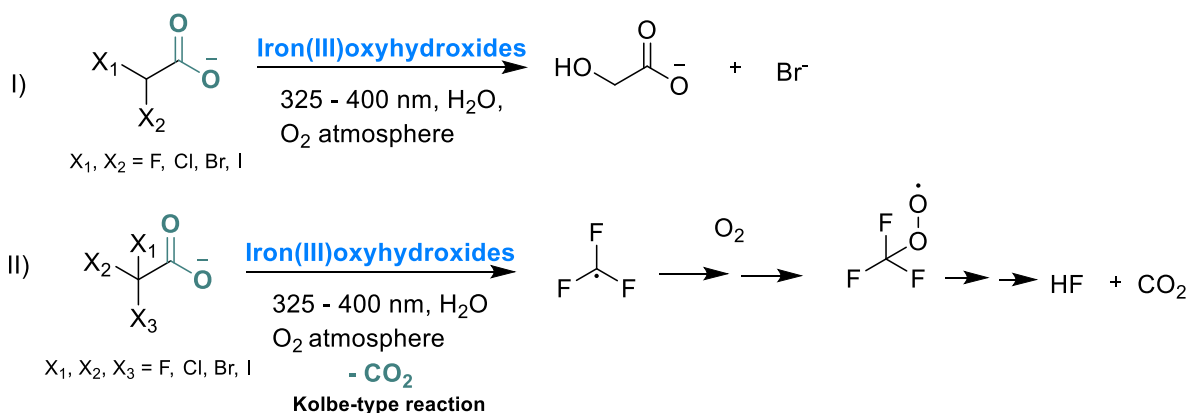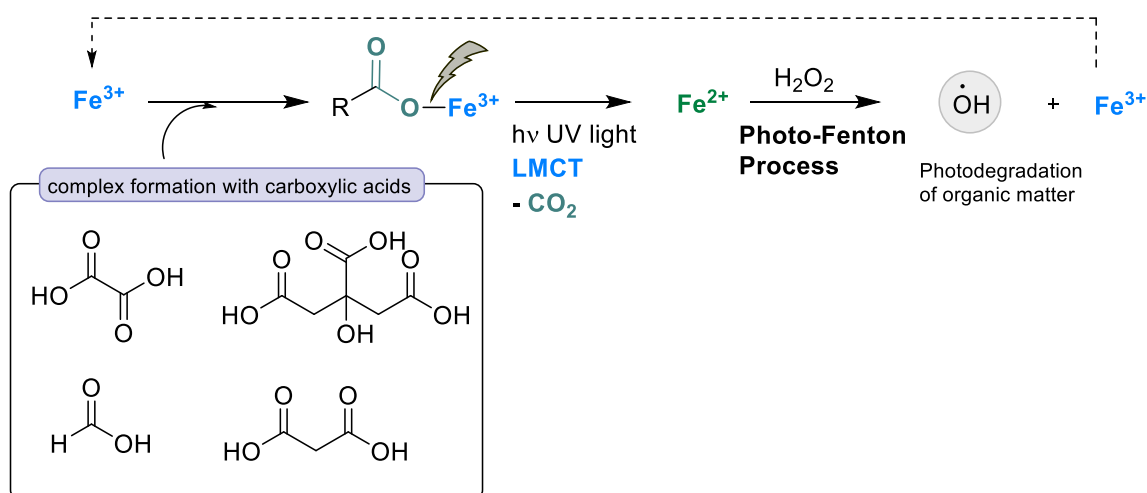
Scheme 1.9. Applications of carboxylic acid decarboxylation reactions.[60, 69]

Baba and co-workers realised in 2015 that a LMCT in iron(III)-carboxylic acids followed by light-triggered decarboxylation can increase the rate constant for a subsequent photo-Fenton process initiated by the previously generated Fe(II) (Scheme 1.9).[60] Once being coordinated to oxalic acid, citric acid, formic acid or malonic acid a coloured iron(III) species is formed whose LMCT transition can be excited at 352 – 400 nm and the fast bond homolysis as exothermic reaction produces Fe(II) in large amounts. The hydroxy radicals originating from the Fenton reaction were used for the photo-degradation of organic matter such as coumarin. Compared to reactions without carboxylic acids the kinetic of the iron redox cycle was

increased by 26% for oxalic acid as most successful entry.[60] The group did not find a direct correlation between the application of carboxylic acids and the generation of hydroxy radicals.

The ligand-to-metal charge transfer principle can also be applied to the functionalisation, transformation or synthesis of biomolecules.[61, 70] Siderophores are low molecular-weight chelators that are produced by many bacteria to facilitate iron acquisition.[71] Citric acid-containing Aerobactin (Scheme 1.10) is generated by marine bacteria such as Vibrio sp. DS40M5 and binds iron(III) on overall six coordination sites in the molecule. By exciting the complex with UV light, the ligand-iron LMCT can be triggered, whereat the α-hydroxy carboxylic acid part is affected most as photo-labile unit. After decarboxylation the molecule undergoes a structural change and iron(III) can be bound in a more efficient way *via* an enolate moiety for iron transport.[72]

Aerobactin with citric acid substructure
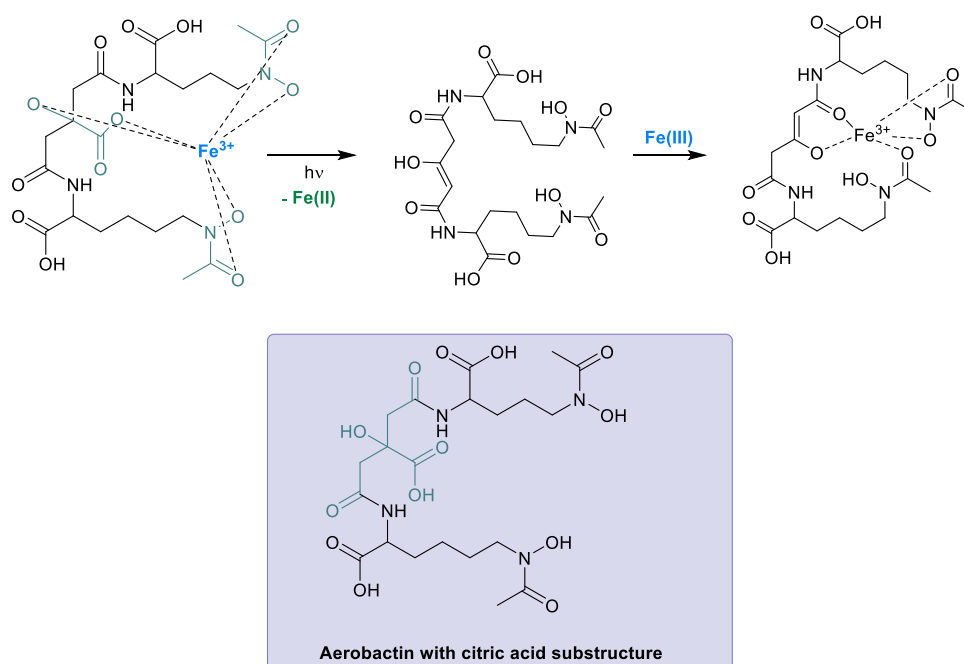
Scheme 1.10. Coordination change of iron(III) in siderophores after light induced decarboxylation.[73]

1.5.2   Catalytic Oxidations

Redox reactions involving iron(III) species in natural waters have been shown to play a crucial role in providing important oxidant species within water drops such as OH·, SO_x^{-}, $H_2O^{·}/O_2^{-}$ and H_2O_2 and are known to be responsible for the atmospheric oxidation of SO_2 to H_2SO_4 to just mention one example.[74-77] Like in most photocatalysed reactions the transformation proceeds *via* single electron transfer and the harder Lewis acid Fe(III) is reduced to the respective +2 species whereat, at the same time one substrate gets oxidised.[30, 78] The redox potential of the Fe(III)/Fe(II) pair in water was determined to be E^0_{calc}: 0.786 V so single electron transformations are feasible in combination with most organic substrates.[79]

Iron(III)chlorides are water-soluble and LMCT-active species whose metal-chloride bond can be cleaved in a homolytic fashion upon irradiation with UV or visible light. The resulting chloride radicals are highly reactive and non-selective hydrogen-atom abstractors that allow for the formation of carbon-centred radicals from C-H precursors with a suitable bond-dissociation energy.[32, 80] In presence of oxygen the nucleophilic carbon-centred radicals can be trapped leading to the formation of overall oxidised substrates.[81] Scheme 10 highlights the interesting application of this methods for the photooxidation of cyclic olefins and the synthesis of exo-Brevicomin in water realised by the group of Kobayashi in 1985 (Scheme 1.11).[81]
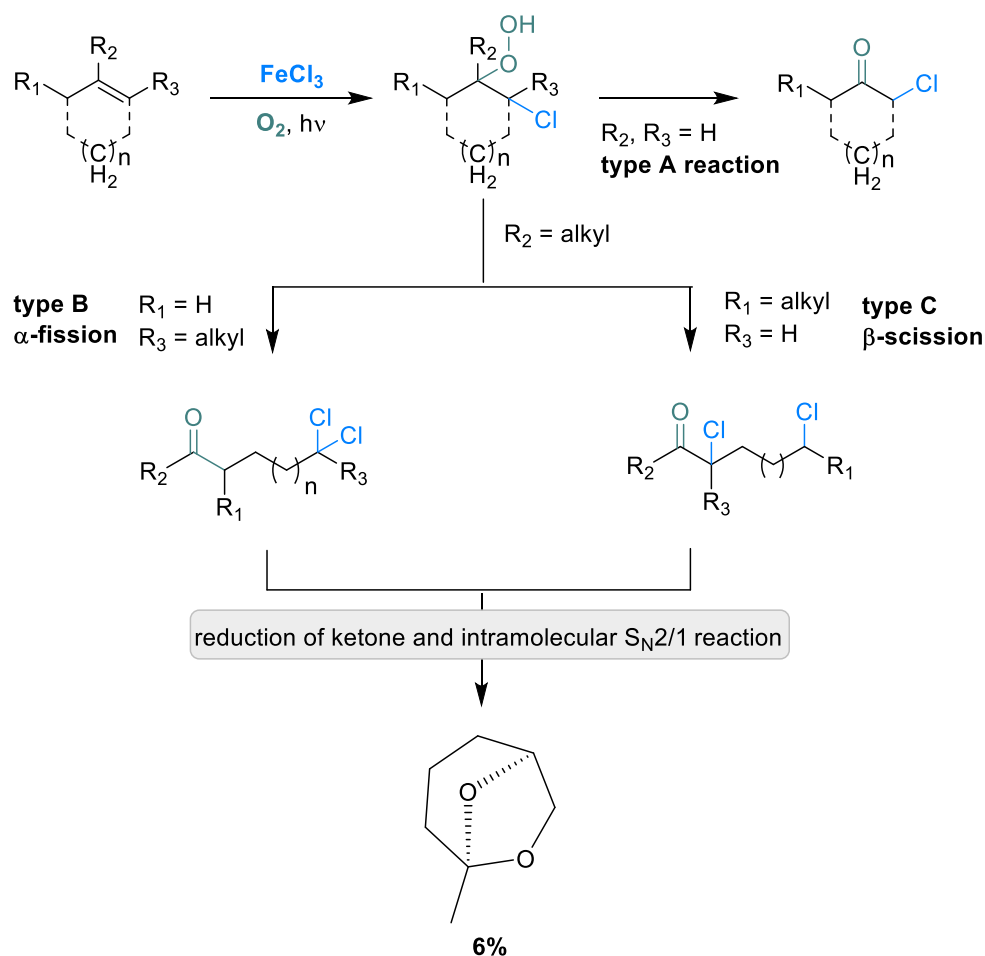
***Scheme 1.11**. Application of iron LMCT on the photooxidation of cyclic ketones.[81]*

A environmentally important application of the iron LMCT in water is represented by the catalytic oxidation of arsenic(III) in waste water under irradiation with near-UV light.[82] Increased amounts of arsenic in ground water and acidic mine waters are found in many different countries such as India or Bangladesh and people are bearing high risk to be intoxicated by contaminated water. It occurs naturally by dissolution of arsenic-containing minerals and soils in respective regions. The group of Khoe found that the oxidation of As(III) to As(V) by oxygen can be accelerated efficiently upon addition of dissolved iron complexes and irradiation with ultraviolet light.[82] They hypothesised that two radical pathways based on a LMCT activation of either a Fe-OH or Fe-Cl bond lead to the formation of highly reactive and oxidising hydroxy or chlorine radicals that enable the stepwise single electron transfer oxidation of arsenic from its 3+ to its 5+ state, the less toxic oxidation state.[83]

The photoreaction was observed to be most efficient in case of chloride being coordinated to the iron(III) centre in presence of oxygen. Lowering the pH of the solution did contribute to an even higher amount of As(V) formed in the photocatalytic process while the presence of Fe(II) had a clear inhibitory effect to the overall reaction (Scheme 1.12).[82]
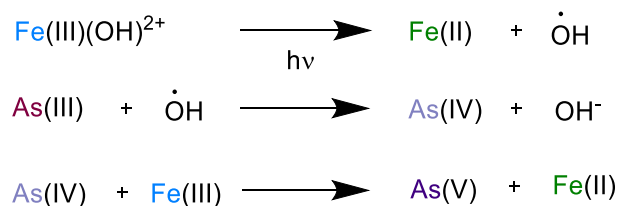
Scheme 1.12. Iron-assisted oxidation of arsenic.[82]

Another oxidative transformation induced by an iron-LMCT reaction is the photolysis of phenol derivatives such as *m*-cresol or tyrosine in aqueous solution investigated by the group of Arnd Vogler.[84] The ligand undergoes fast complex formation in a 1:1 stoichiometry with the oxophilic iron(III), however the two components are only weakly associated and hydrolysis of iron(III) has to be considered as main side reaction.[85, 86] Combining colourless $Fe(III)(ClO_4)_3$ and tyrosine, the resulting metal-ligand complex shows absorptions tailing into the 500 nm region ($\lambda_{max} = 558$ nm for the respective phenol $\rightarrow$ iron transition) and the oxidative Fe-O bond homolysis can be triggered by visible light leading to the formation of reactive phenolate radicals. Based on investigations, the quantum yield for the formation of phenol radicals is rather small ($\varphi \sim 10^{-4}$), which can be explained by an inefficient cage escape in aqueous solution and a fast back electron transfer. Nevertheless, the phenomena offers interesting application in the field of biological investigations on tyrosine-containing enzymes and proteins (Scheme 1.13).[87]
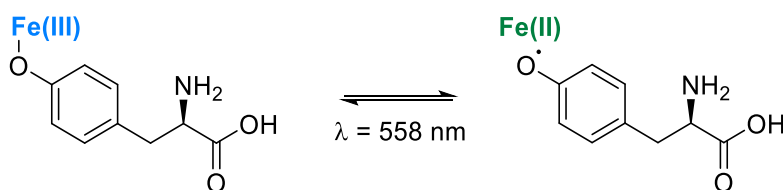
Scheme 1.13. Iron(III)-tyrosine complex and its respective LMCT excitation wavelength.[42]

1.6 Release of Small Molecules

1.6.1 Release of N_2, NO and O_2 by LMCT

The release of low-molecular weight molecules such as NO or N_2 plays an important role especially in the field of biochemistry as those compounds are crucial for biological activities such as cellular signal transport or the key control system of metabolism and immunity.[88] Within the physiological environment of mammalians, degradation of some of these nitrogen-containing molecules can take place given the suitable redox window of water in the blood circulation. Oxidation and reduction pathways are initiated by protein substructures and the resulting molecules, themselves soluble in water, are involved in subsequent signalling steps on receptors in the body of humans and animals.[89]

Already discovered in 1989, Wagner and Nakamoto could show that N_2 is released from the surface of porphyrin after UV light trigged bond cleavage of the iron-nitrogen bond in the catalytic centre of the molecule.[90] However, this process can't be assigned as ligand-to-metal charge transfer as iron(III) undergoes a two-electron oxidation to the +5 species whereas the N_3 ligand is reduced to one molecule of N_2 leaving behind an iron-N triple bond.

The group of Arndt Vogler found, that iron(III) complexes with cupferronate or phenyldiazeniumdiolate ligands can be excited with UV light leading to a bond homolysis of the iron-oxygen bonds. Upon oxidation NO is released and iron(III) reduced to iron(II) (Scheme 1.14).[87] The group discovered that the bond homolysis shows a high efficiency and can also proceed by irradiation with visible light. As this molecule acts like a reservoir for the small molecule NO it can be considered as photo-trigger molecule with huge impact for medical and biological research.[87]
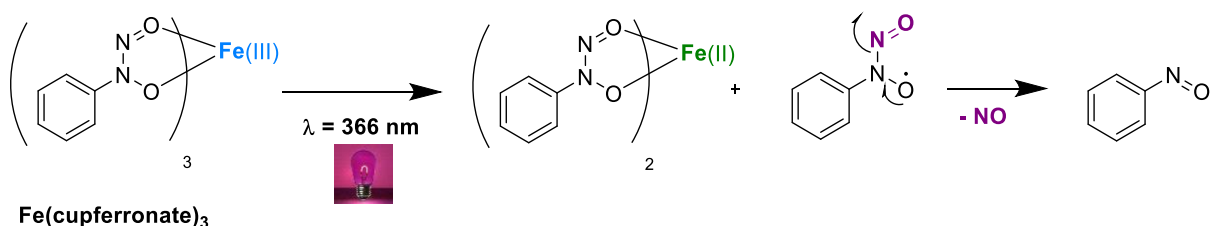
Scheme 1.14. Formation of NO *via* UV light induced bond homolysis of the iron-oxygen bond.[87]

Inspired by the ability of Fe(III)-porphyrins to bind to alcohols and to form the respective oxygen-centred radical after a LMCT activation step,[91, 92] the group of Tsuchida investigated a system consisting of (tetraphenylporphyrinato)Fe(III) complex with four alkyl phosphocholine ligands as well as an axially coordinated imidazole that is forming tubular fibres in water and can bind molecular oxygen reversibly. Iron(III) is generated from iron(II) by a previous autoxidation mechanism. As the compound is handled in saline solution, a chloride anion binds to the iron(III) centre of the porphyrin and the Fe-Cl bond scission is realised by a LMCT step upon irradiation at 362 nm. The resulting iron(II) metal centre is able to reversibly bind molecular oxygen like Haemoglobin.[93] Hyaluronic acid as additive prevents back electron transfer in the system and the efficient radical trapping by the polysaccharide is displayed in the decrease of the reaction solution viscosity.[94] In case the hyaluronic acid or other polysaccharide additives were added in the dark, no prominent spectral change could be observed (Figure 1.2).[94]
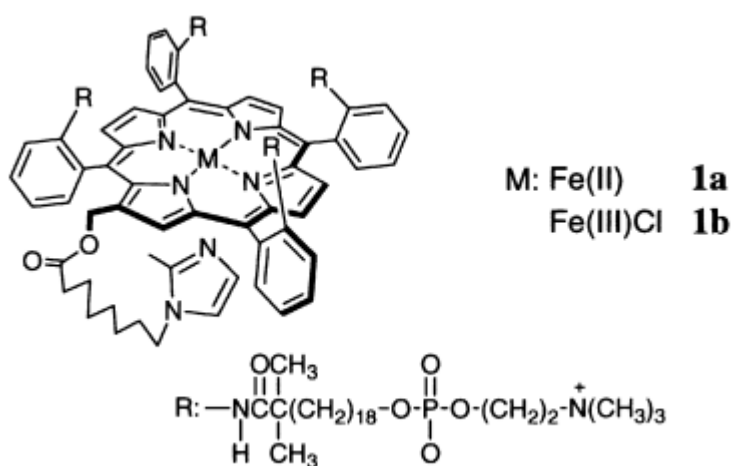
Figure 1.2. Iron(III) and iron(II)-porphyrin complexes with alkyl phosphocholine ligands. **1b)** Fe(III) bound to chloride anion; LMCT-active form; right structure: **1a)** reduced iron-centre that can bind molecular oxygen reversibly.[94] Reproduced from ref. [94] with permission from *Bull. Chem. Soc. Jpn.*, copyright 2001.

1.7 Conclusion

Water is an interesting and underrated solvent for organic transformations. It allows the tuning of reaction selectivity based on physical characteristics of the medium such as hydrogen-bonding or the high bond-dissociation energy of the O-H bond that suppresses competitive hydrogen atom abstraction events in the field of radical chemistry. Even reaction rates of photochemical transformations can be positively influenced in presence of water.[95-97] Efforts were made to overcome the solubility problems of organic starting materials by adding phase transfer catalysts or performing reactions in micellar systems.[98, 99] For the research field of ligand-to-metal charge transfer catalysis the hydrolysis of the metal is the main challenge as hydroxy radicals that result from the competitive bond homolysis of a metal-OH_2 bond can hardly be controlled in their reactivity and therefore stable iron complexes are promising candidates for selective LMCT reactions in water.[21, 37, 100] Additionally, performing photoreactions in water reduces the use of harmful chemicals as many organic solvents show medium to high toxicity.[101]

1.8 References

[1]   A. Brack, *Orig. Life Evol. Biosph.* **1993**, *1*, 3-10.

[2]   M. Ahsan, C. Pindi, S. Senapati, *J. Mol. Graph. Model.* **2021**, *105*, 107894.

[3]   X. Liu, J. Yu, *Sci. Rep.* **2019**, *1*, 18562.

[4]   K. Rayat, F. Feyzi, *Colloids Surf.* **2011**, *1*, 61-67.

[5]   Z. Chen, D. Li, K. Tong, Z. Chen, H. Chen, Q. Chen, Y. Xu, *Environ. Sci. Pollut. Res.* **2019**, *7*, 7216-7227.

[6]   A.A. Dietz, M.J. Hofmann, H. Motschmann, *J. Phys. Chem. B* **2016**, *29*, 7143-7147.

[7]   H. Chen, E. Ruckenstein, *J. Phys. Chem. B* **2015**, *39*, 12671-12676.

[8]   M. Andreev, J.J. de Pablo, A. Chremos, J.F. Douglas, *J. Phys. Chem. B* **2018**, *14*, 4029-4034.

[9]   I. Persson, *Pure Appl. Chem.* **2010**, *10*, 1901-1917.

[10]   P. Maksyutenko, T.R. Rizzo, O.V. Boyarkin, *Chem. Phys* **2006**, *18*, 181101.

[11]   O.V. Boyarkin, M.A. Koshelev, O. Aseev, P. Maksyutenko, T.R. Rizzo, N.F. Zobov, L. Lodi, J. Tennyson, O.L. Polyansky, *Chem. Phys. Lett.* **2013**, 568-569, 14-20.

[12]   S.J. Blanksby, G.B. Ellison, *Acc. Chem. Res.* **2003**, *4*, 255-263.

[13]   Z. Lee, C. Hu, S. Shang, K. Du, M. Lewis, R. Arnone, R. Brewin, *J. Geophys. Res.* **2013**, *9*, 4241-4255.

[14]   V. Balzani, G. Bergamini, S. Campagna, F. Puntoriero, *Photochemistry and Photophysics of Coordination Compounds: Overview and GeneralConcepts*, in *Photochemistry and Photophysics of Coordination Compounds I*, V. Balzani , S. Campagna, Editors. 2007, Springer Berlin Heidelberg: Berlin, Heidelberg. p. 1-36.

[15]   V.W.-W. Yam, A.K.-W. Chan, E.Y.-H. Hong, *Nat. Rev. Chem.* **2020**, *10*, 528-541.

[16]   R. Zhao, L. Shi, *Org, Chem. Front.* **2018**, *20*, 3018-3021.

[17]   D. Birnthaler, R. Narobe, E. Lopez-Berguno, C. Haag, B. König, *ACS Catal.* **2023**, *2*, 1125-1132.

[18]   L. Chang, S. Wang, Q. An, L. Liu, H. Wang, Y. Li, K. Feng, Z. Zuo, *Chem. Sci.* **2023**, *25*, 6841-6859.

[19]   M. Zhang, J. Zhang, Q. Li, Y. Shi, *Nat. Commun.* **2022**, *1*, 7880.

[20]   Q. An, Z. Wang, Y. Chen, X. Wang, K. Zhang, H. Pan, W. Liu, Z. Zuo, *J. Am. Chem. Soc.* **2020**, *13*, 6216-6226.

[21]   Z. Li, X. Wang, S. Xia, J. Jin, *Org. Lett.* **2019**, *11*, 4259-4265.

[22]   V.R. Yatham, P. Bellotti, B. König, *Chem. Commun.* **2019**, *24*, 3489-3492.

[23]   J.-L. Tu, H. Gao, M. Luo, L. Zhao, C. Yang, L. Guo, W. Xia, *Green Chem.* **2022**, *14*, 5553-5558.

[24]   T. Xue, Z. Zhang, R. Zeng, *Org. Lett.* **2022**, *3*, 977-982.

[25]   A.S. Mereshchenko, P.K. Olshin, A.M. Karimov, M.Y. Skripkin, K.A. Burkov, Y.S. Tveryanovich, A.N. Tarnovsky, *Chem. Phys. Lett.* **2014**, *615*, 105-110.

[26]   D.A. Cagan, D. Bím, B. Silva, N.P. Kazmierczak, B.J. McNicholas, R.G. Hadt, *J. Am. Chem. Soc.* **2022**, *14*, 6516-6531.

[27]   K.S. Kjær, N. Kaul, O. Prakash, P. Chábera, N.W. Rosemann, A. Honarfar, O. Gordivska, L.A. Fredin, K.-E. Bergquist, L. Häggström, T. Ericsson, L. Lindh, A. Yartsev, S. Styring, P. Huang, J. Uhlig, J. Bendix, D. Strand, V. Sundström, P. Persson, R. Lomoth, K. Wärnmark, *Science* **2019**, *6424*, 249-253.

[28]   S. Mitra, S.R.K. Ainavarapu, J. Dasgupta, *J. Phys. Chem. B* **2022**, *29*, 5390-5399.

[29]   F.J. Millero, W. Yao, J. Aicher, *Mar. Chem.* **1995**, *1*, 21-39.

[30]   Y. Abderrazak, A. Bhattacharyya, O. Reiser, *Angew. Chem. Int. Ed.* **2021**, *39*, 21100-21115.

[31]   F. Juliá, *ChemCatChem* **2022**, *19*, e202200916.

[32]   Y.C. Kang, S.M. Treacy, T. Rovis, *ACS Catal.* **2021**, *12*, 7442-7449.

[33]   M. Passananti, V. Vinatier, A.-M. Delort, G. Mailhot, M. Brigante, *Environ. Sci. Technol.* **2016**, *17*, 9324-9332.

[34]   L. Lopes, J. de Laat, B. Legube, *Inorg. Chem.* **2002**, *9*, 2505-2517.

[35]   M. Radoń, K. Gąssowska, J. Szklarzewicz, E. Broclawik, *J. Chem. Theory Comput.* **2016**, *4*, 1592-1605.

[36]   S. Gligorovski, R. Strekowski, S. Barbati, D. Vione, *Chem. Rev.* **2015**, *24*, 13051-13092.

[37]   F. Collin, *Int.J. Mol. Sci.* **2019**, *10*, 2407.

[38]   D. Vione, M. Minella, V. Maurino, C. Minero, *Chem. Eur. J.* **2014**, *34*, 10590-10606.

[39]   P. Wardman, *J. Phys. Chem. Ref. Data* **1989**, *4*, 1637-1755.

[40]   P. Cieśla, P. Kocot, P. Mytych, Z. Stasicka, *J. Mol. Catal. A Chem.* **2004**, *1*, 17-33.

[41]   H. Kawaguchi, A. Inagaki, *Chemosphere* **1993**, *12*, 2381-2387.

[42]   G. Mailhot, M. Sarakha, B. Lavedrine, J. Cáceres, S. Malato, *Chemosphere* **2002**, *6*, 525-532.

[43]   B.C. Faust, J. Hoigné, *Atmos. Environ.* **1990**, *1*, 79-89.

[44] L. Poulain, G. Mailhot, P. Wong-Wah-Chung, M. Bolte, *J. Photochem. Photobiol. A* **2003**, *1*, 81-88.

[45] G. Mailhot, M. Astruc, M. Bolte, *Appl. Environ. Chem.* **1999**, *1*, 53-61.

[46] J.H. Carey, C.H. Langford, *Can. J. Chem.* **1975**, *16*, 2436-2440.

[47] G. Lente, I. Fábián, *Inorg. Chem.* **2002**, *5*, 1306-1314.

[48] K.H. Park, D. Mohapatra, B.R. Reddy, *Sep. Purif. Technol.* **2006**, *3*, 332-337.

[49] I. Persson, *J. Solution Chem.* **2018**, *5*, 797-805.

[50] G.R. Wentworth, H.A. Al-Abadleh, *Phys. Chem. Chem. Phys.* **2011**, *14*, 6507-6516.

[51] N. Quici, M.I. Litter, *Photochem. Photobiol. Sci.* **2009**, *7*, 975-984.

[52] F. Keppler, R. Borchers, J. Pracht, S. Rheinberger, H.F. Schöler, *Environ. Sci. Technol.* **2002**, *11*, 2479-2483.

[53] N. Quici, M.I. Litter, A.M. Braun, E. Oliveros, *J. Photochem. Photobiol. A* **2008**, *2*, 306-312.

[54] V. A. Nadtochenko, J. Kiwi, *J. Chem. Soc., Perkin trans.2* **1998**, *6*, 1303-1306.

[55] G.H. Khoe, P.L. Brown, R.N. Sylva, R.G. Robins, *J. Chem. Soc., Dalton Trans.* **1986**, *9*, 1901-1906.

[56] G.B. Shul'pin, G.V. Nizova, Y.N. Kozlov, *New J. Chem.* **1996**, 1243-1256.

[57] G.B. Shulpin, M.M. Kats, *React. kinet. catal. lett.* **1990**, *2*, 239-243.

[58] M. Shahid, V.B. Banakar, P.S.K. Prabhakar Ganesh, P. Gopinath, *Asian J. Org. Chem* **2022**, *7*, e202200184.

[59] W.J.I. DeBenedetti, M.A. Hines, *The Journal of Physical Chemistry C* **2019**, *14*, 8836-8842.

[60] Y. Baba, T. Yatagai, T. Harada, Y. Kawase, *Chem. Eng.* **2015**, *277*, 229-241.

[61] S. Gavelle, M. Innocent, T. Aubineau, A. Guérinot, *Adv. Synth. Catal.* **2022**, *24*, 4189-4230.

[62] H.B. Abrahamson, A.B. Rezvani, J.G. Brushmiller, *Inorg. Chim. Acta* **1994**, *1*, 117-127.

[63] X. Huang, Y. Peng, J. Xu, F. Wu, G. Mailhot, *Chemosphere* **2021**, *263*, 128142.

[64] F.-b. Li, J.-j. Chen, C.-s. Liu, J. Dong, T.-x. Liu, *Biol. Fertil. Soils* **2006**, *5*, 409-417.

[65] D.A. Nichela, J.A. Donadelli, B.F. Caram, M. Haddou, F.J. Rodriguez Nieto, E. Oliveros, F.S. García Einschlag, *Appl. Catal. B* **2015**, *170-171*, 312-321.

[66] M. Tedetti, K. Kawamura, B. Charrière, N. Chevalier, R. Sempéré, *Anal. Chem.* **2006**, *17*, 6012-6018.

[67] B.C. Faust, R.G. Zepp, *Environ. Sci. Technol.* **1993**, *27*, 2517-2522.

[68]   J. Utley, *Chem. Soc. Rev.* **1997**, *3*, 157-167.

[69]   S.O. Pehkonen, R.L. Siefert, M.R. Hoffmann, *Environ. Sci. Technol.* **1995**, *5*, 1215-1222.

[70]   N. Xiong, Y. Li, R. Zeng, *ACS Catal.* **2023**, *3*, 1678-1685.

[71]   J.B. Neilands, *J. Biol. Chem.* **1995**, *45*, 26723-26726.

[72]   E.A. Dertz, J. Xu, A. Stintzi, K.N. Raymond, *J. Am. Chem. Soc.* **2006**, *1*, 22-23.

[73]   F.C. Küpper, C.J. Carrano, J.-U. Kuhn, A. Butler, *Inorg. Chem.* **2006**, *106*, 6028-6033.

[74]   C.J. Weschler, M.L. Mandich, T.E. Graedel, *J. Geophys. Res.* **1986**, *D4*, 5189-5204.

[75]   T.E. Graedel, M.L. Mandich, C.J. Weschler, *J. Geophys. Res.* **1986**, *D4*, 5205-5221.

[76]   C. Lee, J. Yoon, *Chemosphere* **2004**, *10*, 1449-1458.

[77]   Y. Zuo, J. Hoigné, *Science* **1993**, *5104*, 71-73.

[78]   L. Marzo, S.K. Pagire, O. Reiser, B. König, *Angew. Chem. Int. Ed.* **2018**, *32*, 10034-10072.

[79]   A.N. Masliy, T.N. Grishaeva, A.M. Kuznetsov, *J. Phys. Chem. A* **2019**, *25*, 5341-5346.

[80]   Y.C. Kang, S.M. Treacy, T. Rovis, *Synlett* **2021**, *17*, 1767-1771.

[81]   T. Sato, T. Oikawa, K. Kobayashi, *J. Org. Chem.* **1985**, *10*, 1646-1651.

[82]   M.T. Emett, G.H. Khoe, *Water Res.* **2001**, *3*, 649-656.

[83]   A. Pawar, S. Singh, P.C. Ramamurthy, A.G. Anil, N. Shehata, D.S. Dhanjal, T.S.S.K. Naik, P. Parihar, R. Prasad, J. Singh, *Int. J. Environ.* **2022**, *5*, 66.

[84]   H. Kunkely, A. Vogler, *Inorg. Chem. Commun.* **2003**, *10*, 1335-1337.

[85]   Y. Wang, F. Liu, N. Yan, S. Sheng, C. Xu, H. Tian, X. Chen, *ACS Biomater. Sci. Eng.* **2019**, *9*, 4700-4707.

[86]   G. Limb, R.J. Robinson, *Anal. Chim. Acta* **1969**, *3*, 451-460.

[87]   H. Kunkely, A. Vogler, *Inorg. Chim. Acta* **2003**, 275-277.

[88]   J.O. Lundberg, E. Weitzberg, *Cell* **2022**, *16*, 2853-2878.

[89]   P.C. Ford, K.M. Miranda, *Nitric Oxide* **2020**, *103*, 31-46.

[90]   W.D. Wagner, K. Nakamoto, *J. Am. Chem. Soc.* **1989**, *5*, 1590-1598.

[91]   A. Maldotti, R. Amadelli, C. Bartocci, V. Carassiti, E. Polo, G. Varani, *Coord. Chem. Rev.* **1993**, *1*, 143-154.

[92]   C. Bizet, P. Morlière, D. Brault, O. Delgado, M. Bazin, R. Santus, *Photochem. Photobiol.* **1981**, *3*, 315-321.

[93]   I.A. Lavrinenko, G.A. Vashanov, A.S. Buchelnikov, Y.D. Nechipurenko, *Biophysics* **2022**, *3*, 327-337.

[94]   T. Yanagimoto, A. Nakagawa, T. Komatsu, E. Tsuchida, *Bull. Chem. Soc. Jpn.* **2001**, *74*, 2123-2128.

[95]   R. Schulte, M. Löcker, H. Ihmels, M. Heide, C. Engelhard, *Chem. Eur. J.* **2023**, *9*, e202203203.

[96]   B. Pfund, D.M. Steffen, M.R. Schreier, M.-S. Bertrams, C. Ye, K. Börjesson, O.S. Wenger, C. Kerzig, *J. Am. Chem. Soc.* **2020**, *23*, 10468-10476.

[97]   Y.-M. Tian, E. Hofmann, W. Silva, X. Pu, D. Touraud, R.M. Gschwind, W. Kunz, B. König, *Angew. Chem. Int. Ed.* **2023**, *17*, e202218775.

[98]   L. Brüss, R. Jeyaseelan, J.C.G. Kürschner, M. Utikal, L. Næsborg, *ChemCatChem* **2023**, *1*, e202201146.

[99]   M. Cybularczyk-Cecotka, J. Predygier, S. Crespi, J. Szczepanik, M. Giedyk, *ACS Catal.* **2022**, *6*, 3543-3549.

[100]   S. Tomyn, S.I. Shylin, D. Bykov, V. Ksenofontov, E. Gumienna-Kontecka, V. Bon, I.O. Fritsky, *Nat. Commun.* **2017**, *1*, 14099.

[101]   C. van Thriel, *Toxicology of Solvents (Including Alcohol)*, in *Reference Module in Biomedical Sciences* 2014, Elsevier.

2 Caesium Carbonate Catalysed Oxa-Michael Addition of Oximes to Acrylonitrile
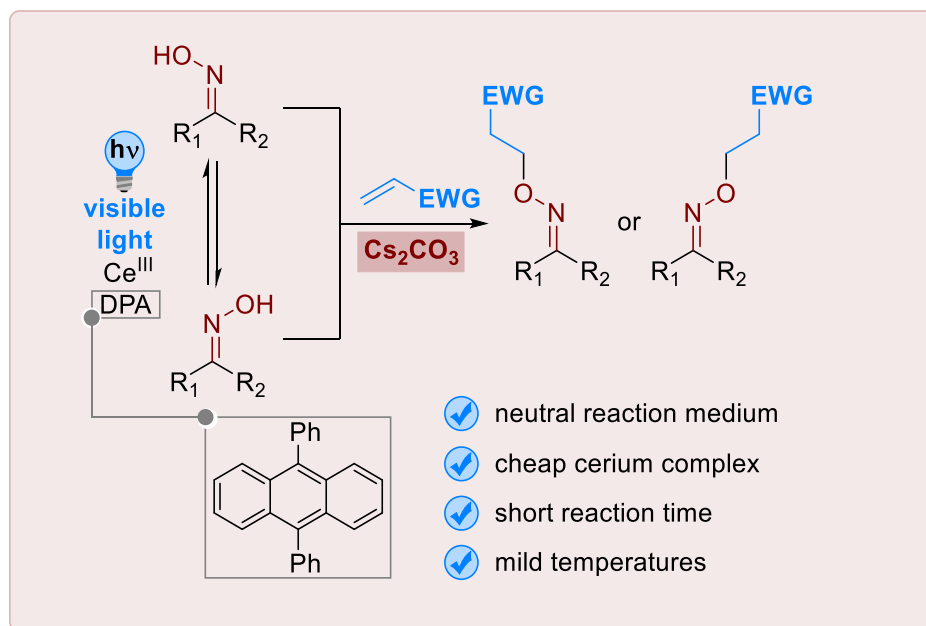
Veera Reddy Yatham gave the idea for the project, Jessica Stahl performed all the experiments described in the manuscript and the Supporting Information, if not otherwise stated. Stefano Crespi did the calculations about *E-Z* Isomerisation of oximes in the Supporting Information; Burkhard König supervised the project.

CHAPTER 2

This chapter was published in:

Abstract

The photochemical controlled transformation of none functionalised oximes was achieved using a Ce(III)DOTA (2,2',2''.2'''-(1,4,7,10-tetraazacyclododecane-1,4,7,10-tetrayl)tetraacetic acid complex and 9,10-diphenyl anthracene (DPA) as photosensitiser.

We report the O-alkylation of oximes with Michael acceptors using Cs_2CO_3 as catalyst. The transformation proceeds stereospecific under mild reaction conditions with retention of the oxime configuration. Irradiated with visible light in the presence of diphenyl anthracene and cerium complexes affects the *E* to *Z* configuration ratio of the oxime ether products significantly, but a complete stereo-control was not achieved. The operationally simple protocol allows the synthesis of various O-alkylated oxime products that are useful precursors for further chemical transformations.

2.1 Introduction

Oxime ethers and the respective ester derivatives are important structural elements in organic chemistry. They are present in natural products, in anti-bacterial or anti-inflammatory drugs or cancer therapeutics.[1-4] Heterocyclic oxime ethers such as Oxicanazole are important antifungal drugs that are used in the treatment of mycosis.[5]
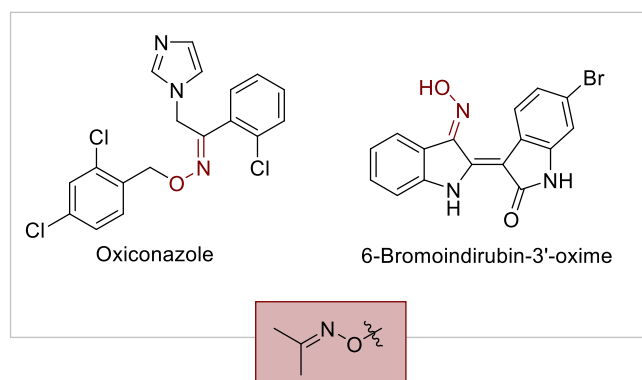

Figure 2.1. Oxime based drugs.

Different strategies were reported for the synthesis of oxime derivatives *via* oxa-Michael addition.[6] The group of Buchwald functionalised the hydroxyl moiety of an oxime *via* palladium-catalysed cross-coupling with aryl halides yielding the respective aryl-substituted oximes (see Scheme 2.2a).[7] Leonori *et al*. developed photocatalytic strategies for the generation of nitrogen-centred radicals based on hydroxylamine derivatives. They were able to generate nitrogen radicals of various polarities and reactivities by incorporating redox-active substituents on the oxime group.[8] The group of Xiao performed an enantioselective addition of aldoximes to β-CF$_3$-β-disubstituted nitro alkenes (see Scheme 2.2b).[9] By adding chiral alkaloid organo-catalysts, they were able to induce a new stereo centre enantio-selectively on the β-carbon atom of the alkene. Narayanan *et al.* demonstrated that oxime ethers could also be prepared by Michael addition to the hydroxyl group of the oxime (see Scheme 2.2c).[10] Applying PPh$_3$ as the catalyst they were able to synthesise various ethers by addition of malonate derivatives.[10] However, PPh$_3$ can readily be oxidised by atmospheric oxygen to triphenyl phosphine oxide that needs to be removed by recrystallisation or precipitation.[11]

33

Interestingly, none of the reported synthesis strategies considered the possibility to control the product outcome exploiting the photochemical *E-Z* isomerisation of the oximes. The geometric isomerisation of oximes is a well-known photoreaction of this substance class.[12, 13] By direct or sensitised irradiation or by acid catalysis the *E* and *Z* isomers can be interconverted.[14, 15] *E* to *Z* isomerisation of oximes and its derivatives has been investigated by several research groups.[16-18] In 2004, O'Brien *et al.* published the acid-catalysed isomerisation of (*E*)- and (*Z*)-*p*-methoxy benzaldehyde oximes that proceeds through hydrolysis *via* formation of a tetrahedral intermediate. They also observe a bathochromic shift of the oxime absorption when the neutral oxime was protonated.[16] Olsen *et al.* developed the sensitised isomerisation of cinnamic acid oxime derivatives around the carbon-carbon or carbon-nitrogen bond. They propose that the isomerisation behaviour of the respective *E,E* or *E,Z*-derivative can be tuned by sensitisation using triplet sensitisers of different energies.[15]
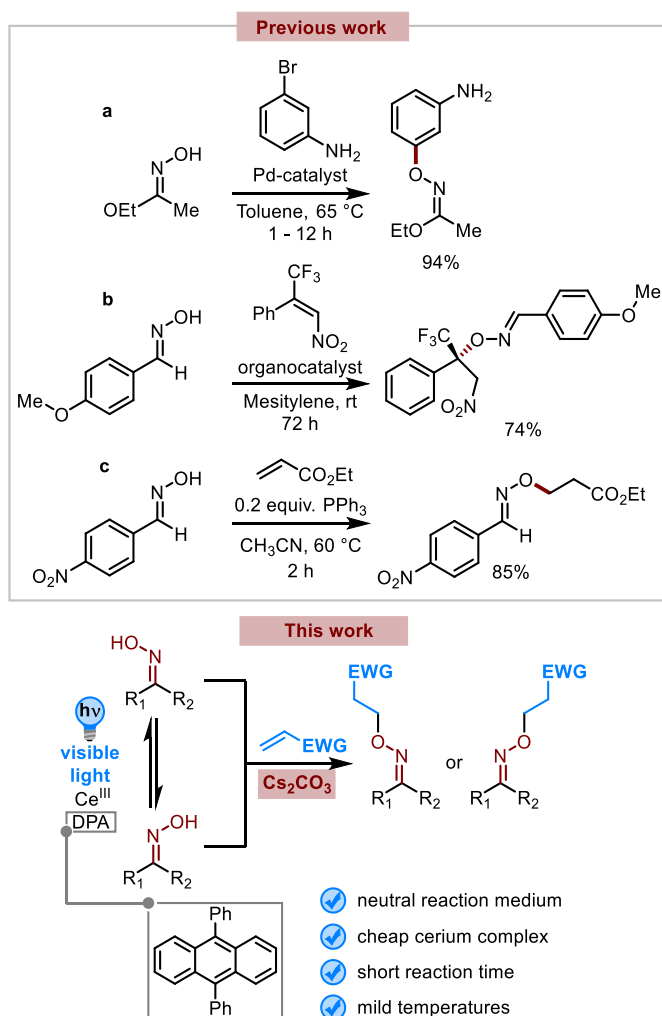
Scheme 2.2. Oxime O-functionalisation in literature.

Herein, we propose a transition metal-free, effective method for the O-alkylation of oximes using Cs_2CO_3 as cheap, non-toxic, and air-stable reagent for the activation of the oxime hydroxyl group. The reaction shows nearly quantitative yield after 2 h with retention of the oxime stereochemistry in the oxime ether if performed in the dark. However, under irradiation in the presence of a cerium Lewis acid and diphenyl anthracene (DPA) as photosensitiser the *E* / *Z* ratio changes significantly from the oxime to the oxime ether.
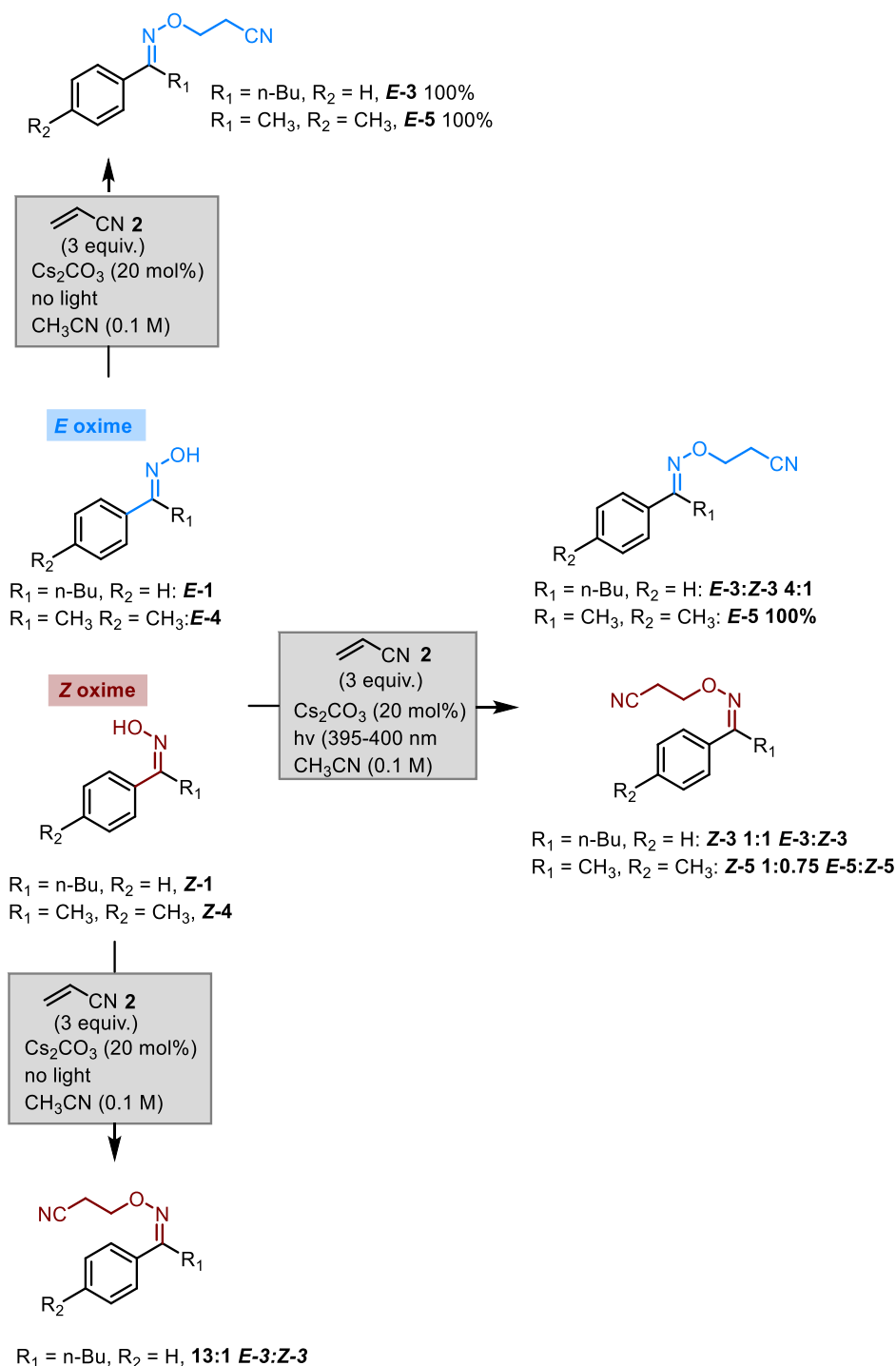
2.2 Results and Discussion

Inorganic salts are widely used in organic synthesis as bases, acids or neutral salts, but also as electrolytes and Lewis acids due to their availability, low costs and effectivity.[19] Especially, caesium salts have gained considerable attention due to their unique characteristics. The caesium cation possesses a larger atom radius compared to other alkali metal ions and it is fully solvated in various polar aprotic organic solvents (e.g. DMSO and DMF).[20, 21] This property, along with the limited solvation of the counterion in the same environment is the principle cause of the "caesium effect".[22, 23] Additionally, caesium salts have a perfectly balanced acid-base character that allows for selective deprotonations.[24]

In an early state of our research, we recognised that we obtain two stereoisomers of the same O-alkylated oxime. This product ratio was highly dependent on the light-driven isomerisation of the oxime starting material around the carbon-nitrogen double bond.

We started our investigations by selectively converting different *E* and *Z* oximes in an Oxa-Michael reaction using acrylonitrile (**2**) as electron-deficient coupling reagent (Scheme 2.3).[25] We added Cs_2CO_3 to our reaction mixture to increase the nucleophilicity of the oxime.[26,27] Running the reaction under irradiation with oxime *E*-**1** or *E*-**3**, the respective products *E*-**3** and *E*-**5** were nearly exclusively obtained as confirmed by NMR. When the same reaction was performed starting with the *Z* oximes (*Z*-**1** and *Z*-**4**), we detected by NMR a 1:1 ratio for *E*-**3**:*Z*-**3** and 1:0.75 for *E*-**5**:*Z*-**5**.

The reactions of *E*-**1** or *E*-**3** were repeated in the dark and again 100% of ***E*-3** and ***E*-5** were formed, respectively. Performing the reaction with *Z*-**1** in absence of light a ratio of 13:1 for *E*-**3**:*Z*-**3** was achieved, indicating that only under irradiation with visible light the respective *Z*-

isomer product can be formed in larger amounts. Additionally, this experimental outcome highlights the capacity of the *Z*-oxime to re-isomerise to its more stable *Z* configuration.

R$_1$ = n-Bu, R$_2$ = H, *E-3* 100%
R$_1$ = CH$_3$, R$_2$ = CH$_3$, *E-5* 100%

CN 2
(3 equiv.)
Cs$_2$CO$_3$ (20 mol%)
no light
CH$_3$CN (0.1 M)

E oxime

R$_1$ = n-Bu, R$_2$ = H: *E-1*
R$_1$ = CH$_3$ R$_2$ = CH$_3$:*E-4*

CN 2
(3 equiv.)
Cs$_2$CO$_3$ (20 mol%)
hv (395-400 nm
CH$_3$CN (0.1 M)

R$_1$ = n-Bu, R$_2$ = H: *E-3:Z-3* 4:1
R$_1$ = CH$_3$, R$_2$ = CH$_3$: *E-5* 100%

Z oxime

R$_1$ = n-Bu, R$_2$ = H, *Z-1*
R$_1$ = CH$_3$, R$_2$ = CH$_3$, *Z-4*

R$_1$ = n-Bu, R$_2$ = H: *Z-3* 1:1 *E-3:Z-3*
R$_1$ = CH$_3$, R$_2$ = CH$_3$: *Z-5* 1:0.75 *E-5:Z-5*

CN 2
(3 equiv.)
Cs$_2$CO$_3$ (20 mol%)
no light
CH$_3$CN (0.1 M)

R$_1$ = n-Bu, R$_2$ = H, **13:1** *E-3:Z-3*

Scheme 2.3. Oxa-Michael addition of *E* and *Z* oximes in presence or absence of light.

Table 2.1. Screening for carbonate bases.

Entry [a]	Deviation from standard condition	Irradiation	Conversion [%] [b]	Product ratio E-3:Z-3 [%] from GC-FID
a	None	yes	93	80:20
b	None	no	94	100:0
c	CsBr (20 mol%)	yes	0	-
d	CsI (20 mol%)	yes	0	-
e	CsF (20 mol%)	yes	0	-
f	CsOAc (20 mol%)	yes	0	-
g	$Cs_2C_2O_4$ (20 mol%)	yes	0	-
h	$MgCO_3$ (20 mol%)	yes	0	-
i	Na_2CO_3 (20 mol%)	yes	0	-
j	K_2CO_3 (20 mol%)	yes	57	80:20

[a] Reactions were performed using **E-1** (0.1 mmol, 1.0 equiv.), acrylonitrile **2** (0.3 mmol, 3.0 equiv.) and an inorganic base (20 mol%, 0.02 equiv.) in acetonitrile (0.1 M) under irradiation with 395-400 nm at 20 °C for 2 h.
[b] Conversion and product ratio were determined using naphthalene as internal standard for GC-FID.

The complete separation of the oxime starting material by column chromatography turned out to be challenging and even short exposition to daylight led to the formation of the sterically and electronically favoured *E*-Oxime from the *Z*-Oxime.[28]

As Cs_2CO_3 was necessary for the formation of the O-alkylated product we investigated the reaction using oxime **1**, acrylonitrile (**2**) and different inorganic bases to find the most reactive ionic species in the reaction mixture.

Interestingly, again two products **E-3** and **Z-3** were observed in GC-FID, showing that the product ratio is highly dependent on irradiation (Table 2.1, entries a and b). Without irradiation, the tendency of *E-Z* isomerisation of the oxime starting material was negligible, leading to the exclusive formation of product *E*-3 (entry b). Adding Cs_2CO_3 in 20 mol%, nearly quantitative conversion of the oxime starting material was achieved and the products were formed in a ratio of 80:20 (entry a). To screen the best reaction conditions and the role of the cation/anion in the transformation, different caesium and carbonate salts were tested. Only K_2CO_3 could catalyse the reaction leading to the same product ratio observed in entry a, but with a lower conversion (entry j). In the case of other caesium or carbonate salts, GC-FID showed no conversion at all. This experimental outcome supports the hypothesis of caesium carbonate provides the perfect conditions for the alkylation of the O-H of the oxime.[24, 29]

Next, we investigated several additives to enhance the effect of irradiation on the stereochemical control of the reaction (Table 2.2). The presence of a cerium complex changes for some oximes the product ratio of the photochemical reaction to a higher amount of the *Z* product in the reaction mixture compared to the entries without lanthanoid salt (Table 2.2, entries a to c). To ensure a defined interaction between the Lewis acid cerium complex and the oxime we used a cerium(III) 1,4,7-10-tetraazacyclododecan-1,4,7,10-tetraacetic acid (DOTA)[30] complex. We observe a yellow colour after mixing oxime and the cerium complex in presence of the base (Figure 2.2). Figure 2.2 shows the broad absorption band of the interacting compounds that is visible around 340 nm tailing into the visible region of the spectrum. The UV/Vis spectrum of the oxime in acetonitrile only shows a slight absorption at this wavelength area.
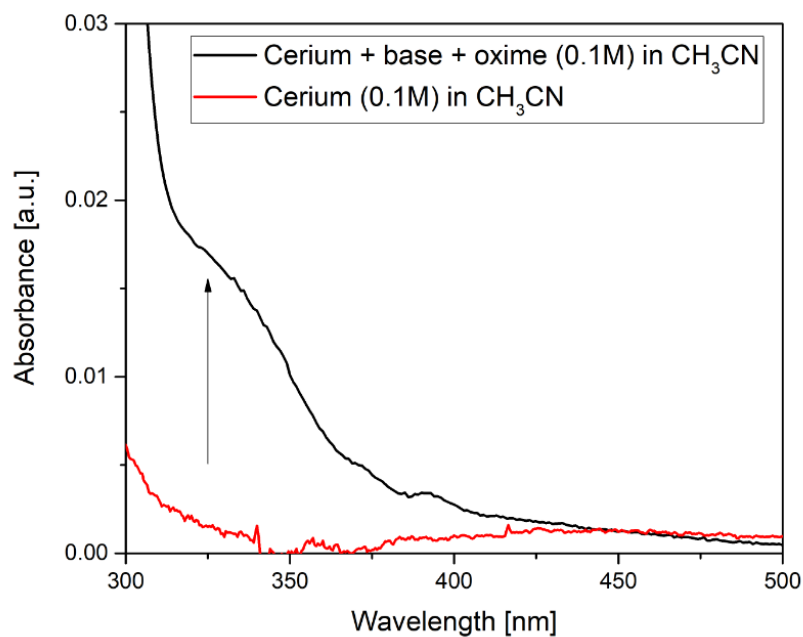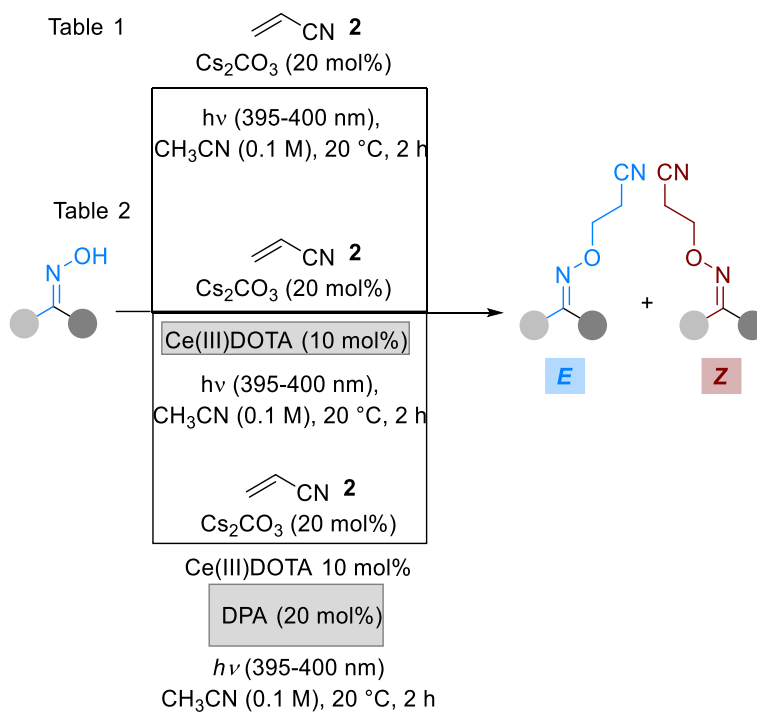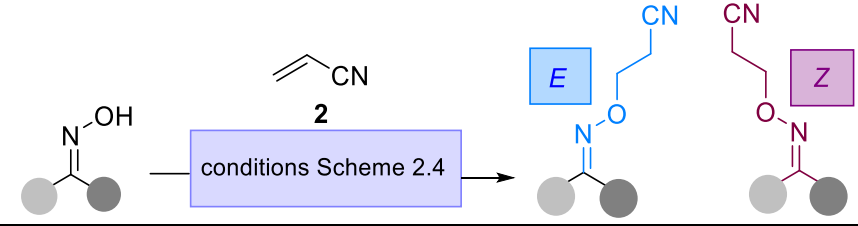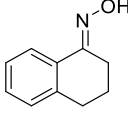
Figure 2.2. Absorption spectra of Ce(III)DOTA (0.1 M) in CH$_3$CN (red curve) and the visible light active cerium, base and oxime mixture (0.1 M) in CH$_3$CN (black curve).

Scheme 2.4. Reaction optimisation for the photochemical control of product formation.

Table 2.2. Survey of parameters controlling the stereochemistry of the products.

Entry	[a] **Oxime starting material**	**Deviation from standard condition**	[b] **Product ratio *E:Z* [%]**
a	***E*-1**	none	[c] 80:20 67:33
b	***E*-4**	none	[c] 83:17 75:25
c	*(structure shown)* **E-7**	none	[c] 67:37 42:58
d	***E*-1**	none	[d] 75:25
e	***Z*-1**	no light	[d] 13:1
f	***E*-1**	no light	[d] 100:0
g	***E*-1**	ZnCl$_2$ as Lewis acid (10 mol%)	[d] n.d.
h	***E*-1**	CeCl$_3$ as Lewis acid (10 mol%)	[d] ***E*-3** > 99
i	***E*-1**	BF$_3$ as Lewis acid (10 mol%)	[d] 26:74
j	***E*-1**	no light	[d] ***E*-3** > 96

[a] Reactions were performed using the *E* or *Z*-oxime (0.1 mmol, 1.0 equiv.), acrylonitrile (**2**) (0.3 mmol, 3.0 equiv.) and Cs$_2$CO$_3$ (20 mol%, 0.02 equiv.) in acetonitrile (0.1 M) [b] Product-ratios were determined by GC-FID using naphthalene as internal standard. [c] Ce(III)DOTA (10 mol%, 0.01 equiv.) was additionally added. [d] Diphenyl anthracene (20 mol%, 0.02 equiv.) was additionally added to the reaction mixture.

Diphenyl anthracene is known as photosensitiser for the *E/Z*-isomerization of the oxime starting material. Reactions with only the presence of diphenyl anthracene and combinations of the cerium complex and diphenyl anthracene show that the isomeric products ***E*-1** and ***Z*-1** are formed in a ratio of 75:25% (entry d). This value only slightly differs from the product ratio that was achieved from the entries with Cs$_2$CO$_3$ and acrylonitrile (**2**) (entry a). Running the reactions starting with ***E*-1** or ***Z*-1** in the dark, respectively the tendency for the *E* oxime to

isomerise was low yielding the respective *Z* product in 100%. Comparable to the results shown in Scheme 2.1, the *E* oxime can isomerise back to its *Z* form, yielding a higher amount of the *Z* product regardless the presence of DPA as photosensitiser (entries e and f).

Table 2.2 and Scheme 2.3 summarise further prominent effects of additives on the stereochemical outcome of the oxime alkylation under irradiation. For additional examples see Supporting Information (Table T2.2 and T2.3). Compared to the cerium complex other Lewis acids such as $ZnCl_2$ (entry g) did not work at all or led to a less prominent shift towards one specifically configured product (entries h and i). With the best conditions and the knowledge of the isomerisation behaviour we expanded the product scope from the first results from Table 2.2. Further oximes were synthesised and tested in the reaction (Table 2.3). Different acrylonitrile derivatives (**2**, **2-CH₃** and **2-Cl**) were screened, and the respective products were isolated.

Acyclic and cyclic alkylated oximes could be synthesised starting from the respective oxime substrate complex. In every case the *E* oxime starting material was dominantly present in thermal equilibrium. GC-FID showed the second product resulting from the *Z* oxime in small amounts and with a similar retention time (**E-3** and **Z-3**). Due to the small amount of the *Z*-configured product formed, we were not always able to isolate it although these products were detected in GC-FID or ¹H-NMR spectroscopy. In general, the yield of the reaction was highly dependent on the starting material structure (**E-3**, **E-14**, and **E-33**) as electron rich substituents increased the nucleophilicity of the oxime anion.

We propose the following mechanistic pathways for the formation of O-alkylated oximes and the light-induced isomerisation. Sensitisation of the oxime starting material with diphenyl anthracene leads to the formation of **E** and **Z** configurational isomers. Even in the photo-stationary state the **E** oxime dominates in the reaction mixture. The respective oxime isomer converts in the presence of the base and the cerium complex into complex **Z-1-OCe(III)DOTA** which shows bathochromically shifted absorption and may also participate in the photo-induced *E*/*Z* isomerisation.[31] Nucleophilic addition of the oxime oxygen to acrylonitrile (**2**) yields intermediate **Z-1-O-alkyl**, which upon protonation yields the O-alkylated product **E-3**.
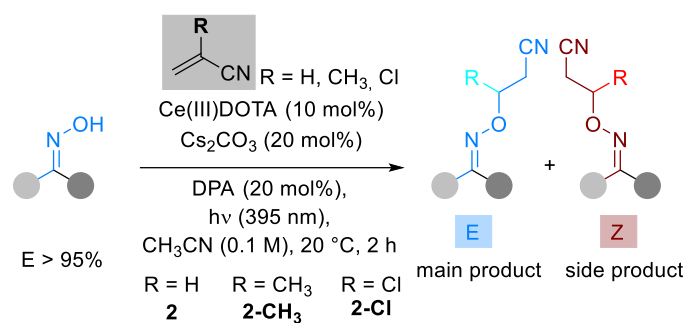
The same reaction pathway operates for the *Z*-configurated oxime. The obtained *Z* products are configurationally stable, if stored in the absence of light.
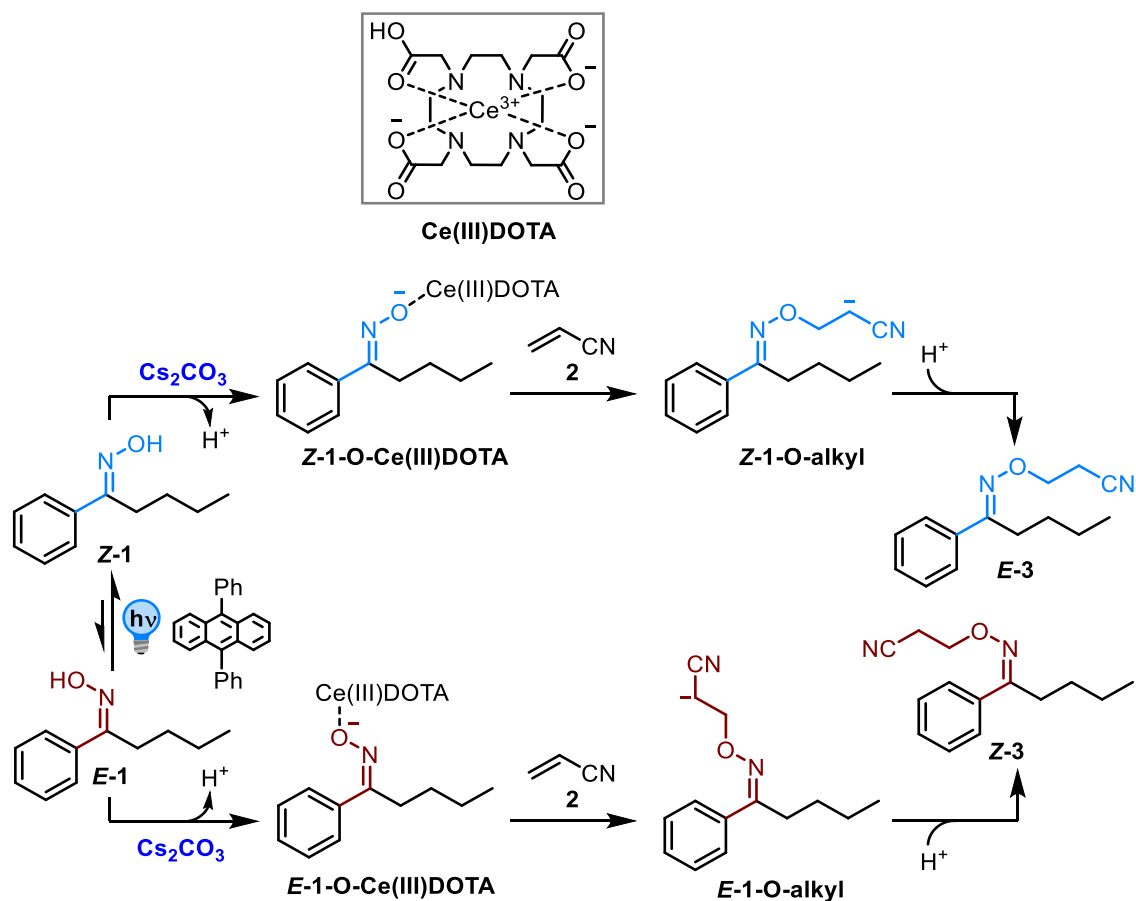
Scheme 2.5. Proposed reaction mechanism.

2.3 Conclusion

In summary, we prepared O-alkyl oxime ethers *via* Oxa-Michael additions to oximes.[32] The caesium salt is cheap and non-toxic and can easily be removed by filtration or aqueous extraction from the reaction mixture. The oxime double bond configuration can in part be controlled by photo-isomerisation; the effect is slightly enhanced by the addition of a cerium complex Lewis acid and diphenyl anthracene as sensitiser. Alkylation of separated configurational oximes isomers proceed under retention of the carbon-nitrogen double bond configuration if performed in the absence of light.

Table 2.3. Product scope.

[a]Oxime	[b] Product trapping reagent	[a] Oxime	[b] Product trapping reagent

[a] Reactions were performed using the respective oxime (*E* > 90%). [b] All given yields are isolated yields if not otherwise stated.

2.4 Experimental Section

General procedure for the synthesis of oximes (for further information see General Considerations)

To a solution of the respective ketone (1.0 equiv.) and hydroxylamine hydrochloride (1.2 equiv.) in methanol (0.5 M, 10 mL), pyridine (2.0 equiv.) was added in one step. The mixture was stirred at room temperature for 3 h. Then MeOH was removed under reduced pressure, the residue was diluted with 1 M HCl (40 mL, aqueous solution) and ethyl acetate (40 mL). The layers were separated, and the aqueous layer was extracted with ethyl acetate (2 x 20 mL). The combined organic phases were washed with a saturated $NaHCO_3$ solution (20 mL) and brine (20 mL). After drying over anhydrous Na_2SO_4 the remaining solvent was removed under reduced pressure to give the respective crude ketone oximes that were purified by flash column chromatography (petroleum ether/ethyl acetate, 9:1).

General procedure for the caesium-catalysed synthesis of O-alkylated oximes (for further information see General Considerations)

A 5 mL crimp neck vial equipped with a magnetic stir bar was loaded with the oxime (0.2 mmol, 1.0 equiv.), DPA (13.2 mg, 20 mol%), anhydrous $CeCl_3$ (5.0 mg, 10 mol%) and Cs_2CO_3 (13.0 mg, 20 mol%). The vial was capped and purged with nitrogen before adding 2 mL of dry degassed acetonitrile *via* syringe. The vial was additionally degassed three times *via* freeze-pump-thaw. After completion the electron poor trapping reagent (0.6 mmol, 3.0 equiv.) was added, and the reaction mixture was stirred and irradiated using a violet high-power LED (395 nm) for 2 h at 25 °C. The progress could be monitored by GC-FID and GC-MS analysis.

After 24 h the completion was tested *via* TLC analysis and the reaction mixture was diluted with 1 M HCl (20 mL) and extracted with ethyl acetate (3 x 20 mL). The combined organic phases were dried over anhydrous $MgSO_4$ and solvent residues were removed under reduced pressure. Purification was performed by automated flash column chromatography on silica (petroleum ether/ethyl acetate, 92:8) to yield the respective Oxa-Michael product.

2.5 References

[1] Z. Mirjafary, M. Abdoli, H. Saeidian, A. Kakanejadifard, S.M.F. Farnia, *RSC Advances* **2016**, *21*, 17740-17758.

[2] H.-J. Park, K. Lee, S.-J. Park, B. Ahn, J.-C. Lee, H. Cho, K.-I. Lee, *Bioorg. Med. Chem. Lett.* **2005**, *13*, 3307-3312.

[3] F. Delmas, M. Gasquet, P. Timon-David, N. Madadi, P. Vanelle, A. Vaille, J. Maldonado, *Eur. J. Med. Chem.* **1993**, *1*, 23-27.

[4] A.K. Surowiak, S. Lochyński, D.J. Strub, *Symmetry* **2020**, *4*, 575.

[5] T. Kosmalski, R. Studzinska, M. Redka, R. Pluskota, B.E. Modzelewska-Banachiewicz, *J. Braz. Chem. Soc.* **2017**, *28*, 2100-2105.

[6] C.F. Nising, S. Bräse, *Chem. Soc. Rev.* **2008**, *6*, 1218-1228.

[7] T.J. Maimone, S.L. Buchwald, *J. Am. Chem. Soc.* **2010**, *29*, 9990-9991.

[8] J. Davies, S.P. Morcillo, J.J. Douglas, D. Leonori, *Chem. Eur. J.* **2018**, *47*, 12154-12163.

[9] F.-L. Liu, J.-R. Chen, B. Feng, X.-Q. Hu, L.-H. Ye, L.-Q. Lu, W.-J. Xiao, *Org. Biomol. Chem.* **2014**, *7*, 1057-1060.

[10] D. Bhuniya, S. Mohan, S. Narayanan, *Synthesis* **2003**, *7*, 1018-1024.

[11] D.C. Batesky, M.J. Goldfogel, D.J. Weix, *J. Org. Chem.* **2017**, *19*, 9931-9936.

[12] T. Kopczyǹski, E. Krzyżanowska, A. Olszanowski, *J. prakt. Chem.* **1989**, *3*, 486-492.

[13] H. Roth, *Light-Induced Chemistry of Oximes and Derivatives*, 2010, Wiley.

[14] S. Nsikabaka, W. Harb, M.F. Ruiz-López, *J. Mol. Struct.* **2006**, *1*, 161-166.

[15] R.J. Olsen, *J. Photochem. Photobiol. A* **1997**, *1*, 91-94.

[16] R.A.M. O'Ferrall, D. O'Brien, *J. Phys. Org. Chem.* **2004**, *6-7*, 631-640.

[17] A. Padwa, F. Albrecht, *J. Am. Chem. Soc.* **1972**, *3*, 1000-1002.

[18] J.E. Johnson, N.M. Morales, A.M. Gorczyca, D.D. Dolliver, M.A. McAllister, *J. Org. Chem.* **2001**, *24*, 7979-7985.

[19] D. Joshi, N. Adhikari, *Chem. Asian J.* **2019**, *4*, 1-11.

[20] G. Dijkstra, W.H. Kruizinga, R.M. Kellogg, *J. Org. Chem.* **1987**, *19*, 4230-4234.

[21] R. Rabie, M.M. Hammouda, K.M. Elattar, *Res. Chem. Intermediat.* **2017**, *4*, 1979-2015.

[22] B.F. Gisin, *Helv. Chim. Acta* **1973**, *5*, 1476-1482.

[23] S.-S. Wang, B.F. Gisin, D.P. Winter, R. Makofske, I.D. Kulesha, C. Tzougraki, J. Meienhofer, *J. Org. Chem.* **1977**, *8*, 1286-1290.

[24]   S. Putatunda, A. Chakraborty, *C. r. Chim.* **2014**, *10*, 1057-1064.

[25]   C.D. Vanderwal, E.N. Jacobsen, *J. Am. Chem. Soc.* **2004**, *45*, 14724-14725.

[26]   T. Flessner, S. Doye, *J. prakt. Chem.* **1999**, *2*, 186-190.

[27]   R. Rabie, M. Hammouda, K. Elattar, *Res. Chem. Intermediat.* **2016**, *43*, 37.

[28]   D.K. Kölmel, E.T. Kool, *Chem. Rev.* **2017**, *15*, 10358-10376.

[29]   H. Huang, F. Li, Z. Xu, J. Cai, X. Ji, G.-J. Deng, *Adv. Synth. Catal.* **2017**, *18*, 3102-3107.

[30]   H.F. Schmitthenner, D.E. Dobson, K.G. Jones, N. Akporji, D.Q.M. Soika, K.L. Nastiuk, J.P. Hornak, *Chem. Eur. J.* **2019**, *61*, 13848-13854.

[31]   Z. Wang, L. He, B. Liu, L.-P. Zhou, L.-X. Cai, S.-J. Hu, X.-Z. Li, Z. Li, T. Chen, X. Li, Q.-F. Sun, *J. Am. Chem. Soc.* **2020**, *142*, 16409-16419.

[32]   C. Nising, S. Bräse, *Chem. Soc. Rev.* **2008**, *37*, 1218-1228.

2.6 General Considerations

Materials

Starting materials and reagents were purchased from commercial suppliers (Sigma Aldrich, Alfa Aesar, Acros, Fluka, TCI or VWR) and used without further purification. Anhydrous $CeCl_3$ was flushed with nitrogen after use. Solvents were used as p.a. grade or purified by distillation from reagent grade and stored over molecular sieve.

Analytical Methods

For automated flash column chromatography industrial grade of solvents was used. All reactions with oxygen- or moisture-sensitive reagents were carried out in glassware, which was dried before use by heating under vacuum. Dry nitrogen was used as inert gas atmosphere. Liquids were added *via* syringe unless otherwise stated. All NMR spectra were measured at room temperature using a Bruker Advance 300 (300 MHz for ^{1}H, 75 MHz for ^{13}C) or a Bruker Advance 400 (400 MHz for ^{1}H, 101 MHz for ^{13}C, NMR spectrometer.[1] All chemical shifts are reported in δ-scale as parts per million [ppm], relative to the solvent residual peaks as the internal standard.[2] Coupling constants J are given in Hertz [Hz]. Abbreviations used for signal multiplicity: ^{1}H-NMR: b = broad, s = singlet, d = doublet, t = triplet, q = quartet, hept = heptet dd = doublet of doublets, dt = doublet of triplets, dq = doublet of quartets, and m = multiplet; ^{13}C-NMR: (+) = primary/tertiary, (–) = secondary, (Cq) = quaternary carbon. ^{1}H-^{13}C HSQC spectra were acquired using the hsqcedetgp sequence (multiplicity-edited HSQC using echo-antiecho), ^{1}H-^{1}H-COSY using the cosygpqf sequence, ^{1}H-^{13}C-HMBC using the hmbcetgpl2nd sequence (HMBC with 2nd order low pass J-filter). The mass spectrometric measurements were performed at the Central Analytical Laboratory of the University of Regensburg. All mass spectra were recorded on a Finnigan MAT 95, ThermoQuest Finnigan TSQ 7000, Finnigan MAT SSQ 710 A or an Agilent Q-TOF 6540 UHD instrument. GC measurements were performed on a GC 7890 from Agilent Technologies. Data acquisition and evaluation was done with Agilent ChemStation Rev.C.01.04. GC-MS measurements were performed on a 7890A GC system from Agilent Technologies with an Agilent 5975 MSD

Detector. Data acquisition and evaluation was done with MSD ChemStation E.02.02.1431.A capillary column HP-5MS/30 m x 0.25 mm/0.25 μM film and helium as carrier gas (flow rate of 1 mL/min) were used.

Experimental Procedures

For irradiation with blue light OSRAM Oslon SSL 80 LDCQ7P1U3U (blue, λ_{max} = 455 nm, I_{max} = 1000 mA, 1.12 W) was used. For irradiation with green light Cree XPEGRN L1 G4 Q4 (green, λ_{max} = 528 nm, I_{max} = 1000 mA, 1.12 W) was used. For irradiation with violet light LT-2115 (violet, λ_{max} = 395 – 419 nm, I_{max} = 0.7 A, 3 W) was used which was installed on a passive cooling system at the bottom (7 mm from the bottom-plane of the vials) of a custom made six-vials reactor (aluminium), which was equipped with a liquid cooling system (25 ºC) and a magnetic stirrer (≈ 250 rpm). Purification by column chromatography was performed with silica gel 60 M (40-63 μm, 230-440 mesh, Merck) on a Biotage® IsoleraTM Spectra One device using plastic cartridges. Petroleum ether and ethyl acetate (both: purification by distillation from technical grade) were used as mobile phase. Solvent removal under reduced pressure was performed using Büchi Rotavapor® R-100 rotary evaporators equipped with water baths at 40 ºC.

2.7 Synthesis and Characterisation of Starting Materials and Products

All synthesized oximes are literature known and were prepared according to published procedures; spectroscopic data match the published data.[3],[4]

### 2.7.1 General Procedure for the Preparation of Oxime Starting Materials

To a solution of the respective ketone (1.0 equiv.) and hydroxylamine hydrochloride (1.2 equiv.) in methanol (0.5 M, 10 mL), pyridine (2.0 equiv.) was added in one step. The mixture was stirred at room temperature for 3 h. Then MeOH was removed under reduced pressure, the residue was diluted with 1 M HCl (40 mL, aqueous solution) and ethyl acetate (40 mL). The layers were separated, and the aqueous layer was extracted with ethyl acetate (2 x 20 mL). The combined organic phases were washed with a saturated $NaHCO_3$ solution (20 mL) and brine (20 mL). After drying over anhydrous Na_2SO_4 the remaining solvent was removed under reduced pressure to give the respective crude ketone derived oximes that were purified by flash column chromatography (petrol ether/ethyl acetate, 10% ethyl acetate).

E-1
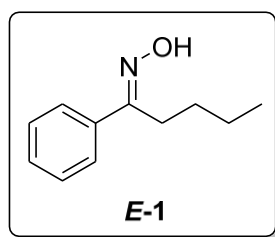
(E)-1-Phenylpentan-1-one oxime (E-1) [5]

Following the general procedure using valerophenone (16.9 mmol, 2.77 mL, 1.0 0equiv.) as ketone starting material **(E)-1-phenylpentan-1-one oxime (E-1)** was synthesized as white solid in 59% yield (1.81 g, 10.2 mmol).

^{1}H-NMR (300 MHz, DMSO-d_6, δ_H) 11.13 (s, 1H), 7.79 –7.57 (m, 2H), 7.57 - 7.25 (m, 3H), 2.72 (t, J = 7.5 Hz, 2H), 1.57 – 1.17 (m, 4H), 1.37 – 1.21 (m, 2H), 0.87 (t, J = 7.1 Hz, 3H).

^{13}C-NMR (101 MHz, Chloroform-d, δ_C) 159.9 (C_q), 135.9 (C_q), 129.1 (+), 128.6.1 (+), 126.3 (+), 28.5 (-), 26.0 (-), 23.0 (-), 13.9 (+).

E-4
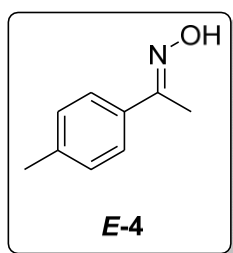
(E)-1-(p-Tolyl) ethan-1-one oxime (E-4) [5]

Following the general procedure using (E/Z)-1-(p-tolyl) ethan-1-one (16.78 mmol, 2.25 g, 1.00 equiv.) as starting material, **(E)-1-(p-tolyl) ethan-1-one oxime (E-4)** was synthesized as white solid in 61% (1.53 g, 10.3 mmol).

^{1}H-NMR (400 MHz, DMSO-d_6, δ_H) 11.25 (s, 1H), 8.00 – 7.69 (m, 2H), 7.51 – 7.26 (m, 2H), 2.49 (s, 3H), 2.31 (s, 3H).

^{13}C-NMR (101 MHz, DMSO-d_6, δ_C) 153.2 (C_q), 138.4 (C_q), 134.7 (C_q), 129.4 (+), 125.9 (+), 21.2 (+), 12.0 (+).

E-7
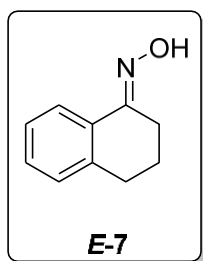
(*E*)-3,4-Dihydronaphthalen-1(2H)-one oxime (*E*-7) [4a]

Following the general procedure using 3,4-dihydronaphthalen -1(2H)-one (Tetralon) (1.00 equiv.) as starting material **(*E*)-3,4-dihydronaphthalen-1(2H)-one oxime (*E*-7)** could be synthesized as pale orange solid in 27% yield (0.54 g, 3.35 mmol).

^{1}H-NMR (300 MHz, DMSO-d_6, δ_H) 11.08 (s, 1H), 7.85 (dd, J = 8.0, 1.6 Hz, 1H), 7.38 – 7.11 (m, 3H), 2.67 (dt, J = 16.2, 6.3 Hz, 4H), 1.83 – 1.66 (m, 2H).

^{13}C-NMR (75 MHz, DMSO-δ_6, δ_C) 152.8 (C_q), 139.4 (C_q), 131.6 (C_q), 129.1 (+), 128.8 (+), 126.6 (+), 123.7 (+), 29.6 (-), 23.9 (-), 21.5 (-).


E-10
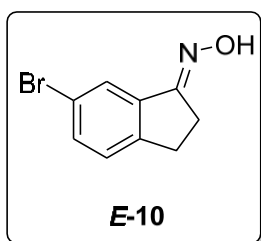
(*E*)-6-Bromo-2,3-dihydro-1H-inden-1-one oxime (*E*-10) [6]

Following the general procedure using (*E/Z*)-6-bromo-2,3-dihydro-1H-iden-1-one (1.66 mmol,

0.35 g, 1.00 equiv.) as starting material, **(*E*)-6-bromo-2,3-dihydro-1H-inden-1-one oxime (*E*-10)** was synthesized as white solid in 61% yield (0.23 g, 1.03 mmol).

^{1}H-NMR (300 MHz, DMSO-d_6, δ_H) 11.16 (s, 1H), 7.61 (dd, J = 1.9, 0.6 Hz, 1H), 7.47 (dd, J = 8.1, 2.0 Hz, 1H), 7.35 – 7.24 (m, 1H), 3.03 – 2.86 (m, 2H), 2.77 (ddd, J = 7.3, 4.6, 1.7 Hz, 2H).

^{13}C-NMR (75 MHz, DMSO-d_6, δ_C) 160.8 (C_q), 147.5 (C_q), 139.3 (C_q), 132.8 (+), 128.4 (+), 123.4 (+), 120.4 (+), 28.0 (-), 26.4 (-).

E-12
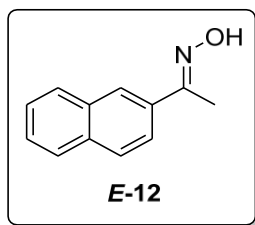
(*E*)-1-(Naphthalen-2-yl) ethan-1-one oxime (E-12) [5]

Following the general procedure using (*E/Z*)-1-(naphthalen-2-yl) ethan-1-one (13.5 mmol, 2.30 g, 1.0 equiv.) as starting material, **(*E*)-1-(naphthalen-2-yl) ethan-1-one oxime (*E*-12)** was synthesized as white solid in 41% yield (1.02 g, 5.51 mmol).

¹H-NMR (300 MHz, DMSO-d_6, δ_H) 11.35 (s, 1H), 8.22 – 8.10 (m, 1H), 8.05 – 7.80 (m, 4H), 7.60 – 7.46 (m, 2H), 2.28 (s, 3H).

¹³C-NMR (75 MHz, DMSO-d_6, δ_C) 153.2 (C_q), 134.8 (C_q), 133.4 (C_q), 133.3 (C_q), 128.8 (+), 128.1 (+), 127.9 (+), 126.9 (+), 126.8 (+), 125.6 (+), 123.5 (+), 11.8 (+).
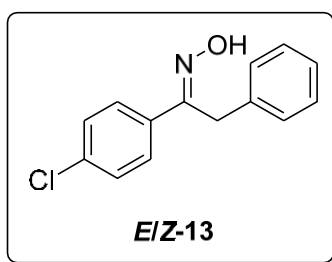
E/Z-13

(*E/Z*)-1-(4-Chlorophenyl)-2-phenylethan-1-one oxime (*E/Z*-13) [7]
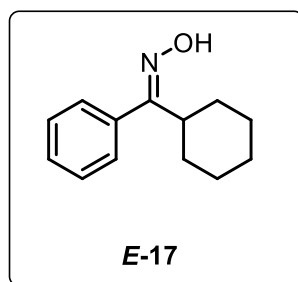
Following the general procedure using (*E/Z*)1-(4-chlorophenyl)-2-phenylethan-1-one (8.14 mmol, 1.88 g, 1.00 equiv.) as starting material, **(*E/Z*)-1-(4-chlorophenyl)-2-phenylethan- 1-one oxime (*E/Z*-13)** was synthesized as white solid in 79% yield (1.58 g, 6.40 mmol).

¹H- NMR (300 MHz, DMSO-d_6, δ_H) *Z*-Isomer: 11.63 (s, 1H), 7.75 – 7.60 (m, 2H), 7.51 – 7.36 (m, 2H), 7.34 – 7.09 (m, 5H), 4.15 (s, 2H).

¹³C-NMR (75 MHz, DMSO-d_6, δ_C) *Z*-Isomer: 154.4 (C_q), 137.4 (C_q), 135.1 (C_q), 133.8 (C_q), 128.9 (+), 128.9 (+), 128.8 (+), 128.1(+), 126.6(+), 30.8(-).

¹H-NMR (300 MHz, DMSO-d_6, δ_H) *E*-Isomer: 11.65 (s, 1H), 7.73-7-66 (m, 2H), 7.53 – 7.45 (m, 2H), 7.43 – 7.34 (m, 5H), 4.16 (s, 2H).

¹³C-NMR (75 MHz, DMSO-d_6, δ_C) *E*- Isomer: 154.4(C_q), 153.6 (C_q), 137.9 (C_q), 133.4 (C_q), 132.5 (+), 130.8 (+), 129.2 (+), 128.3 (+), 128.1 (+), 126.8 (+), 126.6 (+), 40.8 (-).

E-17

(*E*)-Cyclohexyl(phenyl)methanone oxime (*E*-17) [8]

Following the general procedure using cyclohexyl phenyl ketone (12.4 mmol, 1.66 mL, 1.00 equiv.) as starting material **(*E*) cyclohexyl(phenyl)methanone oxime (*E*-17)** could be synthesized as white solid in 72% yield (1.85 g, 9.84 mmol).

^{1}H-NMR (400 MHz, DMSO-d_6, δ_H) *E*- and *Z* Isomer (63:37%): 10.94 (s, 1H), 10.41 (s, 1H), 7.58 – 7.07 (m, 10H), 3.17 (tt, *J* = 12.1, 3.2 Hz, 1H), 2.48 (m, 1H), 1.82 – 1.54 (m, 10H), 1.54 - 0.95 (m, 10H).

^{13}C-NMR (101 MHz, DMSO-d_6, δ_C) 161.8 (C_q), 160.2 (C_q), 137.2 (C_q), 135.4 (C_q), 128.4 (+), 128.4 (+), 128.3 (+), 128.1 (+), 128.1 (+), 128.0 (+), 43.7 (+), 37.9 (+), 30.9 (+), 29.2 (+), 26.5 (+), 26.2 (+), 26.1 (+).

***E*-20**
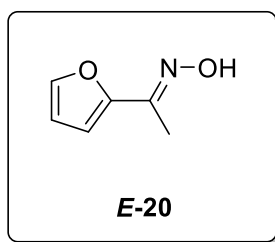
(*E*)-1-(Furan-2-yl) ethan-1-one oxime (*E*-20) [9]

Following the general procedure using (*E*/*Z*)-1-(furan-2-yl) ethan-1-one (20.0 mmol, 2.20 g, 1.00 equiv.) as starting material, **(*E*)-1-(furan-2-yl) ethan-1-one oxime (*E*-20)** was synthesized as white solid in 24% yield (0.59 g, 4.72 mmol).

^{1}H-NMR (300 MHz, DMSO-d_6, δ_H) 11.17 (s, 1H), 7.70 (dd, J = 1.8, 0.8 Hz, 1H), 6.74 (dd, J = 3.4, 0.8 Hz, 1H), 6.54 (dd, J = 3.4, 1.8 Hz, 1H), 2.06 (s, 3H).

**^{13}C-NMR** (75 MHz, DMSO-d_6, δ_C) 151.1 (C_q), 146.1 (C_q), 144.0 (+), 111.9 (+), 109.5 (+), 11.5 (+).

***E*-22**
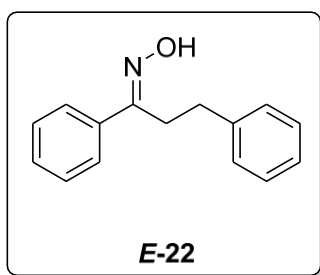
(*E*)-2-Hydroxy-1,2-diphenylethan-1-one oxime (*E*-22) [4b]

Following the general procedure using (*E*/*Z*)-2-hydroxy-1,2-diphenylethan-1-one (8.88 mol, 1.87 g, 1.00 equiv.) as starting material, **(*E*)-2-hydroxy-1,2-diphenylethan-1-one oxime (*E*-22)** was synthesized as white solid in 58% yield (1.17 g, 5.19 mmol).

^{1}H-NMR (300 MHz, DMSO- d_6, δ_H) 11.29 (s, 1H), 7.73 – 7.60 (m, 2H), 7.50 – 7.15 (m, 8H), 3.07 – 2.92 (m, 2H), 2.86 – 2.71 (m, 2H).

^{13}C-NMR (75 MHz, DMSO-d_6, δ_C) 156.5 (C_q), 141.8 (C_q), 136.4 (C_q), 129.1 (+), 128.9 (+), 128.8 (+), 128.6 (+), 126.4 (+), 126.2 (+), 40.8 (+), 32.2 (-), 27.7 (-).
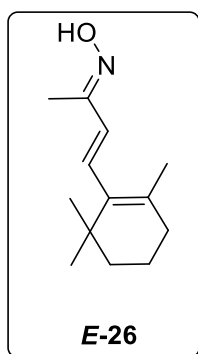
E-24
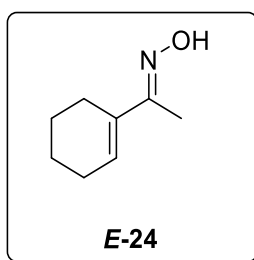
(*E*)-1-(Cyclohex-1-en-1-yl) ethan-1-one oxime (*E*-24) [10]

Following the general procedure using (*E*/*Z*)-1(cyclohex-1-en-1-yl) ethan-1-one (3.60 mmol, 0.46 ml, 1.00 equiv.) as starting material, **(*E*)-1-(cyclohex-1-en-1-yl) ethan-1-one oxime (*E*-24)** was synthesized as white solid in 86% yield (0.43 g, 3.10 mmol).

^{1}H-NMR (300 MHz, DMSO- d_6, δ_H) 10.78 (s, 1H), 6.10 (tt, J = 4.1, 1.5 Hz, 1H), 2.21 (tq, J = 6.0, 1.7 Hz, 2H), 2.13 (dtt, J = 5.6, 3.8, 2.0 Hz, 2H), 1.86 (s, 3H), 1.56 (pd, J = 5.6, 2.8 Hz, 4H).

^{13}C-NMR (75 MHz, DMSO- d_6, δ_C) 154.6 (C$_q$), 135.3 (C$_q$), 128.0 (+), 25.8 (-), 24.6 (-), 22.6 (-), 22.3 (-), 9.9 (+).


E-26

(*E*)(2E,3E)-4-(2,6,6-Trimethylcyclohex-1-en-1-yl)but-3-en-2-one oxime (*E*-26) [10]
Following the general procedure using **(*E*/*Z*) (2E,3E)-4-(2,6,6-trimethylcyclohex-1-en-1- yl)but-3-en-2-one** (9.65 mmol, 1.96 ml, 1.00 equiv.) as starting material, **(*E*) (2E,3E)-4-(2,6,6- trimethylcyclohex-1-en-1-yl)but-3-en-2-one oxime (*E*-26)** was synthesized as white solid in 28% yield (0.56 g, 2.70 mmol).

^{1}H-NMR (400 MHz, DMSO-d_6, δ_H) 10.55 (s, 1H), 6.74 (d, J = 16.8 Hz, 1H), 6.50 - 6.43 (m, 1H), 1.99 (t, J = 6.4 Hz, 2H), 1.92 (s, 3H), 1.71-1.63 (m, 3H), 1.62 - 1.51 (m, 2H), 1.49 - 1.39 (m, 2H), 1.00 (s, 6H).

^{13}C-NMR (101 MHz, DMSO-d_6, δ_C) 151.2 (C$_q$), 137.2 (C$_q$), 133.5 (+), 131.3 (C$_q$), 122.1 (+), 34.1 (-), 33.0 (-), 29.1 (+), 21.8 (+),19.1 (-), 16.9 (+).

E-28
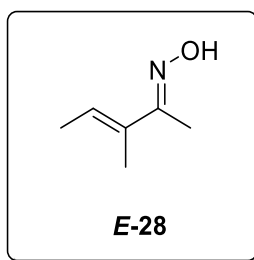
(2Z,3E)-3-Methylpent-3-en-2-one oxime (E-28) [11]

Following the general procedure using (2Z,3E/Z)-3-methylpent-3-en-2-one (17.7 mmol, 1.99 ml, 1.00 equiv.) as starting material **(2Z,3E)-3-methylpent-3-en-2-one oxime (E-28)** was synthesized as white solid in 78% yield (1.56 g, 13.8 mmol).

^{1}H-NMR (400 MHz, DMSO-d_6, δ_H) 10.77 (s,1H), 5.90 (qq, J = 6.8, 1.3 Hz, 1H), 1.86 (s, 3H), 1.76 (t, J = 1.2 Hz, 3H), 1.72 (dt, J = 6.9, 1.0 Hz, 3H).

^{13}C-NMR (101 MHz, DMSO-d_6, δ_C) 155.4 (C_q), 134.2 (C_q), 125.3 (+), 14.2 (+), 12.7 (+), 10.0 (+).


E-30
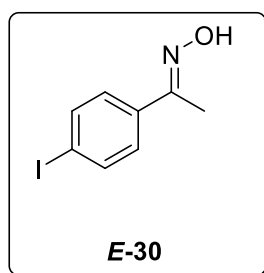
(E/Z)-1-(4-Iodophenyl) ethan-1-one oxime (E-30) [12]

Following the genera procedure using (E/Z)-1-(4-iodophenyl) ethan-1-one (7.66 mmol, 1.88 g, 1.00 equiv.) as starting material **(E)-1-(4-iodophenyl) ethan-1-one oxime (E-30)** was synthesized as pale-yellow solid in 93% yield (0.87 g, 7.16 mmol).

^{1}H-NMR (400 MHz, DMSO-d_6, δ_H) 11.29 (s, 1H), 7.90 – 7.62 (m, 2H), 7.55 – 7.36 (m, 2H), 2.11 (s, 3H).

^{13}C-NMR (101 MHz, DMSO-d_6, δ_C) 152.7 (C_q), 137.6 (+), 136.9 (C_q), 128.1 (+), 95.5 (C_q), 11.7 (+).

E-32
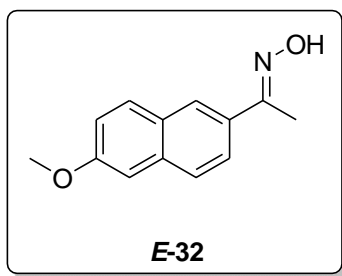
(*E*)-1-(6-Methoxynaphthalen-2-yl) ethan-1-one oxime (*E*-32) [13]

Following the general procedure using (*E/Z*)-1-(6-methoxynaphthalen-2-yl) ethan-1-one (9.29 mmol, 1.86 g, 1.00 equiv.) as starting material **(*E*)-1-(6-methoxynaphthalen-2-yl) ethan- 1-one oxime (*E*-32)** was synthesized as pale-yellow solid in 58% yield (5.39 mmol, 1.16 g).

¹H-NMR (300 MHz, DMSO-d_6, δ_H) 11.8 (s, 1H), 8.04 (d, J = 1.7 Hz, 1H), 7.92 – 7.84 (m, 2H), 7.77 (d, J = 8.7 Hz, 1H), 7.31 (d, J = 2.5 Hz, 1H), 7.18 (dd, J = 8.9, 2.6 Hz, 1H), 3.88 (s, 3H), 2.25 (s, 3H).

¹³C-NMR (75 MHz, DMSO-d_6, δ_C) 158.2 (C_q), 153.2 (C_q), 134.8 8C_q), 132.6 (C_q), 130.3 (+), 128.6 (C_q), 127.1 (+), 125.5 (+), 124.0 (+), 119.2 (+), 106.4 (+), 55.7 (+), 11.7 (+).

Compounds **E-6**, **E-6b**, **E-3** and **E-5** were synthesized according to a published procedure.[14]

2.7.2 General Procedure for the Oxa-Michael Addition to Oximes

A 5 mL crimp neck vial equipped with a magnetic stir bar was loaded with the oxime (0.20 mmol, 1.00 equiv.), DPA (13.2 mg, 20 mol%), anhydrous CeCl₃ (5.00 mg, 10 mol%) and Cs₂CO₃ (13.0 mg, 20 mol%). The vial was capped and purged with nitrogen before addition of 2 mL of dry degassed acetonitrile *via* syringe. The vial was additionally degassed three times *via* freeze- pump- thaw. After completion the electron poor trapping reagent (0.60 mmol, 3.00 equiv.) was added, and the reaction mixture was stirred and irradiated using a violet high-power LED (395 nm) for 2 h at 25 °C. The progress could be monitored by GC-FID and GC-MS analysis.

After 24 h the completion was tested *via* TLC analysis and the reaction mixture was diluted with 1 M HCl (20.0 mL) and extracted with ethyl acetate (3 x 20.0 mL). The combined organic phases were dried over anhydrous $MgSO_4$ and solvent residues were removed under reduced pressure. Purification was performed by automated flash column chromatography on silica (petroleum ether/ethyl acetate, 92:8) to yield the respective Oxa-Michael product.

For the other O-alkylated oximes listed, Ce(III)DOTA (10.8 mg, 10 mol%) instead of anhydrous $CeCl_3$ was used.[15]

A 5 mL crimp neck vial equipped with a magnetic stir bar was loaded with the oxime (0.20 mmol, 1.0 equiv.), DPA (13.2 mg, 20 mol%), Ce(III)DOTA (10.8 mg, 10 mol%) and Cs_2CO_3 (13.0 mg, 20 mol%). The vial was capped and purged with nitrogen before adding 2 mL of dry degassed acetonitrile *via* syringe. The vial was additionally degassed three times *via* freeze-pump-thaw. After completion the electron poor trapping reagent (0.60 mmol, 3.00 equiv.) was added, and the reaction mixture was stirred and irradiated using a violet high-power LED (395 nm) for 2 h at 25 °C. The progress could be monitored by GC-FID and GC-MS analysis.

After 24 h the completion was tested *via* TLC analysis and the reaction mixture was diluted with 1 M HCl (20.0 mL) and extracted with ethyl acetate (3 x 20.0 mL). The combined organic phases were dried over anhydrous $MgSO_4$ and solvent residues were removed under reduced pressure. Purification was performed by automated flash column chromatography on silica (petroleum ether/ethyl acetate, 92:8) to yield the respective Oxa-Michael product. TLC experiments in petroleum ether/ethyl acetate were performed and the result before column chromatography and after purification was compared for oxime *E*-1.
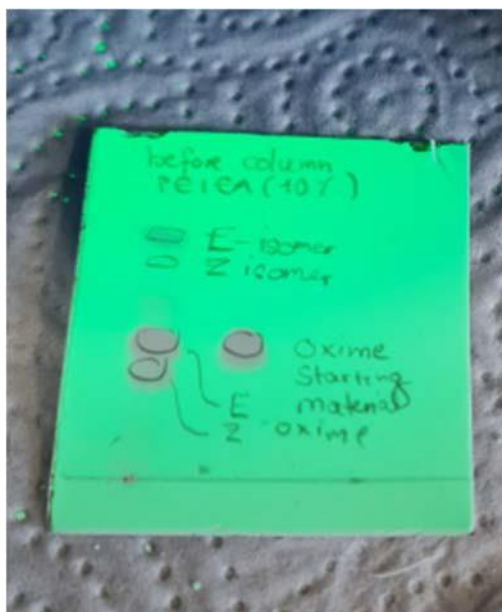
Figure S2.1. TLC analysis of the reaction mixture before purification.

The *E*-product showed an R$_f$ value of about 0.9, the *Z*-product the value was about 0.8. In general, the spots appear close.
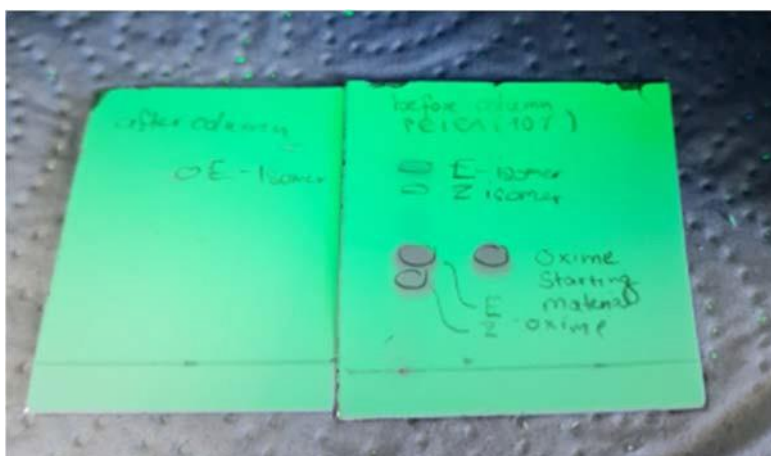

Figure S2.2. Comparison of products before and after purification.

After purification of the products by column chromatography only the *E*-product was visible on the TLC plate. Due to low amounts of the *Z* product being formed during the reaction, this compound could not or not exclusively be isolated (see NMR-spectra for compound ***E-3*** and ***Z- 3***). The separation of *E* and *Z* isomer on TLC indicates that the *Z* isomer of the alkylated oxime is stable on silica gel. However, we cannot exclude an effect on the *E*/*Z* ratio during extended periods of silica gel and ambient light exposure.
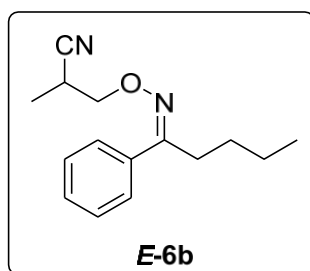
59

E-6
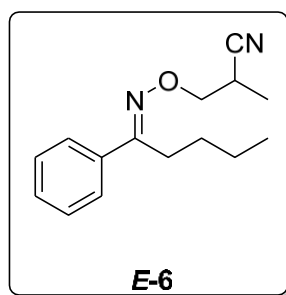
N-(2-Cyanopropyl)-N-phenyl pentane amide (*E*-6)

^{1}H-NMR (400 MHz, Chloroform-*d*, δ_H) 7.79 – 7.64 (m, 2H), 7.50 – 7.38 (m, 3H), 4.46 – 4.17 (m, 2H), 3.19 (pd, *J* = 7.2, 6.1 Hz, 1H), 2.96 – 2.75 (m, 2H), 1.74 – 1.52 (m, 2H), 1.44 (dd, *J* = 16.0, 7.1 Hz, 5H), 0.97 (t, *J* = 7.3 Hz, 3H).

^{13}C-NMR (101 MHz, Chloroform-*d*, δ_C) 160.6 (C_q), 135.4 (C_q), 129.4 (+), 128.5 (+), 126.4 (+), 121.3 (+), 74.1 (-), 28.7 (-), 26.7 (-), 26.1 (+), 22.9 (-), 14.4 (+), 13.8 (+).

HRMS (ESI) (m/z): [M+H]$^+$($C_{15}H_{20}N_2O$) calc.: 245.1648, found: 245.1651.

**Yield:** 16%, 7.85 mg, 0.032 mmol, colourless oil.

E-6b

3-(Cyanomethyl)-N-phenylpentan amide (*E*-6b)

^{1}H-NMR (300 MHz, Chloroform-*d*, δ_H) 7.62 (dtdd, *J* = 5.8, 4.0, 3.0, 1.9 Hz, 2H), 7.51 – 7.31 (m, 3H), 3.15 (pd, *J* = 7.2, 6.1 Hz, 1H), 3.01 – 2.89 (m, 1H), 2.82 – 2.71 (m, 2H), 1.61 – 1.47 (m, 2H), 1.46 – 1.32 (m, 5H), 0.97 – 0.90 (m, 3H).

^{13}C-NMR (75 MHz, Chloroform-*d*, δ_C) 160.6 (C_q), 135.4 (C_q), 129.4 (+), 128.5 (C_q), 126.4 (+), 121.3 (+), 28.7 (-), 26.7 (-), 26.1 (+), 22.9 (+), 22.5 (-), 14.4 (+), 13.9 (+).

HRMS (ESI) (m/z): [M+H]$^+$ ($C_{15}H_{20}N_2O$) calc.: 245.1648, found: 245,1651.

Yield: from GC-FID: product ratio *E*-6:*E*-6b 80:20%, product *E*-6b could not be isolated by column chromatography; ^{1}H-NMR and ^{13}C-NMR spectra together with *E*-6.
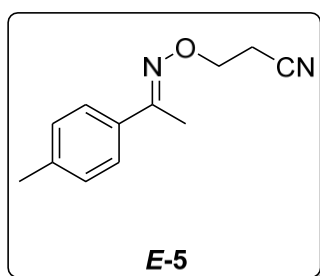
E-3
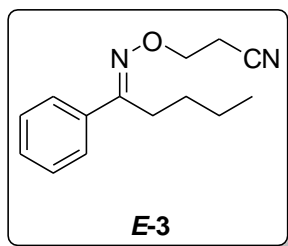
N-(2-Cyanoethyl)-N-phenylpentan amide (E-3)

^{1}H-NMR (300 MHz, Chloroform-*d*, δ_H) 7.68 – 7.61 (m, 2H), 7.43 – 7.36 (m, 3H), 4.37 (t, *J* = 6.2 Hz, 2H), 2.82 – 2.74 (m, 4H), 1.65 – 1.51 (m, 2H), 1.49 – 1.32 (m, 2H), 0.93 (t, *J* = 7.2 Hz, 3H).

^{13}C-NMR (75 MHz, Chloroform-*d*, δ_C) 160.8 (C$_q$), 135.3 (C$_q$), 129.4 (+), 128.5 (+), 126.4 (+), 117.8 (C$_q$), 68.1(-), 28.7 (-), 26.7 (-), 22.9 (-), 18.6 (-), 13.9 (+).

HRMS (EI+) (m/z): [M]$^+$ (C$_{14}$H$_{18}$N$_2$O): calc.:230.1414, found: 230.1408.

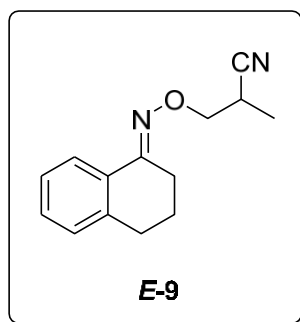**Yield:** 65%, 29.9 mg, 0.13 mmol, colourless oil.

E-5

N-(2-Cyanoethyl)-N-(p-tolyl) acetamide (E-5)

^{1}H-NMR (300 MHz, Chloroform-*d*, δ_H) 7.63 – 7.51 (m, 2H), 7.26 – 7.09 (m, 2H), 4.37 (t, *J* = 6.2 Hz, 2H), 2.78 (t, *J* = 6.3 Hz, 2H), 2.37 (s, 3H), 2.25 (s, 3H).

^{13}C-NMR (75 MHz, Chloroform-*d*, δ_C) 156.6 (C$_q$), 139.6 (C$_q$), 133.2 (C$_q$), 129.2 (+), 126.1 (+), 117.9 (C$_q$), 68.1(-), 21.3 (+), 18.6 (-), 12.9 (+).

HRMS (EI+) (m/z): [M]$^+$ (C$_{12}$H$_{14}$N$_2$O) calc.: 202.1101, found: 202.1098.

**Yield:** 42%, 17.0 mg, 0.084 mmol, colourless oil.

E-9

2-Methyl-3-(2-oxo-2,3,4,5-tetrahydro-1H-benzo[*b*]azepin-1-yl) propane nitrile (*E*-9)

¹H-NMR (400 MHz, Chloroform-*d*, δ_H) 7.94 (dd, *J* = 7.9, 1.4 Hz, 1H), 7.27 (td, *J* = 7.4, 1.5 Hz, 1H), 7.20 (dd, *J* = 7.7, 1.5 Hz, 1H), 7.16 – 7.09 (m, 1H), 4.38 – 4.11 (m, 2H), 3.15 (dd, *J* = 7.2, 6.1 Hz, 1H), 2.91 – 2.55 (m, 4H), 2.21 – 1.75 (m, 2H), 1.37 (d, *J* = 7.2 Hz, 3H).

¹³C-NMR (101 MHz, Chloroform-*d*, δ_C) 155.8 (C_q), 139.9 (C_q), 130.2 (C_q), 129.4 (+), 128.7 (+), 126.4 (+), 124.3 (C_q), 121.4 (+), 74.1 (-), 39.2 (-), 29.7 (-), 26.1 (-), 24.5 (-), 21.3 (+), 14.4 (+).

HRMS (EI+) (m/z): [M]⁺ ($C_{14}H_{16}N_2O$) calc.: 228.1257, found: 228.1254.

**Yield**: 18%, 8.21 mg, 0.036 mmol, pale yellow oil.

E-8
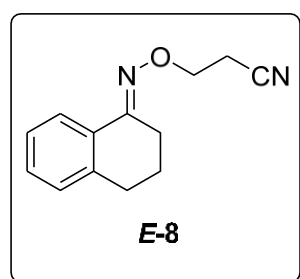
3-(2-Oxo-2,3,4,5-tetrahydro-1H-benzo[*b*]azepin-1-yl) propane nitrile (*E*-8)

¹H-NMR (300 MHz, Chloroform-*d*, δ_H) 7.96 (dd, *J* = 7.8, 1.5 Hz, 1H), 7.38 – 7.07 (m, 3H), 4.38 (t, *J* = 6.2 Hz, 2H), 2.88 – 2.70 (m, 6H), 1.86 (dtd, *J* = 7.1, 6.3, 4.9 Hz, 2H).

¹³C-NMR (75 MHz, Chloroform-*d*, δ_C) 156.0 (C_q), 139.9 (C_q), 130.2 (C_q), 129.4 (+), 128.7 (+), 126.4 (+), 124.3 (+), 117.9 (C_q), 68.2 (-), 29.7 (-), 24.5 (-), 21.3 (-), 18.6 (-).

HRMS (EI+) (m/z): [M]⁺ ($C_{13}H_{14}N_2O$): calc.:214.110, found: 214.110.

Yield: 45%, 19.3 mg, 0.09 mmol, colourless oil.

E-11
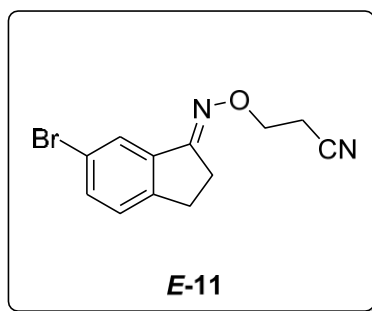
**3-(7-Bromo-2-oxo-3,4-dihydroquinolin-1(2H)-yl) propane nitrile (*E*-11)**

¹H-NMR (300 MHz, Chloroform-*d*, δ_H) 7.80 (d, *J* = 1.9 Hz, 1H), 7.45 (dd, *J* = 8.2, 1.9 Hz, 1H), 7.24 – 7.16 (m, 1H), 4.36 (t, *J* = 6.2 Hz, 2H), 3.04 – 2.97 (m, 2H), 2.96 – 2.90 (m, 2H), 2.80 (t, *J* = 6.2 Hz, 2H).

¹³C-NMR (101 MHz, Chloroform-*d*, δ_C) 163.3 (C_q), 147.2 (C_q), 137.8 (C_q), 133.5 (+), 127.1 (+), 124.7(+), 121.0 (C_q), 117 (C_q), 68.3 (-), 28.2 (-), 26.8 (-), 18.5 (-).

HRMS (EI+) (m/z): [M]⁺ ($C_{12}H_{11}BrN_2O$) calc.:279.0128, found: 279.0132.

Yield:55%, 30.7 mg, 0.11 mmol, pale yellow solid.
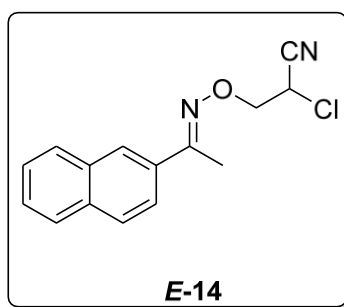
T_m: 123°C.

E-13
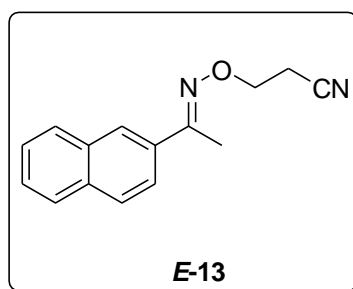
_N_-(2-Cyanoethyl) -_N_-(naphthalen-2-yl) acetamide (*E*-13)

¹H-NMR (300 MHz, Chloroform-*d*, δ_H) 8.02 (dd, *J* = 1.7, 0.8 Hz, 1H), 7.97 – 7.80 (m, 4H), 7.59 – 7.49 (m, 2H), 4.44 (t, *J* = 6.3 Hz, 2H), 2.84 (d, *J* = 6.3 Hz, 2H), 2.39 (s, 3H).

¹³C-NMR (75 MHz, Chloroform-*d*, δ_C) 156.5 (C_q), 133.8 (C_q), 133.4 (C_q), 133.1 (C_q), 128.5 (C_q), 128.1 (+), 127.7 (+), 126.8 (+), 126.5 (+), 126.1 (+), 123.3 (+), 117.8 (+), 68.3 (-), 18.6 (-), 12.8 (+).

HRMS (EI+) (m/z): [M]⁺ ($C_{15}H_{14}N_2O$) calc.: 238.1179, found: 238.1107.

**Yield**: 35%, 16.7 mg, 0.07 mmol, pale yellow oil.

E-14

N-(2-Chloro-2-cyano-ethyl) -N-(naphthalen-2-yl) acetamide (*E*-14)

^{1}H-NMR (400 MHz, Chloroform-*d*, δ_H) 8.11 – 8.00 (m, 1H), 7.86 (qd, *J* = 9.1, 8.6, 5.4 Hz, 4H), 7.61 – 7.44 (m, 2H), 4.88 (dd, *J* = 7.4, 6.5 Hz, 1H), 4.65 – 4.50 (m, 2H), 2.41 (s, 3H).

^{13}C-NMR (101 MHz, Chloroform-*d*, δ_C) 157.9 (C_q), 133.9 (C_q), 133.0 (C_q), 132.8 (C_q), 128.6 (+), 128.2 (+), 127.7 (+), 127.0 (+), 126.6 (+), 126.4 (+), 123.2 (+), 115.8 (C_q), 74.0 (-), 40.6 (+), 12.9 (+).

HRMS (EI+) (m/z): [M]$^+$ ($C_{15}H_{13}ClN_2O$) calc.: 272.0789, found: 272.07790.

Yield: 72%, 38.1 mg, 0.14 mmol, colourless oil.

E-16
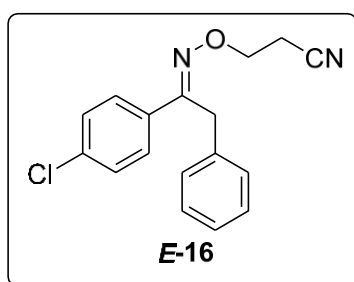
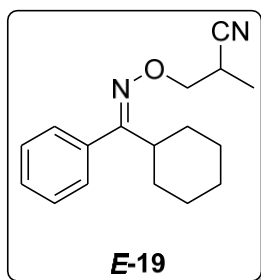**N-(4-Chlorophenyl)-N-(2-cyanoethyl)-2-phenylacetamide (*E*-16)**

^{1}H-NMR (300 MHz, Chloroform-*d*, δ_H) 7.68 – 7.53 (m, 2H), 7.35 – 7.27 (m, 3H), 7.25 – 7.15 (m, 4H), 4.43 (t, *J* = 6.3 Hz, 2H), 4.21 – 4.12 (m, 2H), 2.79 (t, *J* = 6.2 Hz, 2H).

^{13}C-NMR (101 MHz, Chloroform-*d*, δ_C) 157.1 (C_q), 135.9 (C_q), 135.6 (C_q), 133.5 (+), 128.7 (+), 128.4 (+), 127.9 (+), 126.6 (+), 117.5 (C_q), 68.5 (-) 32.7 (-), 18.6 (-).

HRMS (EI+) (m/z): [M]$^+$ ($C_{17}H_{15}ClN_2O$) calc.: 298.0946, found: 298.0872.

Yield: 30%, 17.9 mg, 0.06 mmol, pale yellow solid.
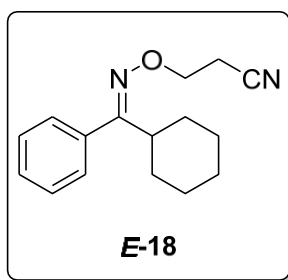
T_m: 100°C

E-19

N-(2-Cyanopropyl)-N-phenyl cyclohexane carboxamide (E-19)

^{1}H-NMR (300 MHz, Chloroform-*d*, δ_H) 7.42 – 7.32 (m, 3H), 7.24 – 7.19 (m, 2H), 4.22 – 3.93 (m, 2H), 3.15 – 2.98 (m, 1H), 2.44 (td, *J* = 11.2, 4.4 Hz, 1H), 1.28 – 1.22 (m, 13H).

^{13}C-NMR (101 MHz, Chloroform-*d*, δ_C) 164.0 (C_q), 139.8 (C_q), 128.3 (+), 128.0 (+), 127.3 (+), 122.5 (C_q), 121.3 (+), 73.7 (-), 44.3, (+) 30.6 (-), 30.4 (-), 29.7 (-), 26.1 (+), 14.4 (+).

HRMS (EI+) (m/z): [M]$^+$ ($C_{17}H_{22}N_2O$) calc.: 270.1727 found: 270.1722.

Yield: 15%, 8.11 mg, 0.03 mmol, colourless oil.
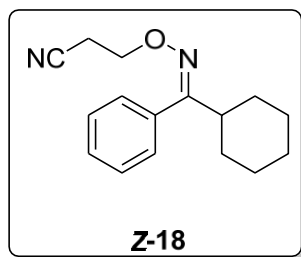

E-18

N-(2-Cyanoethyl)-N-phenyl cyclohexane carboxamide (E-18)

^{1}H-NMR (400 MHz, Chloroform-*d*, δ_H) 7.45 – 7.35 (m, 3H), 7.27 – 7.23 (m, 2H), 4.20 (t, *J* = 6.2 Hz, 2H), 2.72 (t, *J* = 6.4 Hz, 2H), 2.50 (tt, *J* = 11.3, 3.3 Hz, 1H), 2.01 – 1.65 (m, 5H), 1.44 – 1.11 (m, 5H).

^{13}C-NMR (101 MHz, Chloroform-*d*, δ_C) 161.1 (C_q), 134.1 (C_q), 128.4 (+), 128.1 (+), 127.4 (+), 117.8 (C_q), 67.7 (-), 44.4 (+), 30.5 (-), 26.1 (-), 26.0 (-), 18.3 (-).

HRMS (EI+) (m/z): [M]$^+$ ($C_{16}H_{20}N_2O$): calc.:256.1570, found: 256.1564.

**Yield:** 45%, 23.1 mg, 0.09 mmol, colourless oil.

_N_-(2-Cyano-ethyl)-_N_-cyclohexyl benzamide (_Z_-18)

^{1}H-NMR (400 MHz, Chloroform-_d_, δ_H) 7.45 – 7.37 (m, 3H), 7.23 – 7.19 (m, 2H), 4.18 (t, J = 6.4 Hz, 2H), 2.76 (t, J = 6.3 Hz, 2H), 2.46 (ddd, J = 11.2, 7.9, 3.2 Hz, 1H), 1.76 (d, J = 10.7 Hz, 6H), 1.72 – 1.53 (m, 4H).

^{13}C-NMR (101 MHz, Chloroform-_d_, δ_C) 161.3 (C_q), 128.7 (C_q), 128.4 (+), 128.1 (+),127.9 (+), 127.4 (C_q), 67.7 (-), 39.3 (+), 30.5 (-), 29.3 (-), 26.3 (-), 18.2(-).

HRMS (ESI+) (m/z): [M]$^+$ ($C_{16}H_{20}N_2O$): calc.: 256.1650, found: 256.1648.

Yield: 4%, 2.04 mg, 0.008 mmol, colourless oil.
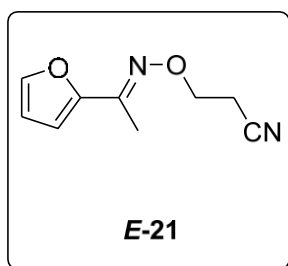
_N_-(2-Cyanoethyl)-_N_-(furan-2-yl) acetamide (_E_-21)

^{1}H-NMR (300 MHz, Chloroform-_d_, δ_H) 7.46 (dd, J = 1.8, 0.8 Hz, 1H), 7.33 (dd, J = 3.5, 0.7 Hz, 1H), 6.53 (dd, J = 3.5, 1.8 Hz, 1H), 4.36 (t, J = 6.3 Hz, 2H), 2.79 (t, J = 6.3 Hz, 2H), 2.24 (s, 3H).

^{13}C-NMR (75 MHz, Chloroform-_d_, δ_C) 178.8 (C_q), 145.3 (C_q), 142.9 (+), 118.3 (+), 117.7 (C_q) 112.2 (+), 68.5 (-), 18.5 (+), 17.4 (-).

HRMS (EI+) (m/z): [M]$^+$ ($C_9H_{10}N_2O2$): calc.: 178.0737, found: 178.0730.

**Yield**: 42%, 15.0 mg, 0.084 mmol, red oil.

E-23
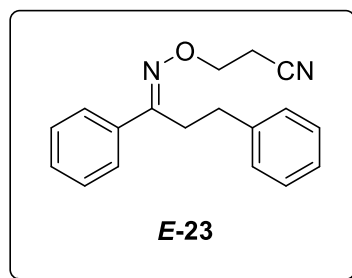
_N_-(2-Cyano-ethyl) -_N_-3-diphenylpropanamide (_E_-23)

¹H-NMR (300 MHz, Chloroform-_d_, δ$_H$) 7.72 – 7.57 (m, 2H), 7.45 – 7.36 (m, 3H), 7.35 – 7.27 (m, 2H), 7.27 – 7.18 (m, 3H), 4.35 (t, _J_ = 6.3 Hz, 2H), 3.17 – 3.05 (m, 2H), 2.88 (dd, _J_ = 9.8, 6.3 Hz, 2H), 2.72 (t, _J_ = 6.3, 1 Hz, 2H).

¹³C-NMR (75 MHz, Chloroform-_d_, δ$_C$) 159.7 (C$_q$), 141.1 (C$_q$), 135.0 (C$_q$), 129.6 (+), 128.6 (+), 128.5 (+), 128.4 (+), 126.4 (+), 126.2 (+), 117.8 (C$_q$), 68.2 (-), 32.5 (-), 29.0 (-), 18.5 (-).

HRMS (EI+) (m/z): [M]$^+$ (C$_{18}$H$_{18}$N$_2$O): calc.: 278.1414, found: 278.1410.

**Yield:** 35%, 19.5 mg, 0.07 mmol, colourless oil.

E-25
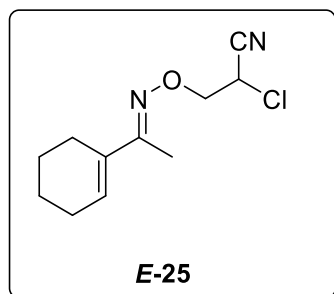
_N_-(2-Chloro-2-cyanoethyl)-_N_-(cyclohex-1-en-1-yl) acetamide (_E_-25)

¹H-NMR (300 MHz, Chloroform-_d_, δ$_H$) 6.21 (tt, _J_ = 4.0, 1.5 Hz, 1H), 4.76 (dd, _J_ = 7.3, 6.5 Hz, 1H), 4.51 - 4.29 (m, 2H), 2.34 - 2-13 (m, 4H), 1.99 (s, 3H), 1.79-1.53 (m, 4H).

¹³C-NMR (75 MHz, Chloroform-_d_, δ$_C$) 159.1 (C$_q$), 134.3 (C$_q$), 131.0 (+), 115.9 (C$_q$), 73.7 (-), 40.5 (-), 26.0 (-), 24.4 (-), 22.3 (-), 22.0 (+), 10.6 (+).

HRMS (EI+) (m/z): [M]$^+$ (C$_{11}$H$_{15}$ClN$_2$O): calc.: 226.0946 found: 226.0949.

**Yield:** 15%, 6.78 mg, 0.03 mmol, colourless oil.

E-27
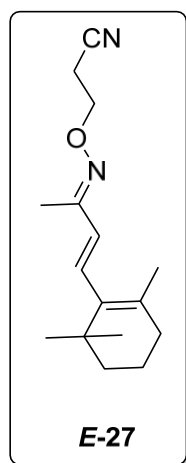
(*E*/*Z*)-*N*-(2-Cyanoethyl)-*N*-(2-(2,6,6-trimethylcyclohex-1-en-1-yl) vinyl) acetamide (*E*-27)

¹H-NMR (400 MHz, Chloroform-*d*, δ_H) 6.51 (d, *J* = 12.5 Hz, 1H), 6.26 (ddq, *J* = 12.6, 2.6, 1.4 Hz, 1H), 4.24 (t, *J* = 6.3 Hz, 2H), 2.71 (t, *J* = 6.4 Hz, 2H), 2.01 – 1.93 (m, 2H), 1.88 (s, 3H), 1.62 (dtt, *J* = 8.7, 5.3, 2.7 Hz, 2H), 1.50 (d, *J* = 1.1 Hz, 3H), 1.47 (dd, *J* = 5.8, 3.2 Hz, 2H), 1.04 (d, *J* = 2.1 Hz, 6H).

¹³C-NMR (101 MHz, Chloroform-*d*, δ_C): 156.6 (C_q), 135.9 (C_q), 134.8 (+), 131.9 (C_q), 122.3 (+), 117.7 (C_q), 67.7 (-), 39.1 (-), 34.3 (+), 32.5 (-), 28.8 (+), 21.5 (+), 19.0 (-), 18.4 (-), 18.0 (+).

HRMS (EI+) (m/z): [M]⁺ ($C_{16}H_{24}N_2O$): calc.:260.1961, found: 260.1966.

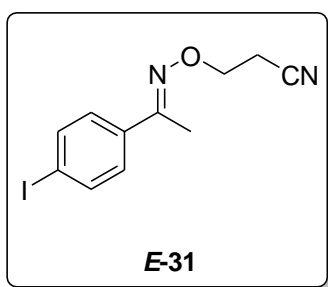**Yield**: 20%, 10.4 mg, 0.04 mmol, red oil.

E-29
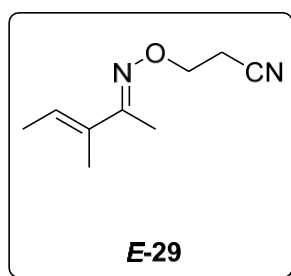
(*E*/*Z*)-*N*-(But-2-en-2-yl)-*N*-(2-cyanoethyl) acetamide (*E*-29)

¹H-NMR (300 MHz, Chloroform-*d*, δ_H) 5.97 (qq, *J* = 6.8, 1.3 Hz, 1H), 4.27 (t, *J* = 6.3 Hz, 2H), 2.72 (t, *J* = 6.3 Hz, 2H), 1.96 (s, 3H), 1.84 – 1.73 (m, 6H).

¹³C-NMR (75 MHz, Chloroform-*d*, δ_C) 158.6 (C_q), 133.4 (C_q), 127.4 (+), 117.9 (C_q), 67.8 (-), 18.4 (-), 14.1 (+), 12.2 (+), 10.8 (+).

HRMS (EI+) (m/z): [M]⁺ ($C_9H_{14}N_2O$): calc.:166.1179, found: 166.1181.

Yield: 41%, 136 mg, 0.082 mmol, colourless oil.

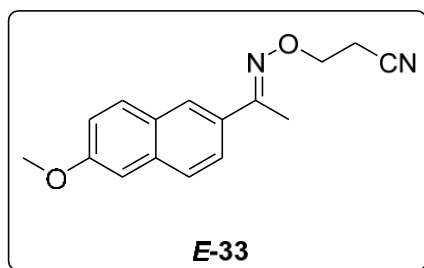*E*-31

N-(2-Cyanoethyl)-N-(4-iodophenyl) acetamide (E-31)

¹H-NMR (300 MHz, Chloroform-*d*, δ_H) 7.87 – 7.61 (m, 2H), 7.49 – 7.26 (m, 2H), 4.38 (t, *J* = 6.1 Hz, 2H), 2.78 (t, *J* = 6.2 Hz, 2H), 2.23 (s, 3H).

¹³C-NMR (75 MHz, Chloroform-*d*, δ_C) 155.88 (C_q), 137.6 (+), 135.5 (C_q), 127.8 (+), 117.7 (C_q), 95.7 (C_q), 68.3 (-), 18.6 (-), 12.7 (+).

HRMS (EI+) (m/z): [M]$^+$ ($C_{11}H_{11}IN_2O$): calc. 313.9989, found: 313.9993.

Yield: 35%, 22.0 mg, 0.07 mmol, white solid

T$_m$: 110°C

E-33

N-(2-Cyanoethyl)-N-(6-methoxynaphthalen-2-yl) acetamide (E-33)

¹H-NMR (300 MHz, Chloroform-*d*, δ_H) 7.95 (d, *J* = 1.8 Hz, 1H), 7.94 – 7.64 (m, 3H), 7.32 -7.03 (m, 2H), 4.42 (t, *J* = 6.3 Hz, 2H), 3.93 (s, 3H), 2.82 (t, *J* = 6.3 Hz, 2H), 2.36 (s, 3H).

¹³C-NMR (75 MHz, Chloroform-*d*, δ_C): 158.4 (C_q), 156.6 (C_q), 135.1 (C_q), 131.2 (C_q), 130.0 (+), 128.4 (C_q), 127.0 (+), 125.9 (+), 123.9 (+), 119.2 (+), 117.9 (C_q), 105.8 (+), 68.2 (-), 55.4 (+), 18.6 (-), 12.7 (+).

HRMS (EI+) (m/z): [M]$^+$ ($C_{16}H_{16}N_2O_2$): calc.268.1285, found:268.1289.

Yield: 65%, 34.9 mg, 0.130 mmol, white solid.

T$_m$: 142°C.

Effects on the *E/Z* Isomerization

Table T2.1. Effects on the E/Z isomerisation.
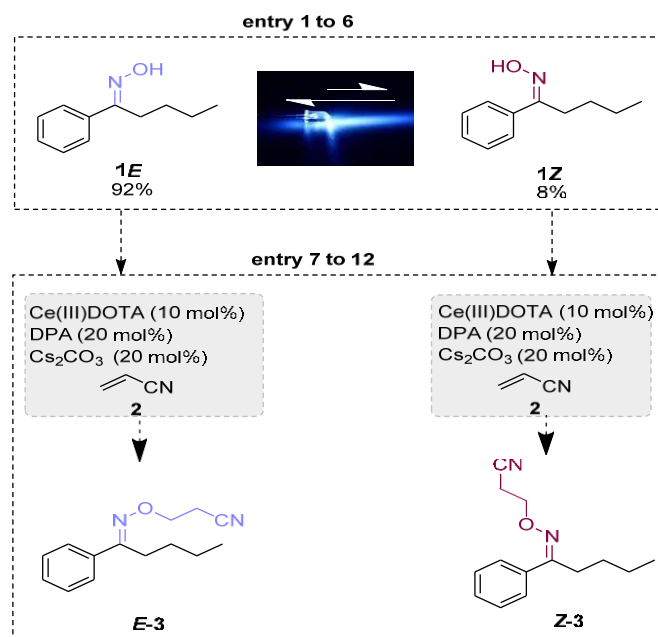
| Entry	Oxime[a]	Conditions	Irradiation[b]	Oxime *E:Z* [%][c]
1	*E*	25 °C, acetonitrile (1 mL), 7 h	no	100:0
2	*E*	0 °C, acetonitrile (1 mL), 7 h	no	100:0
3	*Z*	25 °C, acetonitrile (1 mL), 7 h	no	30:70
4	*Z*	0 °C, acetonitrile (1 mL), 7 h	no	29:71
5	*E* > 95%	25 °C, acetonitrile (1 mL), 2 h	yes	50:50
6	*E* > 95%	25 °C, acetonitrile (1 mL), DPA (20 mol%), 2 h	yes	75:25
				Oxime ether ratio of *E*-3:*Z*-3 [%][c]
7	*Z*	25 °C, acetonitrile (1 mL),	no	0:100
8	*Z*	0 °C, acetonitrile (1 mL),	no	0:100
9	*E*	25 °C, acetonitrile (1 mL),	no	100:0
10	*E*	0 °C, acetonitrile (1 mL),	no	100:0
11	*E*	25 °C, acetonitrile (1 mL),	yes	75:25

[a] The initial oxime mixture was separated by flash column chromatography on silica with PE/EtOAc (9:1). [b] Irradiation of the respective mixture containing the oxime (0.1 mmol), diphenyl anthracene (0.02 mmol), Ce-catalyst (0.01 mmol), Cs_2CO_3 (0.02 mmol) and acrylonitrile (**2**) (3.00 equiv.) using a 395-400 nm high power LED setup for 2-24 h. [c] Oxime and product ratio were determined by ^{1}H-NMR analysis comparing the signal for the hydroxy protons (10-11.5 ppm) or CH_2 protons (2-5 ppm).

The ratios of the isomerisation experiments are in good agreement with published results from Pavlovic *et al.* [16] When we started to irradiate the pure *E* oxime in acetonitrile the tendency to isomerize to the respective *Z* isomer was low, supporting the thermodynamic stability of the *E* oxime in solution.[17] Irradiating oxime **1Z** resulted in the formation of the *E* oxime after 7 h (entries 3 and 4). In case of irradiating the oxime-isomer mixture consisting of *E* > 95% a 1:1 ratio between both oximes could be detected in ^{1}H-NMR spectroscopy after 24 h (entry 5). When diphenyl anthracene as photosensitiser was added in 20 mol% to the oxime mixture, the *E* isomer was detected predominantly in ^{1}H-NMR (entry 6). The oxime ether product formation follows a similar trend. Oxime ethers are reported to be configurationally more stable under thermal isomerisation conditions.

2.8 UV/Vis Experiments
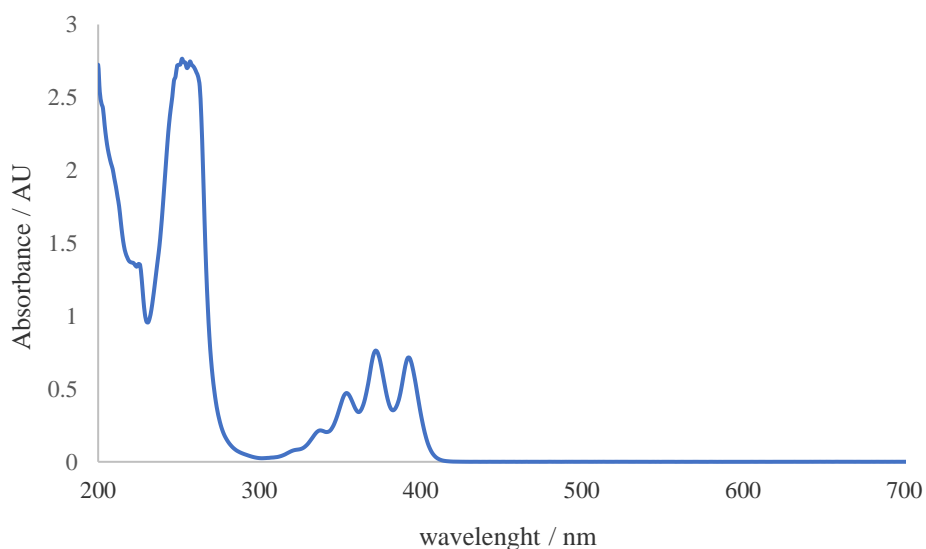
Spectrum S2.1. Spectrum of pure 9 , 1 0 - diphenyl anthracene in acetonitrile (0.01 M, λ_{max} = 390 nm). The three vibronic bands characteristic for DPA are clearly presented between 350 and 400 nm.[18]
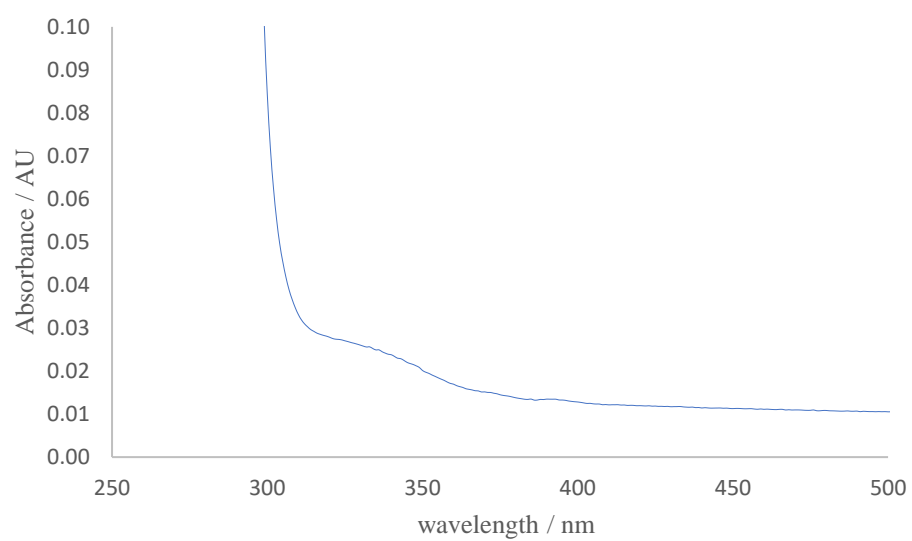
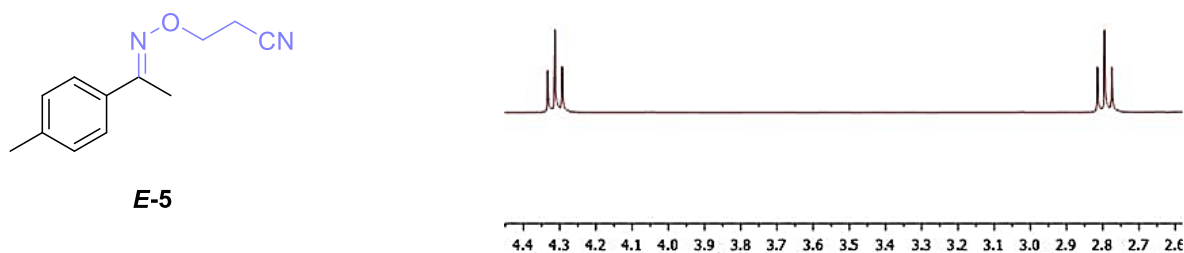***Spectrum S2.2.*** Visible light absorbing complex of Cs_2CO_3, Oxime **1** and Ce^{3+} (0.1 mM in CH_3CN).

2.9 NMR Data of Oxime Ether Isomers

Isomerically pure oxime ethers **E-3** and **E-5**.
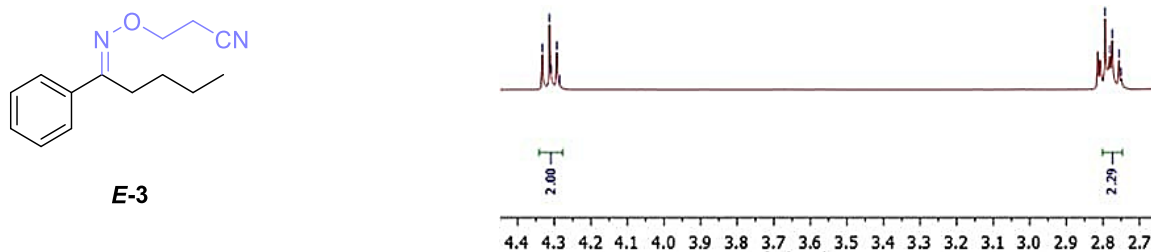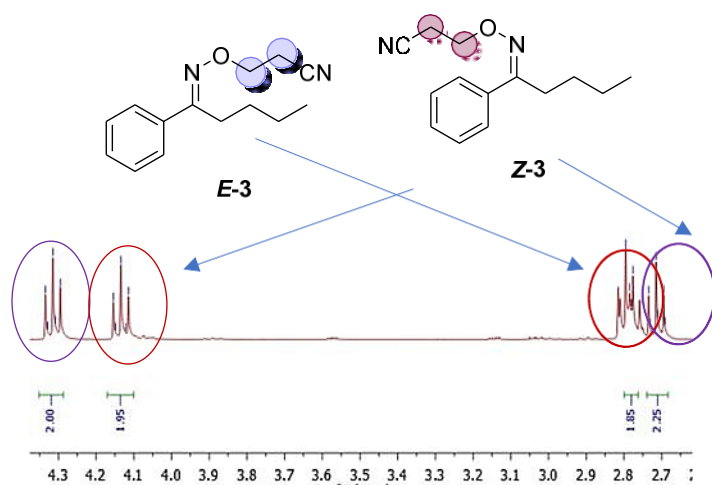

Spectrum S2.5. Pure oxime ether **E-3**.

Spectrum S2.6. Pure oxime ether **E-5**.

Mixture of isomers of **E-3** and **Z-3**

Spectrum S2.7. Mixture of isomers **E-3** and **Z-3**.

2.10 Computational Analysis

Dr. Stefano Crespi performed a DFT optimisation of the *E* and *Z* form of two exemplary oximes to compute the energy difference between the two isomeric forms. The calculations were conducted at the B97X-D/def2-SVP level as implemented in the Gaussian 16 Rev. B.01 software.[19] The stationary points found were confirmed to be minima by the absence of imaginary frequencies upon calculations of the normal vibrational modes.
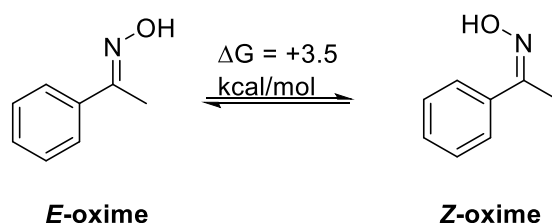

E-oxime $\Delta G = +3.5$ kcal/mol   *Z*-oxime

Table T2.2. *E*-oxime.

C	-4.5555867775	1.6296984809	-0.4644314364
C	-3.2485857325	2.027612322	-0.1741110594
C	-2.2742944906	1.081097958	0.1177535949
C	-2.5841397973	-0.2889648224	0.1263647565
C	-3.8981084489	-0.6761211915	-0.1662943934
C	-4.875444818	0.2753698384	-0.459213544
H	-5.3202202483	2.3751196207	-0.6936186776
H	-2.9875374133	3.0883076579	-0.1756335376
H	-1.2525605626	1.3870349479	0.3450231816
H	-4.1747142864	-1.7316210059	-0.1688698715
H	-5.8936919975	-0.0491063178	-0.6845496139
C	-1.5389000883	-1.3038906745	0.4393872629
C	-1.8921355715	-2.7640892901	0.4462119417
H	-2.2691615986	-3.0730054877	-0.540509626
H	-1.0176799424	-3.3722029696	0.6961486027
H	-2.6860205271	-2.9641100905	1.1816483265
N	-0.366853362	-0.8515629255	0.6909718357
O	0.5604437477	-1.8168735943	0.9726249042
H	1.3614170051	-1.3098933459	1.1324208829

Energy = -439.7277692

Zero-point correction = 0.156424 (Hartree/Particle)

Thermal correction to Gibbs Free Energy = 0.120932

Sum of electronic and zero-point Energies = -439.571345

Sum of electronic and thermal Energies =   -439.562344

Sum of electronic and thermal Enthalpies =   -439.561400

Sum of electronic and thermal Free Energies =   -439.606837

Table T2.3. Z-oxime.

| C	-4.6267165278	1.6042961878	-0.4537507606
C	-3.4511050519	2.0141785639	0.1744162526
C	-2.4287120747	1.1019870964	0.4202865662
C	-2.5704278267	-0.2441027664	0.0517460934
C	-3.7630016658	-0.6470556707	-0.5652968492
C	-4.7787933203	0.270118722	-0.8254490603
H	-5.4241172649	2.3240772243	-0.651353023
H	-3.3262926158	3.0571231901	0.4739074716
H	-1.5088570146	1.4315735784	0.9016922557
H	-3.8996534757	-1.689836122	-0.85890182
H	-5.6952578586	-0.0617374186	-1.3181800137
C	-1.5135702579	-1.2540267539	0.349678123
C	-1.9345322864	-2.5992495279	0.8751973376
H	-2.5192395038	-3.1562959504	0.126660609
H	-1.0454480274	-3.1900066681	1.1281859709
H	-2.5676578824	-2.4870735523	1.7685867995
N	-0.2510054157	-1.090627075	0.2089415532
O	0.1174640706	0.1307008737	-0.2949304344
H	1.0740041797	0.0568571288	-0.3574072815

Energy = -439.723061

Zero-point correction = 0.156298 (Hartree/Particle)

Thermal correction to Gibbs Free Energy =   0.121820

Sum of electronic and zero-point Energies =   -439.566763

Sum of electronic and thermal Energies =   -439.557820

Sum of electronic and thermal Enthalpies =   -439.556875

Sum of electronic and thermal Free Energies =   -439.601241

2.11 NMR Spectra of Oximes and O-alkylated Oximes
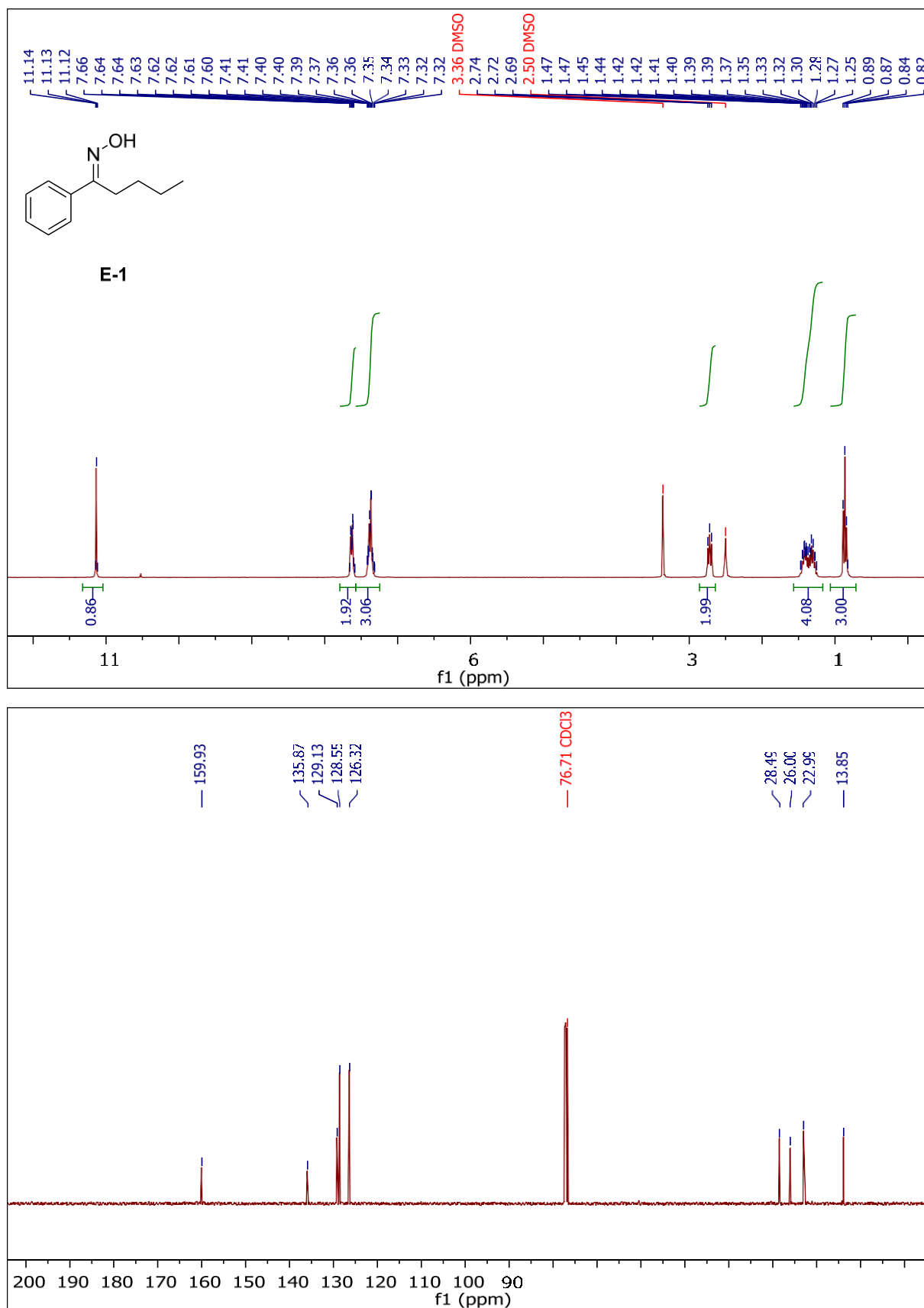
Spectrum S2.8. Compound **E-1**, ^{1}H- and ^{13}C-NMR (DMSO-*d*).
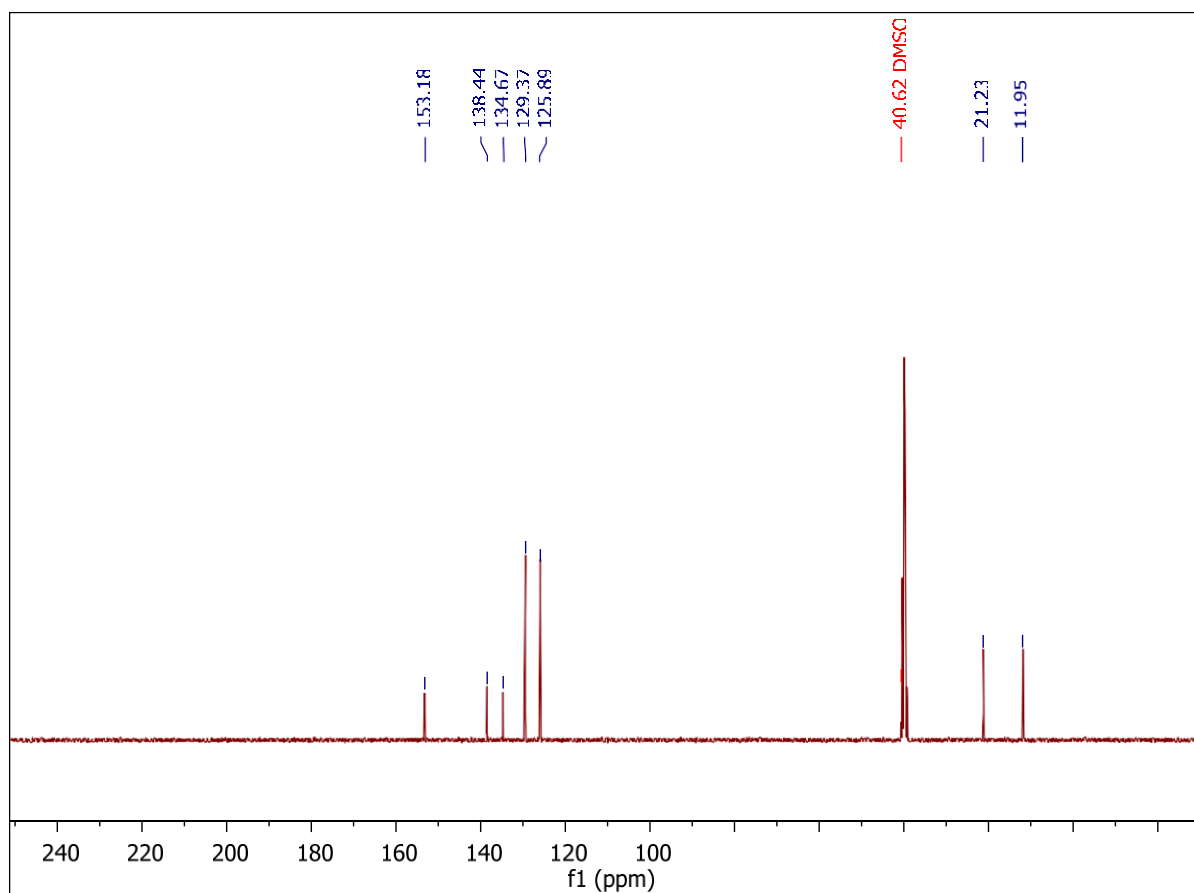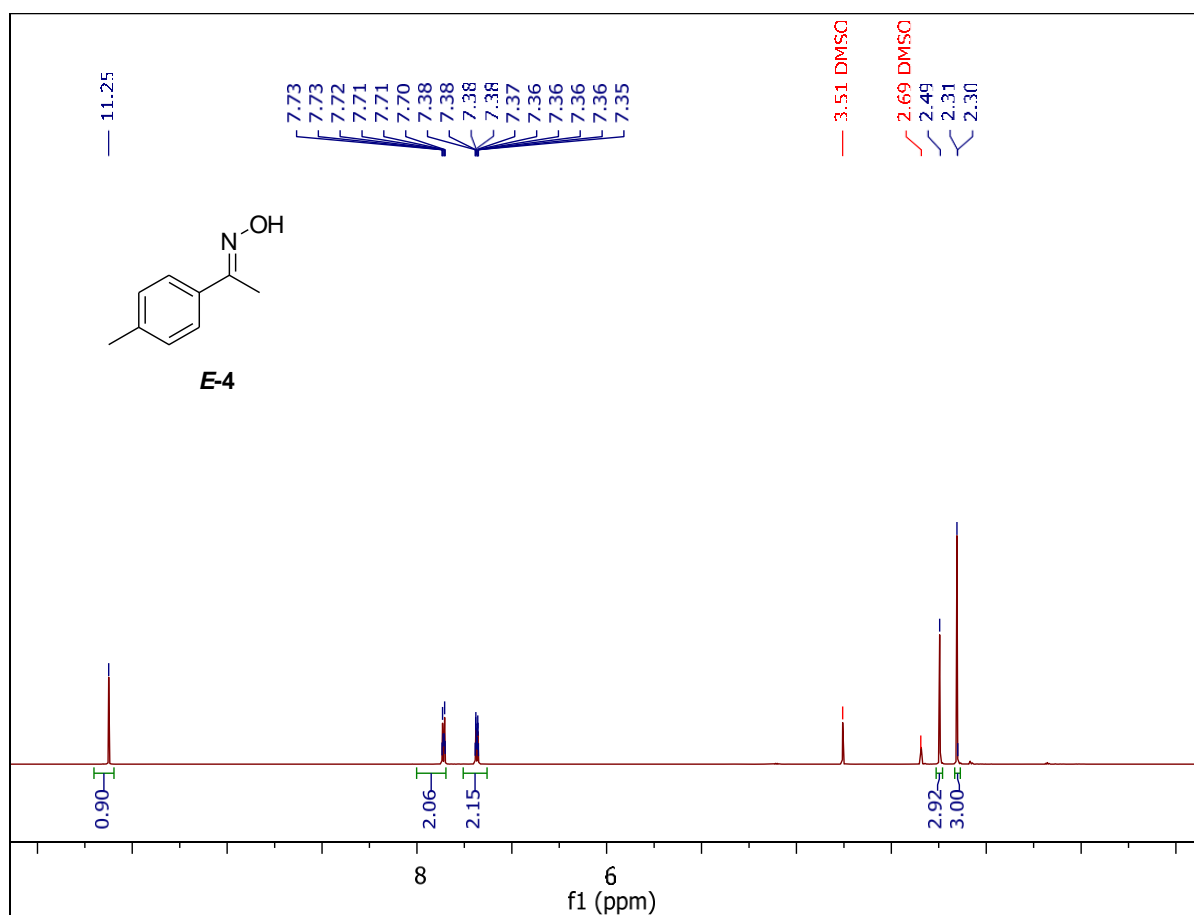
Spectrum S2.9. Compound **E-4**, ^{1}H- and ^{13}C-NMR (DMSO-*d*).
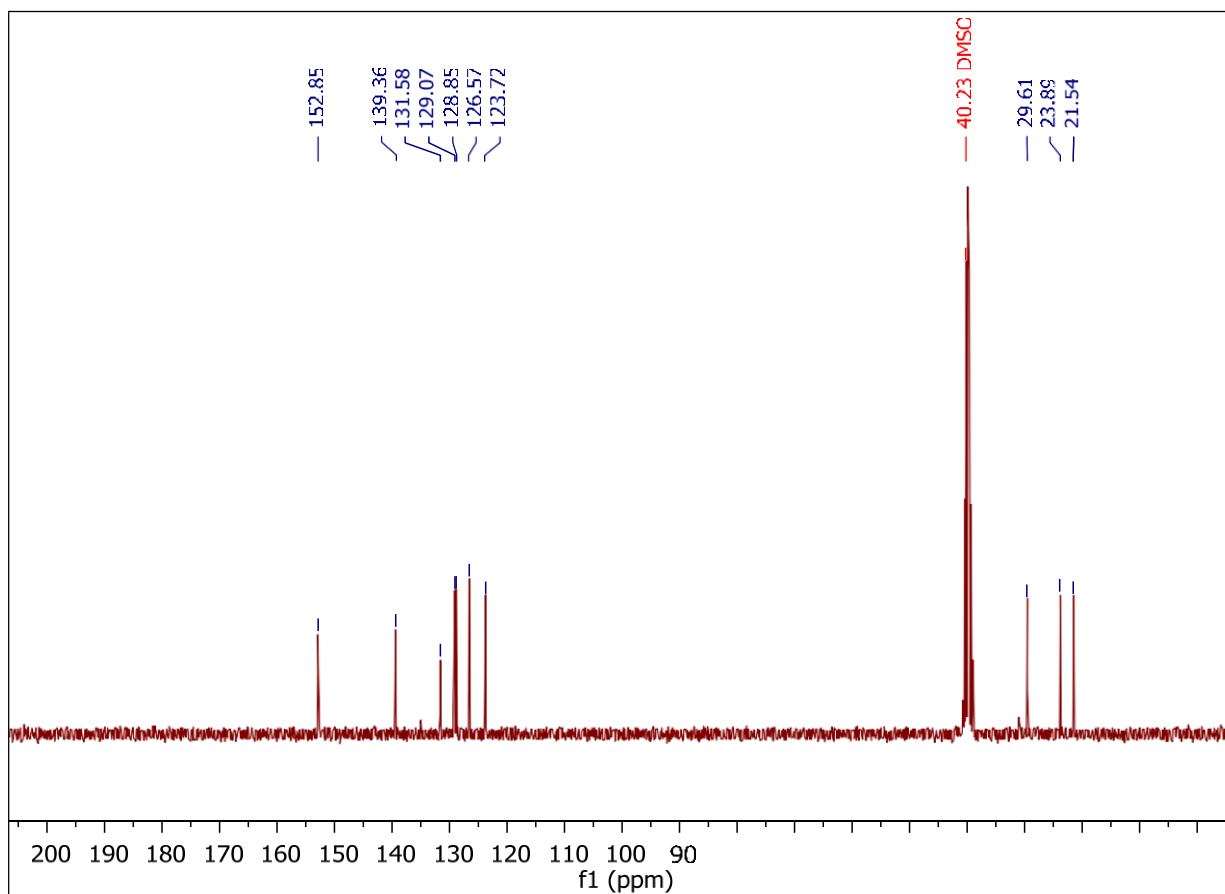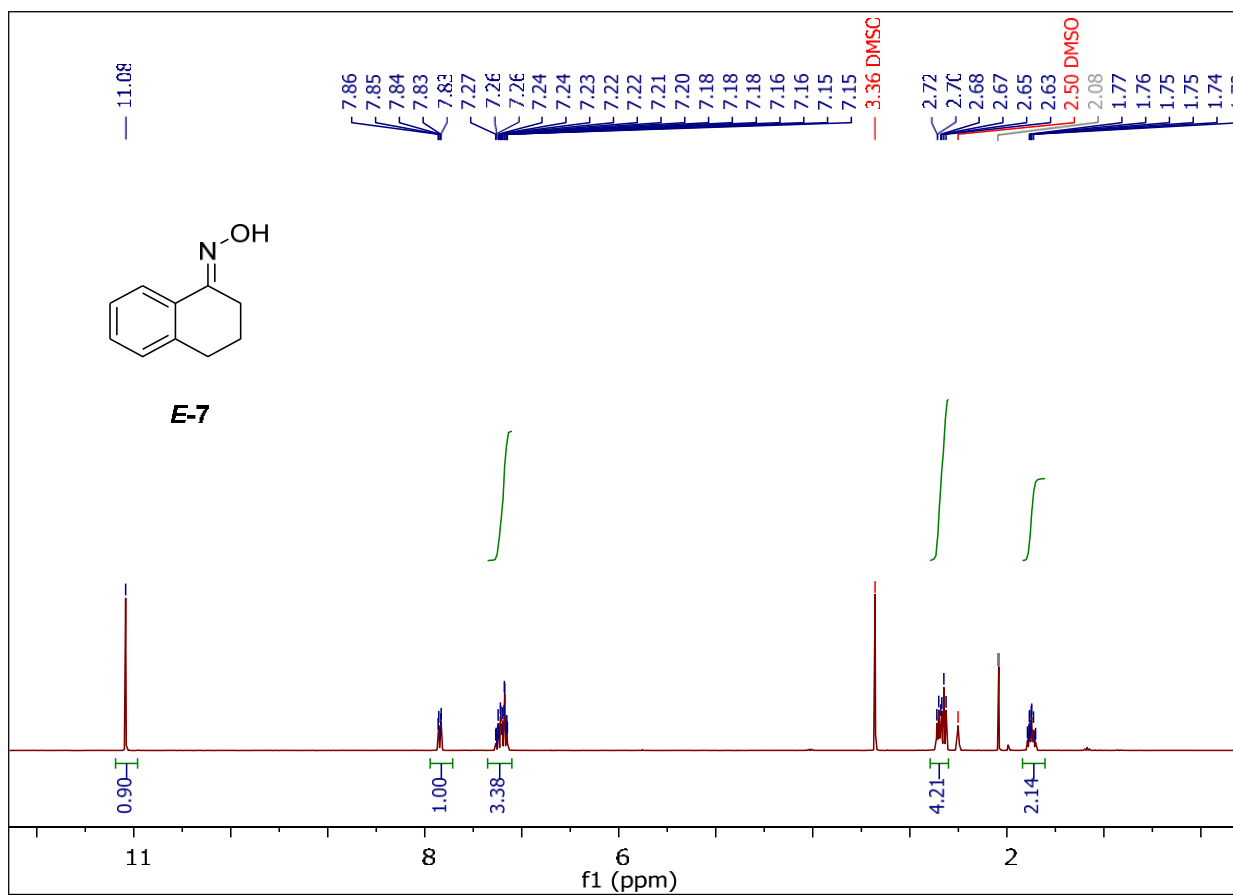
Spectrum S2.10. Compound **E-7**, ^{1}H- and ^{13}C-NMR (DMSO-d).
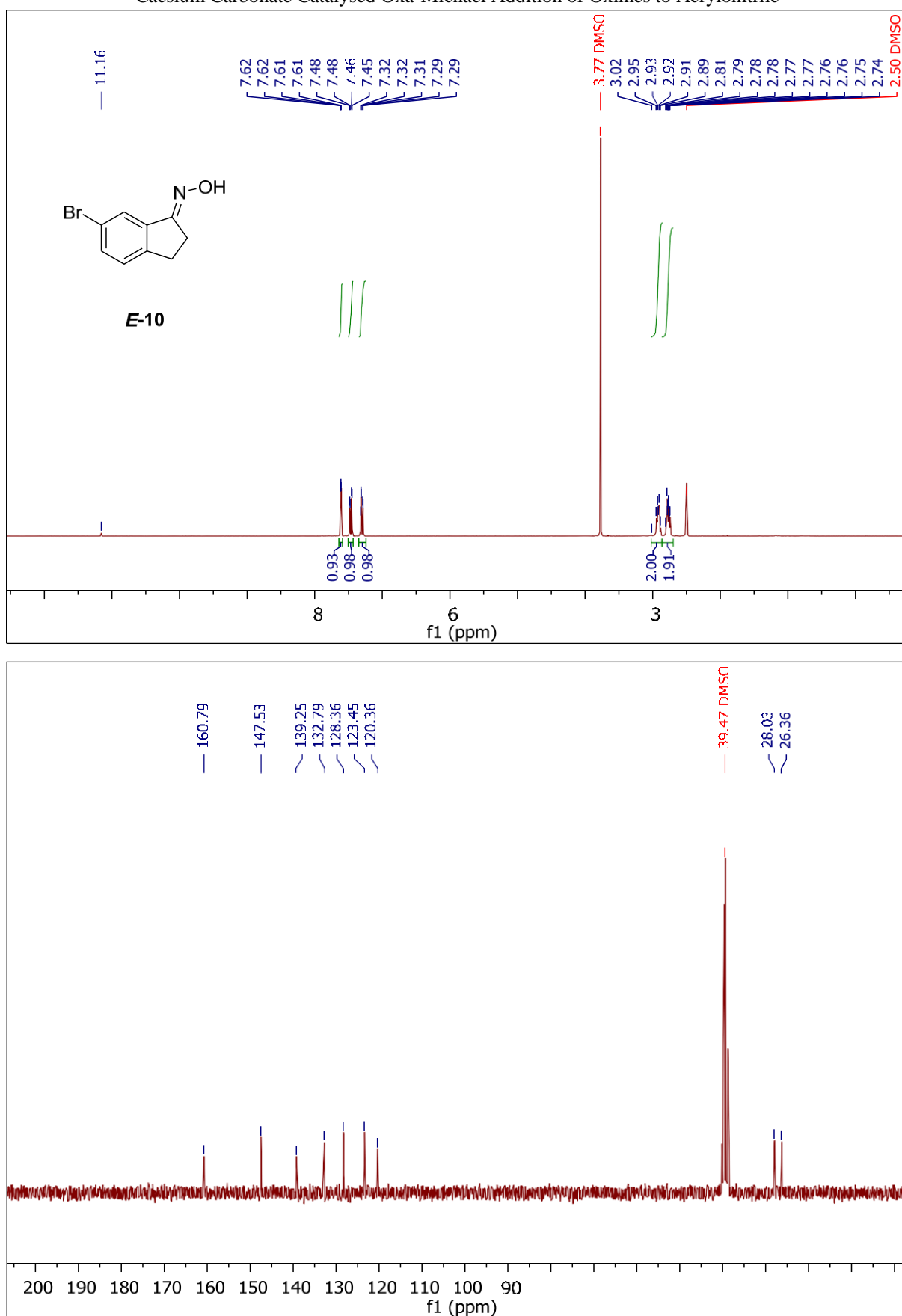
Spectrum S2.11. Compound **E-10**, ¹H- and ¹³C-NMR (DMSO-*d*).
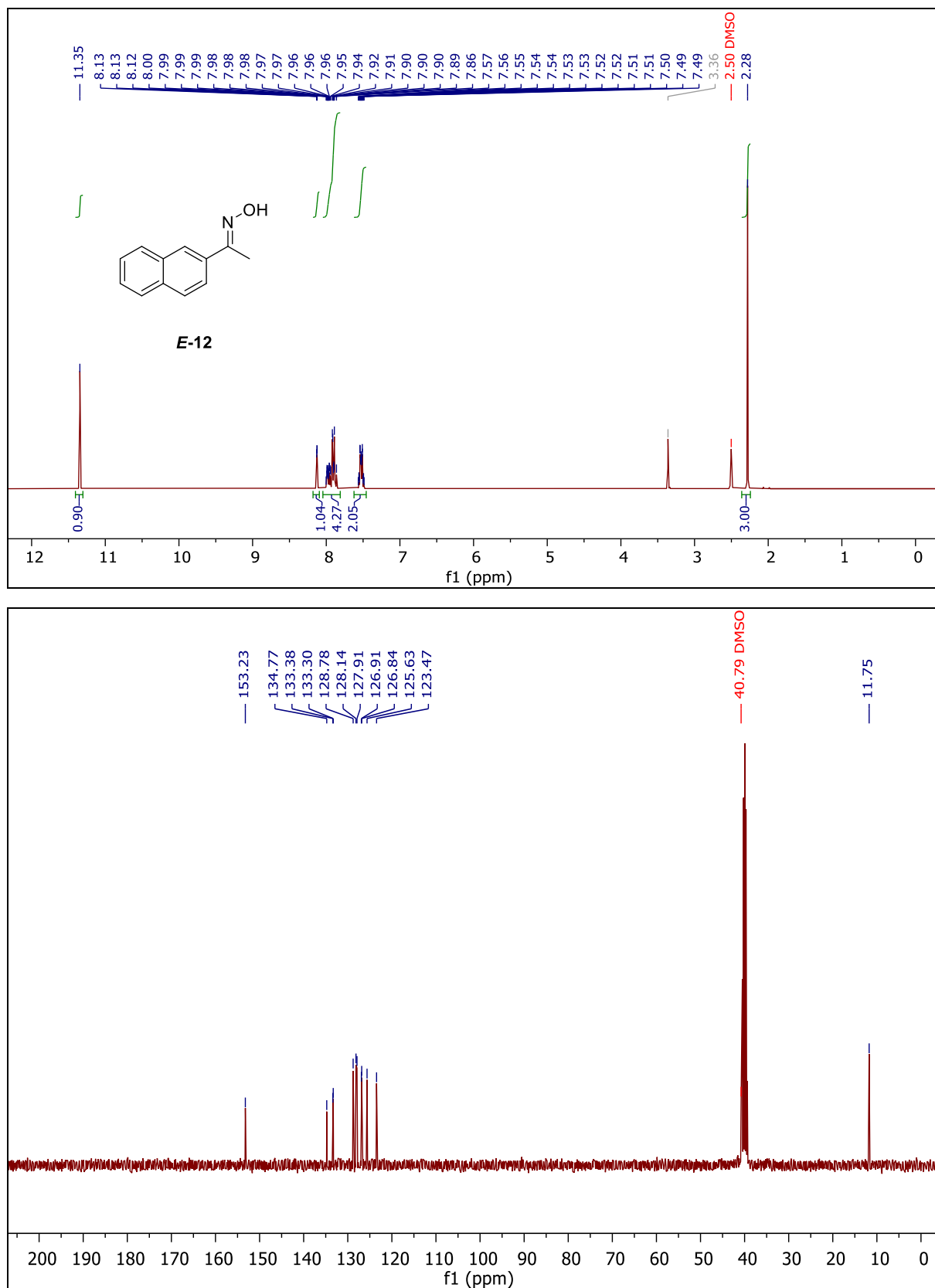
Spectrum S2.12. Compound ***E*-12**, ^{1}H- and ^{13}C-NMR (DMSO-*d*).
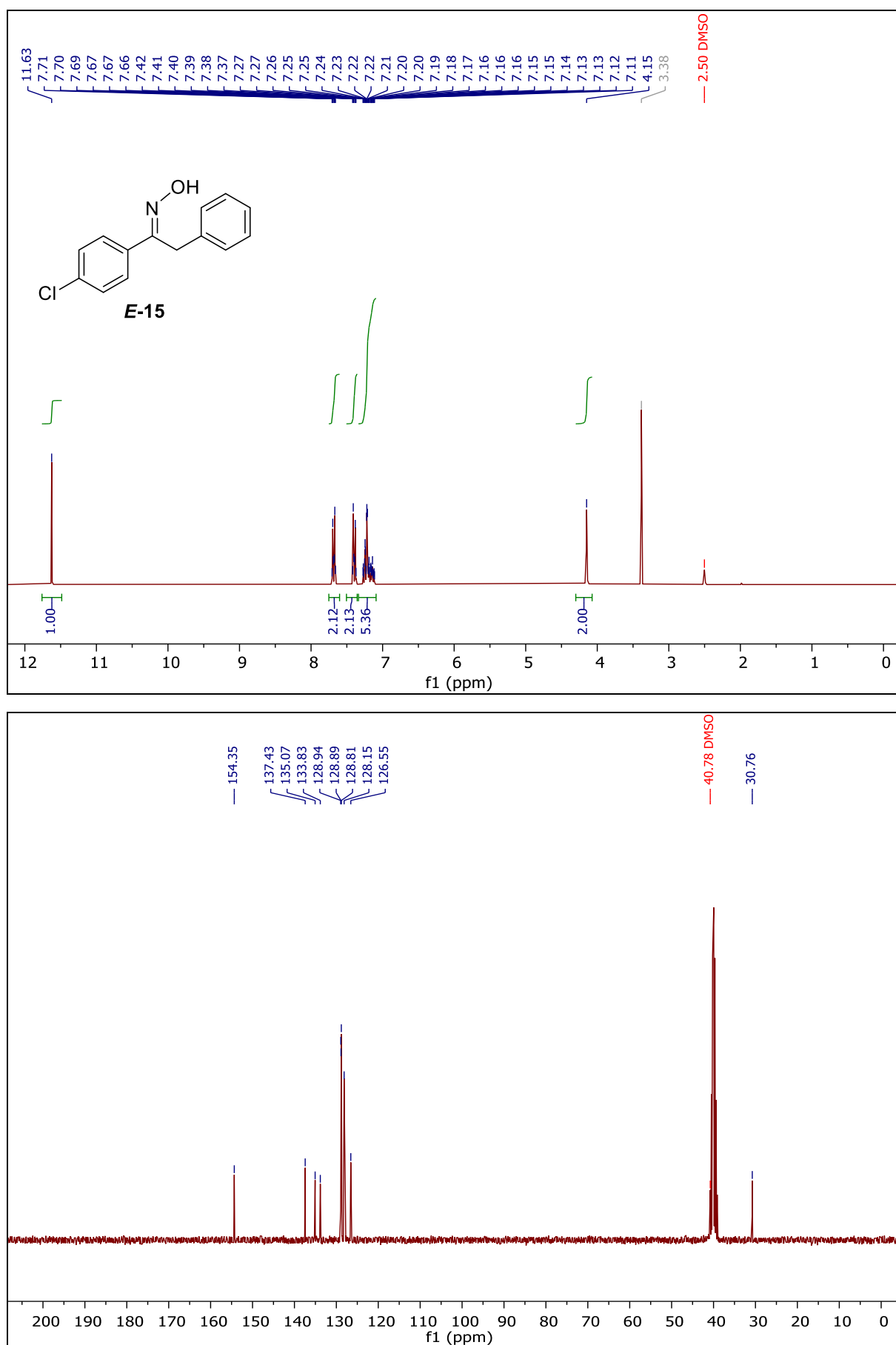
Spectrum S2.13. Compound ***E*-15**, ^{1}H- and ^{13}C-NMR (DMSO-*d*).
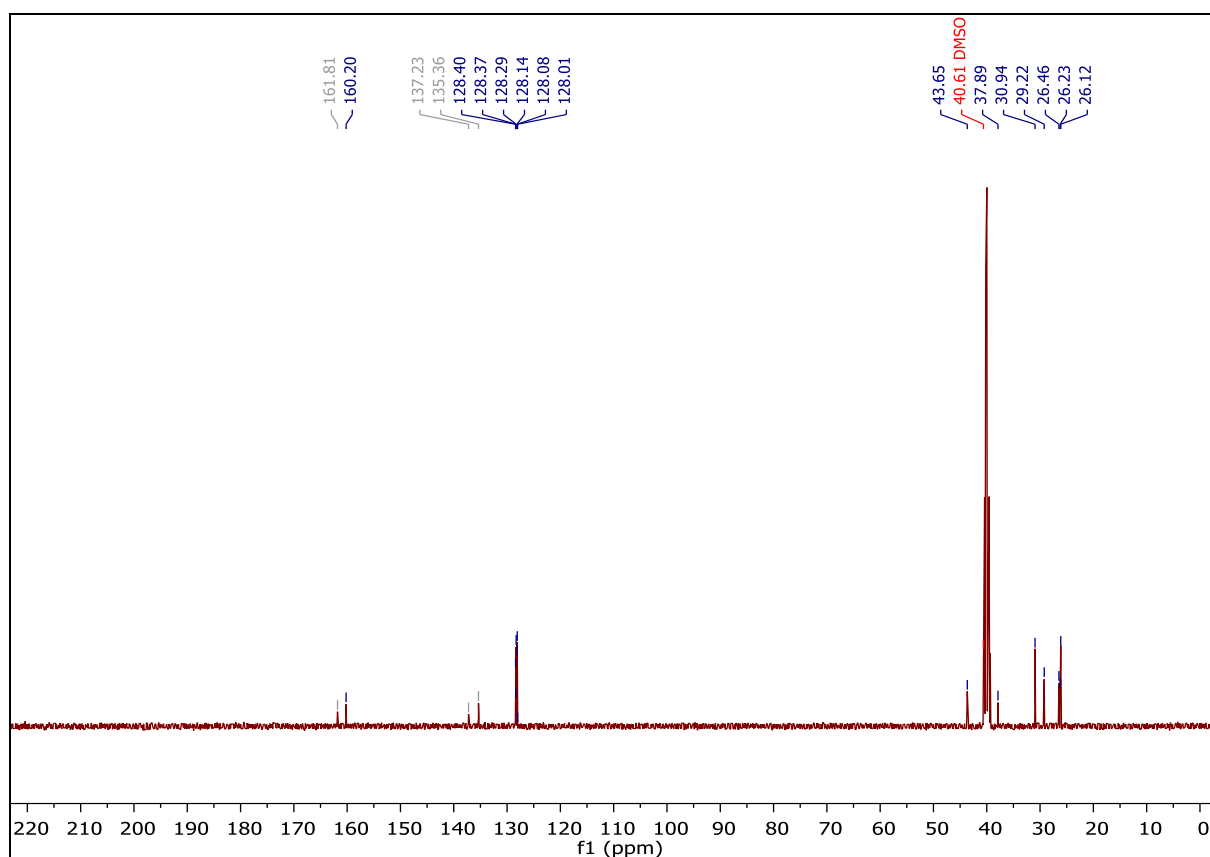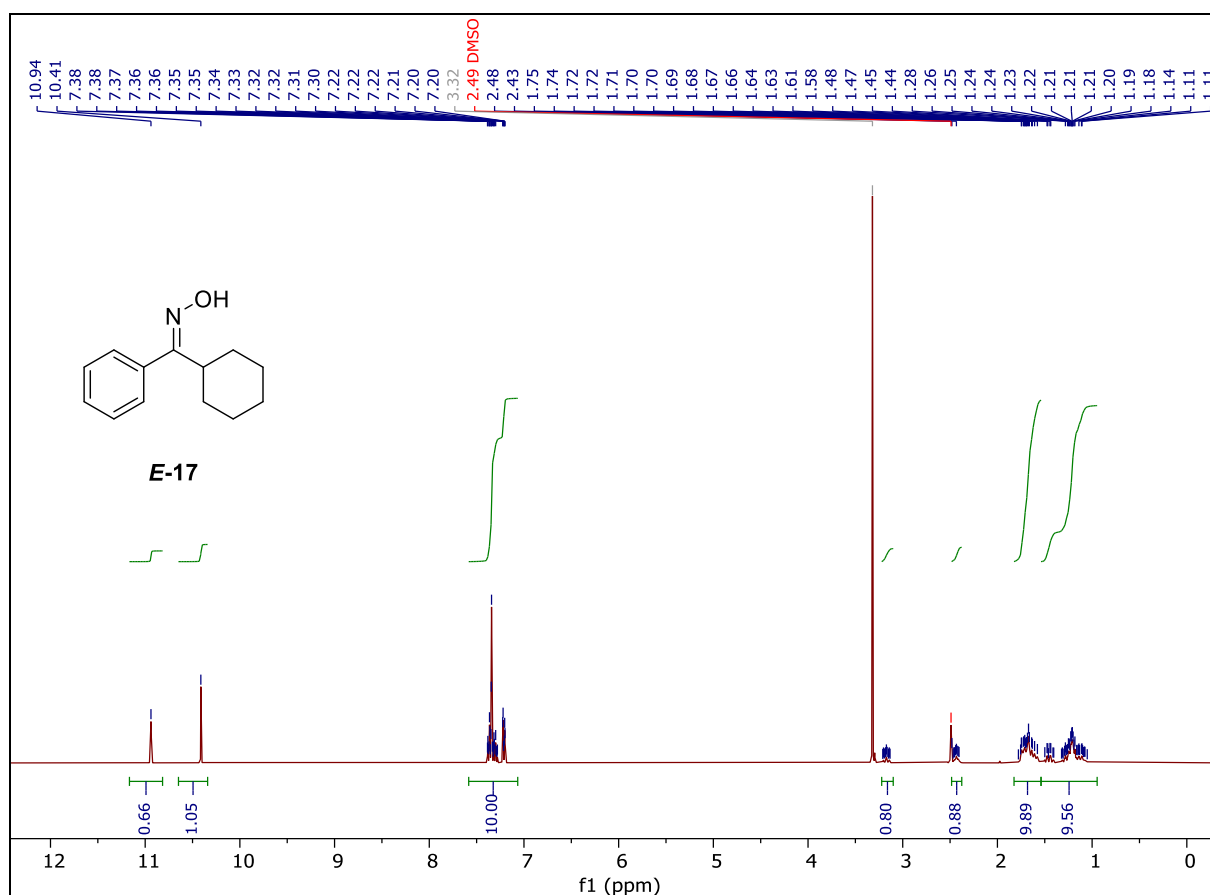
Spectrum S2.14. Compound **E-17**, ^{1}H- and ^{13}C-NMR (DMSO-*d*), *E:Z* (61:39%).
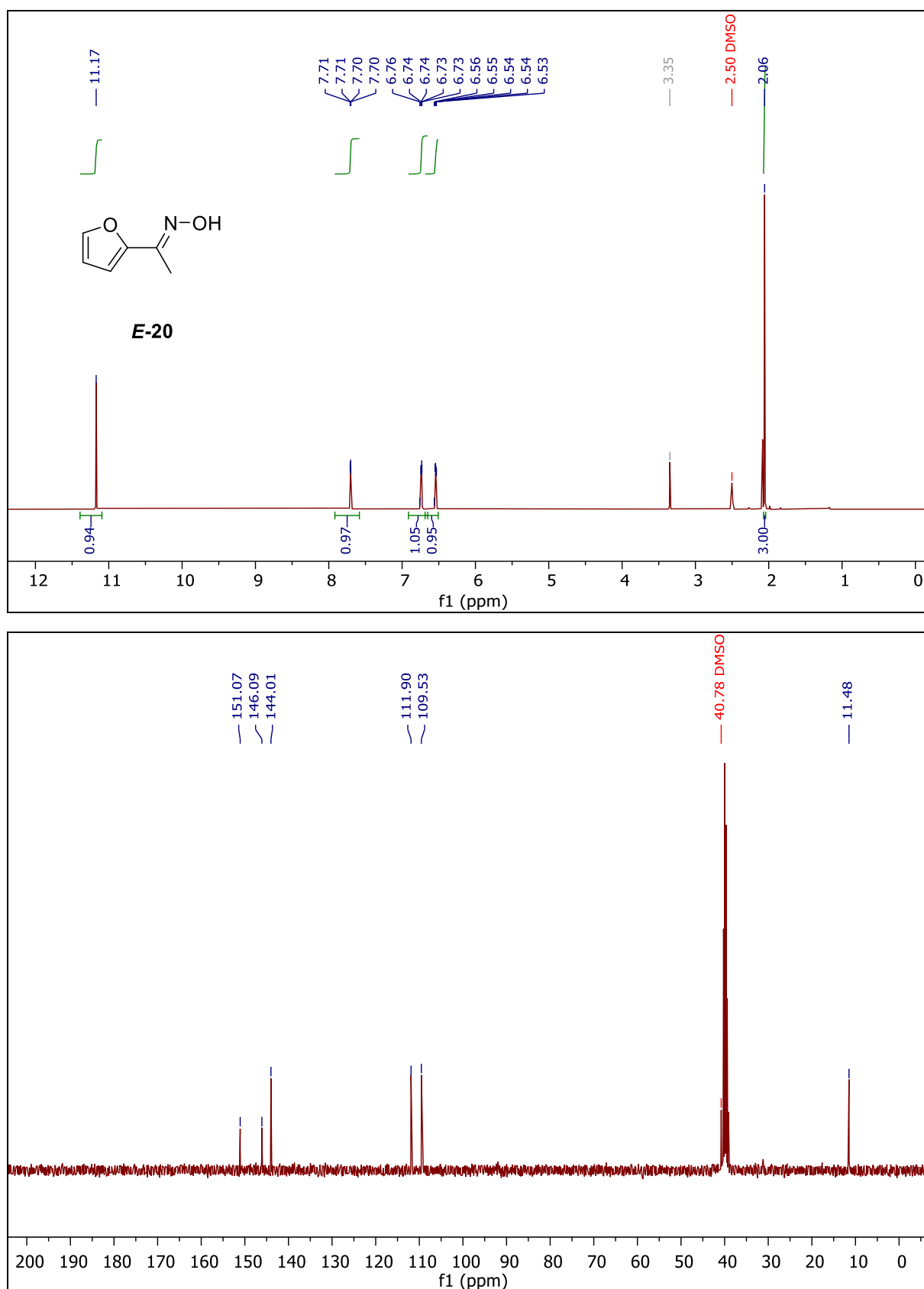
Spectrum S2.15. Compound **E-20**, ^{1}H- and ^{13}C-NMR (DMSO-*d*).
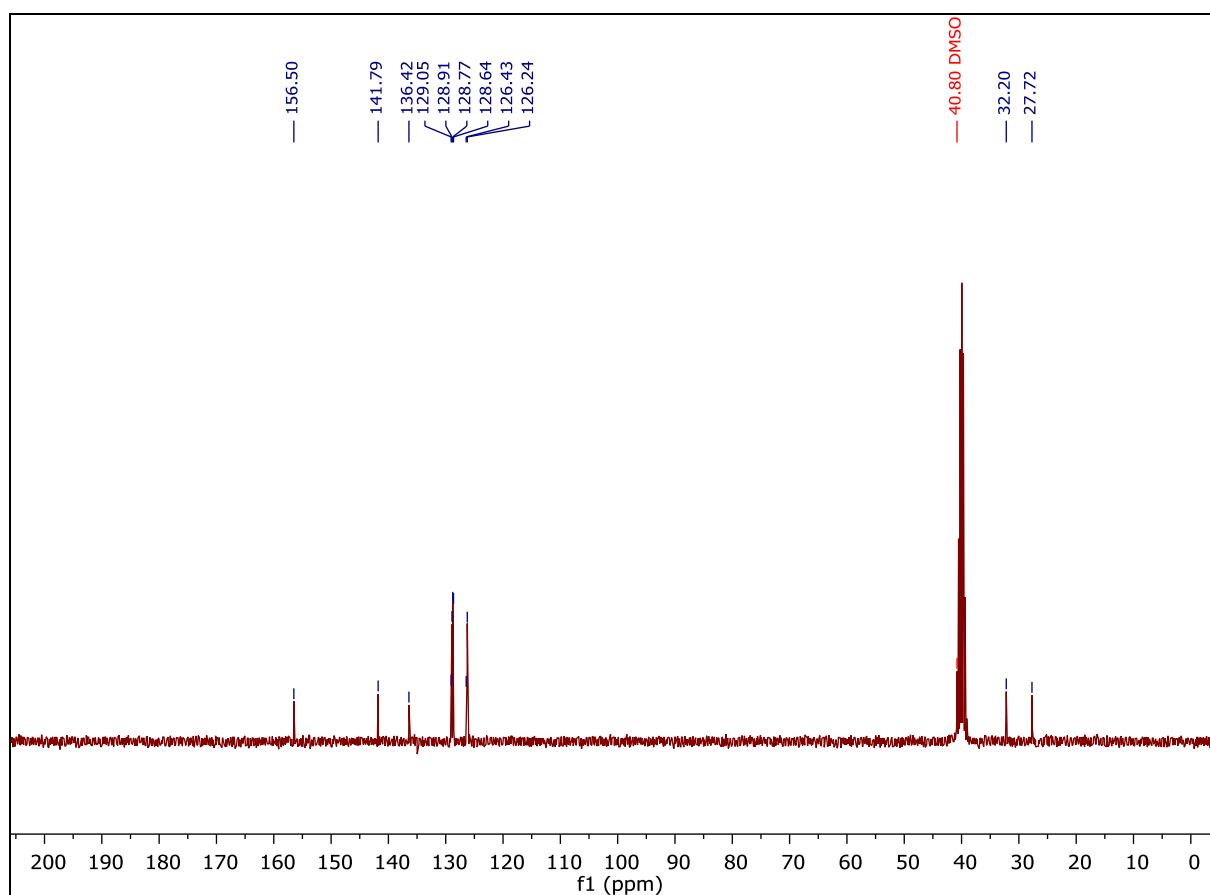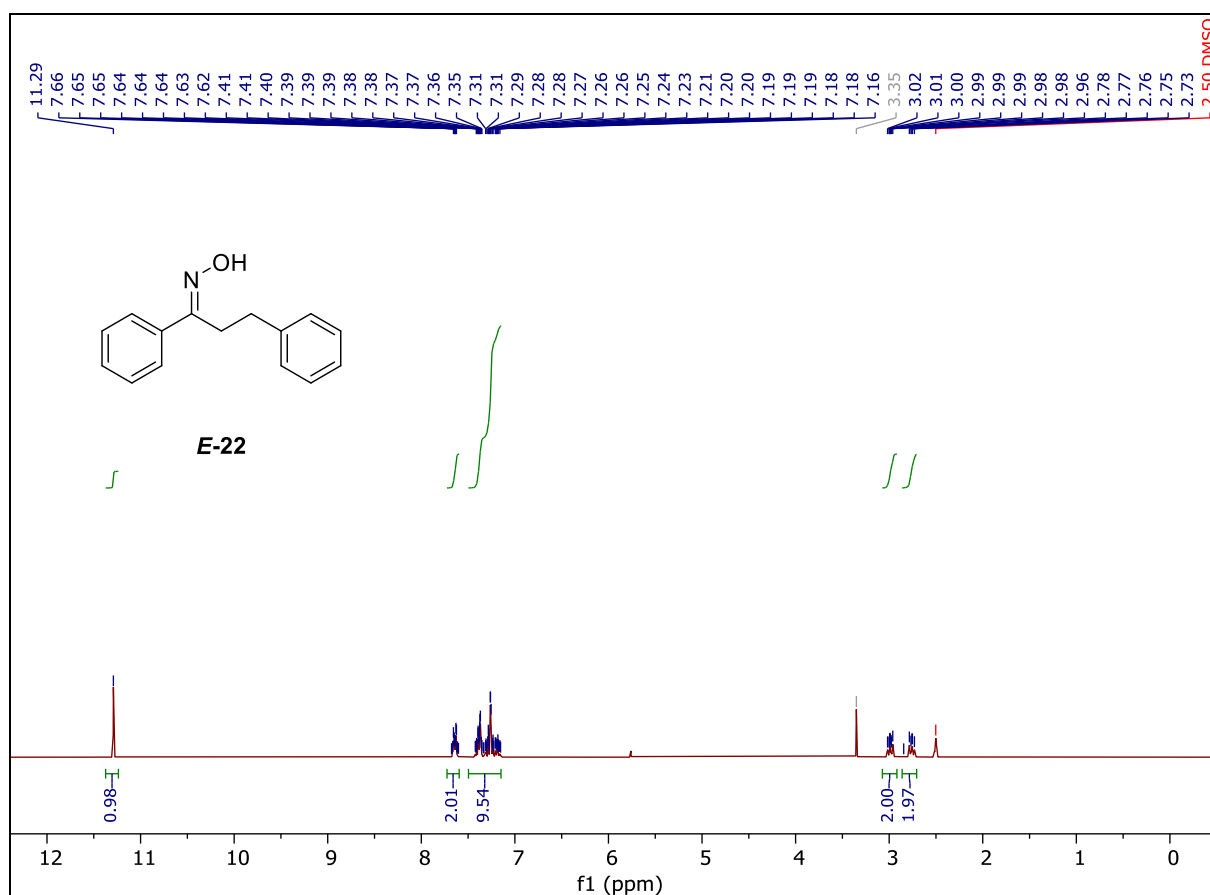
Spectrum S2.16. Compound **E-22**, ¹H- and ¹³C-NMR (DMSO-*d*).
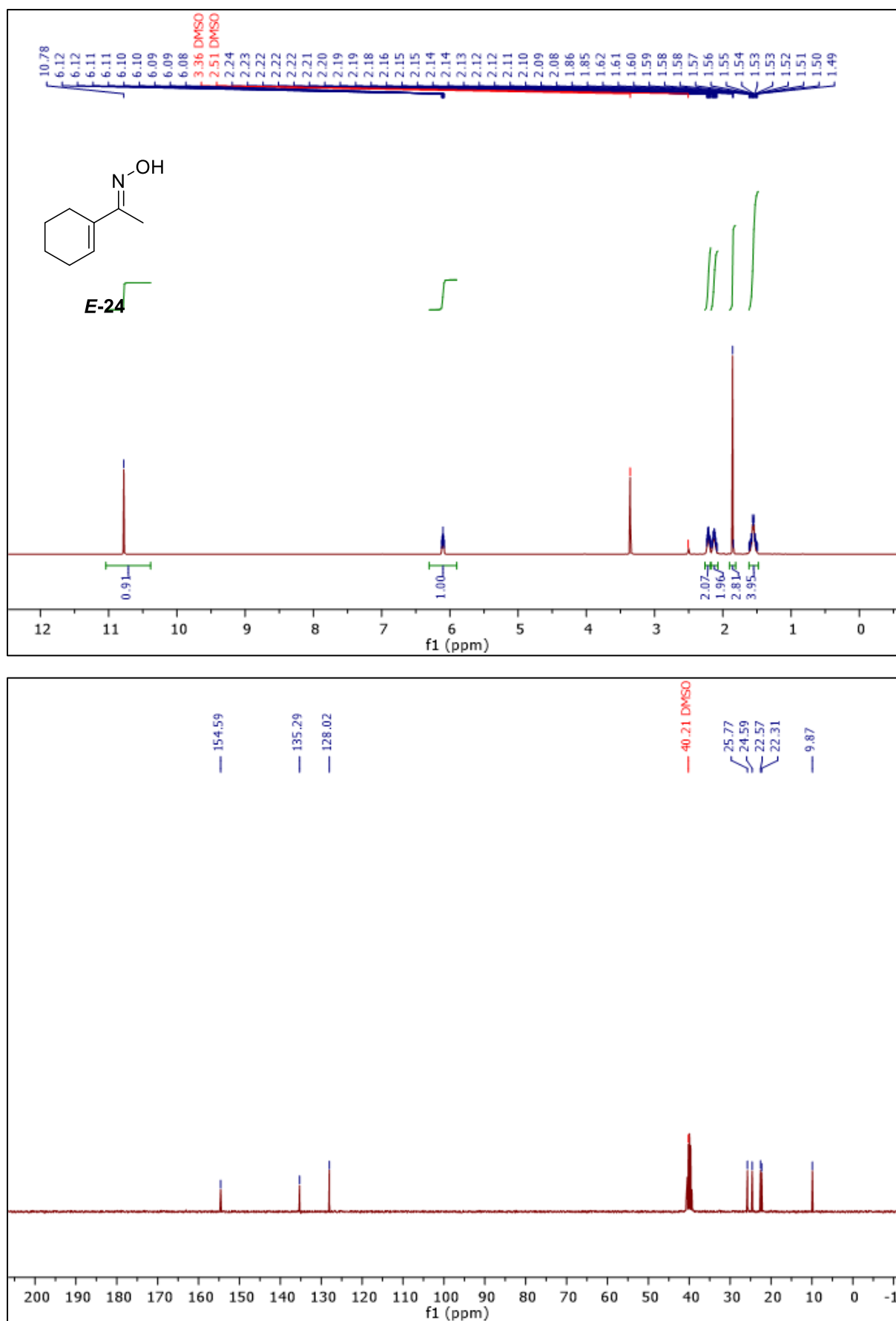
Spectrum S2.17. Compound ***E*-24**, ^{1}H- and ^{13}C-NMR (DMSO-*d*).
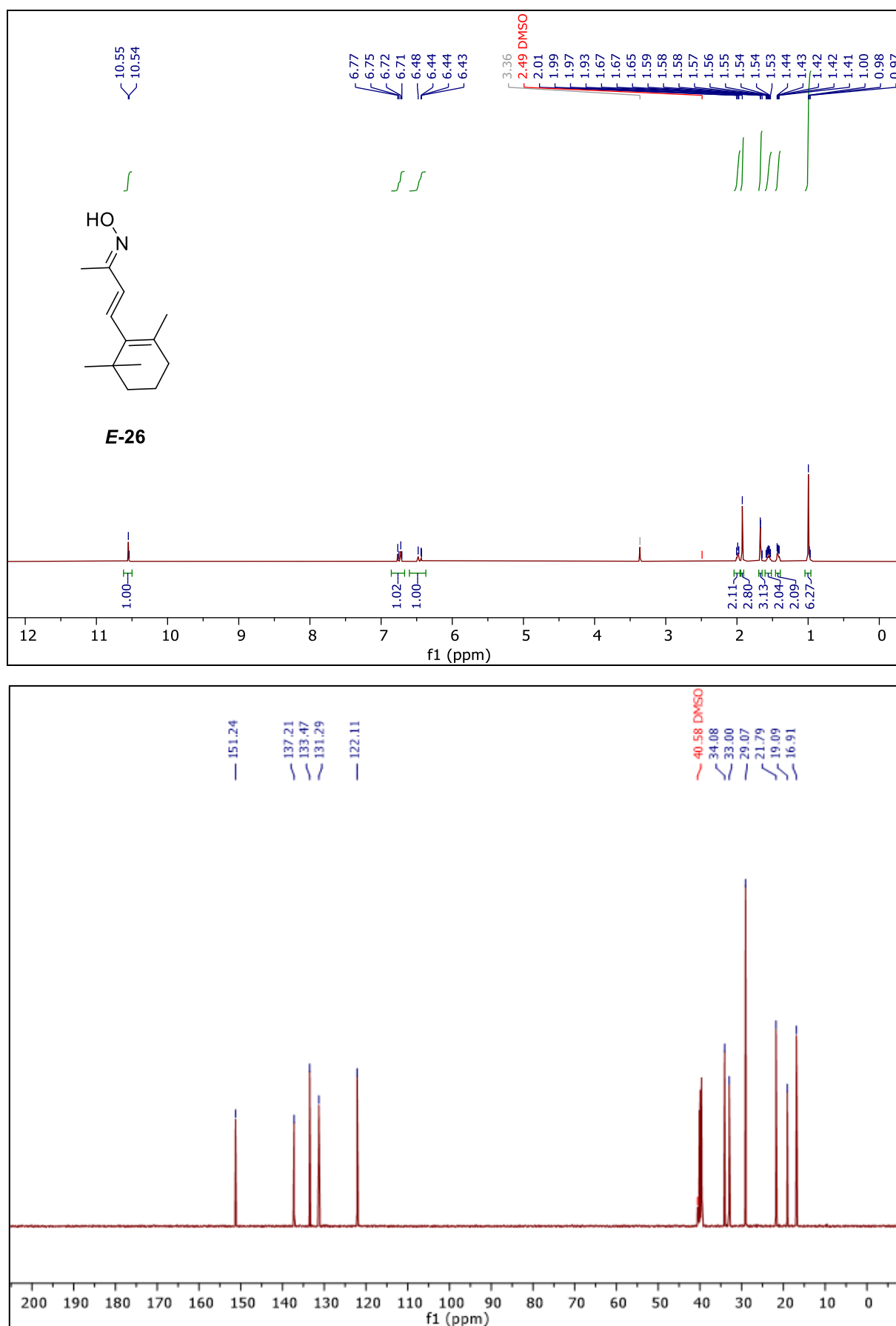
Spectrum S2.18. Compound **E-26**, ^{1}H- and ^{13}C-NMR (DMSO-*d*).
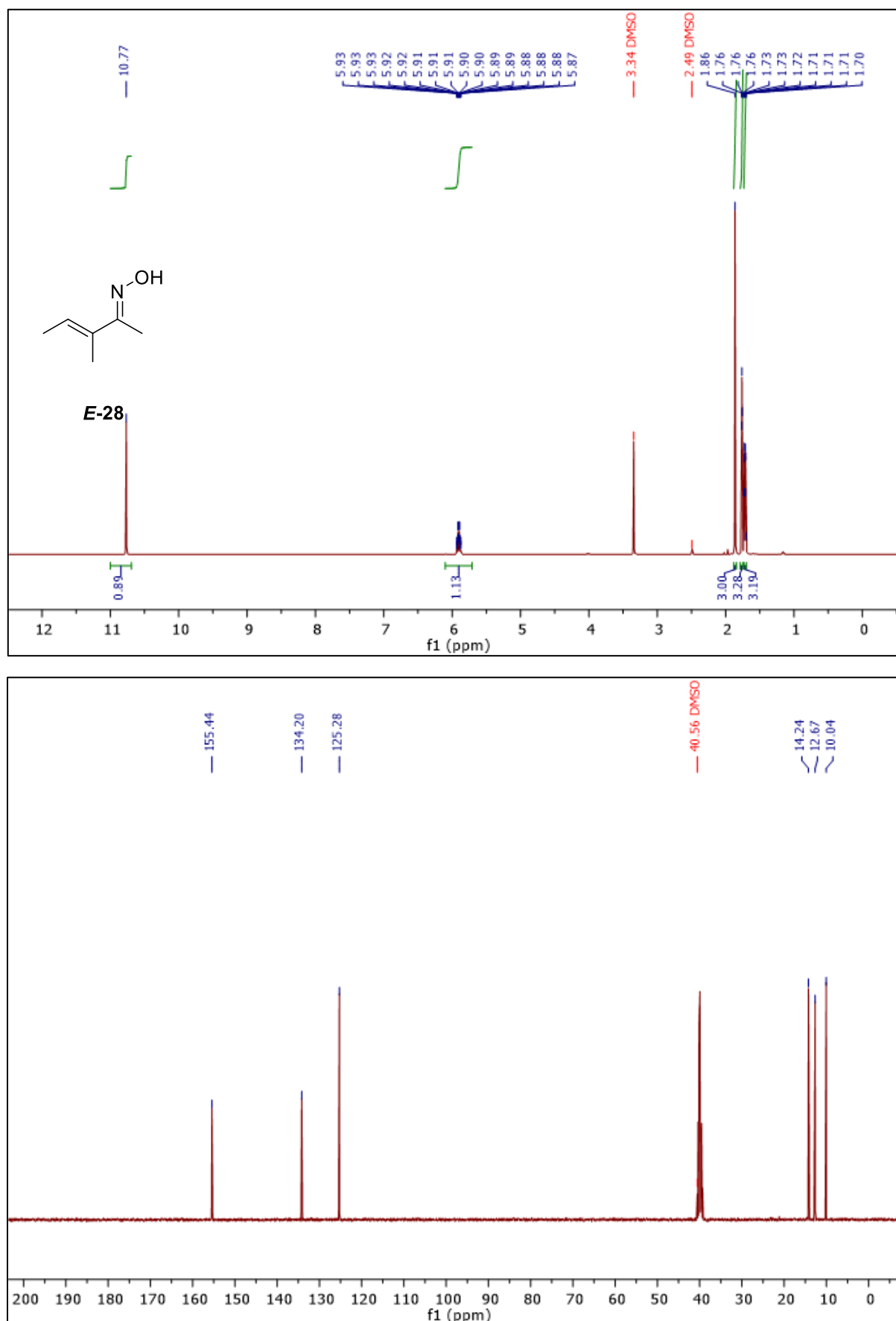
Spectrum S2.19. Compound ***E-28***, ^{1}H- and ^{13}C-NMR (DMSO-*d*).
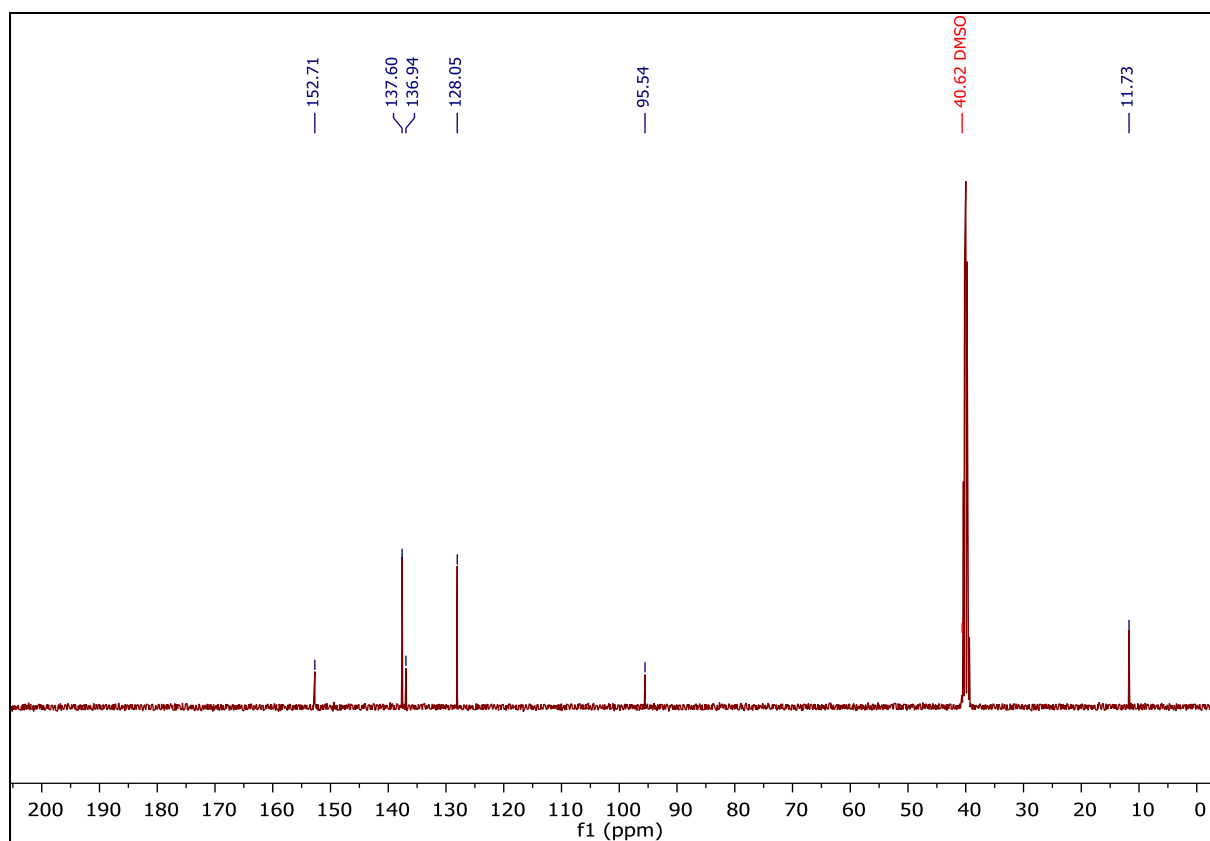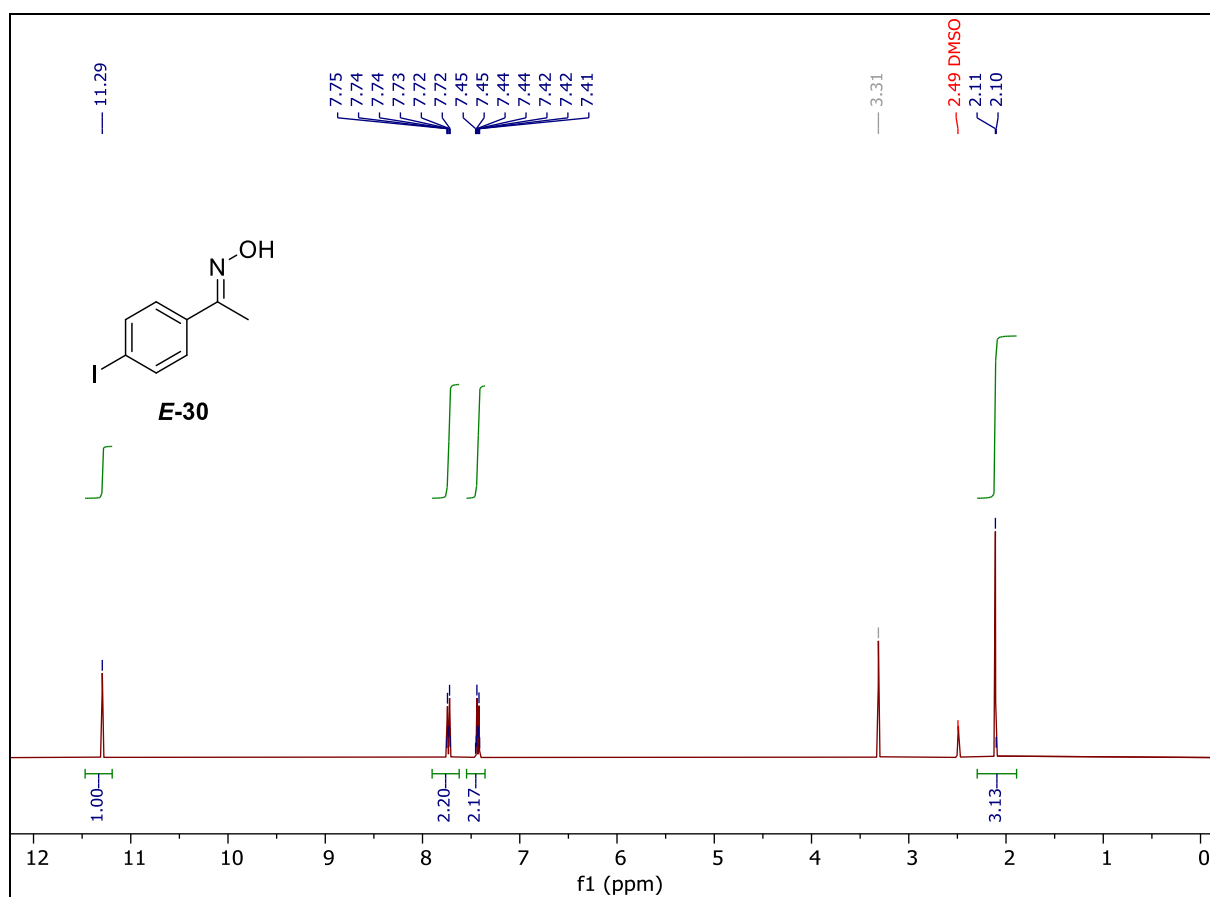
Spectrum S2.20. Compound *E-30*, ^{1}H- and ^{13}C-NMR (DMSO-*d*).
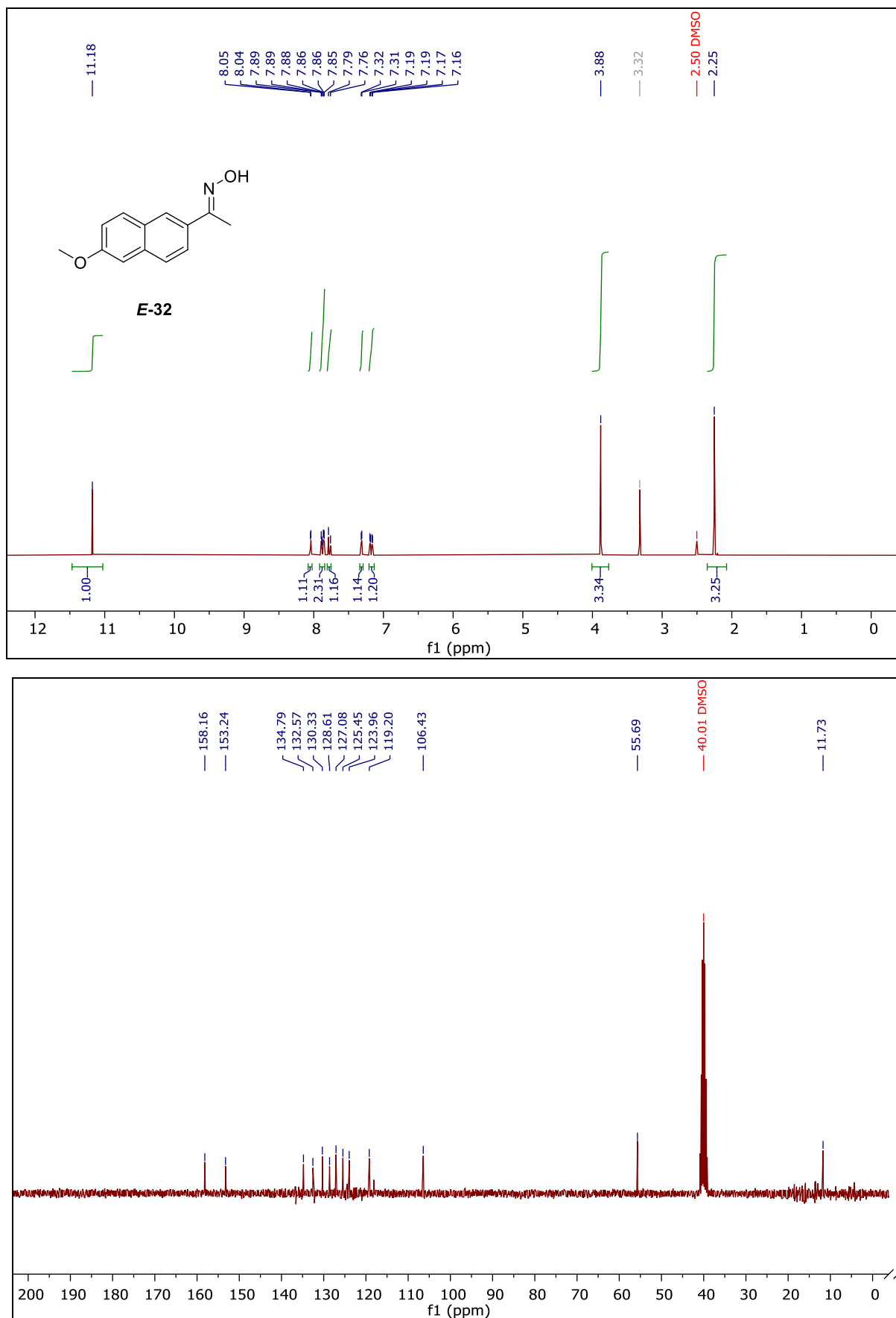
Spectrum S2.21. Compound **E-32**, ^{1}H- and ^{13}C-NMR (DMSO-*d*).
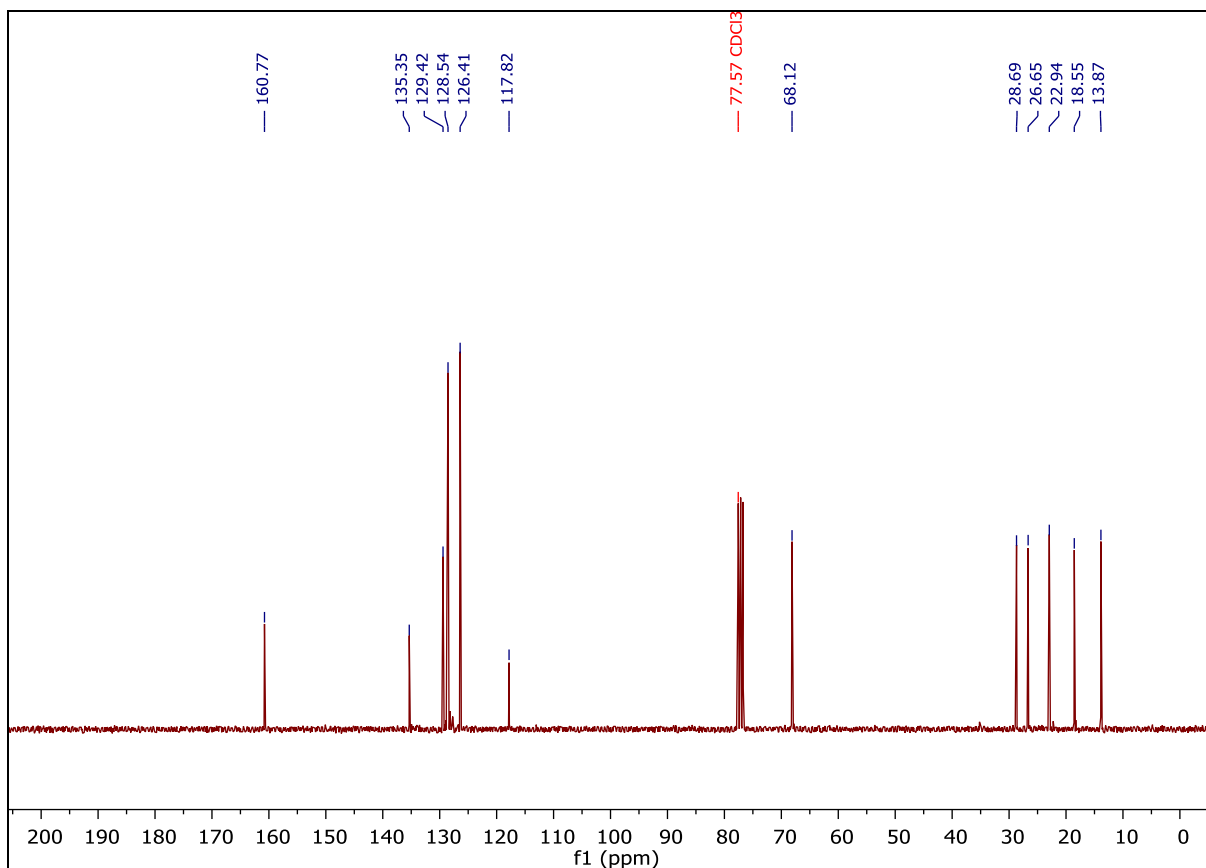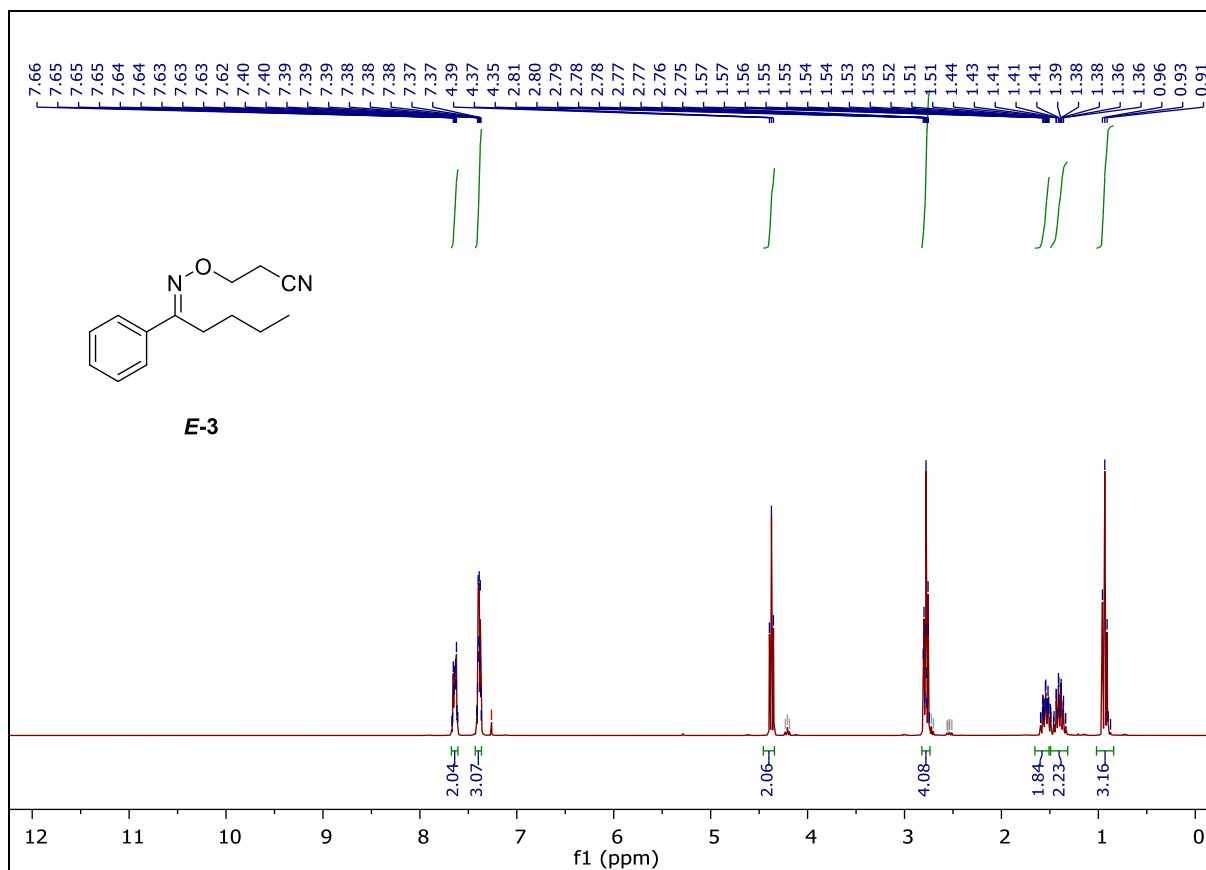
Spectrum S2.22. Compound **E-3**, ^{1}H- and ^{13}C-NMR (Chloroform-*d*).
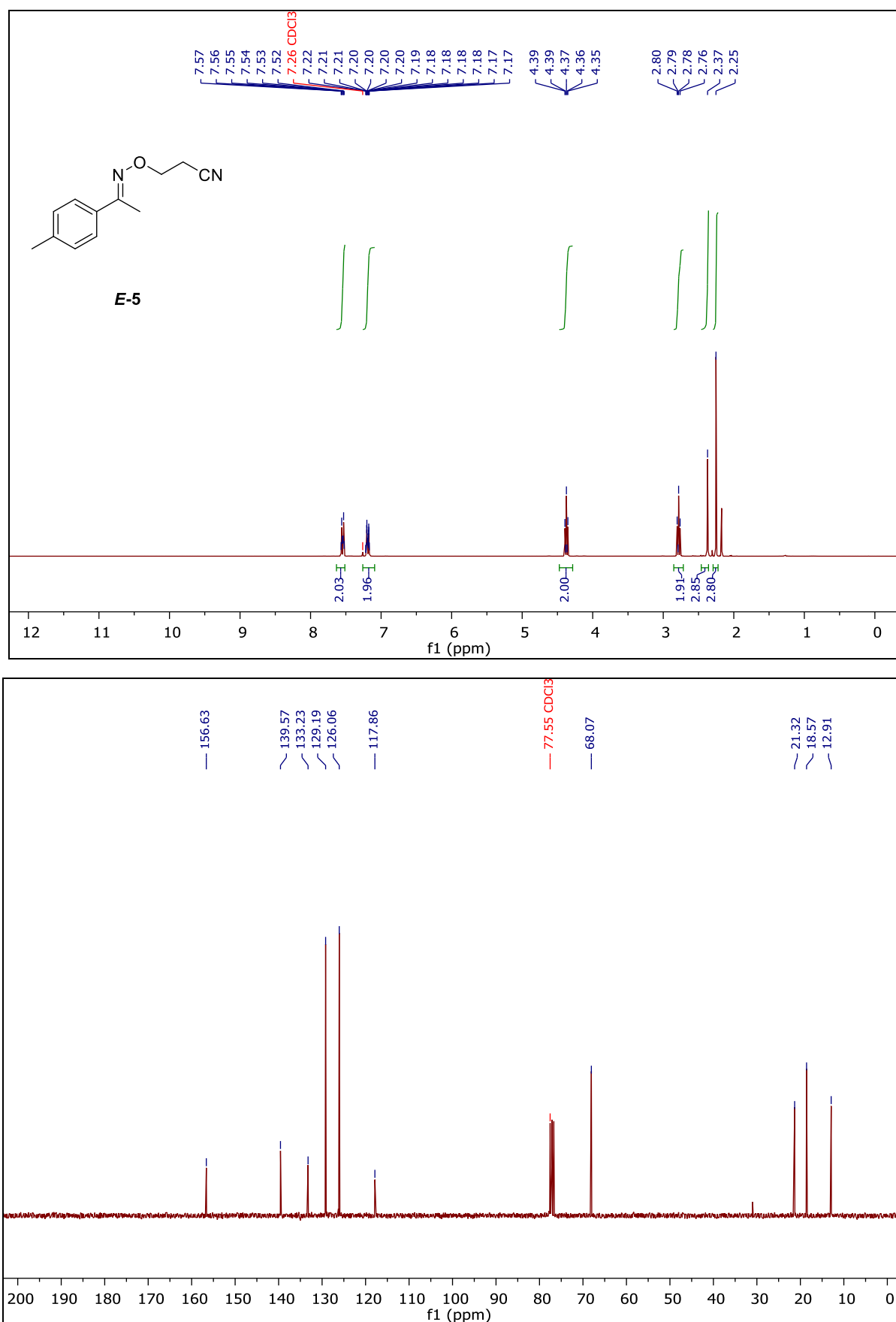
Spectrum S2.23. Compound **E-5**, ^{1}H- and ^{13}C-NMR (Chloroform-d).
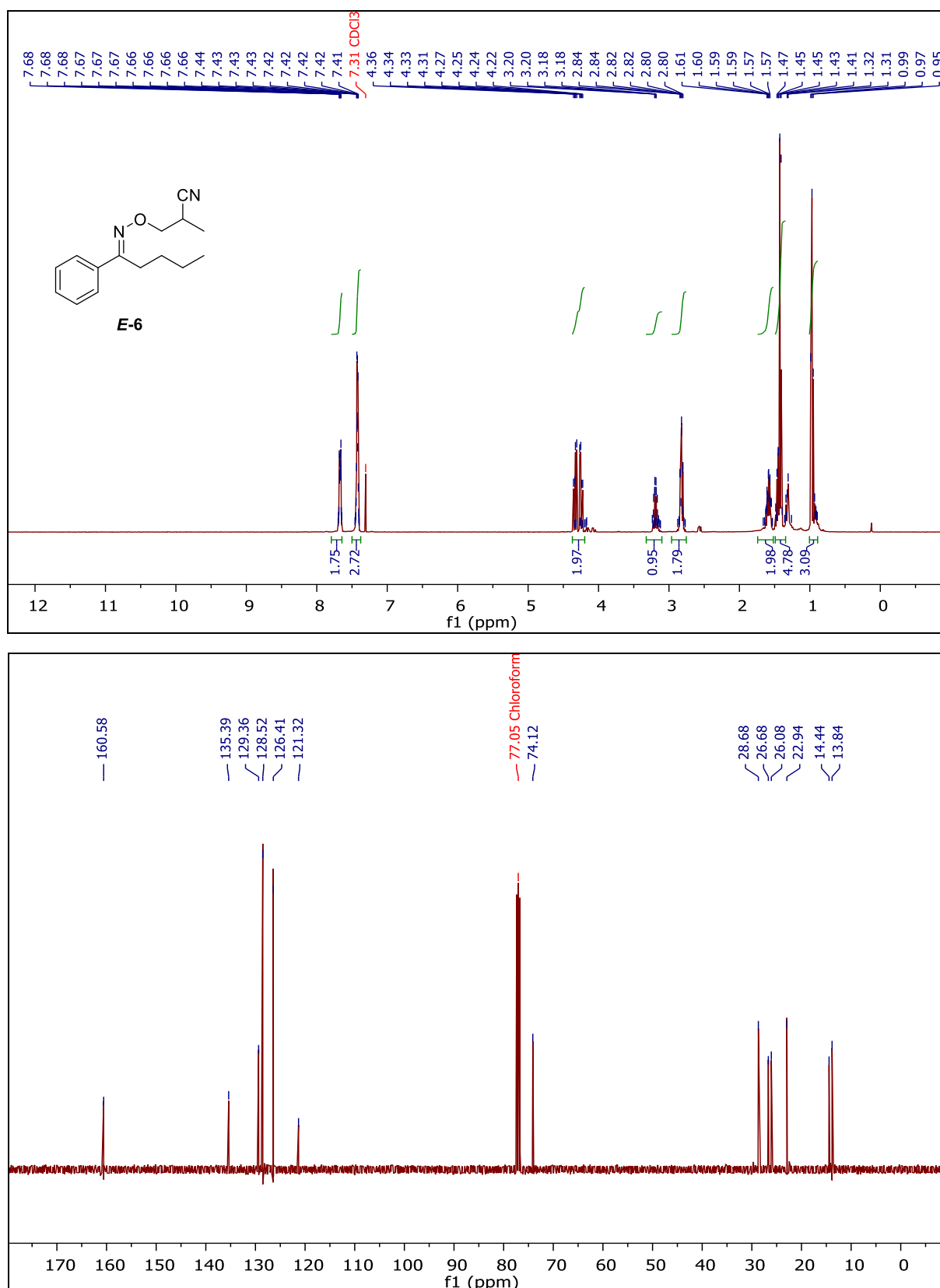
Spectrum S2.24. Compound **E-6**, ^{1}H- and ^{13}C-NMR (Chloroform-d).
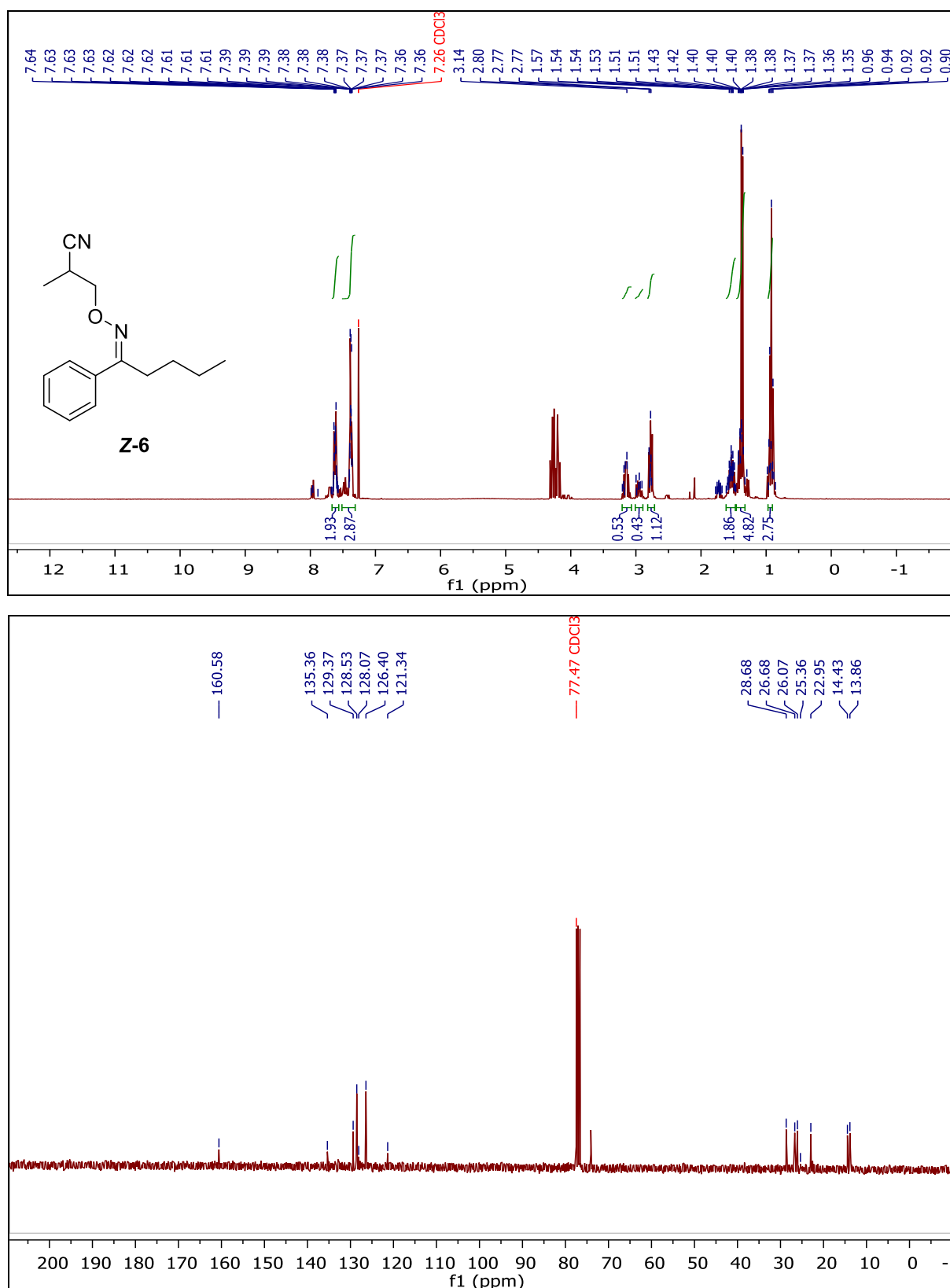
Spectrum S2.25. Compound **Z-6** in combination with **E-6,** [^1]H- and [^13]C-NMR (Chloroform-*d*), 80:20% from GC-FID.
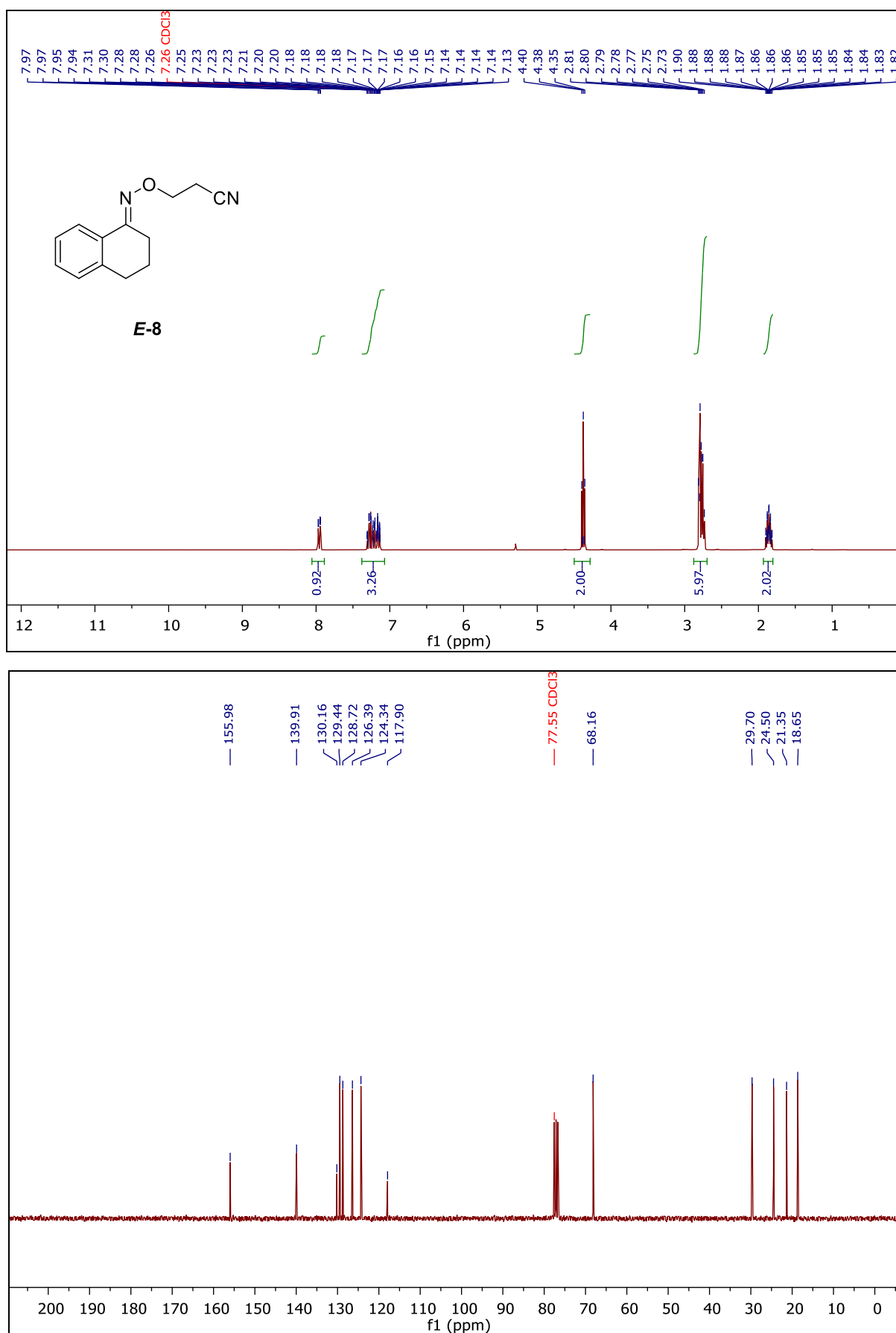
Spectrum S2.26. Compound **E-8**, ^{1}H- and ^{13}C-NMR (Chloroform-d).
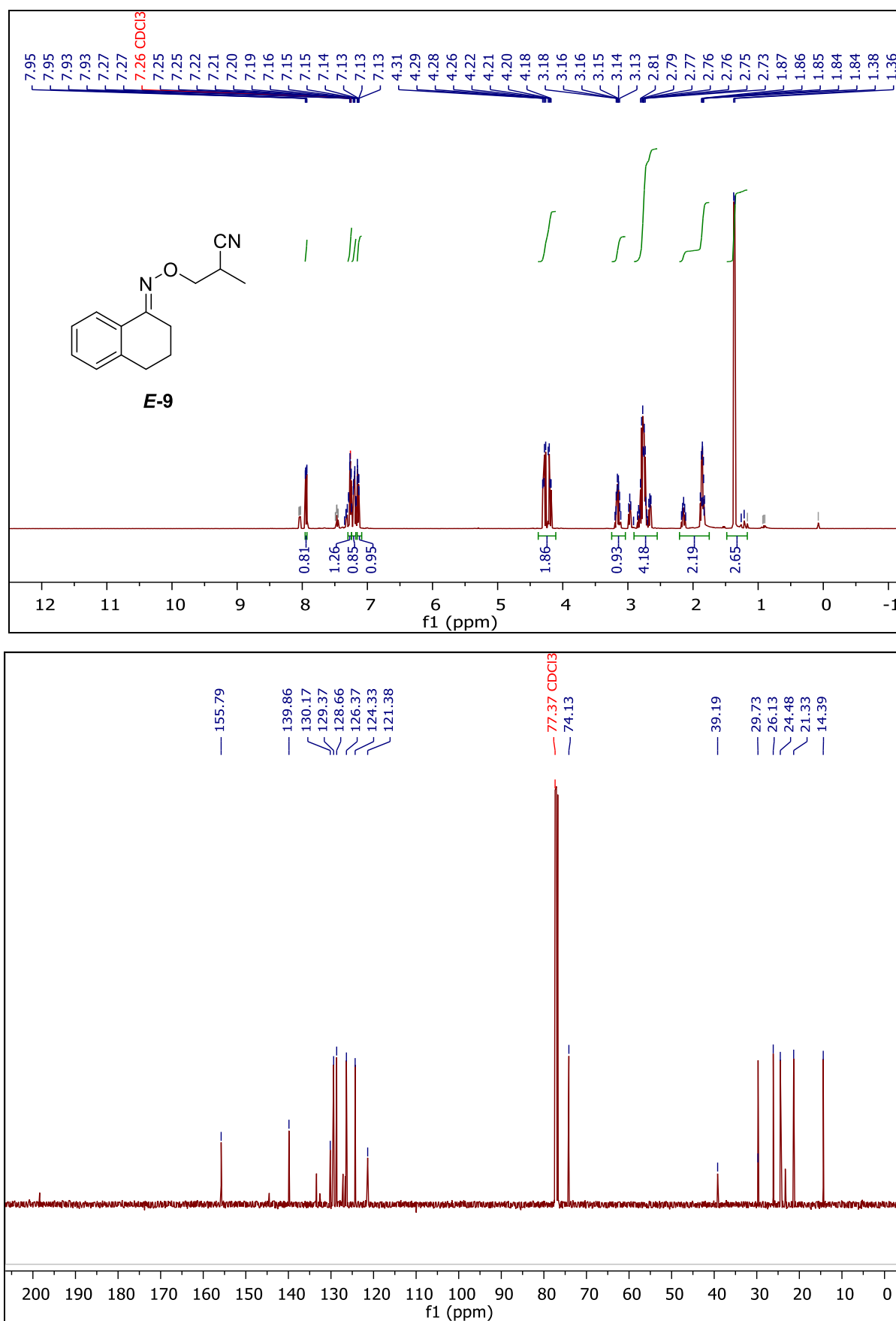
Spectrum S2.27. Compound **E-9**, ^{1}H- and ^{13}C-NMR (Chloroform-*d*).
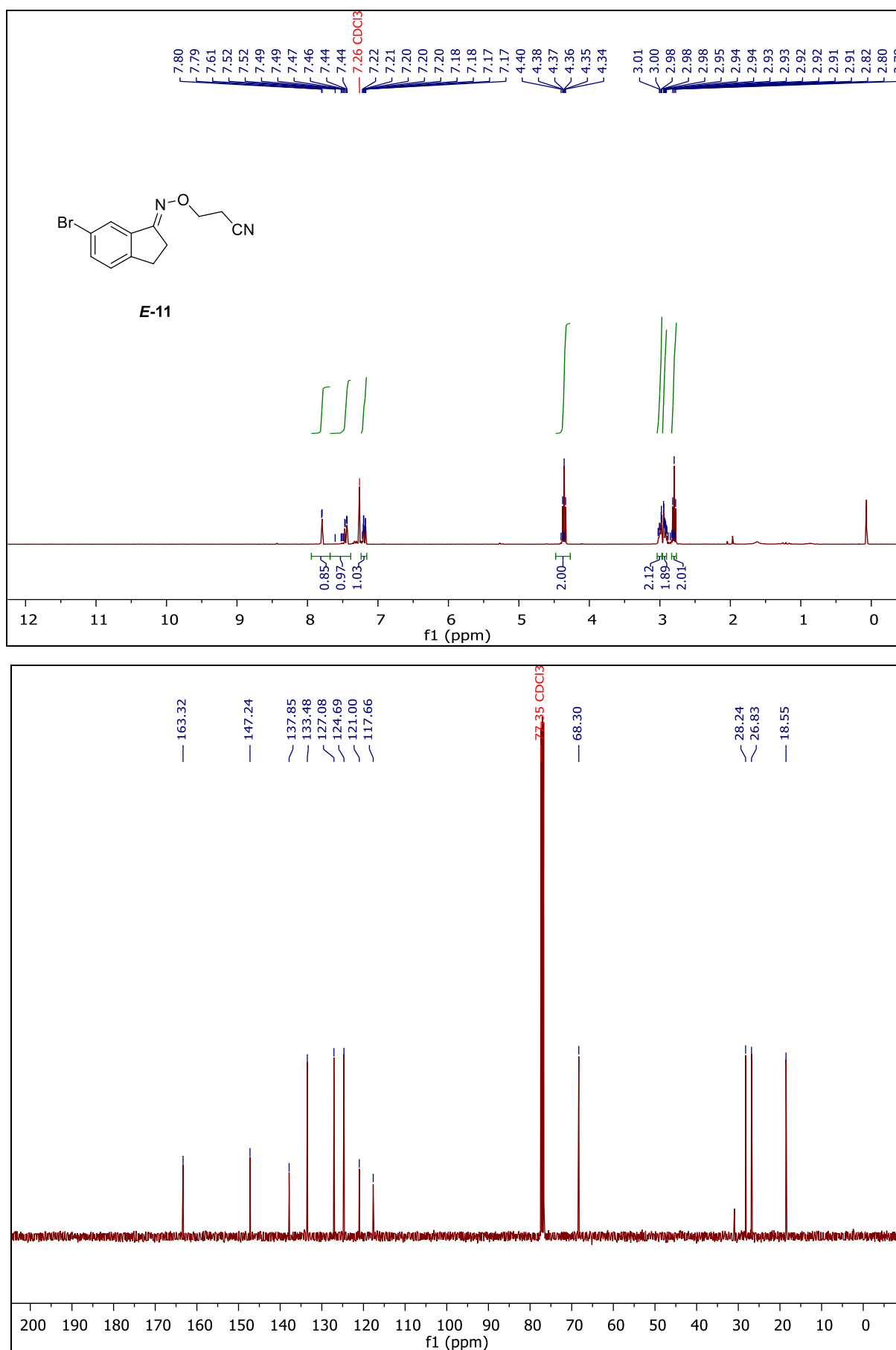
Spectrum S2.28. Compound **E-11**, ¹H- and ¹³C-NMR (Chloroform-*d*).
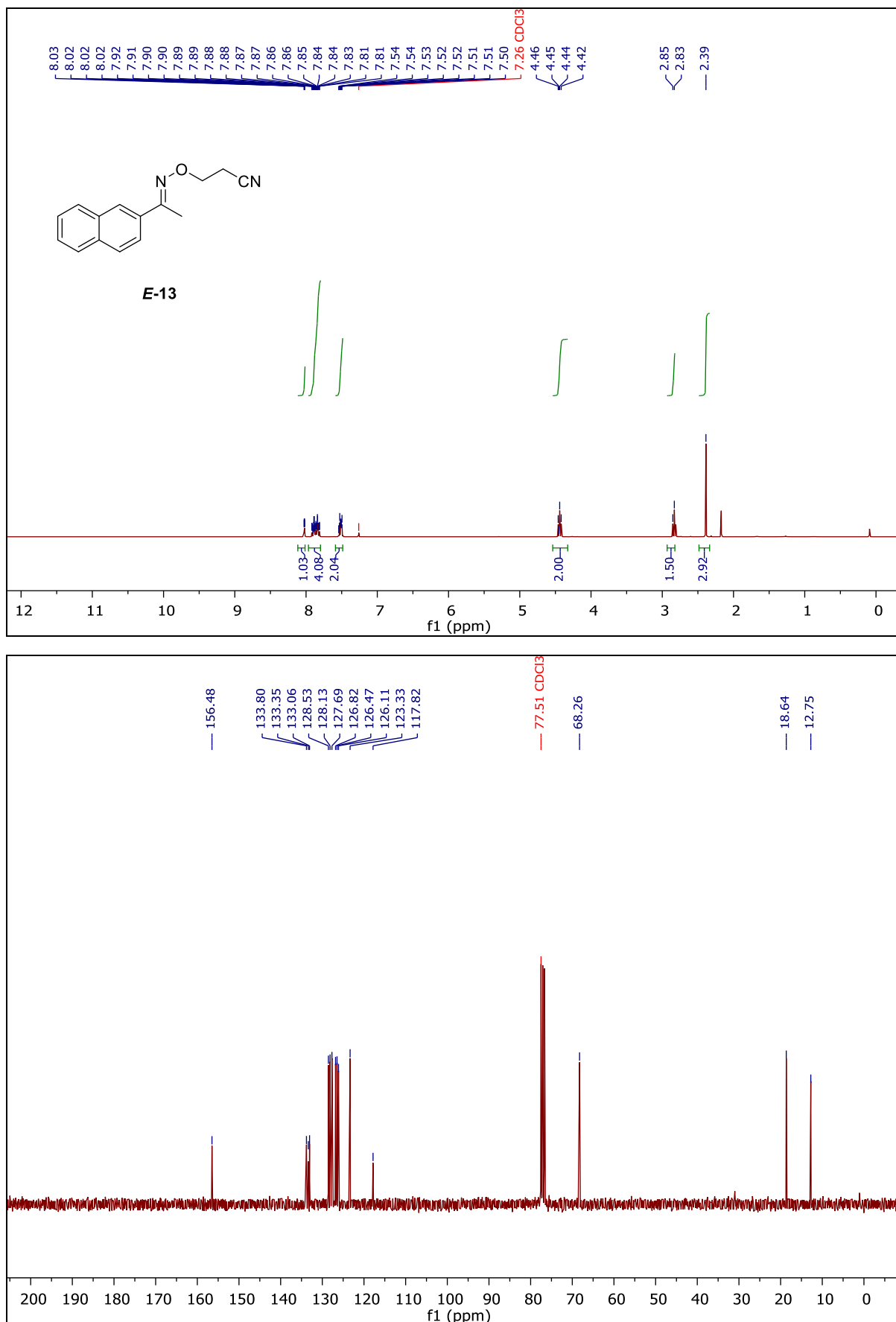
Spectrum S2.29. Compound **E-13**, ^{1}H- and ^{13}C-NMR (Chloroform-*d*).
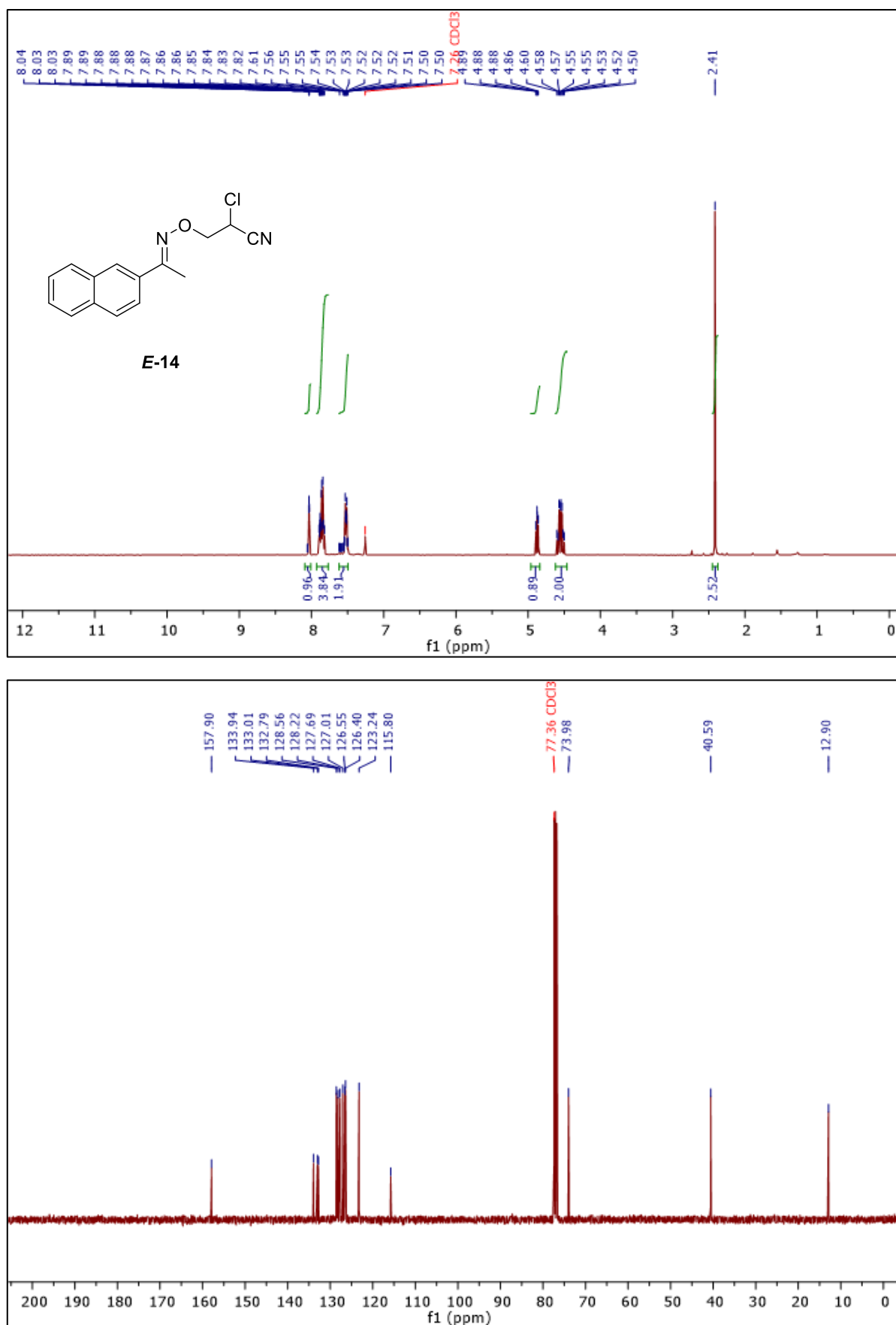
Spectrum S2.30. Compound **E-14**, ¹H- and ¹³C-NMR (Chloroform-*d*).
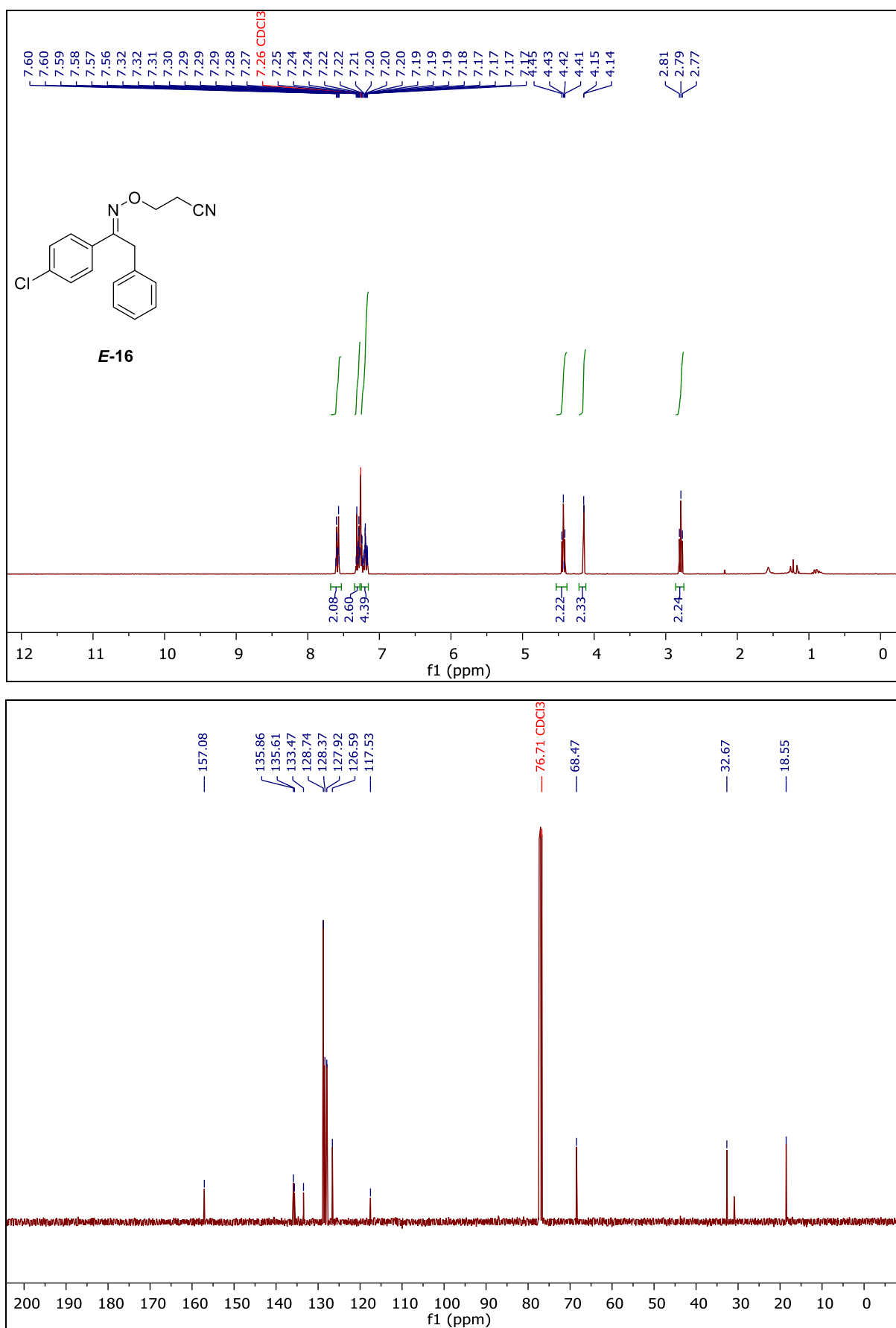
Spectrum S2.31. Compound **E-16**, ^{1}H- and ^{13}C-NMR (Chloroform-*d*).
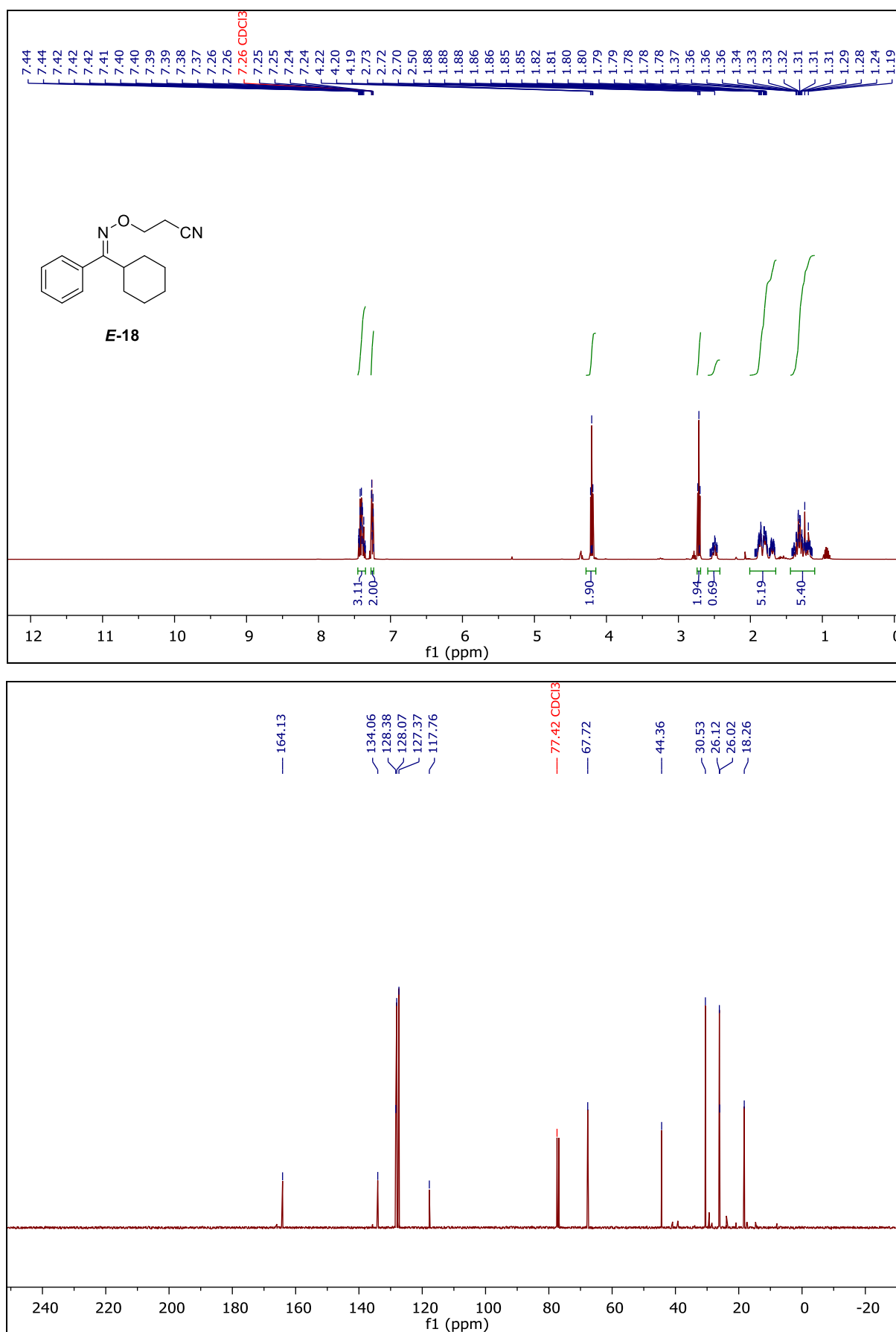
Spectrum S2.32. Compound **E-18**, ¹H- and ¹³C-NMR (Chloroform-*d*).
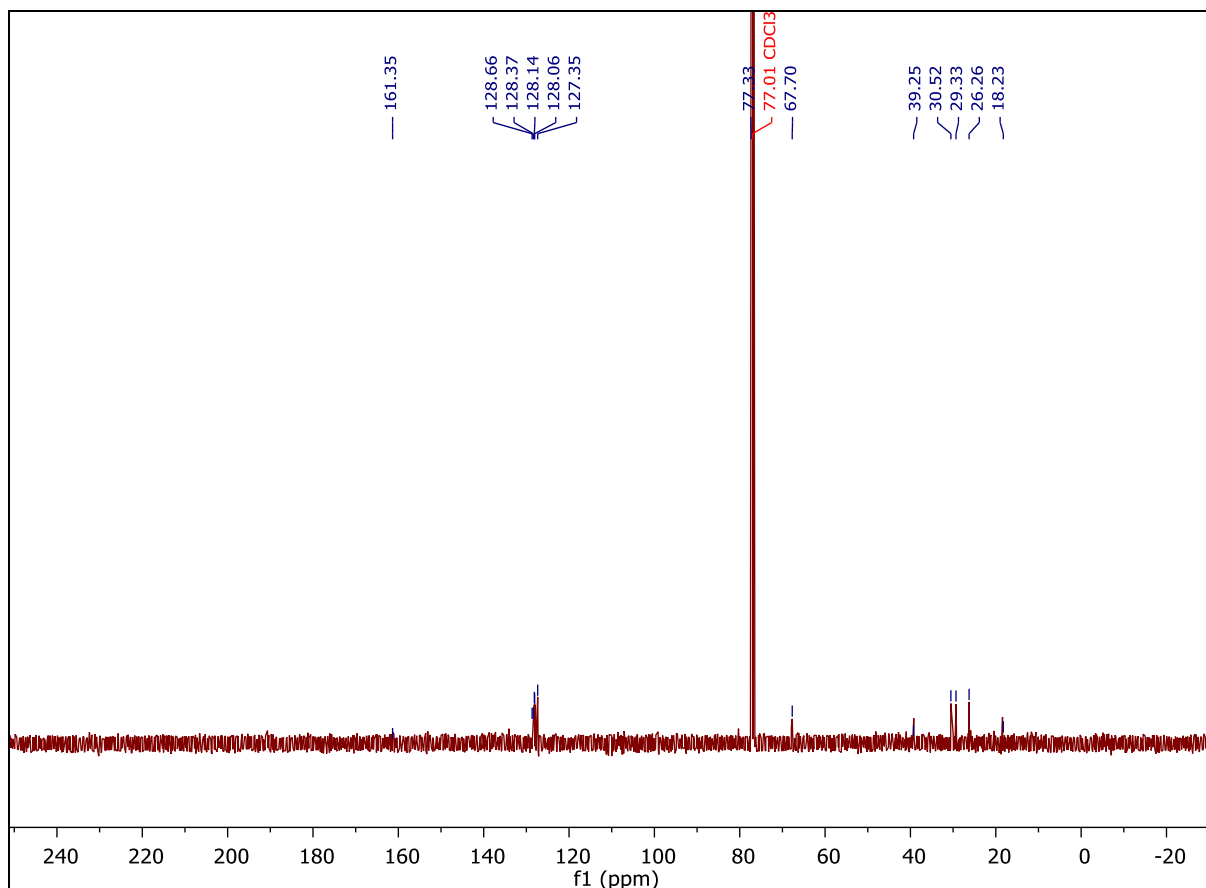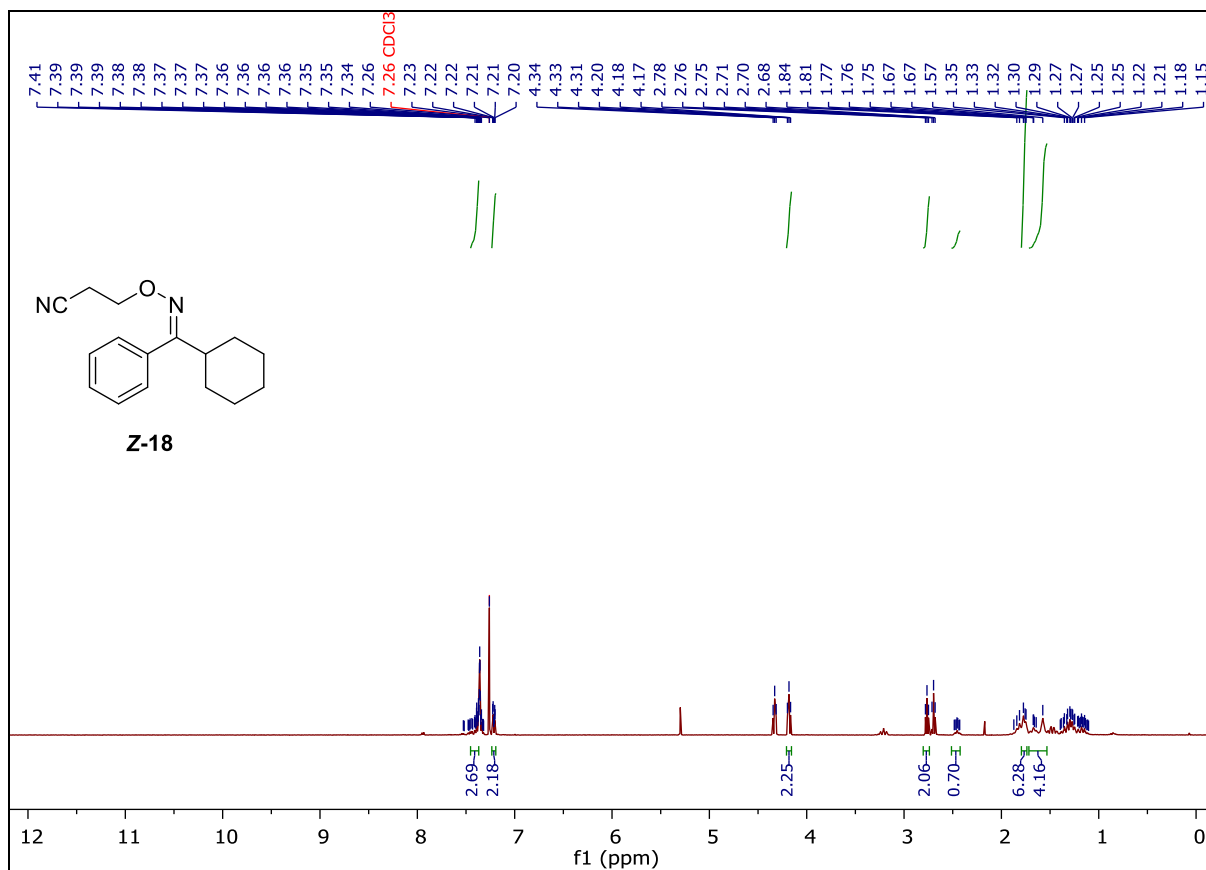
Spectrum S2.33. Compound **Z-18**, ^{1}H- and ^{13}C-NMR (Chloroform-*d*).
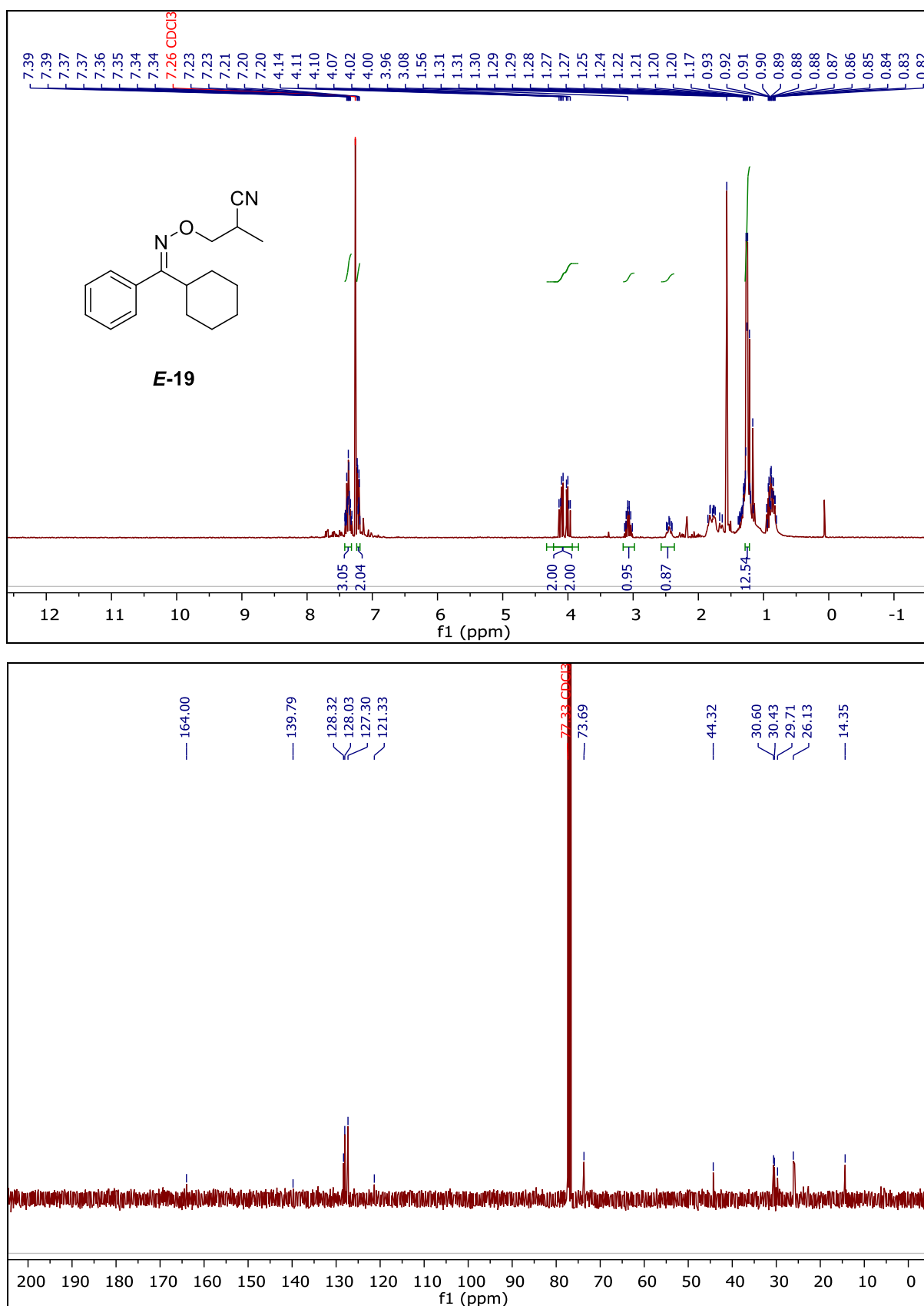
Spectrum S2.34. Compound ***E*-19**, ^{1}H- and ^{13}C-NMR (Chloroform-*d*).
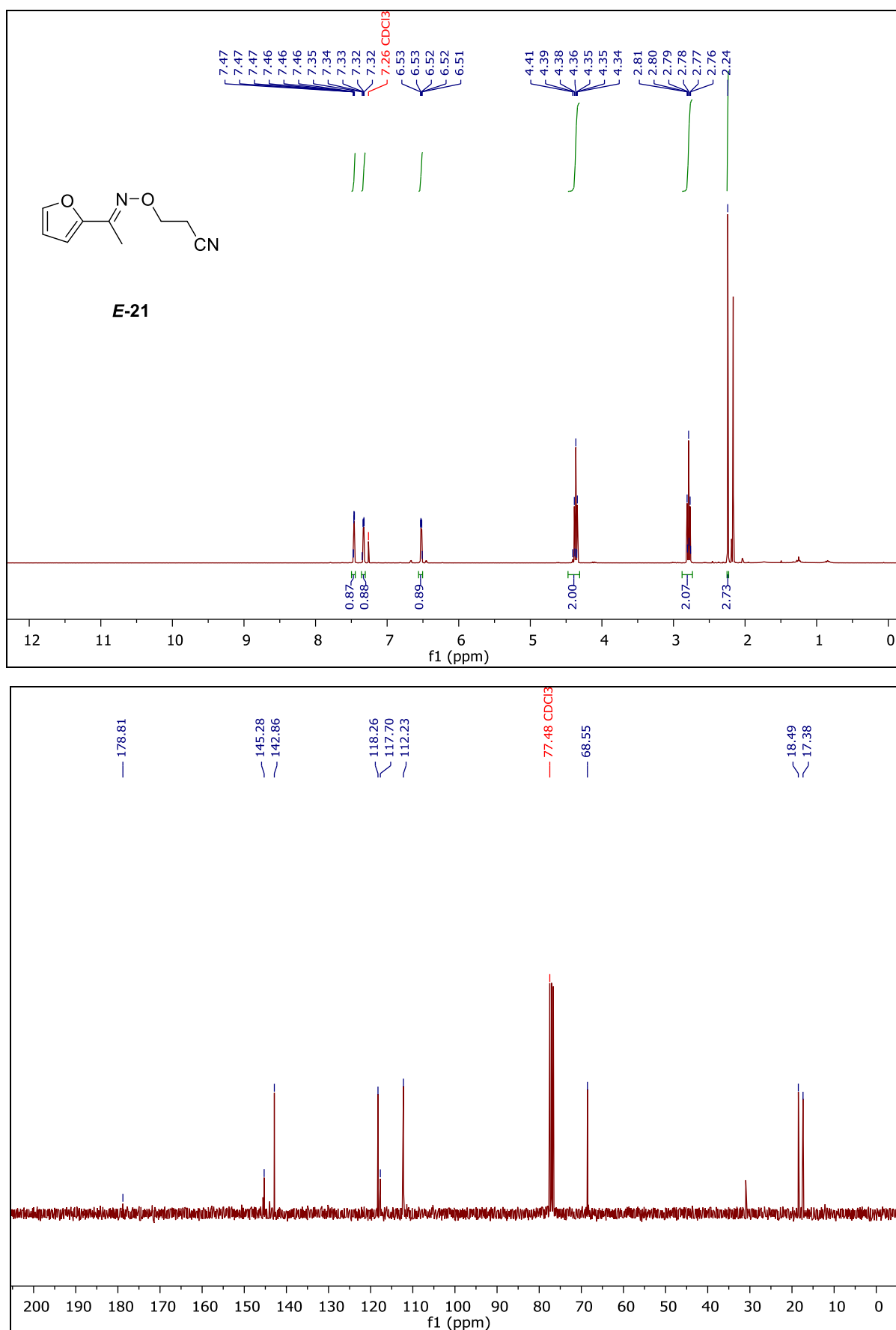
Spectrum S2.35. Compound **E-21**, ^{1}H- and ^{13}C-NMR (Chloroform-*d*).
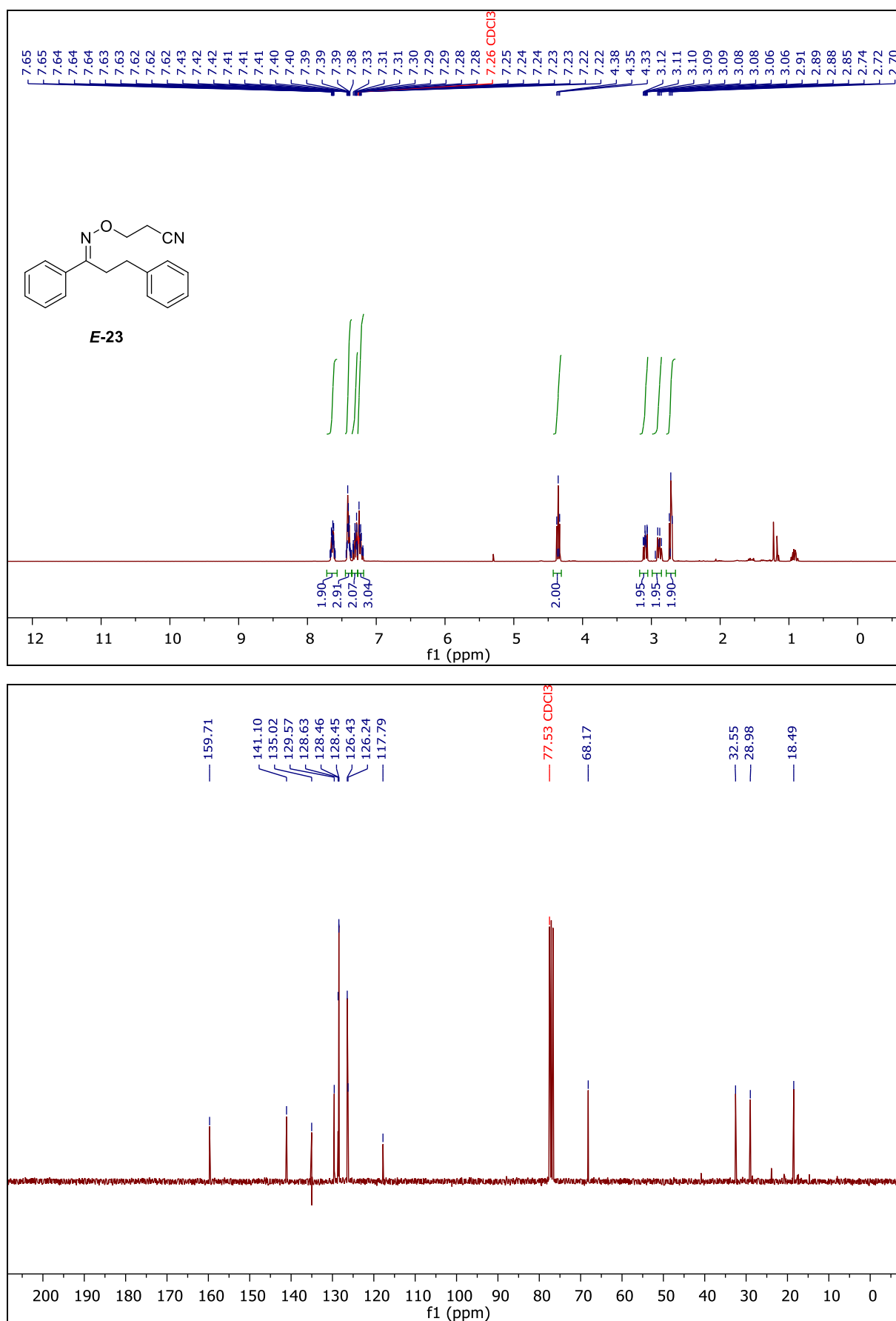
Spectrum S2.36. Compound **E-23**, ^{1}H- and ^{13}C-NMR (Chloroform-d).
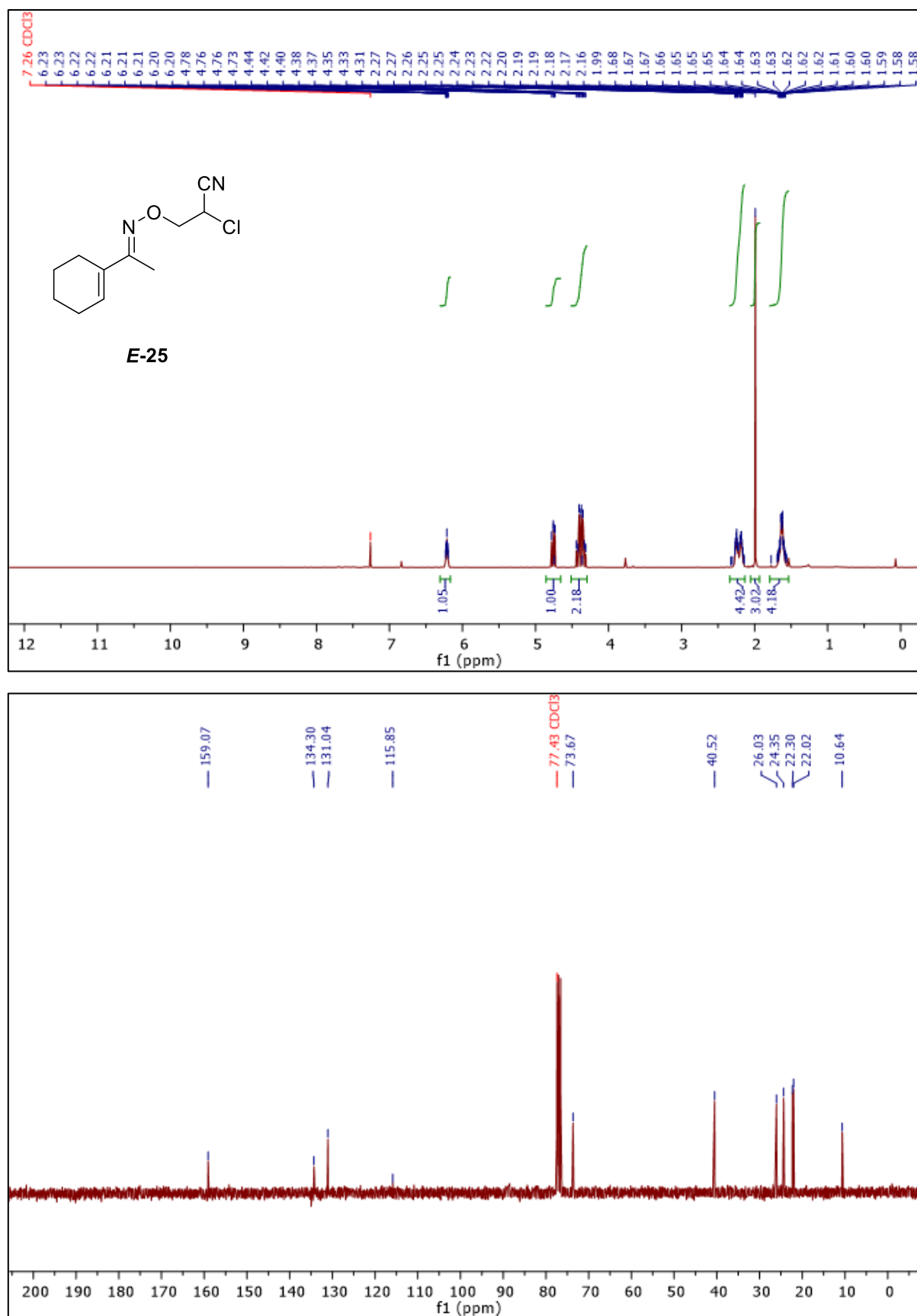
Spectrum S2.37. Compound **E-25**, ^{1}H- and ^{13}C-NMR (Chloroform-*d*).
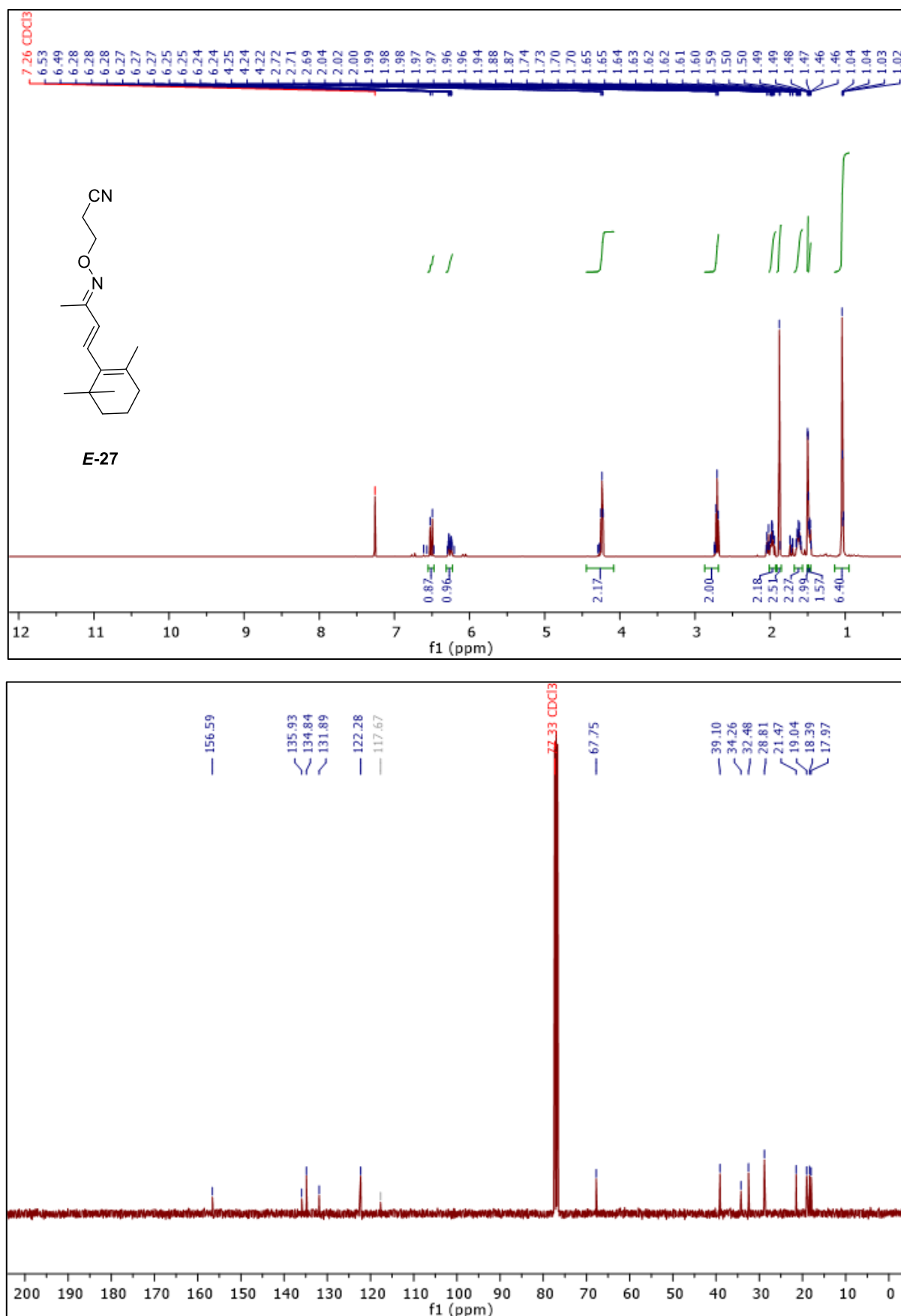
Spectrum S2.38. Compound **E-27**, ^{1}H- and ^{13}C-NMR (Chloroform-*d*).
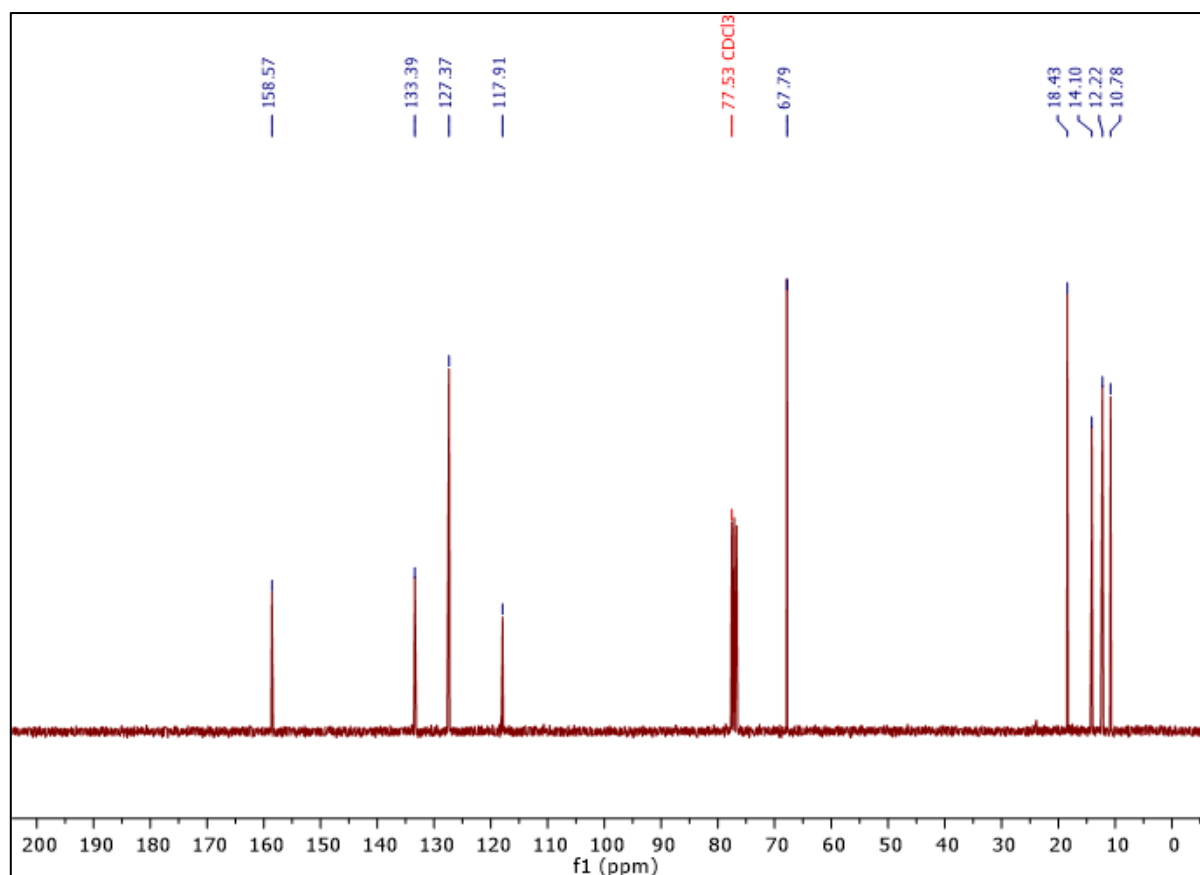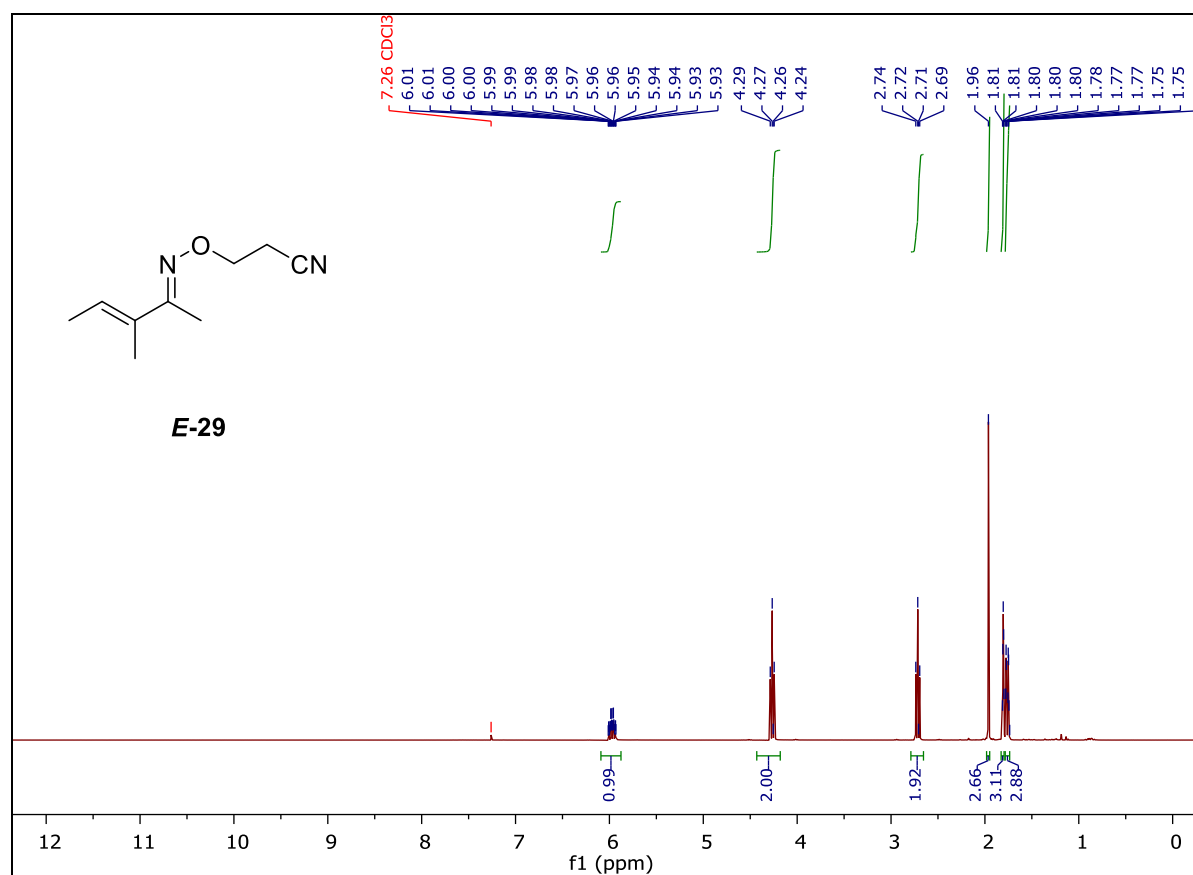
Spectrum S2.39. Compound **E-29**, ^{1}H- and ^{13}C-NMR (Chloroform-*d*).
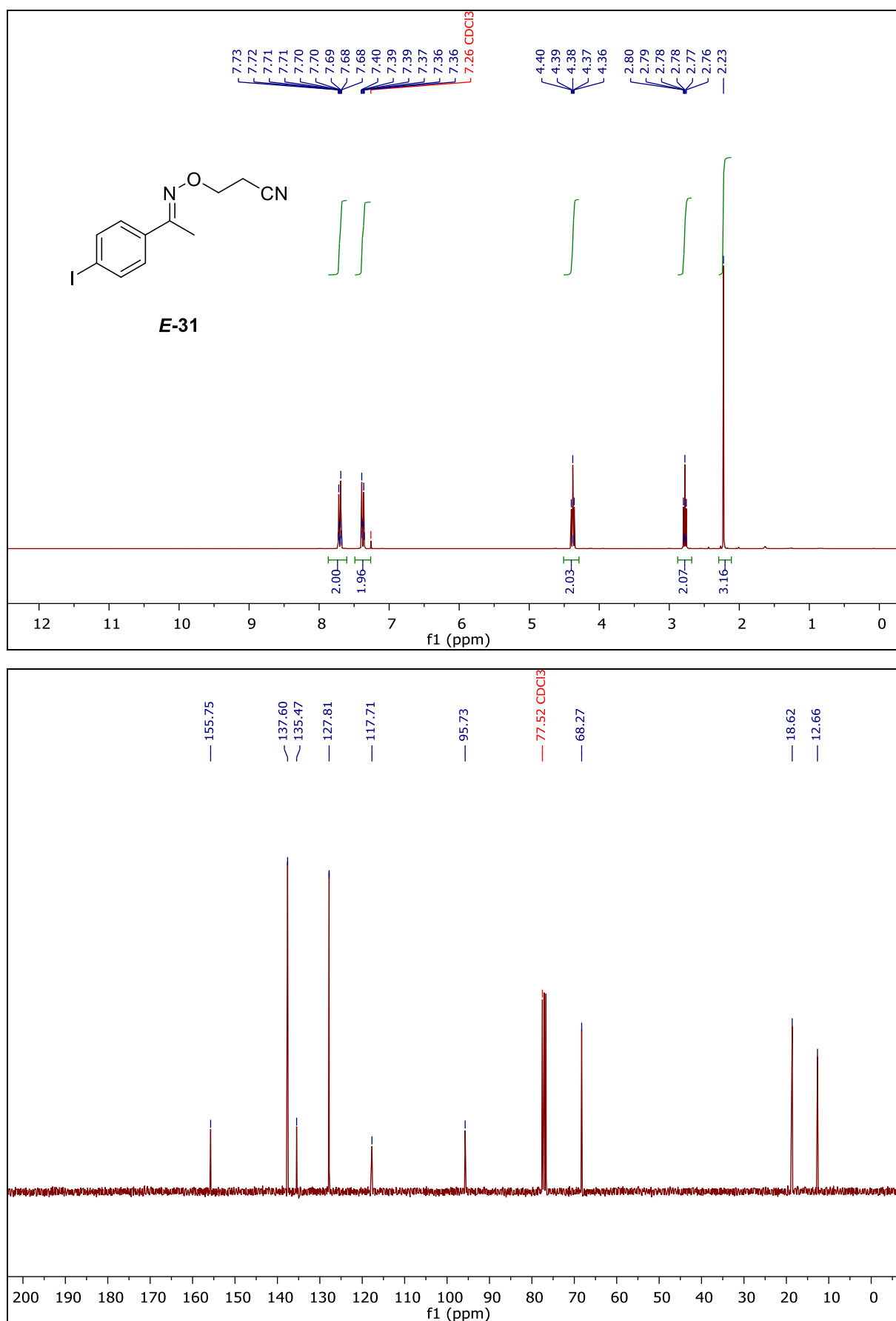
Spectrum S2.40. Compound ***E*-31**, ^{1}H- and ^{13}C-NMR (Chloroform-*d*).
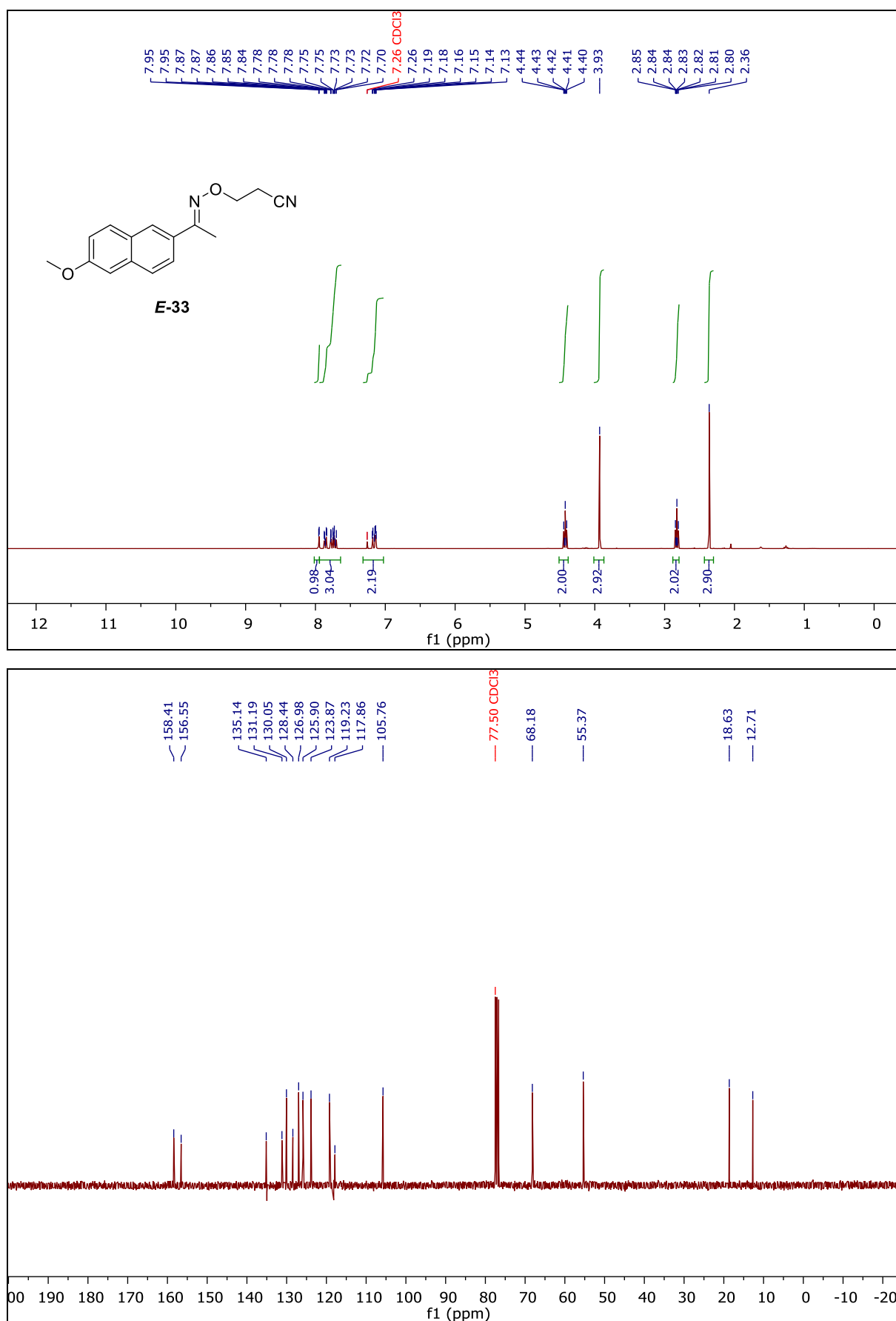
Spectrum S2.41. Compound **E-33**, ^{1}H- and ^{13}C-NMR (Chloroform-*d*).

2.12 References

[1]   R.K. Harris, E.D. Becker, S.M. Cabral de Menezes, R. Goodfellow, P. Granger, *Solid State Nucl. Magn. Reson.* **2002**, *4*, 458-483.

[2]   G.R. Fulmer, A.J.M. Miller, N.H. Sherden, H.E. Gottlieb, A. Nudelman, B.M. Stoltz, J.E. Bercaw, K.I. Goldberg, *Organometallics* **2010**, *9*, 2176-2179.

[3]   Z. Yin, Z. Zhang, Y. Zhang, P.H. Dixneuf, X.-F. Wu, *Chem. Commun.* **2019**, *32*, 4655-4658.

[4]   a) G.A. Honorato, R.V. de Lima, B.R. Manda, D.R. Paiva, T. Pimentel, R. da Silva Gomes, *Tetrahedron Lett.* **2017**, *23*, 2240-2243. b) R.T.   McBurney,   J.C.   Walton, *Beilstein J. Org. Chem.* **2013**, *9*, 1083-1092.

[5]   A. Terent'ev, I. Krylov, V. Vil', Z. Pastukhova, S. Fastov, G. Nikishin, *Open Chem.* **2012**, *2*, 360.

[6]   M.F.T. Koehler, P. Bergeron, E.F. Choo, K. Lau, C. Ndubaku, D. Dudley, P. Gibbons, B.E. Sleebs, C.S. Rye, G. Nikolakopoulos, C. Bui, S. Kulasegaram, W.J.A. Kersten, B.J. Smith, P.E. Czabotar, P.M. Colman, D.C.S. Huang, J.B. Baell, K.G. Watson, L. Hasvold, Z.-F. Tao, L. Wang, A.J. Souers, S.W. Elmore, J.A. Flygare, W.J. Fairbrother, G. Lessene, *ACS Medicinal Chem. Lett.* **2014**, *6*, 662-667.

[7]   H. Wang, Y. Ren, K. Wang, Y. Man, Y. Xiang, N. Li, B. Tang, *Chem. Commun.* **2017**, *69*, 9644-9647.

[8]   D.A. Shabalin, M.Y. Dvorko, E.Y. Schmidt, I.A. Ushakov, N.I. Protsuk, V.B. Kobychev, D.Y. Soshnikov, A.B. Trofimov, N.M. Vitkovskaya, A.b.I. Mikhaleva, B.A. Trofimov, *Tetrahedron* **2015**, *21*, 3273-3281.

[9]   A.S. Demir, Ö. Sesenoglu, D. Ülkü, C. Arıcı, *Helv. Chim. Acta* **2003**, *1*, 91-105.

[10]   P. Too, T. Noji, Y.J. Lim, X. Li, S. Chiba, *Synlett* **2011**, *19*, 2789-2794.

[11]   K. Parthasarathy, M. Jeganmohan, C.-H. Cheng, *Org. Lett.* **2008**, *2*, 325-328.

[12]   C.B. Aakeröy, A.S. Sinha, *RSC Advances* **2013**, *22*, 8168-8171.

[13]   F. Xie, C. Du, Y. Pang, X. Lian, C. Xue, Y. Chen, X. Wang, M. Cheng, C. Guo, B. Lin, Y. Liu, *Tetrahedron Lett.* **2016**, *51*, 5820-5824.

[14]   V.R. Yatham, P. Bellotti, B. König, *Chem. Commun.* **2019**, *24*, 3489-3492.

[15]   Y. Moiseev, Y. Ben-Eliyahu, M. Audras, L. Berthon, P. Moisy, A. Bettelheim, I. Zilbermann, *J. Coord. Chem.* **2016**, *19*, 2895-2907.

[16] N. Krstic, M. Bjelaković, M. Dabovic, L. Lorenc, V. Pavlovic, *J. Serbian Chem. Soc.* **2004**, *69*, 413-420.

[17] L.B. Turner, I. Mueller-Harvey, A.B. McAllan, *Phytochemistry* **1993**, *4*, 791-796.

[18] A. Hu, Y. Chen, J.J. Guo, N. Yu, Q. An, Z. Zuo, *J. Am. Chem. Soc.* **2018**, *140*, 42, 13580-13585.

[19] M.J. Frisch, G.W. Trucks, H.B. Schlegel, G.E. Scuseria, M.A. Robb, J.R. Cheeseman, G. Scalmani, V. Barone, G.A. Petersson, H. Nakatsuji, X. Li, M. Caricato, A.V. Marenich, J. Bloino, B.G. Janesko, R. Gomperts, B. Mennucci, H. P. Hratchian, J.V. Ortiz, A.F. Izmaylov, J.L. Sonnenberg, Williams, F. Ding, F. Lipparini, F Egidi, J. Goings, B. Peng, A. Petrone, T. Henderson, D. Ranasinghe, V.G. Zakrzewski,J. Gao, N. Rega, G. Zheng, W. Liang, M. Hada, M. Ehara, K. Toyota, R. Fukuda, J. Hasegawa, M. Ishida, T. Nakajima,Y. Honda, O. Kitao, H. Nakai, T. Vreven, K. Throssell, J.A. Montgomery Jr., J. E. Peralta, F. Ogliaro, M.J. Bearpark, J.J. Heyd, E.N. Brothers, K.N. Kudin, V. N. Staroverov, T.A. Keith, R. Kobayashi, J. Normand, K. Raghavachari, A.P. Rendell, J.C. Burant, S.S.Iyengar, J.Tomasi, M. Cossi, J.M. Millam, M. Klene, C. Adamo, R. Cammi, J.W. Ochterski, R. L. Martin, K. Morokuma, O. Farkas, J.B. Foresman, D.J. Fox, Wallingford, CT, **2016**.

3 Chemo-Selective Vicinal Dichlorination of Alkenes by Iron Ligand-to-Metal Charge Transfer Catalysis
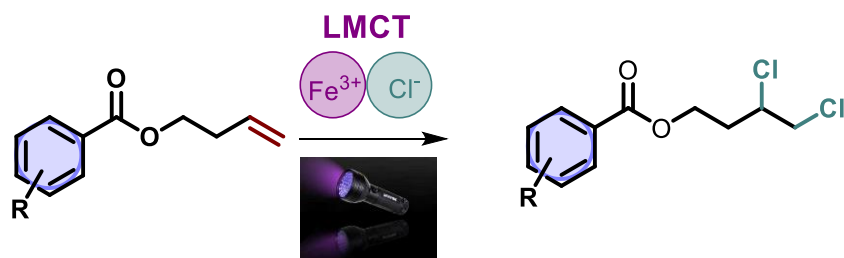
✔ cheap and commercially available iron(III) salt and LiCl as chlorine radical precursor

✔ short reaction time

✔ mild conditions

Jessica Stahl performed the experiments described in the manuscript and the control reactions highlighted in the Supporting Information. Thilo Reiter initiated the project and performed the major reaction optimisation studies shown in the manuscript and the Supporting Information as well as the kinetic reaction studies *via* GC-FID and the GC-FID calibration for yield determination described in the Supporting Information. Burkhard König supervised the project.

Chapter 3

This chapter was published in:

J. Stahl, T. Reiter, B. König, *Synlett*, **2024**, *35*, A-E.

Abstract

We report the photocatalytic functionalisation of terminal alkenes to vicinal dichlorides using visible light and $FeCl_3$ as catalyst, LiCl as chloride source, and air as oxidant. The transformation is proposed to be initiated by ligand-to-metal charge transfer (LMCT) bond homolysis of a Fe-Cl bond giving a highly reactive chlorine radical, able to initiate the functionalisation of olefins. The process shows high chemo-selectivity and functional group tolerance with a yield of up to 94% under mild conditions.

3.1 Introduction

The direct chlorination of alkenes utilising chlorine gas is a well-known reaction from basic organic chemistry und still finds numerous applications in the chemical industry.[1-3] Due to the high oxidation potential of elemental chlorine, in nature chloride is mainly found in its reduced form as anion in inorganic salts, such as sodium chloride.[4, 5] The industrial most relevant application of chlorine gas is the synthesis of vinyl chloride, consuming 33% of the worldwide produced chlorine in 1997. The vinyl chloride monomer is synthesized by thermal cracking of 1,2-dichloroethane, which is produced from the addition reaction of chlorine gas to ethene. An alternative pathway to vinyl chloride, circumventing chorine gas, is by a hydro-chlorination of acetylene.[6] These reaction demonstrated an alternative to toxic chlorine gas, that, applied in a synthesis shows a strongly exothermic reaction profile .[7]

In 2020, the group of Wan reported a photocatalytic method for the vicinal dichlorination of olefins, using 20 mol% of $CuCl_2$ (Scheme 3.1).[8] The reaction is based on the pioneering work of Kochi on the photolysis of $CuCl_2$ in presence of organic compounds.[9] Wan developed a catalytic method using an excess of aqueous HCl as chloride source and air as terminal oxidant. The authors stated that this reaction is initiated by a LMCT process, generating a chlorine radical and Cu(I)Cl.

Iron is the second most abundant metal on Earth and its complexes are frequently discussed in the field of photo-physics and photochemistry.[10-12] Iron as d^8 transition metal has a versatile redox chemistry and, based on its position in the d-block of the periodic table, iron possesses both the character of an early transition metal as well as noble metal behaviour.[13] Therefore, iron can encompass a wide range of different chemical transformations in synthetic ground state.

As known from other metal chlorides $FeCl_3$ is able to generate chlorine radicals upon excitation with visible light.[14] The first reports on the photoreduction of $FeCl_3$ for the oxidation of organic molecules appeared in the 1960s when Imoto and co-workers performed light-driven transformations of 1,2 glycols derivatives. Although not being extensively described the reaction is likely to happen *via* photogenerated chlorine radicals.[15] The research group of Jie Feng described the vicinal dichlorination of acrylamides using a dual photocatalytic system

with FeCl$_3$ in stoichiometric amounts and tetra-*n*-butylammonium decatungstate (TBADT) in catalytic amounts. Upon excitation of decatungstate using 390 nm LEDs, chlorine radicals are formed from the iron salt and the resulting radical species add to the double bond of an acrylate starting material. The method is limited to acrylate substrates, demands an inorganic cluster as photocatalyst, reaction times of 48 h, and DCM as halogenated solvent (Scheme 3.1).[16]

In literature, the application of chlorine radicals as reagent for the direct vicinal addition to electron rich terminal alkenes has not been demonstrated so far using exclusively simple metal salts. Herein, we report a catalytic strategy for the dichlorination of alkenes applying FeCl$_3$ as catalyst and LiCl as source of chlorine radicals in a solvent mixture of acetic acid and acetonitrile. The reaction proceeds within 3 h and shows a certain chemo-selectivity that will be discussed in more detail.
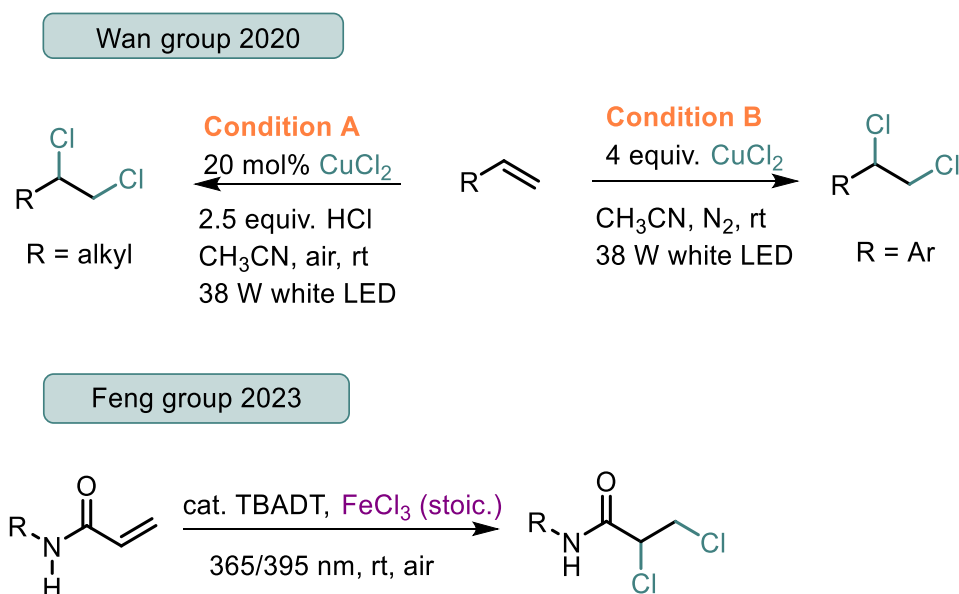
Scheme 3.1. Photocatalytic generation of chlorine radicals for dichlorination procedures *via* Ligand-to Metal charge transfer.

3.2 Results and Discussion

Due to the known ability of iron compounds to generate chlorine radicals in the presence of chlorides and light, we investigated if the halogen radical can add to a carbon-carbon double bond and using FeCl₃ as chlorination agent to obtain 1,2-dichloride products. As depicted in Scheme 3.2, using butenyl benzoate **1** as model substrate, FeCl₃ as photocatalyst, HCl as chloride source, and under visible light irradiation (395 nm) the transformation was successful. As shown in the SI, the reaction does not lead to product formation in the absence of light and iron and only traces of the dichlorinated product are formed under dinitrogen atmosphere.
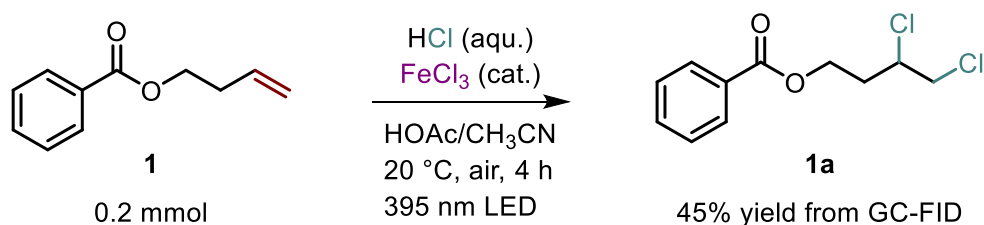
Scheme 3.2. Iron-catalysed photocatalytic dichlorination of butenyl benzoate (**1**) in the presence of concentrated aqueous HCl (2.5 equiv.) and FeCl₃ (20 mol%) in a solvent mixture of HOAc and CH₃CN. The yield was determined with GC-FID using toluene as internal standard.

As shown in Table 1, switching to other iron sources is possible but results in a decrease of product formation, since a Fe(III)-chloride species is supposed to be the active catalyst. Concentrated HCl as chloride source provides quantitative conversion of the starting material, but the moderate isolated yield of the desired product indicates the presence of competitive reactions such as acid catalysed hydrolysis of the ester functional group in the starting material or the product. Hence, the focus was shifted to abundant, less acidic chloride sources that are less likely to induce thermal side reactions with the starting material. LiCl as a cheap and commercially available inorganic salt is already known from previous publications as supporting chloride source in LMCT reactions with metal chloride as active catalysts.[17, 18] It is known from polymerisation reactions that acidic conditions allow for controllable reaction conditions and stabilisation of radical intermediates.[19] As shown in the SI, to maintain the acidic environment, trifluoracetic acid (TFA) was added to the solvent mixture, but the impact on product formation was neglectable or even detrimental as the yield dropped upon increasing

the amount of TFA (**SI**, Table **T3.2**, entry 1-6). This reinforces the previously hypothesised acid-catalysed ester hydrolysis as side reaction. A 9:1 ratio of acetic acid and acetonitrile gave the highest yield of 50% using 10 equiv. of LiCl salt and 0.5 mL of a 9:1 HOAc/CH₃CN solvent mixture. The viscosity of the system increased with higher LiCl loading which could stem from a cluster network consisting of iron(III) ions that are being connected to acetate and chloride ligands increasing the density.[20]

Interestingly, monitoring the concentration of **1** and **1a** revealed a significant product loss if the reaction time is increased to more than 3 h due to degradation indicated by the presence of benzoic acid in GC-MS. Therefore, reactions described in the following are conducted at a reaction time of 3 h (for kinetic study *via* GC-FID, see the SI).
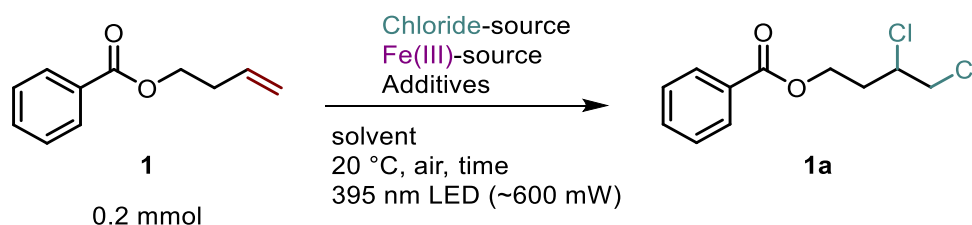
Scheme 3.3. Optimisation of the reaction conditions.

Table 3.1. Selected results from the reaction optimisation study.

Entry	Fe(III) source (20 mol%)	Chloride source	Time [h]	[a] Conv. [%] from GC-FID	[b] Yield [%] from GC-FID
1[a]	$Fe_2(SO_4)_3$	2.5 equiv. HCl (aqu.)	4	100	30
2[a]	$FeCl_3$ (anhydr.)	2.5 equiv. HCl (aqu.)	4	100	45
3[a]	$Fe(NO_3)_3$ $9H_2O$	2.5 equiv. HCl (aqu.)	4	100	33
4[b]	$FeCl_3$ (anhydr.)	2.5 equiv. HCl (aqu.)	4	100	26
5[a]	$FeCl_3$ (anhydr.)	10 equiv. HCl (aqu.)	4	100	45
6[a]	$FeCl_3$ (anhydr.)	10 equiv. LiCl (anhydr.)	4	100	50

[a] [b] Conversion and yield were determined with GC-FID using toluene as internal standard. a) 0.5 mL HOAc/CH_3CN (9:1), b) 1 mL HOAc/CH_3CN (9:1).

With the optimised conditions in hand, we investigated the substrate scope for the iron-catalysed photo-dichlorination of alkenes (Figure 3.1). Various arene substituted alkenes were screened and the majority gave moderate to very good, isolated yields for the dichlorination of the respective terminal double bond.

Very good, isolated yields are achieved for electron-withdrawing and -donating substituents at the *para*-position of the aryl esters (Figure 3.1, compound **6**, **7**, **8**) or substrates with substituents being attached in *ortho*-position to the respective ester moiety (Figure 3.1, substrate **5**, **10**). Starting the reaction from a branched alkene ester led to a decrease of product formation, rationalised by the competitive C-H abstraction of the introduced tertiary carbon (Figure 3.1, compound **2**) and *para*-substituted starting materials performed well in the reaction.

Compound **7** reacted with competitive C-H activation of the methoxy group of the starting material yielding two products **7a** (main) and **7b**. Analogous to **7**, starting material **29** led to a double functionalisation: dichlorination of the double bond (**29a**, major) as well as H-atom abstraction on the *p*-ethyl group on the arene and radical recombination with a chlorine radical (**29b**, traces). *Ortho-* and *meta*-substituted aromatic compounds are tolerated, as demonstrated with compound **4** and direct halogen substitution of the arene has a diminishing effect on the desired reaction (Figure 3.1, compound **5**, **9** and **10**) to the point where no product formation is observed (**SI,** Table **T3.3**, compound **16**). An additional reason for the low performance of **9** is the ability to form a stable benzyl radical after H-atom abstraction at the methyl substituent. Olefins on internal positions could not be functionalised (**SI**, Table **T3.3**, compounds **19**, **20**, **21** and **22**). Using branched esters (**SI**, Table **T3.3**, substrate **18**) led to a complex reaction mixture that was not separable *via* chromatography. The attempt to apply the method to stilbene (**SI**, Table **T3.3**, compound **21**) led to the oxidative cleavage of the C-C double bond and the formation of benzaldehyde (**22**) in 24% ^{1}H-NMR yield. In general, it was observed that insufficient solubility in the polar solvent as well as high hydrolysis kinetics of the ester deteriorated the dichlorination.
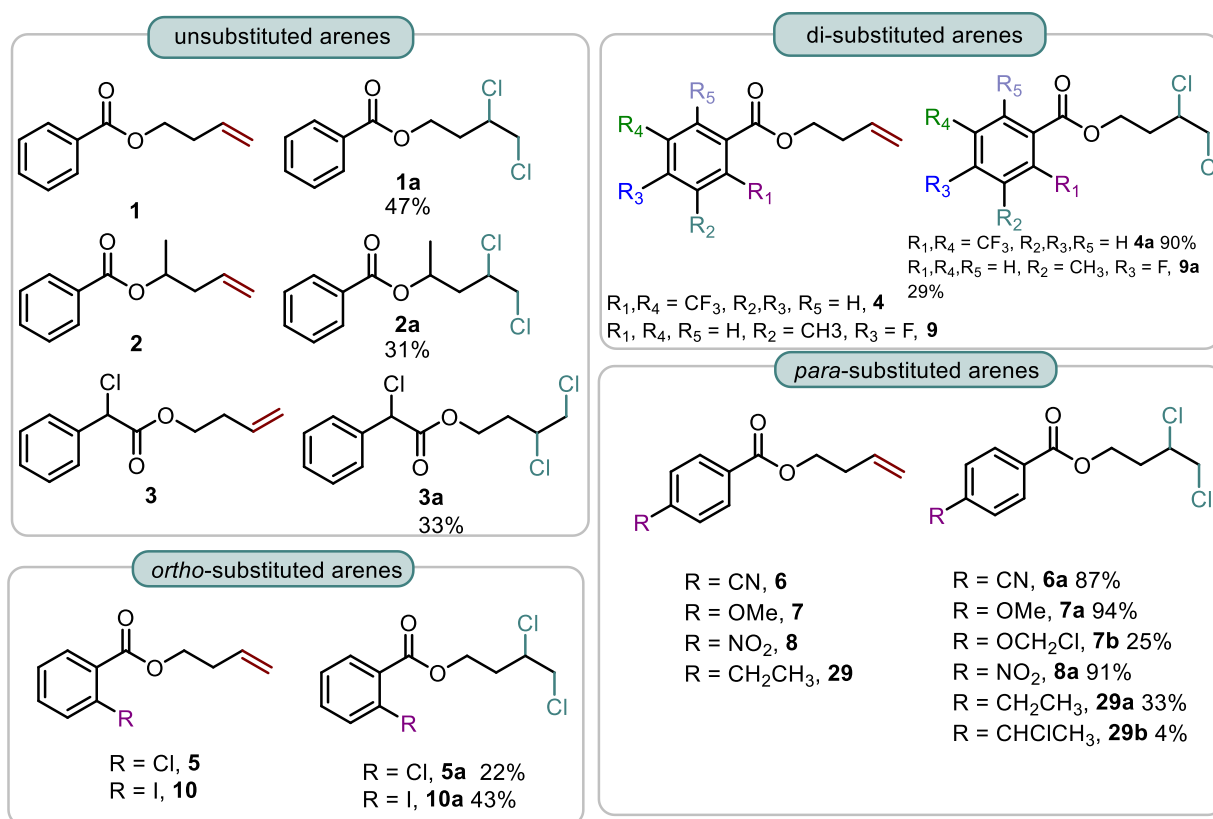
Figure 3.1. Substrate scope for the successful dichlorination of alkenes.

3.3 Mechanistic Investigations

To gain more insights into the mechanism of iron(III)chloride LMCT olefin dichlorination, the overall photoreaction was examined stepwise.

We hypothesised that iron(III) as a Lewis acid can interact with the lone-pair of the carbonyl oxygen of aryl esters, besides acetic acid and acetonitrile solvent molecules. The proposed addition of the chlorine radical to the alkene would benefit from the proximity to the C-C double bond to the bond homolysis event at the iron. Using styrene as test reagent gave 15% yield of a 1,2-dichlorination product in ^{1}H-NMR (Scheme 3.4, entry **I**), next to 24% benzaldehyde for *trans*-stilbene as starting material (Table **T3.3**, SI).

With an additional acetoxy group in *para-* position to the double bond (Scheme 3.4, substrate **12**) the yield increased by factor two, leading to 30% ^{1}H-NMR yield (Scheme 3.4, entry **II**). The constitution isomer of acetoxy styrene, vinyl benzoate (Scheme 3.4, substrate **13,** entry **III**) successfully underwent the photocatalytic halogenation giving 48% of the corresponding product in ^{1}H-NMR.
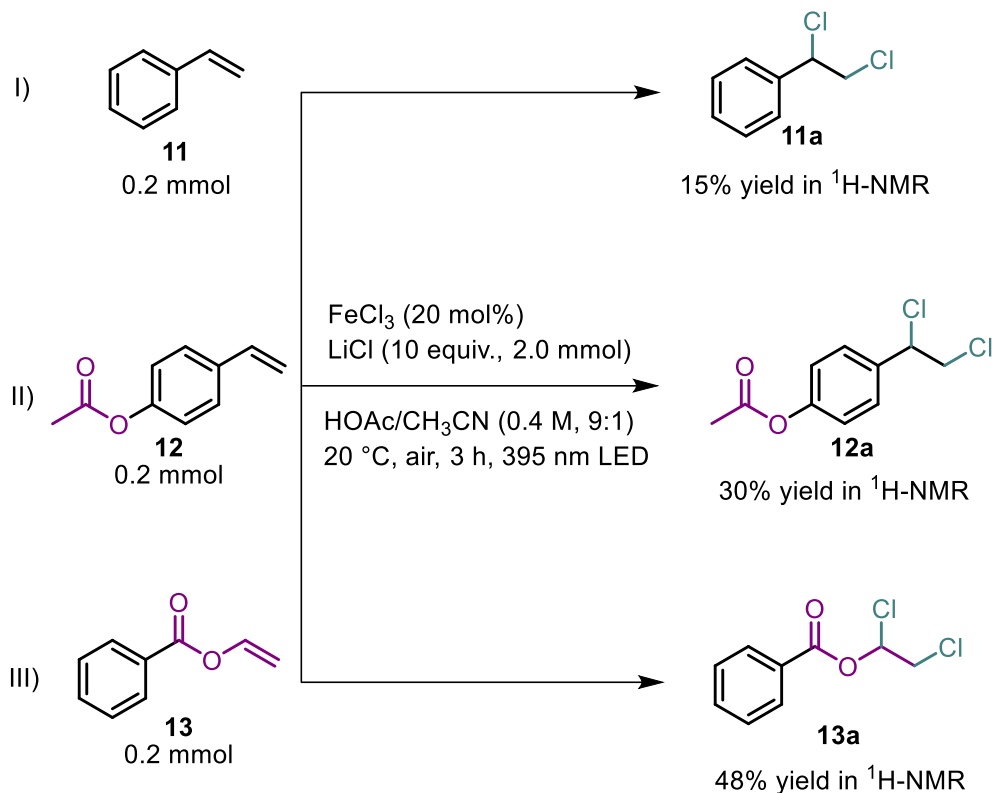
Scheme 3.4. Impact on the additional coordination of iron to a carbonyl function in the molecule.

The examples shown in Scheme 3.5 demonstrate the sensitivity of the electrophilic chlorine radical addition towards the electron density of the carbon-carbon π-bond. For styrene (Scheme 3.5, entry **I**) and *N*-allyl phthalimide (Scheme 3.5, entry **III**) as rather electron rich alkenes the photoreaction result in moderate to good yields of **11a** and **15a**, respectively whereas the electron-poor benzylidene malononitrile (Scheme 3.5, entry **II**) double could not be transformed to the dihalide **14a**. Further mechanistic investigations based on the competing ability of chlorine radicals to either abstract hydrogen atoms or add to a double bond in an electrophilic fashion are highlighted in the Supporting Information.

I)

11
0.2 mmol

FeCl$_3$ (20 mol%)
LiCl (10 equiv., 2.0 mmol)
—————————————————→
HOAc/MeCN (0.4 M, 9:1)
395 nm, 20 °C, 3 h, air

11a
15% yield in ^{1}H-NMR

II)

14
0.2 mmol

FeCl$_3$ (20 mol%)
LiCl (10 equiv., 2.0 mmol)
—————————————————→
HOAc/MeCN (0.4 M, 9:1)
395 nm, 20 °C, 3 h, air

14a
not observed in ^{1}H-NMR

III)

15
0.2 mmol

FeCl$_3$ (20 mol%)
LiCl (10 equiv., 2.0 mmol)
—————————————————→
HOAc/MeCN (0.4 M, 9:1)
395 nm, 20 °C, 3 h, air

15a
45% yield in ^{1}H-NMR
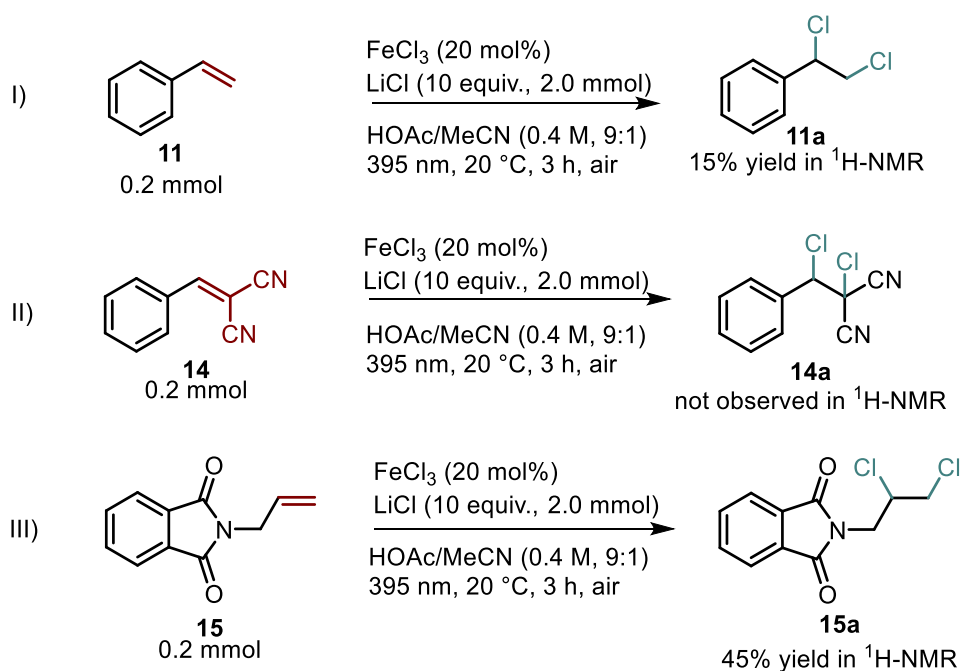
Scheme 3.5. Dependency of the reactivity on the electron density of the starting material double bond.

With the objective for ruling out an ionic second addition step of chloride to the double bond, amines were added to imitate the reaction conditions of a nucleophilic addition to a carbocation being formed during a previous oxidation initiated by traces of Cl$_2$ (for more detailed description see Scheme **S3.5.**, SI). As neither product **30a** nor compound **31a** were detected in ^{1}H-NMR the second addition of a chlorine radical *via* an ionic reaction pathway can be excluded.

I

1
0.2 mmol

+

30
1.0 mmol
5 equiv.

FeCl$_3$ (20 mol%)
LiCl (10 equiv., 2.0 mmol)
—————————————————→
HOAc (0.44 M)
395 nm, 20 °C, 3 h, air

30a
not observed in ^{1}H-NMR

II

1
0.2 mmol

+

31
1.0 mmol
5 equiv.

FeCl$_3$ (20 mol%)
LiCl (10 equiv., 2.0 mmol)
—————————————————→
HOAc (0.44 M)
395 nm, 20 °C, 3 h, air

31a
not observed in ^{1}H-NMR
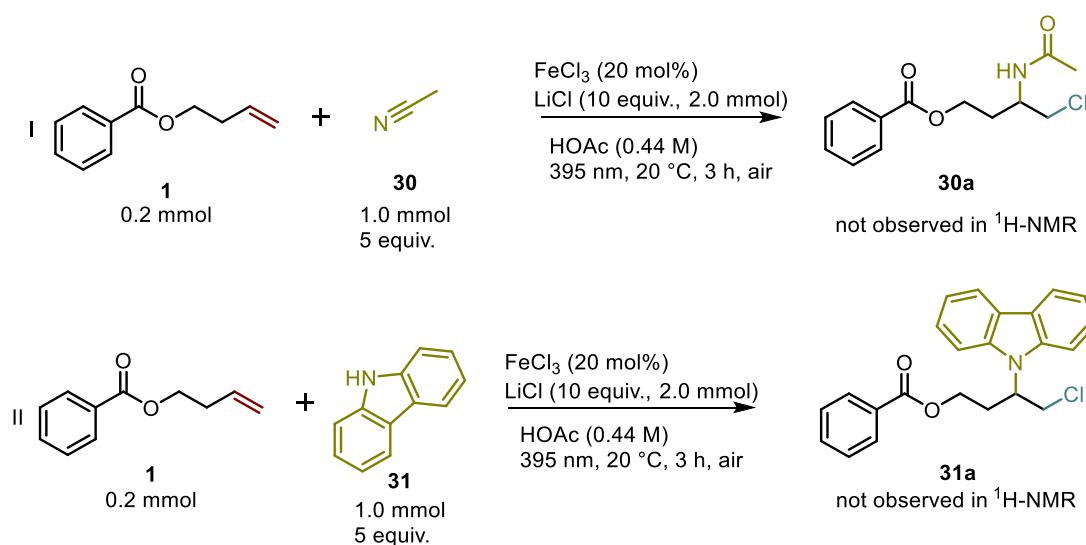
Scheme 3.6. Investigations on a possible second ionic second addition step of chlorine radicals to a carbon-centered radical.

Based on the mechanistic investigations we propose the reaction mechanism highlighted in Scheme 3.6. $FeCl_3$ (Scheme 3.7, **I**) coordinates to chloride anions from LiCl forming a $FeCl_4^-$ complex (Scheme 3.7, **II**) that, upon irradiation with visible light, undergoes a homolytic bond cleavage in a ligand-to-metal charge transfer fashion leading to the formation of chlorine radicals and $FeCl_2$ (Scheme 3.7, **III**). A chlorine radical adds to the terminal double bond resulting in the mono-halogenated product **1'**. The final dichlorinated substrate **1a** is formed from a Radical Ligand Transfer (RLT) described my Bian *et al.*[21] Approaching to a Fe-Cl bond, the carbon-centred radical of intermediate **1'** is able to trigger the bond-homolysis of the metal-ligand bond leading to the formation of chlorine radicals and iron(II). The chlorine radicals undergo an addition to species **1'** and 1,2-dichlorinated species **1a** is formed. The metal-cation is re-oxidised by oxygen from air to Fe(III) to close the overall catalytic cycle.
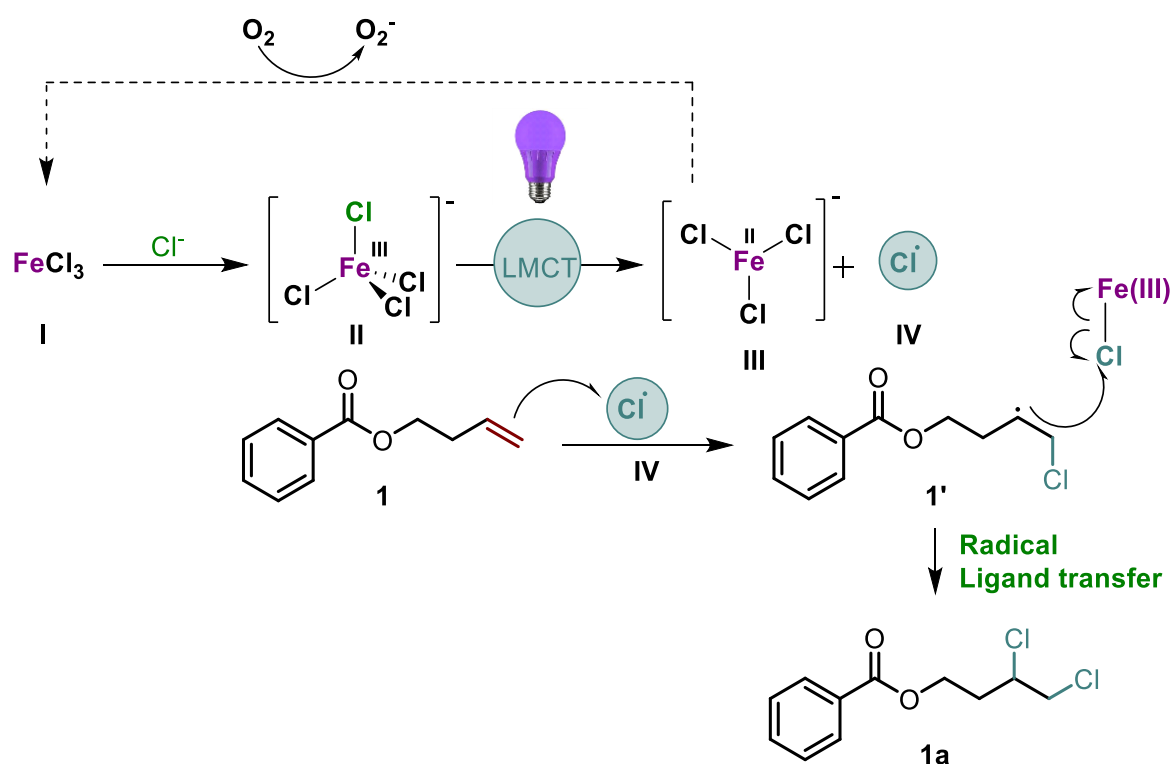
Scheme 3.7. Proposed reaction mechanism for the dichlorination of alkenes by iron LMCT.

3.4 Conclusion

We have developed a photocatalytic method for the chlorine gas free dichlorination of alkenes using cheap and commercially available metal salts and chloride sources. The formation of reactive chlorine radicals is initiated by light-induced ligand-to-metal-charge transfer, followed by a homolysis of the iron-chloride bond. The results illustrate exemplarily a direct synthesis of 1,2-dichloride compounds as important synthetic intermediates from abundant starting materials.

3.5   References

(1) Fauvarque, J. *Pure Appl. Chem.* **1996**, *9*, 1713.

(2) Baldwin, R. T *J. Chem. Ed.* **1927**, *3*, 313.

(3) Rajkumar, D.; Kim, J. D. J *Hazard* **2006**, *2*, 203.

(4) Morosin, B. *Chem. Phys*. **2003**, *7*, 3007.

(5) Recio, J. M; Pendás, A. M.; Francisco, E.; Flórez, M.; Luaña, V. *Phys. Rev. B* **1993**, *9*, 5891.

(6) Dreher, E. -L.; Torkelson, T. L.; Beutel, K. K. Chlorethanes and Chloroethylenes, In *Ullmann's Encyclopedia of Industrial Chemistry*; Wiley-VCH, **2011**.

(7) Achanta, S.; Jordt, S. -E. *Toxicol. Mech. Methods* **2021**, *4*, 244.

(8) Lian, P.; Long, W.; Li, J.; Zheng, Y.; Wan, X. *Angew. Chem. Int. Ed*. **2020**, *52*, 23603.

(9) Kochi, J. K. *J. Am. Chem. Soc.* **1962**, *11*, 2121.

(10) Feng, G.; Wang, X.; Jin, *J. Eur. J. Org. Chem.* **2019**, *39*, 6728.

(11) Chen, J.; Browne, W. R. *Coord. Chem. Rev*. **2018**, *374*, 15.

(12) Wedepohl, K. H. *The Composition of Earth's Upper Crust, Natural Cycles of Elements, Natural Resources*, In *Elements and Their Compounds in the Environment*; Wiley-VCH, **2004**, 3-16.

(13) Fürstner, A. *ACS Cent. Sci.* **2016**, *11*, 778.

(14) Vogler, A.; Kunkely, H. *Coord. Chem. Rev.* **2000**, *1*, 321.

(15) Inoue, H.; Tamaki, K.; Komakine, N.; Imoto, E. *Bull. Chem. Soc. Jpn* **1967**, *40*, 875.

(16) Wang, X.; Shi, C.; Yang, M.; Ma, Y.; Chen, Y.; Lu, T.; Tang, W.; Feng, J. *Asian J. Org. Chem.* **2023**, *6*, e202300077.

(17) Treacy, S. M.; Rovis, T. *J. Am. Chem. Soc.* **2021**, *7*, 2729.

(18) Ding, L.; Niu, K.; Liu, Y.; Wang, Q. *ChemSusChem* **2022**, *10*, e202200367.

(19) Fleischmann, S.; Percec, V. *J. Polym. Sci. A Polym. Chem.* **2010**, *21*, 4889.

(20) Dey, D.; Patra, M.; Al-Hunaiti, A.; Yadav, H. R.; Al-mherat, A.; Arar, S.; Maji, M.; Choudhury, A. R.; Biswas, *B. J. Mol. Struct.* **2019**, *1180*, 220.

(21) Bian, K. -J.; Kao, S. -C.; Nemoto, D.; Chen, X. -W.; West, J. G. *Nat. Commun.* **2022**, *1*, 7881.

(22) General procedure for the preparative scale reactions of the iron-catalysed dichlorination of alkenes

After successful screening in 0.1 mmol scale the preparative scale reactions were set in six to 12 parallel vials to achieve good reproducibility. Each of them was equipped with a magnetic stir bar, the alkene ester starting material (0.20 mmol, 1.00 equiv.), $FeCl_3$ (0.04 mmol, 6.50 mg, 20.0 mol%) and LiCl (2.00 mmol, 85.0 mg, 10.0 equiv.) as well as acetic acid (0.45 mL) and acetonitrile (0.05 mL) in a ratio of 9 to 1. The vials were closed, and air was added *via* septum-compacted syringe to every vial through a semi-permeable septum in the cap of the crimp cap vial. The vials were sealed with parafilm© and placed in the thermostated (20 °C) metal block approximately 2 cm above the 390-395 nm light source. The photoreactions were irradiated for 3 h. After the reaction, the vials were opened to air, combined, filtered through a thin layer of silica in a vacuum filtration device, washed with diethyl ether and collected in a 100 mL round-bottom flask. After reducing the solvent volume under reduced pressure, the residue was extracted with water (2 x 20.0 mL) and $NaHCO_3$ (20.0 mL) and the combined organic layers were dried over anhydrous Na_2SO_4. The crude mixture was filtered, and the solvent was removed in vacuum. The oily residue was dried under reduced pressure and purified by flash column chromatography on silica using acetone (20%) and petroleum ether as the eluent. The purity of the product was confirmed by ^{1}H- and ^{13}C-NMR in $CDCl_3$ using triphenylmethane as internal standard.

3.6   General Considerations

Starting materials and reagents were purchased from commercial suppliers (Sigma Aldrich, Alfa Aesar, Acros or Fluka) and were used without further purification. Solvents were used as p.a. grade. Reactions were monitored by analytic thin layer chromatography (TLC) using Fluka silica gel plates with a fluorescent indicator. Visualisation of the developed TLC chromatogram was performed using 254 nm UV light source or potassium permanganate stain. Organic solutions were concentrated using Büchi rotary evaporator. Flash column chromatography was performed either on a Biotage® IsoleraTM Spektra or by hand for non-UV absorbing products. In both cases we used columns filled with silica gel (60-200 μm). If not otherwise state petroleum ether and acetone were used as the eluent.

NMR Spectroscopy

NMR spectra were recorded at room temperature using a Bruker Advance 300 (300 MHz for ^{1}H, 75 MHz for ^{13}C, 282 MHz for ^{19}F) or a Bruker Advance 400 (400 MHz for ^{1}H, 101 MHz for ^{13}C, 376 MHz for ^{19}F) NMR spectrometer. All chemical shifts are reported in δ-scale as parts per million [ppm], relative to the solvent residual peaks as the internal standard or to an added internal standard. Coupling constants J are given in Hertz [Hz]. Abbreviations used for signal multiplicity: ^{1}H-NMR: br = broad, s = singlet, d = doublet, t = triplet, q = quartet, dd = doublet of doublets, dt = doublet of triplets, and m = multiplet.

Mass Spectrometry

High resolution mass spectrometry (HRMS) was performed at the Central Analytical Laboratory of the University of Regensburg. Mass spectra were measured on a Finnigan MAT 95, ThermoQuest Finnigan TSQ 7000, Finnigan MAT SSQ 710 A or Agilent Q-TOF 6540 UHD instrument and a Waters Acquity UPLC system equipped with Waters PDA, sample manager, sample organiser, column oven and Waters Xevo QTOF mass spectrometer.

UV/Vis spectroscopy

Absorption spectra were measured on an Agilent Cary 100 UV/Vis spectrometer in a 10 mm × 10 mm quartz cuvette at 25.0 °C under air atmosphere. Solvents (acetonitrile and acetic acid) were used from commercial suppliers in HPLC or spectroscopy grade and without further purification.

Gas Chromatography

GC measurements were performed on a GC 7890 from Agilent Technologies system coupled to a flame-ionization detector (FID). The system was equipped with a capillary column (HP-5ms UI, length 30 m, diam. 0.25 mm, film 0.25 µm) and worked with H_2 as carrier gas. GC program: The initial temperature of the GC was set to 40 °C and kept for 1.5 minutes. Subsequently, the oven temperature was increased at a rate of 25 °C/min. until reaching 280 °C, which was maintained for 3 min. Then, the temperature was further increased (42 °C/min) until reaching 300 °C and the final temperature was held for 5 minutes. The injector temperature was set to 280 °C and temperature of the detecting unit to 310 °C. A split ratio of 30:1 (split flow 42 mL/min) was applied, and the column flow was set to 1.4 mL/min. Data acquisition and evaluation were done with Agilent ChemStation Rev.C.01.04.

3.7 Photochemical Setup

The photoreactions were performed in 5 mL crimp cap vials that were equipped with a magnetic stir bar. Before placing them into the cooling block on top of the LED (**Figure S3.1.**, metal cooling block with six available positions for placing samples, fabricated on demand by the mechanical workshop the University of Regensburg), they were crimped and additionally covered with parafilm®. The samples were placed approximately 2 cm above a 390-395 nm LED (**Figure S3.2.**, LED: LED-Modul 6-fold, 6x LT-4795 Luminus SST 10UV, Ser.-Nr.:244-22-1, 609 mW). The reaction temperature was controlled by a thermostat (20 °C) that is connected to every individual metal cooling block.
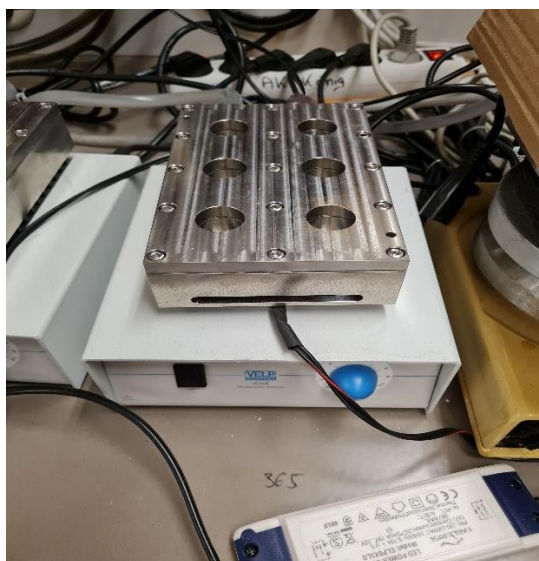
Figure S3.1. Cooling block for the photochemical reactions.

Figure S3.2. LED plate for the irradiation of six samples at the same time at 390-395 nm.

3.8 General Experimental Procedures

3.8.1 General Procedure for Screening and Optimisation Studies

Analysis Method 1 – GC-Yield Determination

In a 5 mL glass vial equipped with a magnetic stir bar, but-3-en-1-yl (**1**) (0.20 mmol, 1.00 equiv., 35.2 mg) was combined with an Fe(III)-salt (20 mol%, respectively) and a chlorine radical precursor (LiCl, NaCl or HCl) and dissolved upon the addition of acetic acid and acetonitrile in various mixing rations. The samples were closed by a septum-containing cap and air (15.0 mL) was added *via* an air-tight syringe to every individual sample. The vials were covered additionally with parafilm© and were placed in a thermostated (20 °C) cooling block and irradiated at 390-395 nm for 3 h. After completion of the reaction 2 mL of water were added and the reaction mixtures were extracted with diethyl ether (reagent grade, 3 x 2 mL). The combined organic phases were dried over anhydrous Na_2SO_4, filtered and GC-FID samples were prepared using toluene (25.0 µL, 0.24 mmol) as internal standard. The calibration data are shown in **Table T3.1** and **Figure F3.1.**

Analysis Method 2 – ^{1}H-NMR-Yield Determination

The photoreactions were prepared and irradiated in the same fashion as described in **analysis method 1.** After finished irradiation, the vials were opened to air and filtered through a 2 cm layer of silica in a vacuum filtration device. Every entry was diluted with diethyl ether and the empty reaction flask were washed three times with diethyl ether (2.0 mL) and soaked through the silica layer. The combined filtrate was collected in a 50 or, 100 mL round bottom flask and slightly diminished in volume under reduced pressure. The residue was extracted with water (2 x 10 mL) and $NaHCO_3$ (10 mL) and the combined organic phases were dried over anhydrous Na_2SO_4. After removing the solvent in vacuum, the residue was mixed with triphenyl methane (10.00 mg, 0.041 mmol) that served as internal standard for ^{1}H-NMR yield determination. The area of two protons in the product was compared with the area of the standard (for 10 mg and

a batch of 0.2 mmol: 0.1 AU at 5.6 ppm). The samples were diluted in 0.7 mL of CDCl$_3$, and a ^{1}H-NMR spectrum was measured.

Table T3.1. GC calibration based on starting material (aryl alkene ester **1**) conversion using toluene as internal standard. The calibration of the reaction was done by Thilo Reiter.

		c / mM	Retention time [min]	GC FID area (A)
Solution A	Internal standard (IS)	0.4097	5.045	1689704.42
	Starting material (SM)	0.3966	12.132	1843783.43
Solution B	IS	0.2088	5.052	1819357.19
	SM	0.3966	12.093	1004264.82
Solution C	IS	0.1073	5.05	1738553.86
	SM	0.3966	12.057	483082.609
Solution D	IS	0.0505	5.052	1796487.23
	SM	0.3966	12.032	246964.078
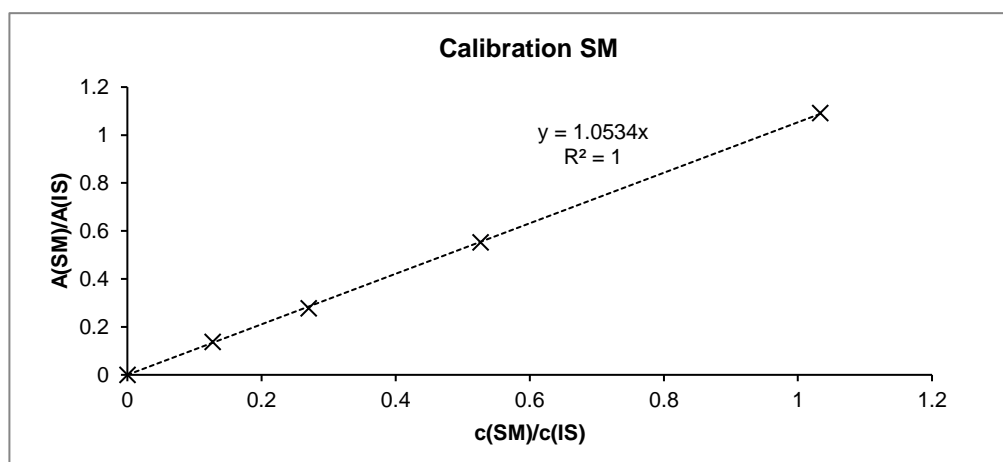
Figure S3.1. GC-calibration evaluation.

3.8.2 General Procedure for the Preparative Scale Reactions

After successful optimisation in small scale (0.1 mmol) the preparative scale reactions were set in six to 12 parallel vials that allowed for controllable reaction procedures. Each of the vials was equipped with a magnetic stir bar, the alkene ester starting material (0.20 mmol, 1.00 equiv.), $FeCl_3$ (0.04 mmol, 6.50 mg, 20.0 mol%) and LiCl (2.00 mmol, 85.0 mg, 10.0 equiv.) as well as acetic acid (0.45 mL) and acetonitrile (0.05 mL) in a ratio of 9 to 1. The vials were closed, and air was added *via* septum-compacted syringe to every vial through a semi-permeable septum in the cap of the glass vial. The vials were sealed with parafilm© and placed in the thermostated (20 °C) metal block approximately 2 cm above the 390-395 nm light source. The photoreactions were irradiated for 3 h. After the reaction, the vials were opened to air, combined, filtered through a thin layer of silica in a vacuum filtration device, washed with diethyl ether and collected in a 100 mL round-bottom flask. After decreasing the solvent volume under reduced pressure, the residue was extracted with water (2 x 20.0 mL) and $NaHCO_3$ (20.0 mL) and the combined organic layers were dried over anhydrous Na_2SO_4. The crude mixture was filtered, and the solvent was removed in vacuum. The oily residue was dried under reduced pressure and purified by flash column chromatography on silica using acetone (20%) and petroleum ether as eluent. The purity of the product was confirmed by ^{1}H- and ^{13}C-NMR in $CDCl_3$. In most cases two subsequent purifications by column chromatography were necessary to achieve the highest purity of the dichlorinated product.

3.9 Optimisation of the Reaction Conditions

The results of the complementary optimisation attempt are shown in Table **T3.2.** The optimisation reactions were conducted by Thilo Reiter and applied in the scope development by Jessica Stahl.
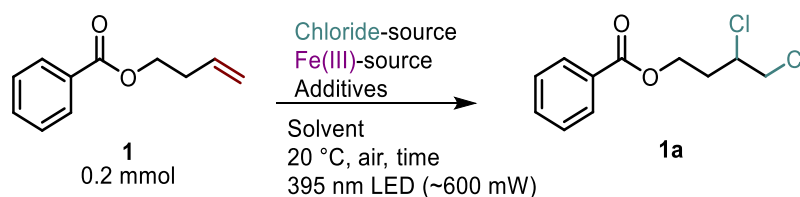
Scheme S3.1. Benchmark reaction for the dichlorination of alkenes via Iron-LMCT.

Table T3.2. Summary of the results from the reaction screening.

Entry	Fe(III)-source (20 mol%)	Cl-source	Additives	Solvent	Time [h]	λ [nm]	Conv [a] [%]	Yield [a] [%]
1	FeCl$_3$	10 equiv. LiCl (anhydr.)	-	0.5 mL HOAc/CH$_3$CN (9:1)	4	-	0	0
2	-	10 equiv. LiCl (anhydr.)	-	0.5 mL HOAc/CH$_3$CN (9:1)	4	390-395	0	0
3	FeCl$_3$	10 equiv. LiCl (anhydr.)	-	0.5 mL HOAc/CH$_3$CN (9:1) under N$_2$ atm.	4	390-395	traces	traces
4	FeCl$_3$	2.5 equiv. LiCl (anhydr.)	4.0 equiv. TFA	0.5 mL HOAc/CH$_3$CN (9:1)	4	390-395	100	39
5	FeCl$_3$	10 equiv. LiCl (anhydr.)	4.0 equiv. TFA	0.5 mL HOAc/CH$_3$CN (9:1)	4	390-395	100	45
6	FeCl$_3$	10 equiv. LiCl (anhydr.)	4.0 equiv. TFA	0.5 mL HOAc/CH$_3$N (1:1)	4	390-395	100	48
7	FeCl$_3$	10 equiv. LiCl (anhydr.)	4.0 equiv. TFA	0.5 mL CH$_3$CN	4	390-395	100	28
8	FeCl$_3$	10 equiv. LiCl (anhydr.)	4.0 equiv. TFA	0.5 mL HOAc	4	390-395	100	43

extension
of Table
T3.2
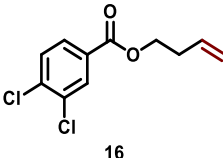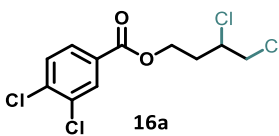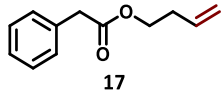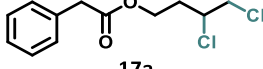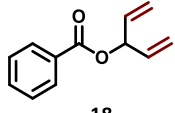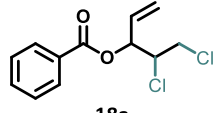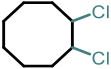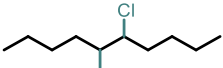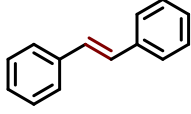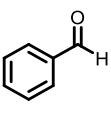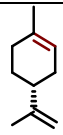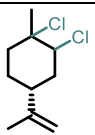
Entry	Fe(III) source (20 mol%)	Cl-source	Additives	Solvent	Time [h]	λ [nm]	Conv.[a] [%]	Yield[a] [%]
9	FeCl₃	10 equiv. LiCl (anhydr.)	10 equiv. TFA	0.5 mL HOAc/CH₃CN (9:1)	4	390-395	100	37
10	FeCl₃	10 equiv. LiCl (anhydr.)	-	0.5 mL HOAc/CH₃CN (1:1)	4	390-395	100	40
11	FeCl₃	10 equiv. LiCl (anhydr.)	-	0.5 mL HOAc/H₂O	4	390-395	100	21
12	FeCl₃	10 equiv. LiCl (anhydr.)	-	0.5 mL HOAc/CH₃CN (9:1)	21	390-395	100	24

[a][b] Conversion and yields were determined by GC-FID using toluene as internal standard.

3.10 Unsuccessful Reactions

As already described in the manuscript, applying the general reaction conditions described in chapter 3.8 of the SI the following products could not be detected in GC-FID or ^{1}H-NMR (**Table T3.3.**).

Table T3.3. Unsuccessful dichlorination attempts.

Alkene starting material	Dichlorinated product or alternative product	[a] Detected in GC-FID or ^{1}H-NMR
16	16a	no
17	17a	no
18	18a	complex reaction mixture; no analysis *via* GC-FID or purification *via* chromatography possible
19	19a	no
20	20a	no
21	21	24% detected in ^{1}H-NMR
22	22a	no

[a] Photoreactions were performed as described in section **3.8** of the SI and after workup submitted to GC-FID using toluene as internal standard or ^{1}H-NMR with triphenyl methane as internal standard.

3.11 Applicability of the Method to Recently Published Dichlorination Reactions

In May 2023 the group of Jie Feng published an alternative method for the photo-catalysed vicinal (and geminal) dichlorination of alkenes using decatungstate as photocatalyst and $FeCl_3$ in stoichiometric amounts as chlorine radical precursor.[1] Using UV light they were able to functionalise differently substituted acrylamides. The substrate **23** was chosen as model as it was available in the König group storage room to investigate the applicability of the method of the Feng group to our photocatalytic procedure for the iron-catalysed dichlorination of alkenes. 13% of the dichlorination product **23a** could be detected in ^{1}H-NMR. The geminal product **23b** was not formed at all (**Scheme S3.2.**).
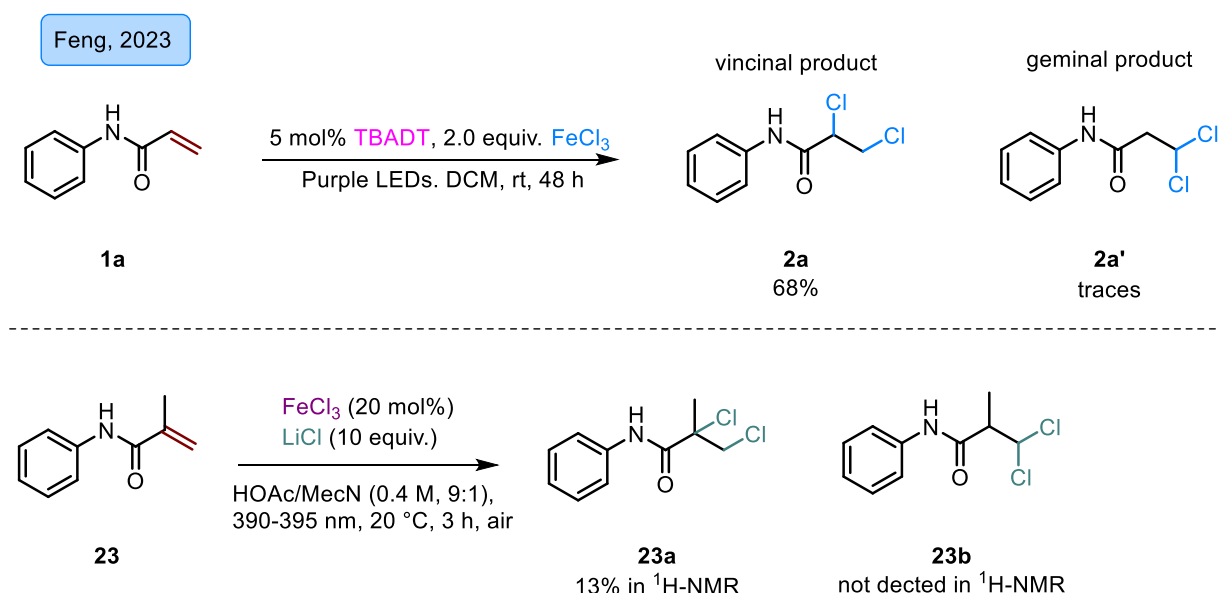
Scheme S3.2. Investigation of acrylamides as substrates for the photocatalytic dichlorination of alkenes *via* iron LMCT. Triphenyl methane (10.0 mg) was used as internal standard for ^{1}H-NMR yield determination of compound **23a** and **23b**.

3.12 Regioselectivity of the Dichlorination Reaction

The effect of the distance between the C-C double bond to the aromatic core of the substrate on the product yield was investigated. Therefore, terephthalic acid dichloride (**24**) was reacted with 1-butan-3-ol (**25**) and 1-butan-5-ol (**26**) to the corresponding diester **27** (**Scheme S3.3.**, entry I). The starting material was reacted under the photocatalytic conditions (procedure described in chapter **3.8.1**, analysis method 2, SI) to product **27a** showing a selective dichlorination on the chain with the shorter alkene-ester distance. The yield was determined *via* ^{1}H-NMR spectroscopy using triphenyl methane as internal standard (**Scheme S3.3.**, entry II).
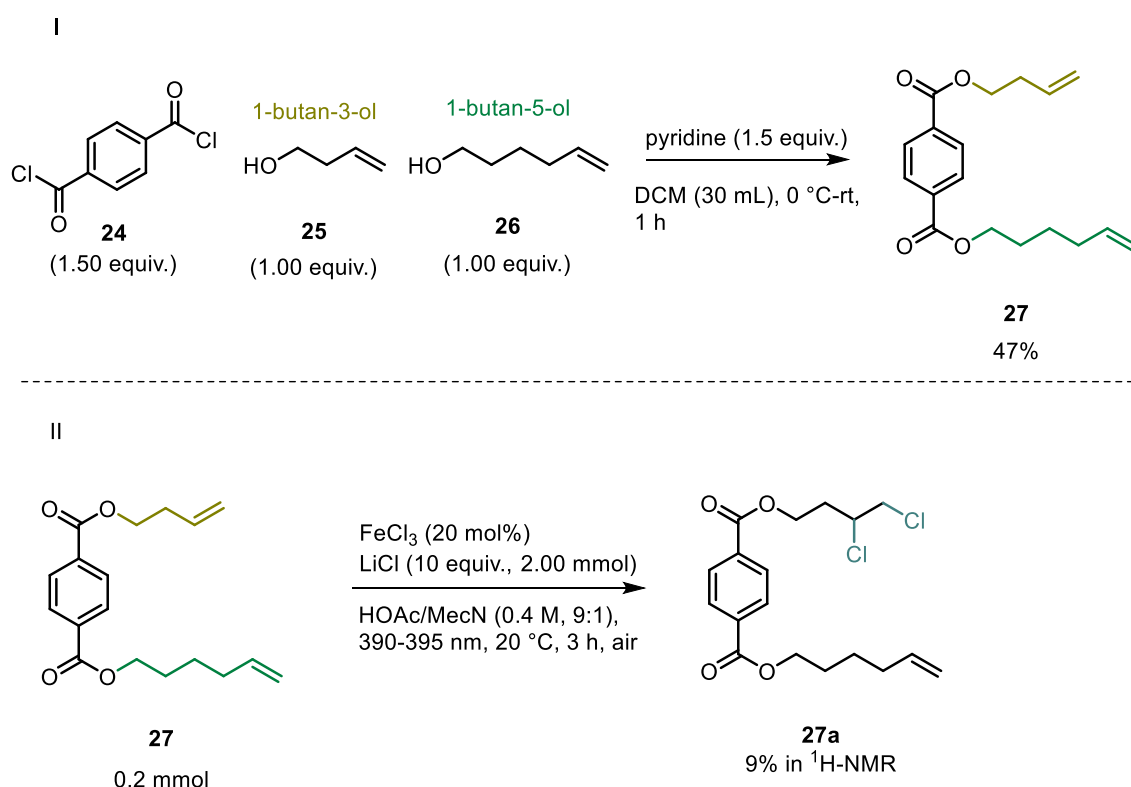
Scheme S3.3. Regioselectivity of the dichlorination reaction.

The low yield may be explained by the poor solubility of the non-polar organic molecule in the solvent mixture of acetic acid and acetonitrile (9:1).

3.13 Mechanistic Investigations

3.13.1 Inter-, or Intramolecular HAT versus Addition to Double Bond

Chlorine radicals do show the characteristics of being highly electrophilic and able to act as hydrogen atom transfer reagent in competition to the trapping reactivity in the presented work. Both, an intramolecular as well as an intermolecular radical trapping study was performed and the ratio between the dichlorinated and the chlorinated product after HAT was analysed by ^{1}H-NMR spectroscopy (**Scheme S3.4.**). Entry **I** revealed that the addition of the chlorine radical to the double bond is more prominent compared to the hydrogen atom abstraction on the methyl group of the aromatic ketone **28**, as model substrate for a compound with an accessible H-atom to be abstracted. Entry **II** highlights the possibility of an intramolecular hydrogen atom abstraction as competitive pathway for the addition of chlorine radicals to the carbon-carbon double bond in molecule **29** leading to **29a** as main product (33%) and traces of multi-halogenated product **29b** (4%).
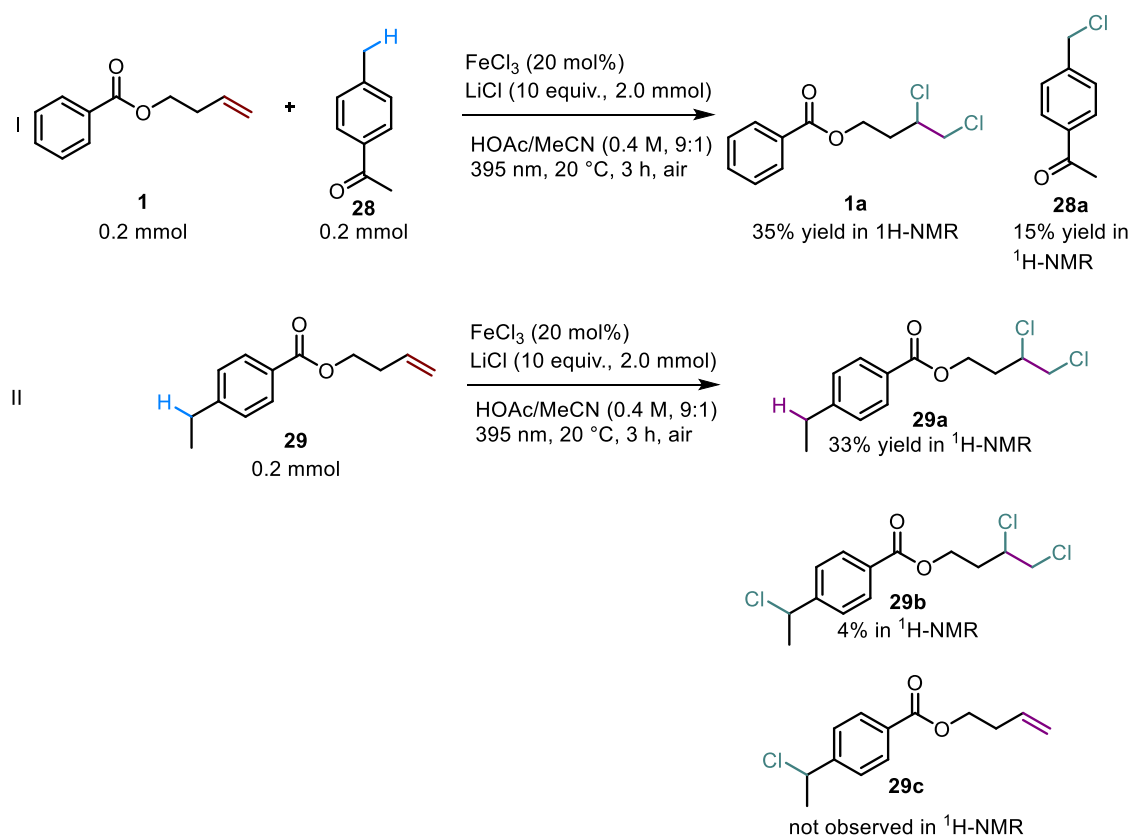
Scheme S3.4. Inter- and intramolecular hydrogen atom transfer and dichlorination of the carbon-carbon double bond.

3.14 Radical Mechanism versus Ionic Second Addition Step (Entry I, Ritter-type amination)
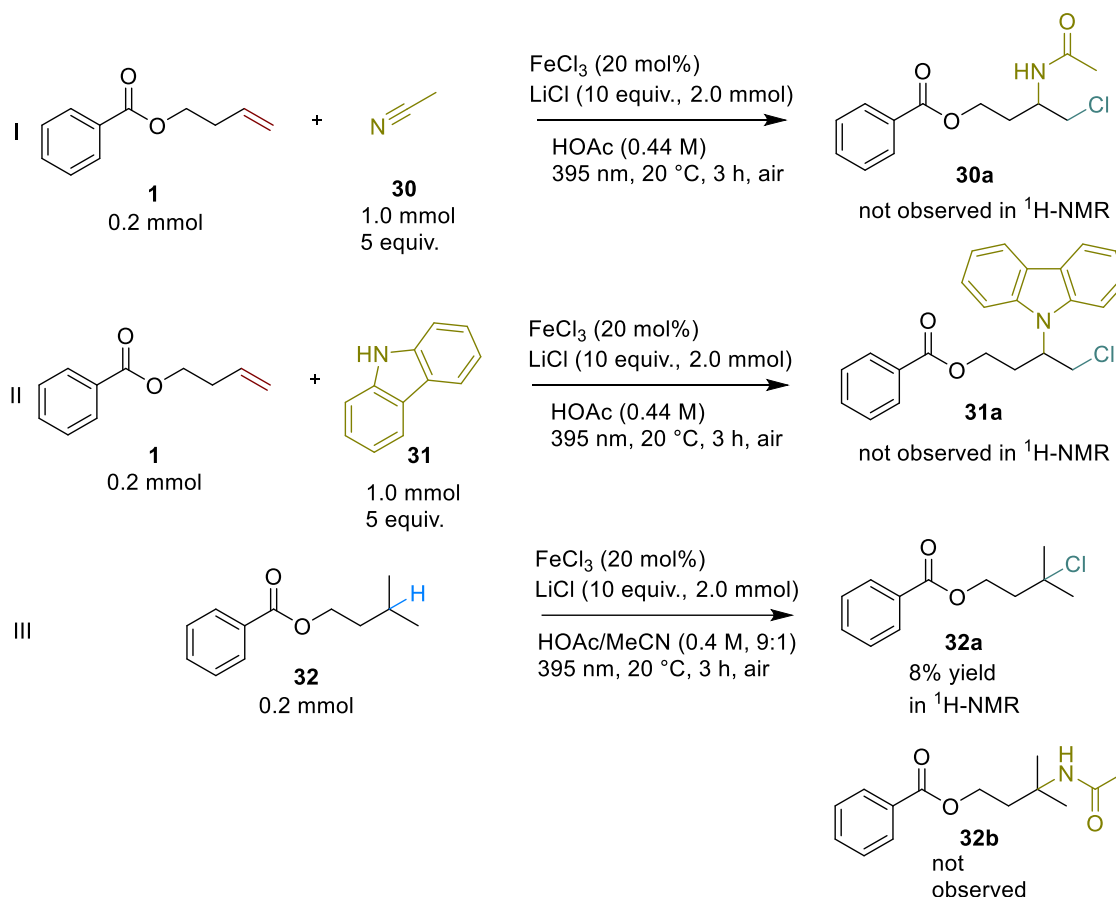
Scheme S3.5. Radical mechanism or ionic reaction for the second addition of chloride atoms.

Finally, the nature of the single reaction steps was investigated. Two mechanistic proposals can be considered: two subsequent chlorine radical additions to the double bond or first radical addition followed by a radical polar crossover step, leading to a carbocation after oxidation of the carbon-centred radical by Cl_2 as transient species in the photoreaction. Trapping the cation by a nitrile nucleophile corresponds to the class of Ritter-type aminations and therefore acetonitrile as weak and carbazole as strong nucleophiles were added in excess (Scheme **S3.5.**, entry **I** and **II**). In none of the two entries a mixed chloride-amide product could be detected but the nucleophile in high concentrations led to a complete shut-down of the photo transformation.

In a similar way, isopentyl benzoate (**32**) in entry **III** was not engaged in a radical polar crossover reaction pathway that generates a stabilized tertiary carbocation. Traces of the chlorinated product resulting from a hydrogen atom abstraction by a chloride radical that has been generated *via* light-induced homolytic Fe-Cl bond cleavage were visible in ^{1}H-NMR.

3.15 TEMPO-Trapping Experiment

A TEMPO-trapping experiment was performed to prove for stable radical intermediates, in this case a carbon-centred radical. In mass spectrometry a m/z of 368.199 was detected, that correlates to the monochlorinated TEMPO-trapped product **1-TEMPO** (**Scheme S3.6.**). For this test reaction the irradiation time was extended from 3 h to 24 h to compensate for the poor solubility of TEMPO in the solvent mixture.
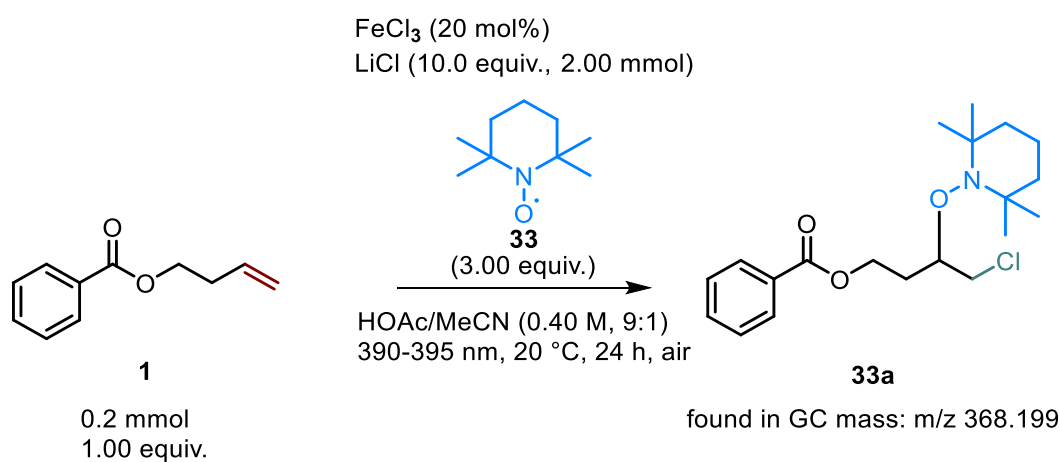
Scheme S3.6. TEMPO trapping experiment.

3.16 UV/Vis Measurements of the Reagents

To understand the interplay of the reagents in the photoreaction, UV/Vis studies were performed.

3.16.1 Interaction of FeCl₃ with Aryl Ester Compound 1

$FeCl_3$ (anhydrous, 6.50 mg, 0.04 mmol, 0.04 M) was dissolved in HPLC-grade acetonitrile (1.00 mL) and stirred for 10 min for the homogenisation of the solution. From this mixture 6.00 µL were drawn by a Hamilton syringe and added to 3.00 mL of acetonitrile in a 1 x 1 cm quartz cuvette (Spectrum **S3.1.**, red curve). Aryl ester **1** (35.2 mg, 0.20 mmol, 0.20 M) was dissolved in 1.00 mL of acetonitrile, stirred for 10 min. and 2.5 µL of the solution were added to 3.00 mL of acetonitrile in the cuvette *via* Hamilton syringe (Spectrum **S3.1.**, green curve). For the third measurement 6 µL of $FeCl_3$ (6.50 mg, 0.04 mmol, 0.04 M) in 1 mL of a 9:1 mixture acetic acid and acetonitrile was mixed with 2.5 µL of aryl benzoate **1** (35.2 mg, 0.20 mmol, 0.20 M) in 1.00 mL of acetonitrile in the 1 x 1 cm quartz cuvette containing 3.00 mL of acetonitrile (Spectrum **S1**, blue curve).
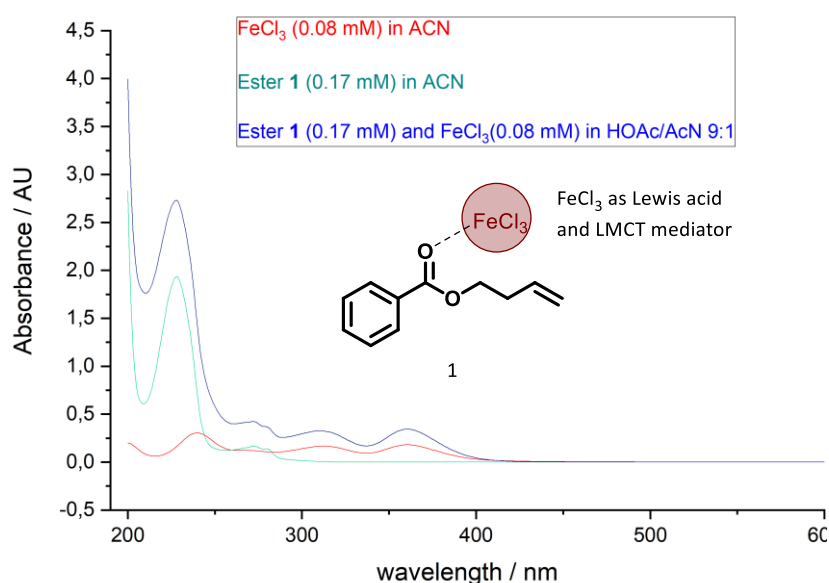
Spectrum S3.1. UV/Vis interaction of $FeCl_3$ (0.04 mM) with ester starting material **1** (0.2 mM) in the reaction mixture of acetic acid and acetonitrile (9:1) and in pure acetonitrile.
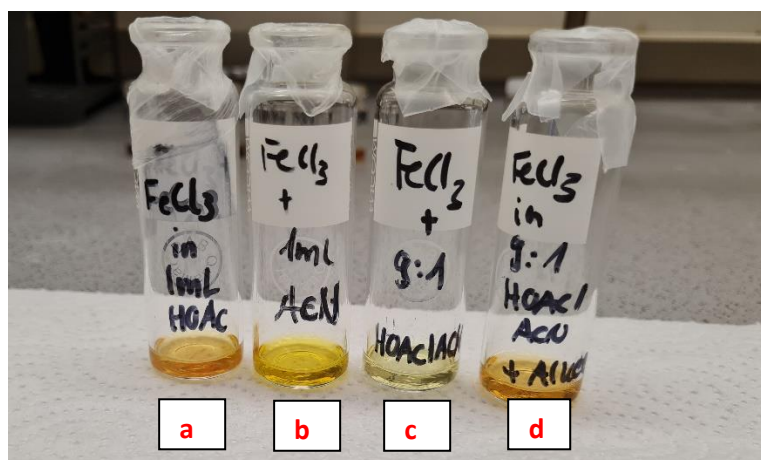
Figure F3.2. Colour change depending on the constitution of the individual solutions. **a**) FeCl$_3$ in 1 mL of pure acetic acid; orange colour; **b**) FeCl$_3$ in 1 mL of pure acetonitrile; colour change towards yellow shade. **c**) FeCl$_3$ in the 9:1 mixture of acetic acid and acetonitrile, **d**) FeCl$_3$ in 9:1 acetic acid/acetonitrile; slight colour-change upon addition of alkene aryl ester starting material **1**.

3.16.2 UV/Vis Titration of FeCl$_3$ with LiCl

Several aliquots of LiCl were added to a stock solution of FeCl$_3$ (6.50 mg, 0.04 mmol, 0.040 M) in 1 mL of HOAc/CH$_3$CN (9:1). For homogenisation of the mixtures, stirring was performed before spectroscopic measurements. For each UV/Vis measurement 6.00 µL of the mixtures were drawn and diluted in 3.00 mL of acetonitrile (HPLC-grade). The measurements were performed in a 1 x 1 cm quartz cuvette.

Table T3.4. UV/Vis titration of FeCl$_3$ solution with LiCl.

Addition step	Equivalents of LiCl	Molarity of the solutions
1	1.00	0.20 mmol, 8.50 mg, 0.20 mM
2	2.00	0.40 mmol, (+ 8.50 mg to overall 17.0 mg), 0.40 mM
3	5.00	1.00 mmol (+ 25.5 mg to overall 42.5 mg), 1.00 mM
4	10.0	2.00 mmol (+ 42.5 mg to overall 85 mg), 2.00 M
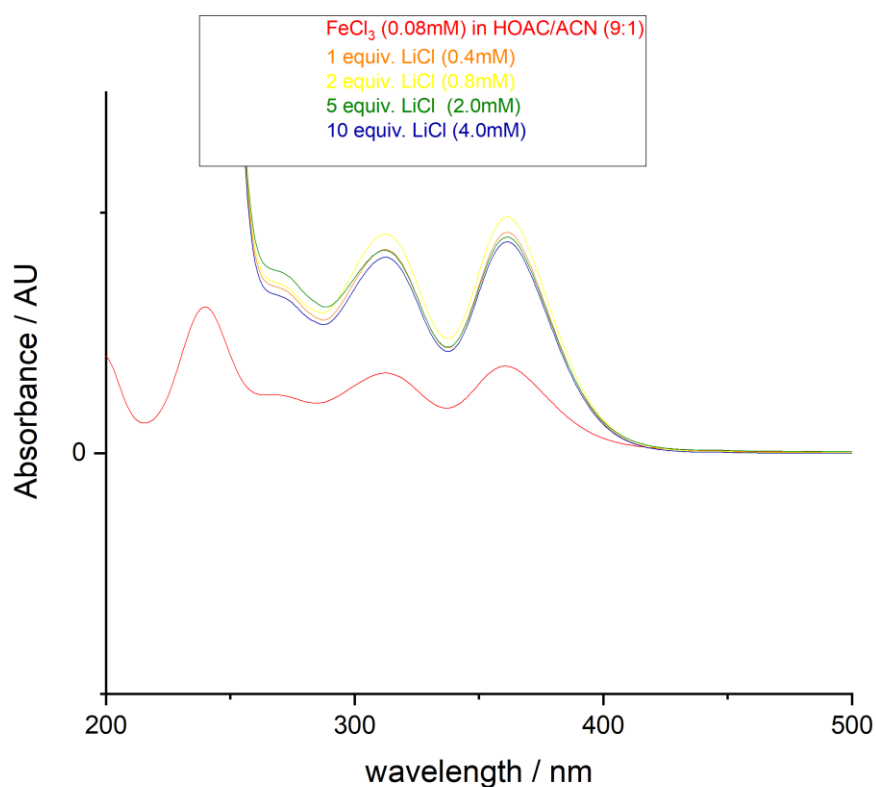
Spectrum S3.2. UV/Vis titration with LiCl.

The addition of LiCl to the FeCl$_3$ solution led to a bathochromic shift of the absorption band at 361 nm, now tailing into the 400 nm region. After the addition of 5.00 equivalents of LiCl, the band at 361 nm does not show a prominent increase and can be considered as quasi-stable regime in absorption intensity given by an equilibrium state. At 380-395 nm a new absorption band is observed that can be assigned to FeCl$_4^-$ as iron cluster formed in the mixture.[2] A similar experimental outcome was achieved for Torras *et al.* who investigated the spectral change of FeCl$_3$ upon addition of aqueous HCl at a concentration of 0.057 M regarding the iron content.[3]

3.16.3 Irradiation Experiment of the FeCl₃ Solution

This UV/Vis study was based on the results of the research group of Rovis on the HAT reactions of chlorine radicals initiated by an iron-chloride bond homolysis under visible light irradiation.[4]

FeCl₃ (13.0 mg, 0.08 mmol, 0.08 M) was dissolved in 1.00 mL of a 9:1 mixture of acetic acid and acetonitrile. An aliquot of 3.00 µL was drawn and added to 3.00 mL of HPLC-grade acetonitrile in a 1 x 1 cm quartz cuvette.
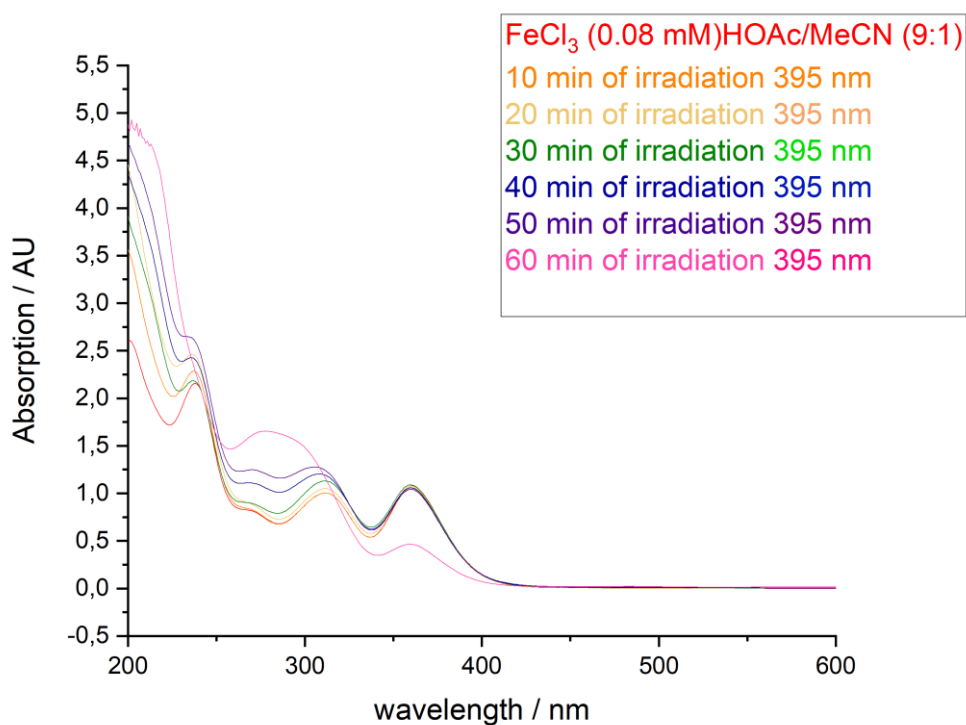
Spectrum S3.3. Irradiation of the iron(III) solution.

Irradiating the mixture did not lead to a prominent change of absorption intensity at 361 nm but an increase in absorption intensity for the region around 280-300 nm. After 1h of irradiation the absorption band at 361 nm decreased strongly while showing an increase of absorption intensity in the region of 280-300 nm. This absorption band again refers to $FeCl_4^-$ clusters.[2]

144

3.17 Reaction Kinetics

The kinetics of the photoreaction were studied using GC-FID with toluene as internal standard. Thilo Reiter performed the kinetic measurements and plotted the respective results (Figure F3.3).
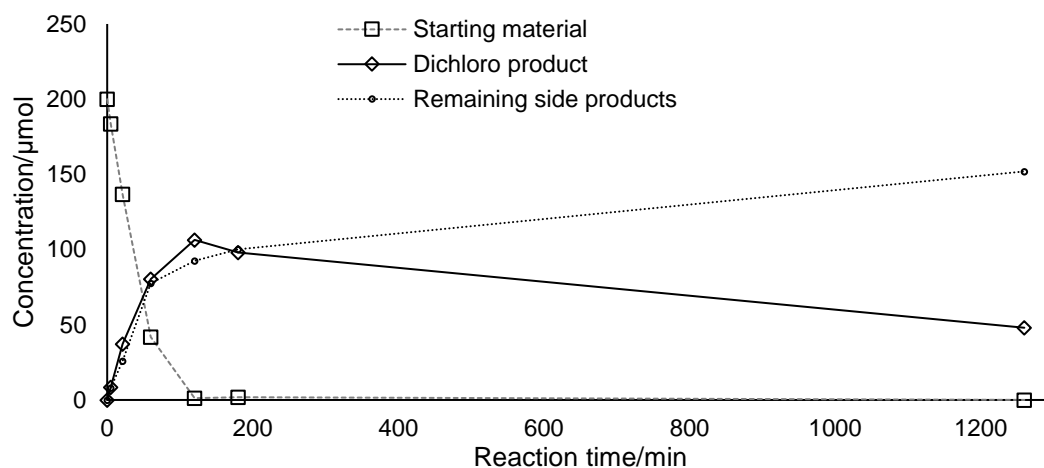
Figure F3.3. Kinetic evaluation of the iron-catalysed dichlorination. Reaction conditions: but-3-en-1-yl benzoate (**1**) (35.2 mg, 0.20 mmol, 1.00 equiv.), FeCl$_3$ (20 mol%), LiCl (85.0 mg, 2.00 mmol, 10.0 equiv.), 0.5 mL of HOAc/CH$_3$CN (9:1), 20 °C irradiated with 395 nm LED. The measurement of dichlorination yield (consistent black curve) and starting material consumption (streaked graph) was monitored with GC-FID using toluene as internal standard. The difference between the amount of product **1a** and olefin with respect to the added amount of compound **1** are undesired side products and depicted as dotted line.

3.18 Starting Material Synthesis and Spectroscopic Evaluation

3.18.1 General Procedure for the Formation of Aryl Esters

The synthesis of the starting materials for the iron-catalysed photo-dichlorination of alkenes was successfully performed according to published literature.[5]

The benzoyl chloride derivative (1.50 equiv.) was dropwise added to a stirred solution of an (terminal) alkene alcohol (1.00 equiv.) and pyridine (2.00 equiv.) in dichloromethane at 0 °C. After completion of addition the mixture was allowed to slowly warm to room temperature and was stirred for another 60 min. After this time the solution was quenched with water (30.0 mL) and stepwise washed with 1 M HCl (30.0 mL), NaHCO₃ (sat., 30.0 mL) and water (30.0 mL). The combined organic phases were dried over anhydrous Na_2SO_4 and the residual solvent was removed under reduced pressure. The crude aryl ester was purified by flash column chromatography on silica in petroleum ether/ethyl acetate (95:5). The final products were isolated in moderate to good yields and the NMR data are in good accordance with the literature.
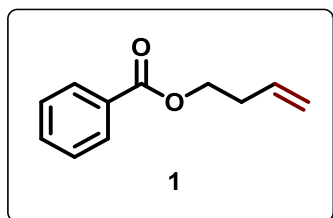
but-3-en-1-yl benzoate (1)

The synthesis was performed according to the general procedure described above mixing benzoyl chloride (2.07 mL, 18.0 mmol, 1.50 equiv.), pyridine (1.94 mL; 24.0 mmol, 2.00 equiv.) and 3-buten-1-ol (1.03 mL, 12.0 mmol, 1.00 equiv.) in 50 mL of DCM and **but-3-en-1-yl benzoate (1)** could be isolated as colourless oil in 75% yield (1.58 g, 8.97 mmol). The experimental outcome is in good accordance with the published literature.[5]

¹H-NMR (400 MHz, CDCl$_3$, δ_H) 8.10 – 7.96 (m, 2H), 7.61 – 7.50 (m, 1H), 7.50 – 7.36 (m, 2H), 5.88 (ddt, J = 17.0, 10.2, 6.7 Hz, 1H), 5.23 – 5.07 (m, 2H), 4.38 (t, J = 6.7 Hz, 2H), 2.53 (qt, J = 6.7, 1.4 Hz, 2H).

¹³C-NMR (101 MHz, CDCl$_3$, δ_C) 166.7 (C$_q$), 134.2 (+), 133.0 (+), 130.5 (C$_q$), 129.7 (+), 128.5 (+), 117.5 (-), 64.1 (-), 33.3 (-).

Yield: 75%, 1.58 g, 8.97 mmol, colourless oil

2
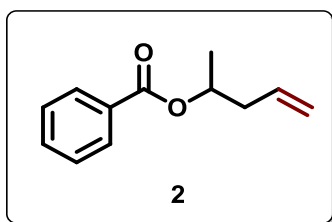
Pent-4-en-2-yl benzoate (**2**)

The reaction was performed with benzoyl chloride (1.73 mL, 15.0 mmol, 1.50 equiv.), pyridine (1.61 mL, 20.0 mmol, 2.00 equiv.) and pent-4-en-2-ol (1.03 mL, 10.0 mmol, 1.00 equiv.) in 30 mL of DCM to yield **pent-4-en-2yl benzoate** (**2**) in 64% (1.23 g, 6.44 mmol) as colourless oil. The result is in good accordance with published literature.[6]

¹H-NMR (300 MHz, CDCl$_3$, δ_H) 8.07 – 8.01 (m, 2H), 7.58 – 7.51 (m, 1H), 7.47 – 7.39 (m, 2H), 5.84 (ddt, J = 17.2, 10.2, 7.0 Hz, 1H), 5.22 (q, J = 6.3 Hz, 1H), 5.18 – 5.15 (m, 1H), 5.09 (ddt, J = 10.0, 2.1, 1.1 Hz, 1H), 2.55 – 2.36 (m, 2H), 1.36 (d, J = 6.3 Hz, 3H).

¹³C-NMR (75 MHz, CDCl$_3$, δ_C) 166.1 (C$_q$), 133.7 (+), 132.8 (+), 130.8 (C$_q$), 129.5 (+), 128.3 (+), 117.9 (-), 70.8 (+), 40.4 (+), 20.5 (+).

Yield: 64%, 1.23 g, 6.44 mmol, colourless oil.

3
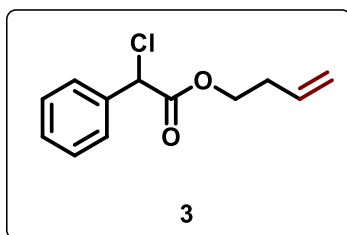
but-3-en-1-yl 2-chloro-2-phenylacetate (3)

The reaction was performed using 2-chloro-2-phenylacetylchloride (2.36 mL, 15.0 mmol, 1.50 equiv.), pyridine (1.61 mL, 20.0 mmol, 2.00 equiv.) and 3-buten-1-ol (0.86 mL, 10.0 mmol, 1.00 equiv.) in 30 mL of DMC to receive **but-3-en-1-yl 2-chloro-2-phenylacetate (3)** in 35% yield as colourless oil (0.78 g, 3.50 mmol). The spectroscopic data fit to the published literature about terminal alkynes of the same substitution.[7]

¹H-NMR (300 MHz, CDCl₃, δ_H) 7.54 – 7.45 (m, 2H), 7.42 – 7.33 (m, 3H), 5.78 – 5.61 (m, 1H), 5.35 (s, 1H), 5.08 – 5.03 (m, 1H), 5.00 (t, J = 1.4 Hz, 1H), 4.22 (td, J = 6.7, 0.7 Hz, 2H), 2.37 (qt, J = 6.7, 1.3 Hz, 2H).

¹³C-NMR (75 MHz, CDCl₃, δ_C) 168.4 (C_q), 135.8 (C_q), 133.3 (+), 129.3 (+), 128.8 (+), 128.0 (+), 117.7 (+), 65.4 (+), 59.1 (-), 32.8 (-).

Yield: 35%, 0.78 g, 3.50 mmol, colourless oil.

4
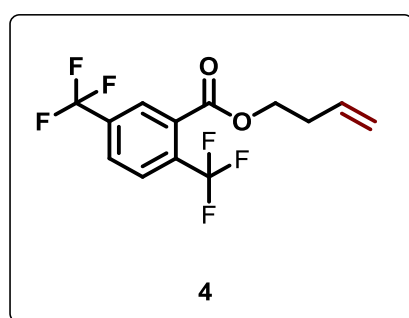
but-3-en-1-yl 2,5-bis(trifluoromethyl)benzoate (4)

The synthesis was performed using 2,5-bis(trifluoromethyl)benzoyl chloride (1.36 mL, 7.50 mmol, 1.50 equiv.), pyridine (0.81 mL, 10.0 mmol, 2.00 equiv.) and 3-buten-1-ol (0.43 mL, 5.00 mmol, 1.00 equiv.) in 30 mL of DCM to get **but-3-en-1-yl 2,5-bis(trifluoromethyl)benzoate (4)** in 73% yield (1.14 g, 3.66 mmol) as colourless oil. The spectroscopic analysis fits to the published results.[8]

¹H-NMR (300 MHz, CDCl₃, δ_H) 8.48 (d, J = 1.8 Hz, 2H), 8.06 (td, J = 1.8, 1.0 Hz, 1H), 5.86 (ddt, J = 17.0, 10.2, 6.8 Hz, 1H), 5.25 – 5.09 (m, 2H), 4.46 (t, J = 6.7 Hz, 2H), 2.57 (qt, J = 6.7, 1.4 Hz, 2H).

¹³C-NMR (75 MHz, CDCl$_3$, δ$_C$) 163.9 (C$_q$), 133.4 (C$_q$), 132.5 (C$_q$), 132.4 (C$_q$), 129.7 (+), 126.5 (+), 124.7 (C$_q$), 121.1 (C$_q$), 117.9 (-), 65.1 (-), 33.1 (-).

Yield: 73%, 1.14 g, 3.66 mmol, colourless oil.

5
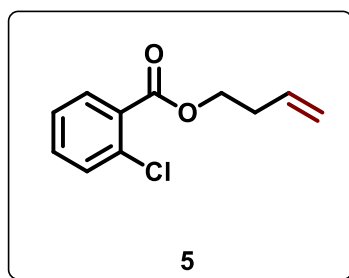
but-3-en-1-yl 2-chlorobenzoate (**5**)

The reaction was conducted with 1-chloro benzoyl chloride (1.90 mL, 15.0 mmol, 1.50 equiv.), pyridine (1.61 mL, 20.0 mmol, 2.00 equiv.) and 3-buten-1-ol (0.86 mL, 10.0 mmol, 1.00 equiv.) in 30 mL of DCM to obtain **but-3-en-1-yl 2-chlorobenzoate** (**5**) in 71% yield (1.50 g, 7.12 mmol) as colourless oil. The spectroscopic data of the pure product fit to the results from published literature.[8]

¹H-NMR (300 MHz, CDCl$_3$, δ$_H$) δ 7.91 – 7.73 (m, 1H), 7.52 – 7.35 (m, 2H), 7.30 (ddd, J = 7.6, 6.9, 1.8 Hz, 1H), 5.87 (ddt, J = 17.0, 10.2, 6.7 Hz, 1H), 5.25 – 5.05 (m, 2H), 4.39 (t, J = 6.7 Hz, 2H), 2.53 (qt, J = 6.7, 1.4 Hz, 2H).

¹³C-NMR (75 MHz, CDCl$_3$, δ$_C$) 165.7 (C$_q$), 134.0 (C$_q$), 133.7, 132.5, 131.4, 131.1, 130.3, 126.6, 117.5 (C$_q$), 64.6 (-), 33.1 (-).

Yield: 71%, 1.50 g, 7.12 mmol, colourless oil.
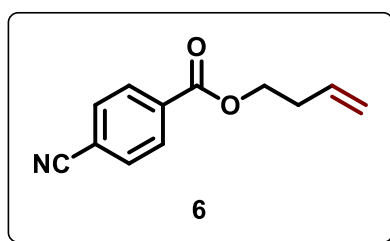
but-3-en-1-yl 4-cyano benzoate (**6**)

The reaction was performed adding 4-cyanobenzoyl chloride (0.98 g, 5.89 mmol, 1.50 equiv.) to 3-but-en-1-ol (0.34 mL, 3.93 mmol, 1.00 equiv.) and pyridine (1.61 mmol, 20.0 mmol, 2.00 equiv.) in 10 mL of DCM. **But-3-en-1-yl 4-cyano benzoate** (**6**) was received in 16% yield as slightly yellow oil (0.13 g, 0.62 mmol). The results are in good accordance with published literature.[9]

^{1}H-NMR (300 MHz, CDCl$_3$, δ_H) 8.14 – 8.04 (m, 2H), 7.75 – 7.65 (m, 2H), 5.82 (ddt, J = 17.0, 10.2, 6.7 Hz, 1H), 5.19 – 5.02 (m, 2H), 4.37 (t, J = 6.6 Hz, 2H), 2.50 (qt, J = 6.7, 1.4 Hz, 2H).

^{13}C-NMR (75 MHz, CDCl$_3$, δ_C) 164.8 (C$_q$), 134.1 (C$_q$), 133.7 (+), 132.2 (+), 130.1 (+), 118.0 (C$_q$), 117.7 (+), 116.3 (C$_q$), 64.7 (-), 33.0 (-).

Yield: 16%, 0.13 g, 0.62 mmol, off-yellow oil.
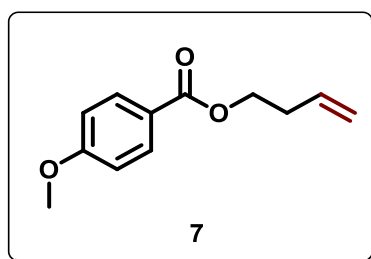
but-3-en-1-yl 4-methoxybenzoate (**7**)

The synthesis was performed by reacting 4-methoxy benzoyl chloride (2.03 mL, 15.0 mmol, 1.50 equiv.), pyridine (1.61 mL, 20.0 mmol, 2.00 equiv.) and 3-but-en-1-ol (0.86 mL, 10.0 mmol, 1.00 equiv.) in 30 mL of DCM. **But-3-en-1-yl 4-methoxybenzoate** (**7**) was isolated in 77% yield as colourless oil (1.58 g, 7.66 mmol). The spectroscopic data for the obtained compound accurately match the published literature.[10]

^{1}H-NMR (300 MHz, CDCl$_3$, δ_H) 8.04 – 7.93 (m, 2H), 6.95 – 6.84 (m, 2H), 5.87 (ddt, J = 17.0, 10.2, 6.7 Hz, 1H), 5.23 – 5.05 (m, 2H), 4.34 (t, J = 6.7 Hz, 2H), 3.85 (s, 3H), 2.51 (qt, J = 6.7, 1.4 Hz, 2H).

^{13}C-NMR (75 MHz, CDCl$_3$, δ_C) 166.3 (C$_q$), 163.3 (C$_q$), 134.2 (+), 131.6 (+), 122.8 (-), 117.3 (+), 113.6 (+), 63.7 (-), 55.4 (+), 33.3 (-).

Yield: 77%, 1.58 g, 7.66 mmol, colourless oil.

8
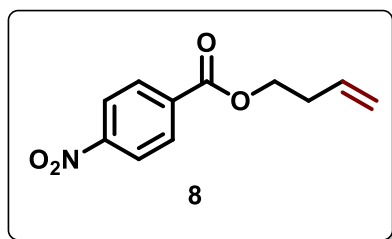
but-3-en-1-yl 4-nitrobenzoate (8)

The compound was synthesised, using 4-nitro benzoyl chloride (2.78 g, 15.0 mmol, 1.50 equiv.), pyridine (1.61 mL, 20.0 mmol, 2.00 equiv.) and 3-buten-1-ol (0.86 mL, 10.0 mmol, 1.00 equiv.) in 30 mL of DCM. **But-3-en-1-yl 4-nitrobenzoate (8)** was isolated as yellow oil in 72% yield (1.60 g, 7.23 mmol). The spectral data of the isolated compound are in good accordance with published results.[11]

^{1}H-NMR (300 MHz, CDCl$_3$, δ_H) 8.34 – 8.12 (m, 4H), 5.86 (ddt, J = 17.0, 10.2, 6.7 Hz, 1H), 5.22 – 5.06 (m, 2H), 4.43 (t, J = 6.6 Hz, 2H), 2.55 (qt, J = 6.6, 1.4 Hz, 2H).

^{13}C-NMR (75 MHz, CDCl$_3$, δ_C) 164.7 (C$_q$), 150.5 (C$_q$), 135.7 (C$_q$), 133.6 (+), 130.7 (+), 123.6 (+), 117.8 (+), 64.9 (-), 33.1 (-).

Yield: 72%, 1.60 g, 7.23 mmol, yellow oil.
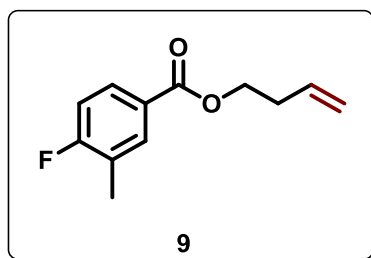
but-3-en-1-yl 4-fluoro-3-methylbenzoate (9)

The compound was synthesised upon addition of 4-fluoro-3-methyl benzoyl chloride (2.12 mL, 15.0 mL, 1.50 equiv.) to 3-but-en-1-ol (0.86 mL, 10.0 mmol, 1.00 equiv.) and pyridine (1.61 mL, 20.0 mmol, 2.00 equiv.) in 30 mL of DMC. **But-3-en-1-yl 4-fluoro-3-methyl benzoate (9)** was obtained as colourless oil in 56% yield (1.37 g, 6.56 mmol).

¹H-NMR (300 MHz, CDCl₃, δ$_H$)7.93 – 7.81 (m, 2H), 7.04 (t, J = 8.9 Hz, 1H), 5.87 (ddt, J = 17.0, 10.2, 6.7 Hz, 1H), 5.22 – 5.06 (m, 2H), 4.35 (t, J = 6.7 Hz, 2H), 2.52 (qt, J = 6.7, 1.4 Hz, 2H), 2.31 (d, J = 2.1 Hz, 3H).

¹³C-NMR (75 MHz, CDCl₃, δ$_C$)166.0 (C$_q$), 134.0 (+), 133.3 (+), 129.4 (+), 126.2 (C$_q$), 125.3 (C$_q$), 117.4 (+), 115.2 (+), 114.9 (+), 64.0 (-), 33.2 (-), 14.5 (+).

Yield: 56%, 1.37 g, 6.56 mmol, colourless oil.
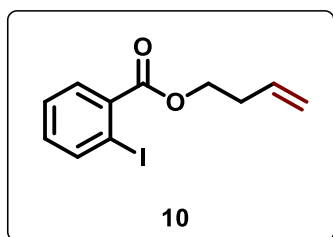
but-3-en-1-yl 2-iodobenzoate (10)

But-3-en-1yl 2-iodobenzoate (10) was synthesised from 2-iodo benzoyl chloride (2.00 g, 7.50 mmol, 1.50 equiv.), pyridine (0.81 mL, 10.0 mmol, 2.00 equiv.) and but-3-en-1-ol (0.43 mL, 5.00 mmol, 1.00 equiv.). The ester could be isolated in 13% yield as colourless oil (0.19 g, 0.63 mmol). The spectroscopic data match results from similar structures published in literature.[12]

¹H-NMR (400 MHz, CDCl₃, δ_H) 7.97 (dd, J = 8.0, 1.2 Hz, 1H), 7.78 (dd, J = 7.8, 1.7 Hz, 1H), 7.38 (td, J = 7.6, 1.2 Hz, 1H), 7.12 (td, J = 7.7, 1.7 Hz, 1H), 5.87 (ddt, J = 17.0, 10.3, 6.7 Hz, 1H), 5.22 – 5.06 (m, 2H), 4.39 (t, J = 6.7 Hz, 2H), 2.54 (qt, J = 6.7, 1.4 Hz, 2H).

¹³C-NMR (101 MHz, CDCl₃, δ_C) 166.4 (C_q), 141.3 (+), 135.2 (C_q), 133.9 (+), 132.6 (+), 130.9 (+), 127.9 (C_q), 117.5 (+), 94.1 (-), 64.8 (-), 33.0 (+).

Yield: 13%, 0.19 g, 0.63 mmol, colourless oil.

27
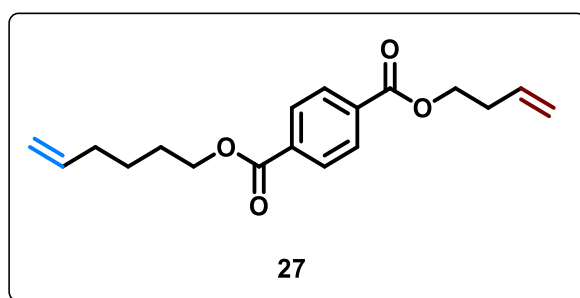
but-3-en-1-yl hex-5-en-1-yl terephthalate (**27**)

Compound **27** was synthesised by reacting 3-buten-1-ol (0.86 mL, 10.0 mmol, 1.00 equiv.), 5-hexen-1-ol (1.20 mL, 10.0 mmol, 1.00 equiv.), pyridine (1.61 mL, 20.0 mmol, 2.00 equiv.) and terephthaloyl dichloride (3.05 g, 15.0 mmol, 1.50 equiv.) to receive the respective di-ester **27** in 47% yield as colourless oil.[10]

¹H-NMR (300 MHz, CDCl₃, δ_H) 8.09 (t, J = 1.0 Hz, 4H), 5.84 (dddt, J = 16.9, 15.1, 10.2, 6.7 Hz, 2H), 5.24 – 4.92 (m, 4H), 4.37 (dt, J = 15.0, 6.6 Hz, 4H), 2.54 (qt, J = 6.7, 1.4 Hz, 2H), 2.19 – 2.07 (m, 2H), 1.87 – 1.73 (m, 2H), 1.65 – 1.51 (m, 2H).

¹³C-NMR (75 MHz, CDCl₃, δ_C) 165.9 (C_q), 138.3 (+), 133.9 (C_q), 129.5 (+), 117.6 (+), 115.0 (+), 65.4 (-), 64.4 (-), 33.3 (-), 28.1 (-), 25.3 (-).

Yield: 47%, 1.42 g, 4.70 mmol, colourless oil.

29
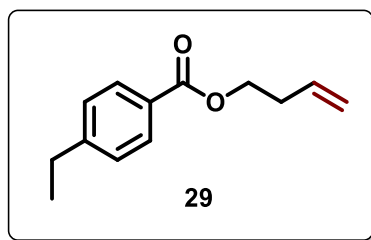
but-3-en-1-yl 4-ethylbenzoate (**29**)

Aryl ester **29** was synthesised from 3-buten-1-ol (0.66 mL, 7.53 mmol, 1.00 equiv.), pyridine (1.22 mL, 15.06 mmol, 2.00 mmol) and 4-ethyl benzoyl chloride (1.1 mL, 11.3 mmol, 1.50 equiv.) to obtain compound **29** in 66% yield as colourless oil.[10]

^{1}H-NMR (400 MHz, CDCl$_3$, δ_H) 8.02 – 7.93 (m, 2H), 7.31 – 7.27 (m, 2H), 5.90 (ddt, J = 17.0, 10.2, 6.7 Hz, 1H), 5.25 – 5.10 (m, 2H), 4.38 (t, J = 6.7 Hz, 2H), 2.72 (q, J = 7.6 Hz, 2H), 2.54 (qt, J = 6.7, 1.4 Hz, 2H), 1.28 (t, J = 7.6 Hz, 3H).

^{13}C-NMR (101 MHz, CDCl$_3$, δ_C) 166.6 (C$_q$), 149.7 (C$_q$), 134.1 (+), 129.7 (+), 127.9 (C$_q$), 117.3 (+), 63.8 (-), 33.2 (-), 29.0 (-), 15.3 (+).

Yield: 66%, 1.02 g, 4.99 mmol, colourless oil.

3.19 NMR Spectra of the Starting Materials
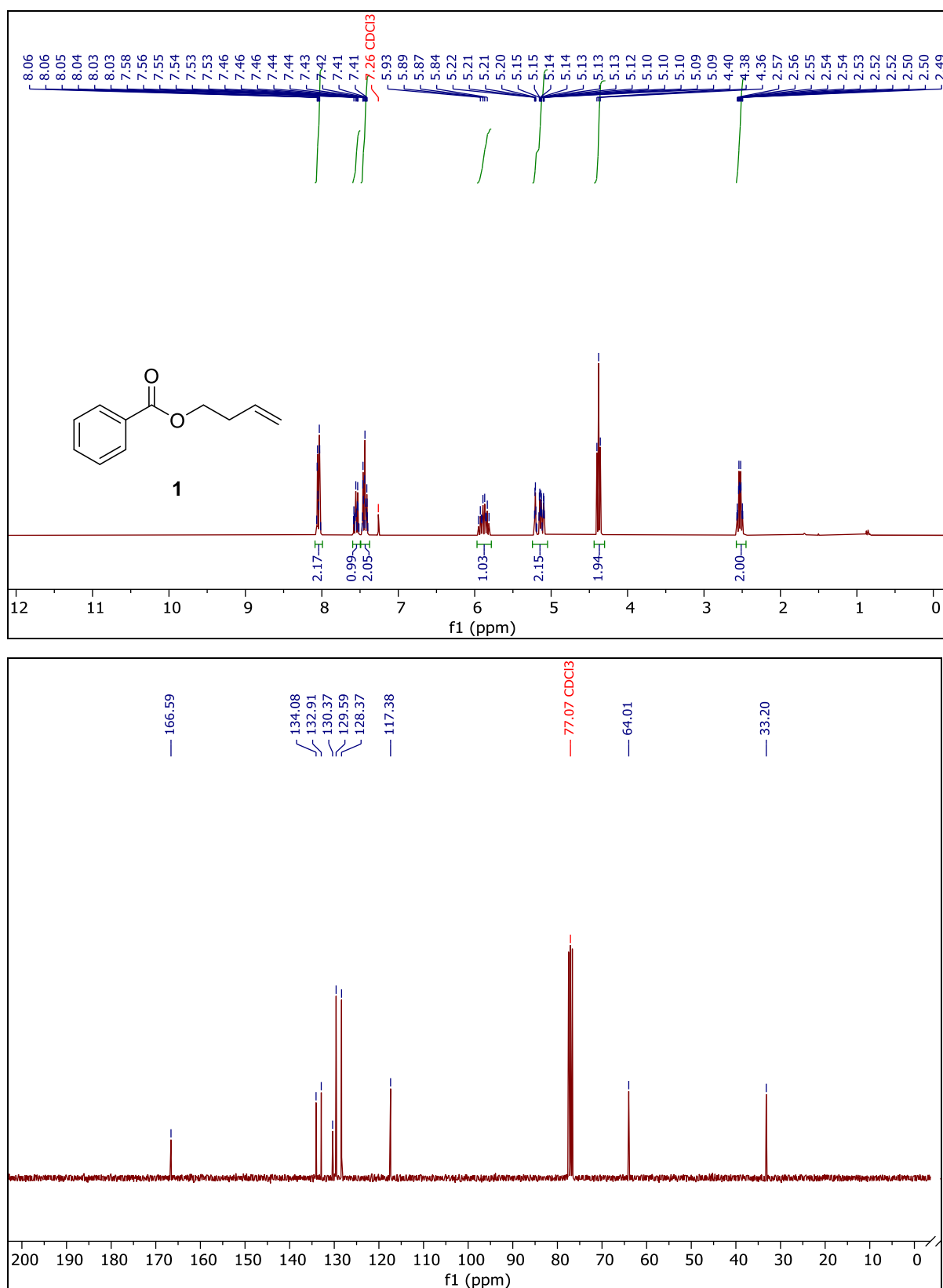
Spectrum S3.4. Compound **1**, ^{1}H- and ^{13}C-NMR (Chloroform-*d*).
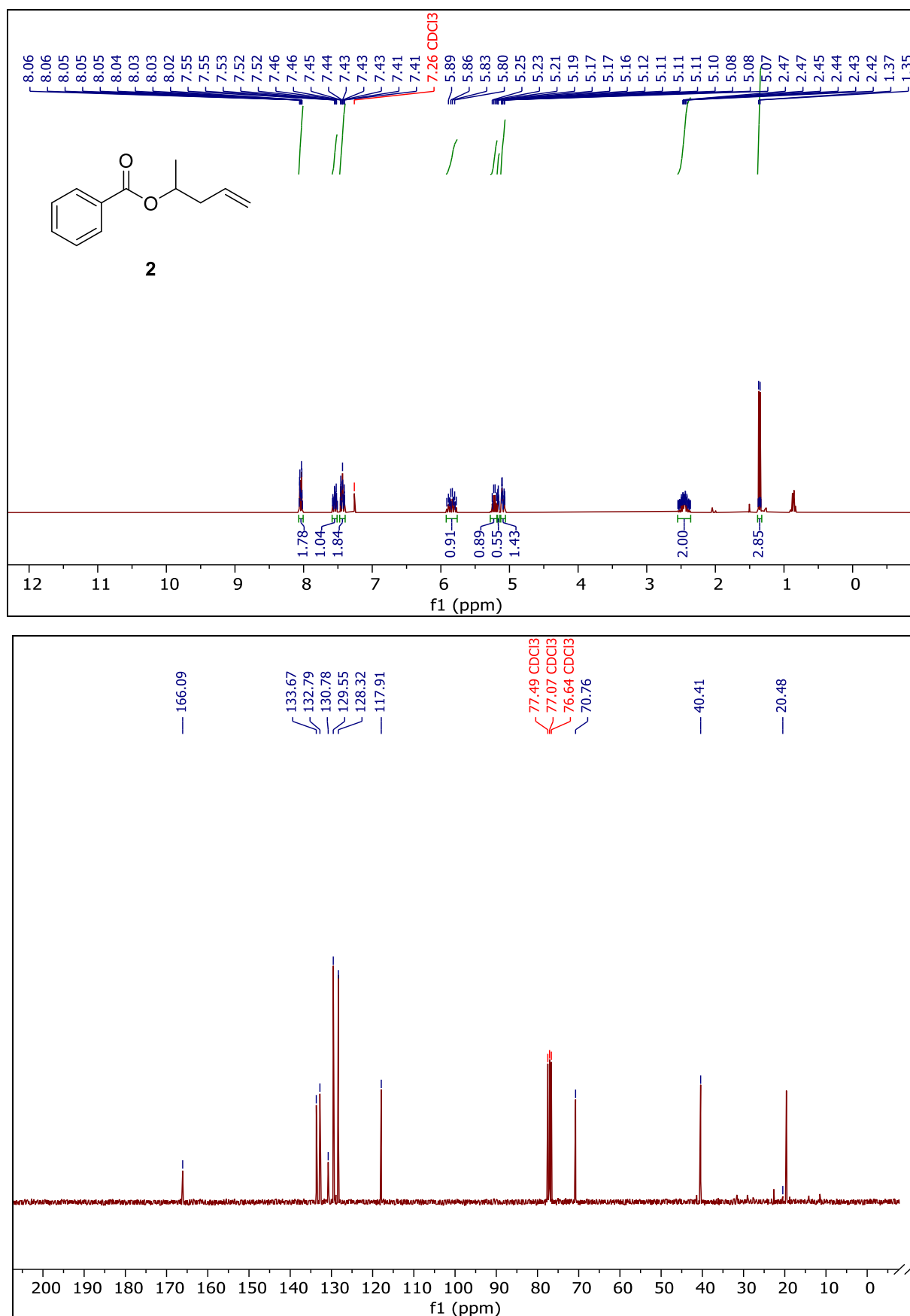
Spectrum S3.5. Compound **2**, ¹H- and ¹³C-NMR (Chloroform-*d*).
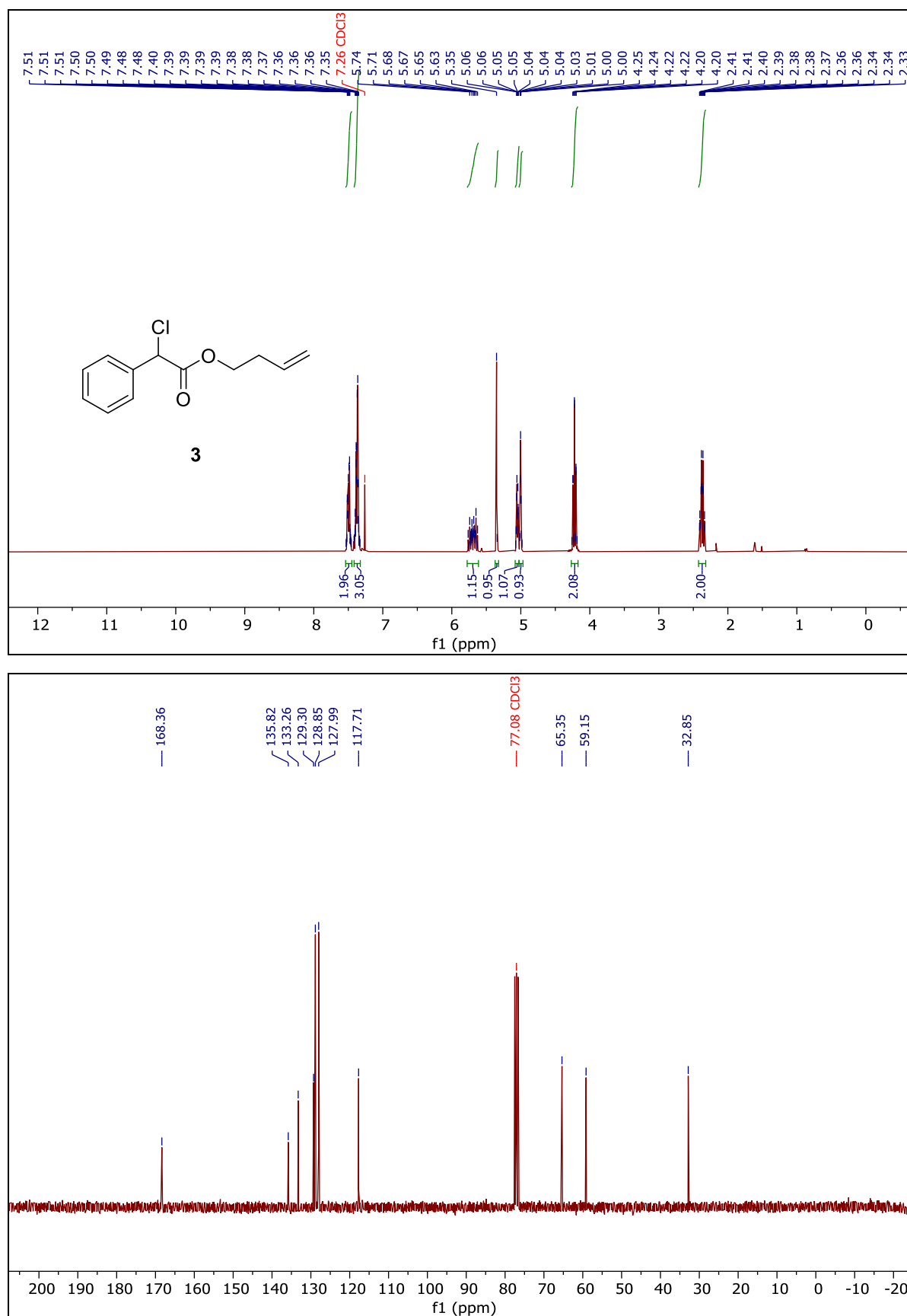
Spectrum S.3.6. Compound **3**, ^{1}H- and ^{13}C-NMR (Chloroform-*d*).
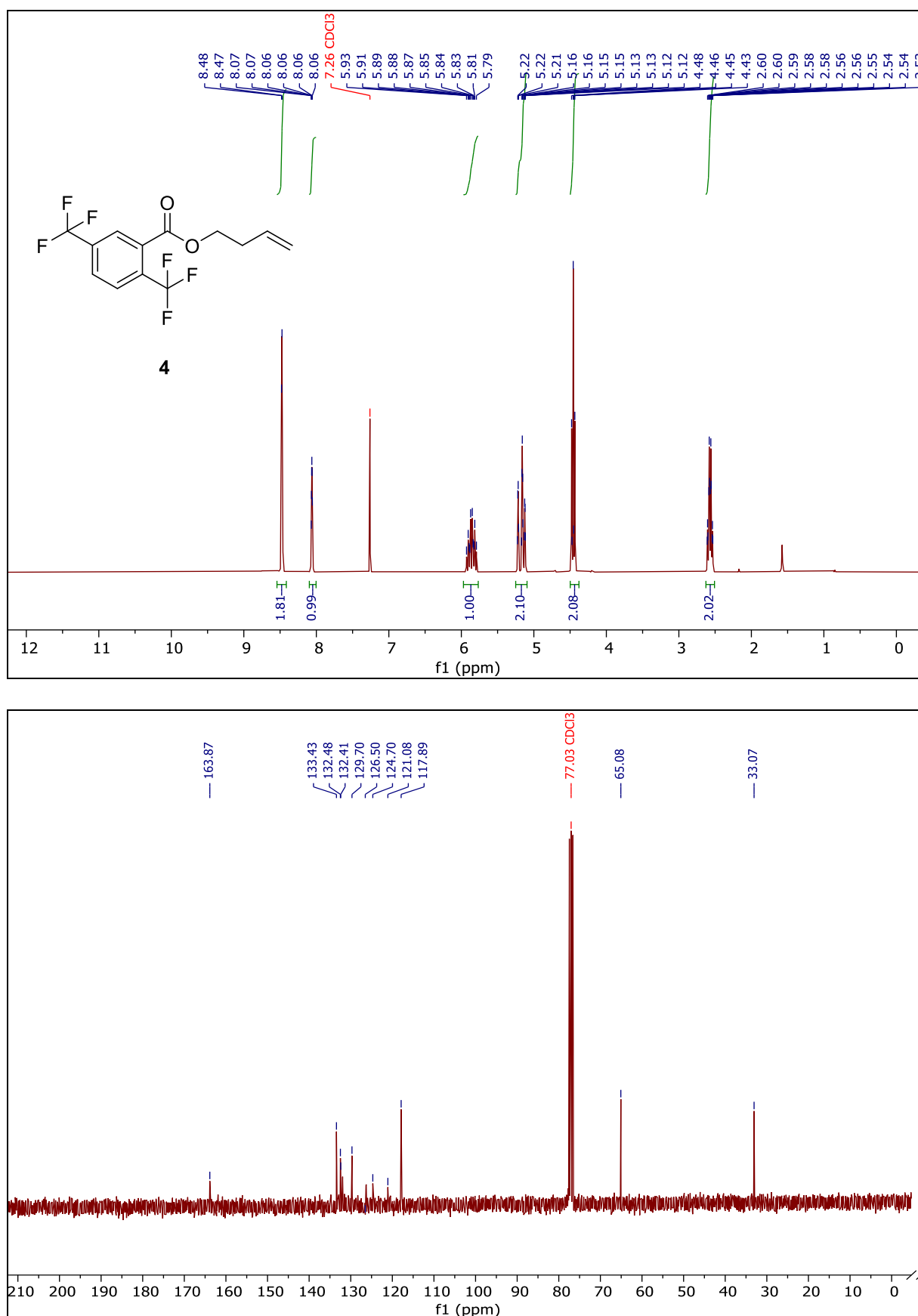
Spectrum S3.7. Compound **4**, ^{1}H- and ^{13}C-NMR (Chloroform-*d*).
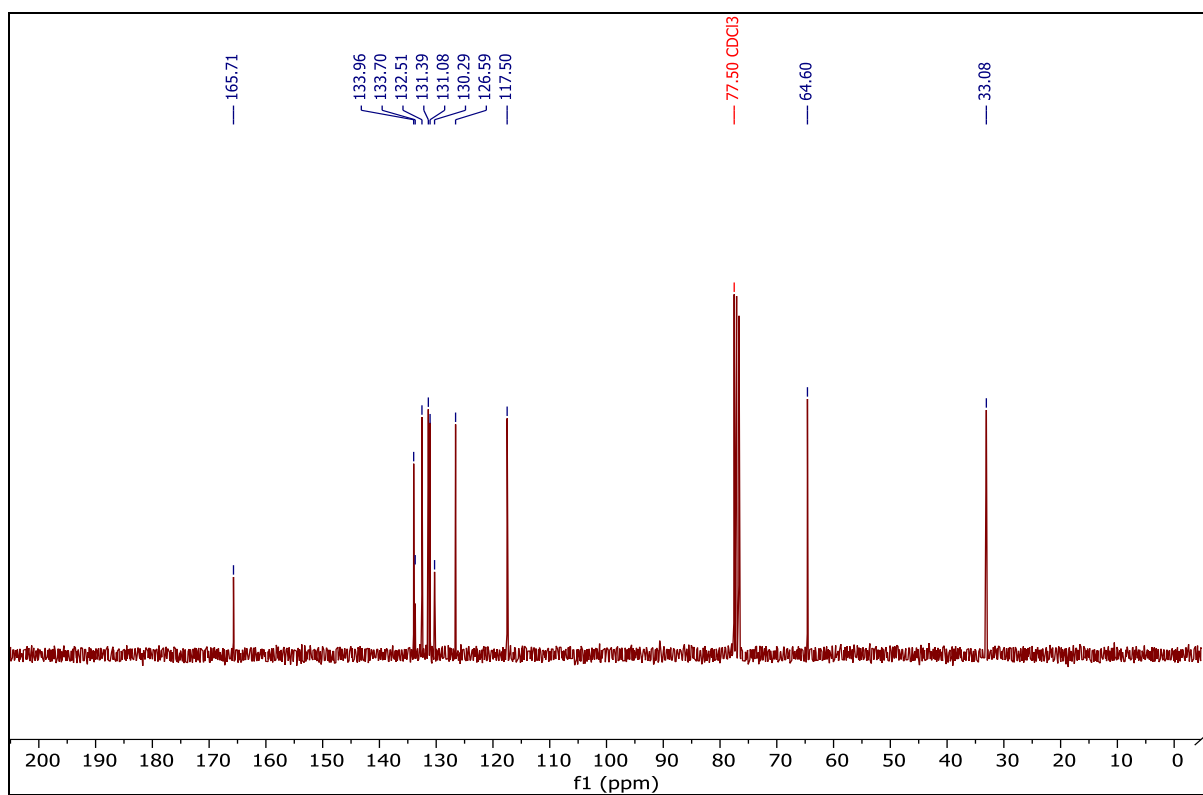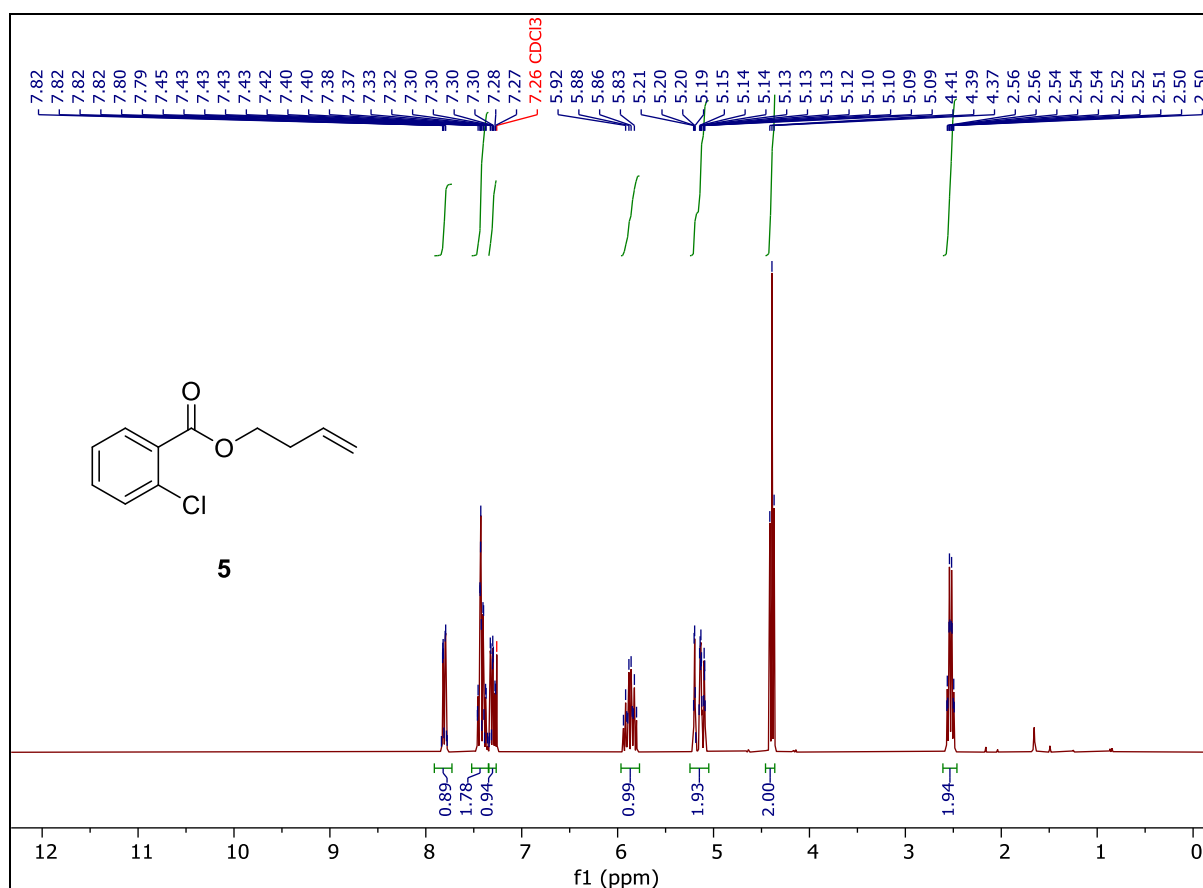
Spectrum *S3.8.* Compound **5**, ^{1}H- and ^{13}C-NMR (Chloroform-*d*).
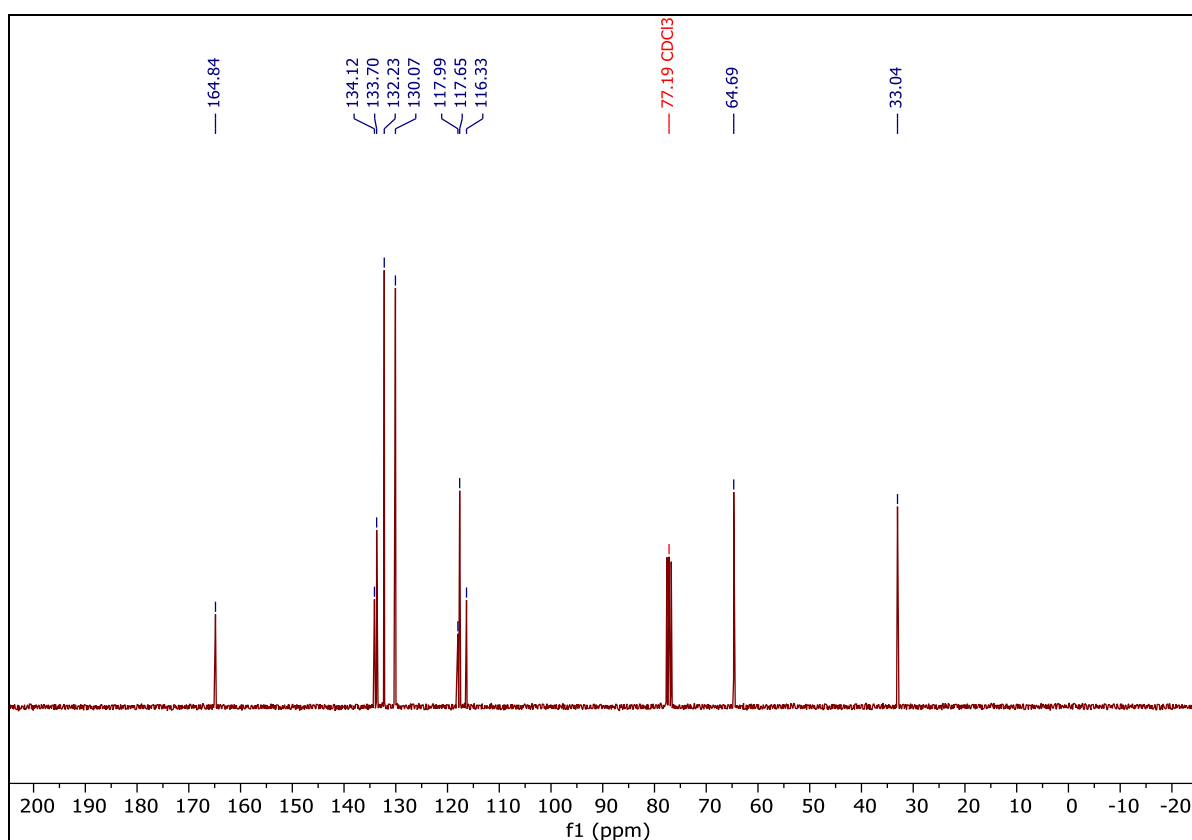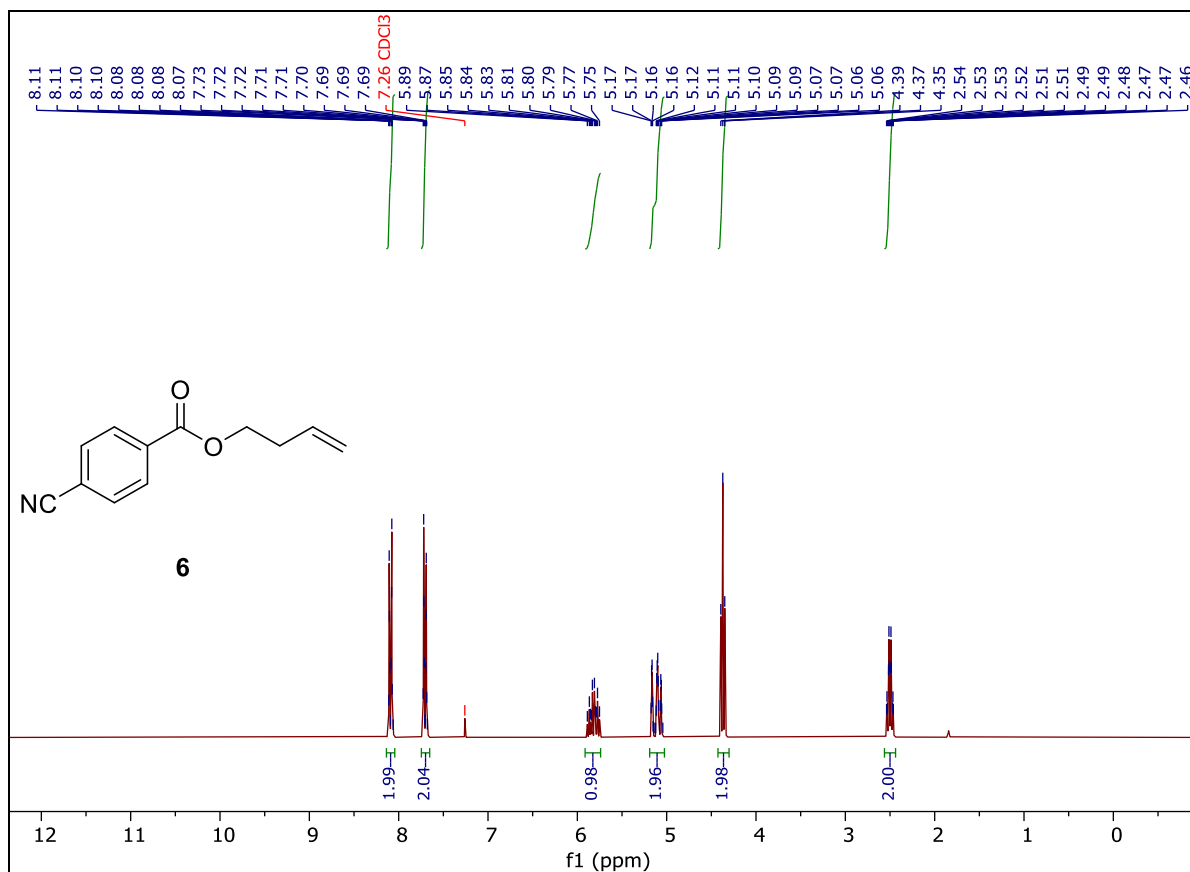
Spectrum S3.9. Compound **6**, ^{1}H- and ^{13}C-NMR (Chloroform-*d*).
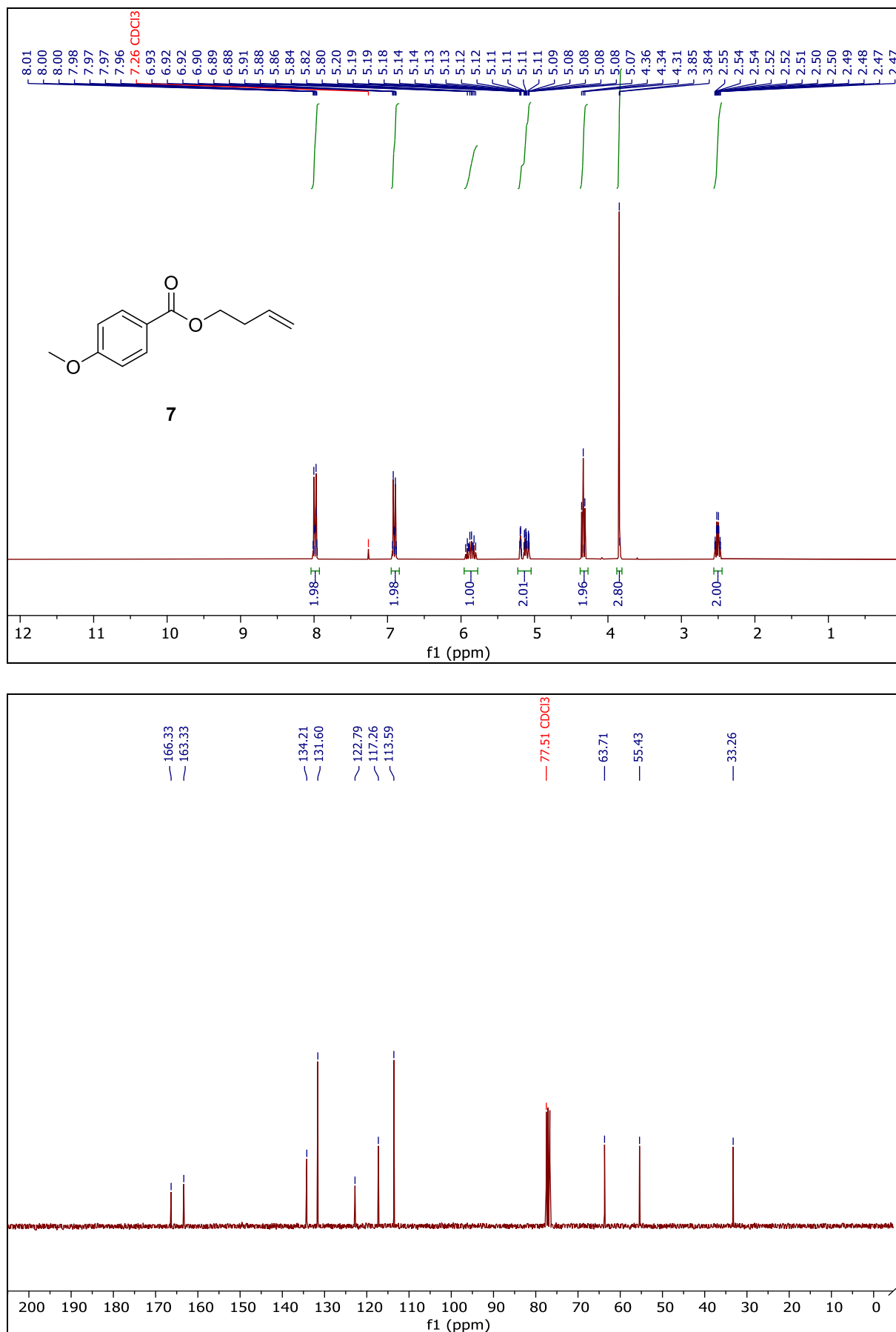
Spectrum S3.10. Compound **7**, ^{1}H- and ^{13}C-NMR (Chloroform-*d*).
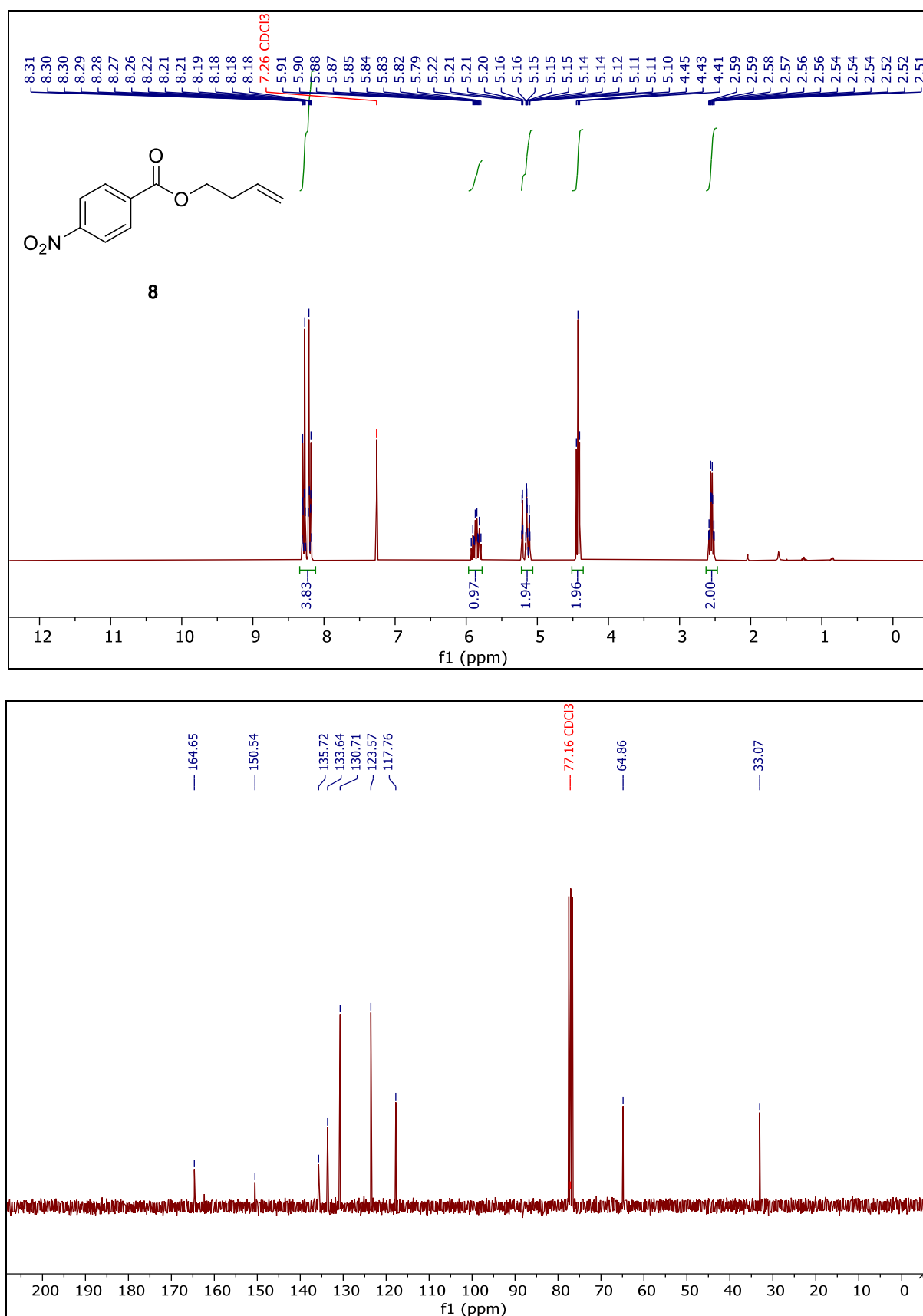
Spectrum S3.11. Compound **8**, [^1]H- and [^13]C-NMR (Chloroform-*d*).
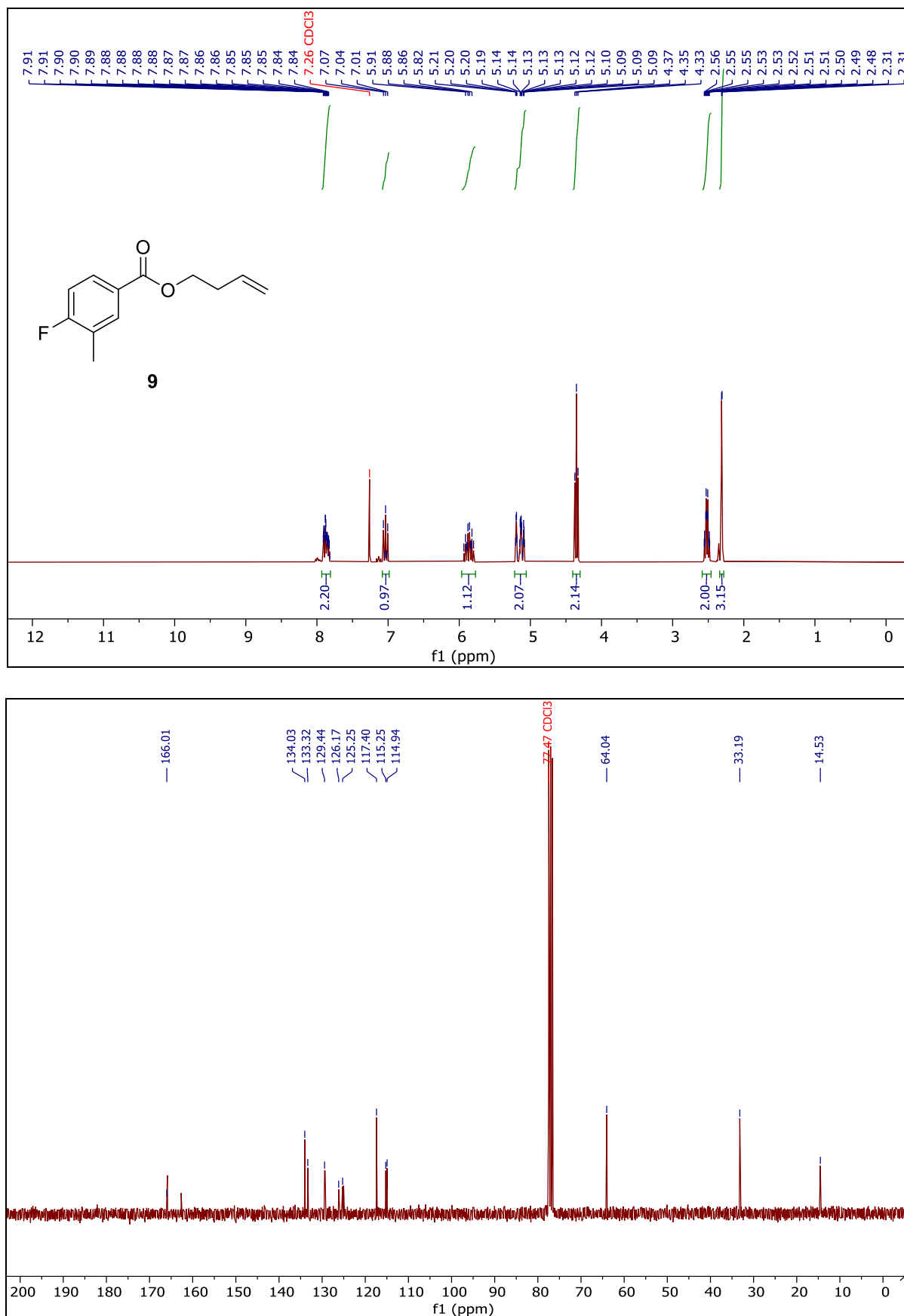
Spectrum S3.12. Compound **9**, ^{1}H- and ^{13}C-NMR (Chloroform-*d*).
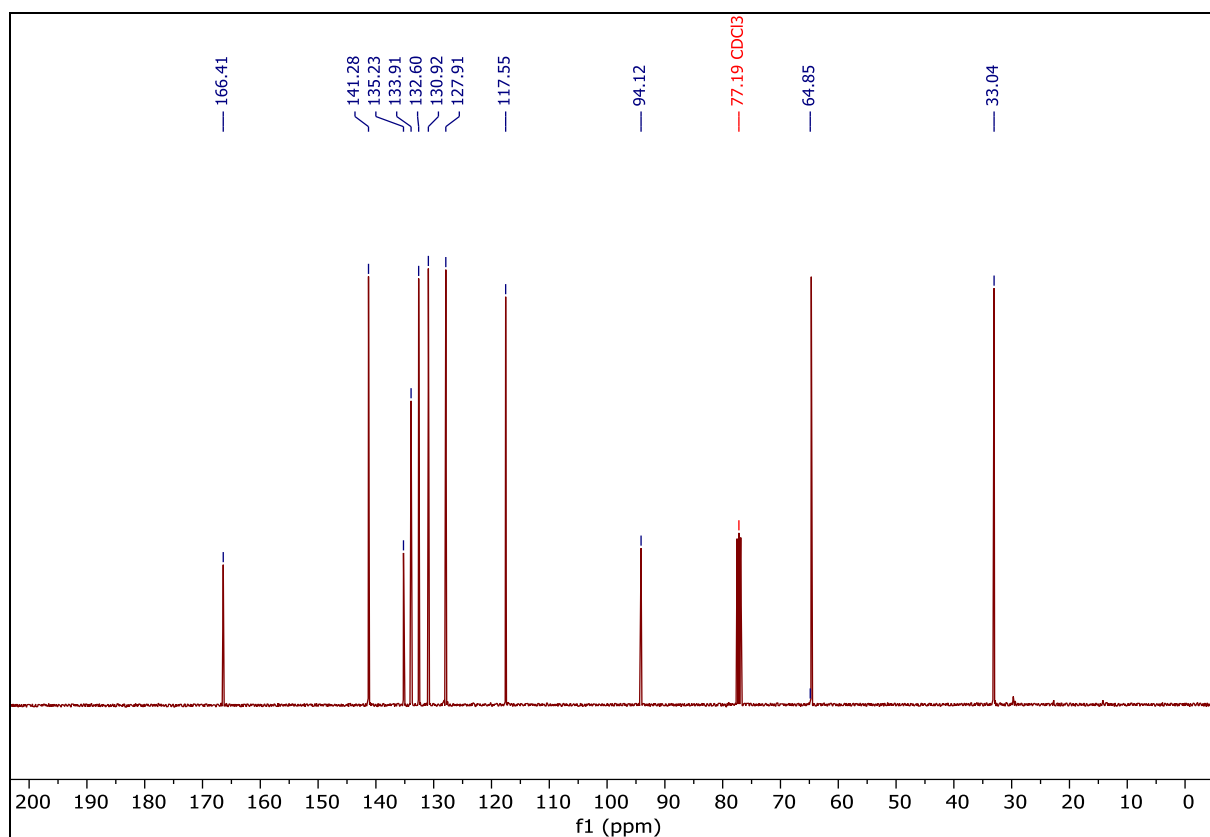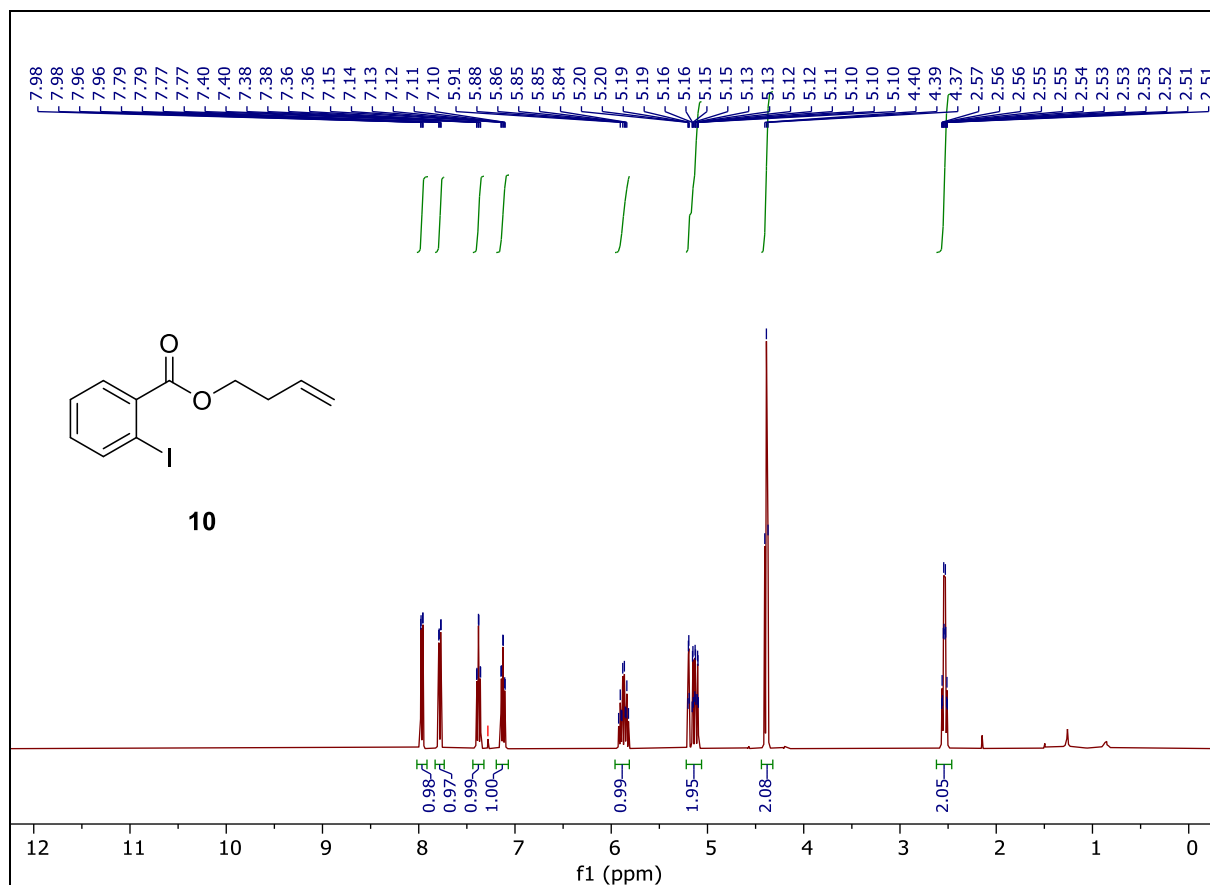
Spectrum S3.13. Compound **10**, [^1]H- and [^13]C-NMR (Chloroform-*d*).
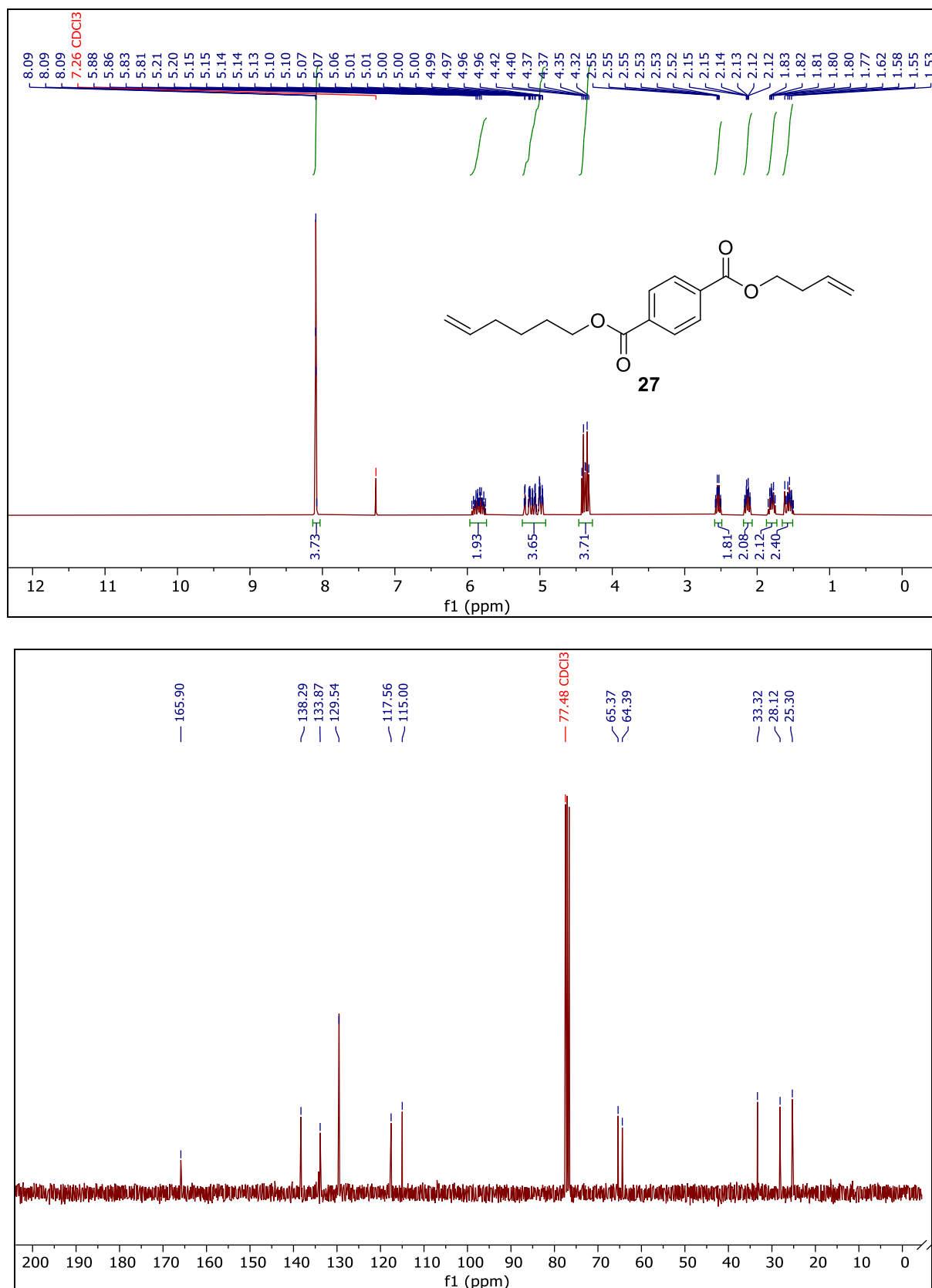
Spectrum S3.14. Compound **27**, ¹H-NMR (Chloroform-*d*).
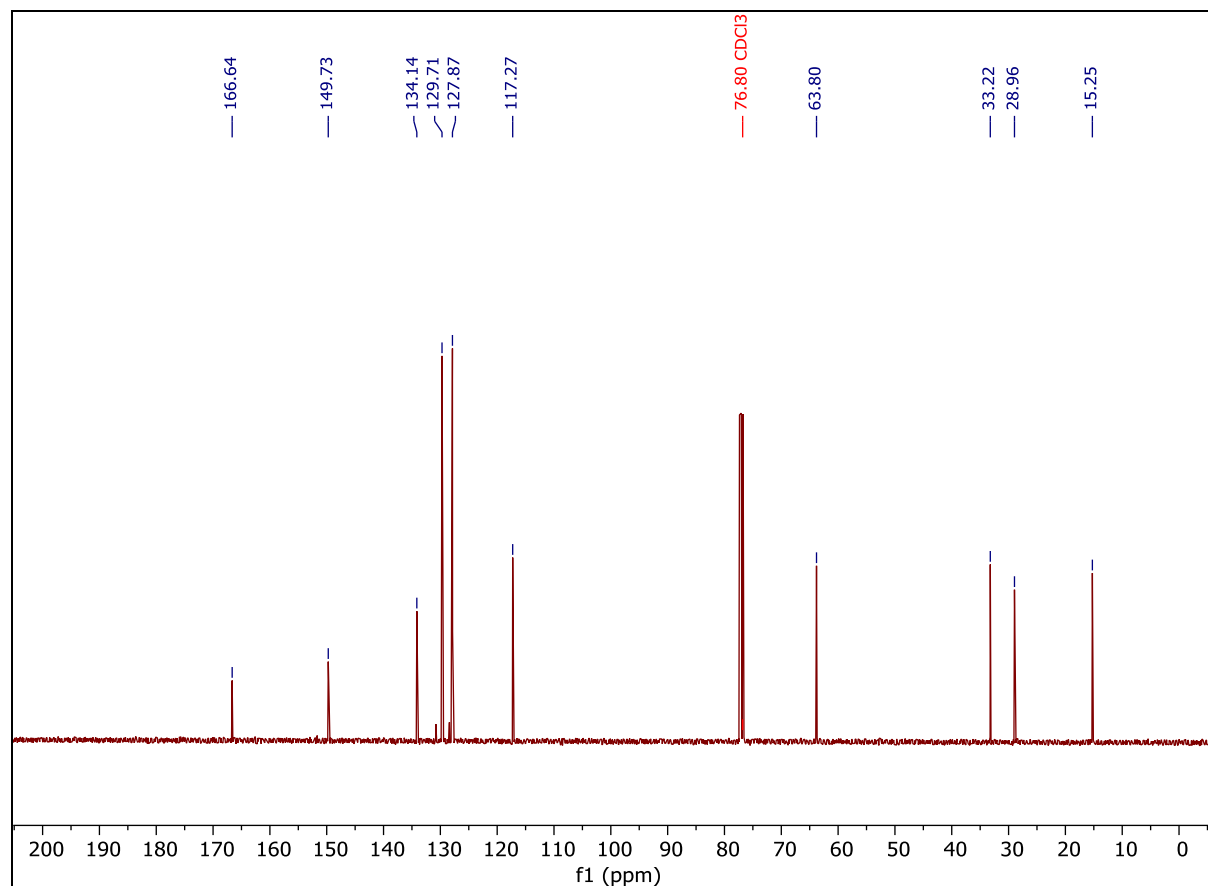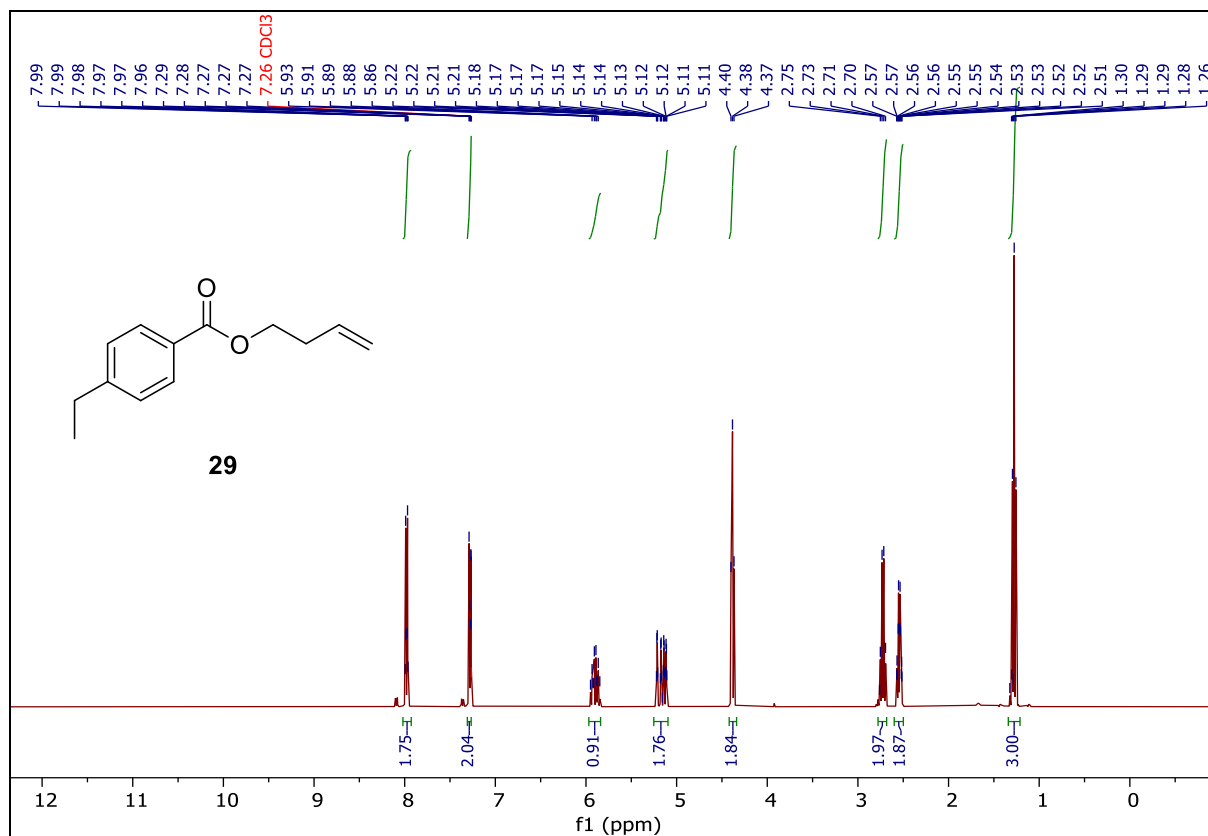
Spectrum S3.15. Compound **29**, ^{1}H- and ^{13}C-NMR (Chloroform-*d*).

3.19.1 Analysis of the Dichlorinated Products

The reagents were obtained following the general procedure for the iron-catalysed photo-dichlorination of alkenes (**SI**, chapter 3.8).

1a
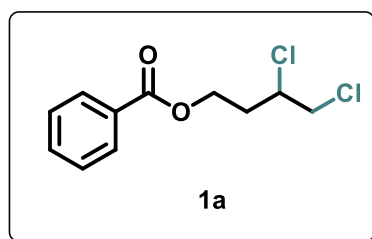
3,4-dichlorobutyl benzoate (**1a**)

Dichlorinated product **1a** could be isolated in moderate yields (47%) starting from alkene aryl ester **1**. The spectroscopic results are in good accordance with the published literature.[10]

^{1}H-NMR (300 MHz, CDCl$_3$, δ$_H$) 8.12 – 7.99 (m, 2H), 7.62 – 7.49 (m, 1H), 7.47 – 7.35 (m, 2H), 4.62 – 4.41 (m, 2H), 4.26 (dddd, J = 9.5, 7.3, 5.0, 3.5 Hz, 1H), 3.83 (dd, J = 11.4, 5.0 Hz, 1H), 3.72 (dd, J = 11.4, 7.3 Hz, 1H), 2.50 (dddd, J = 14.5, 8.9, 5.8, 3.4 Hz, 1H), 2.11 (ddt, J = 14.6, 9.7, 4.9 Hz, 1H).

^{13}C-NMR (75 MHz, CDCl$_3$, δ$_C$) 166.3 (C$_q$), 133.2 (+), 129.9 (C$_q$), 129.6 (+), 128.5 (+), 61.4 (-), 57.6 (+), 48.3 (-), 34.3 (-).

Yield: 47%, 0.023 g, 0.09 mmol, colourless oil.

2a
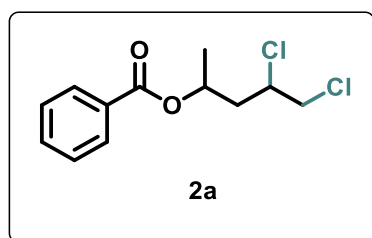
4,5-dichloropentan-2-yl benzoate (**2a**)

Product **3a** was obtained in moderate yields (31%) from the respective alkene starting material **2**.[13]

¹H-NMR (300 MHz, CDCl₃, δ$_H$) δ 8.11 – 7.98 (m, 2H), 7.62 – 7.52 (m, 1H), 7.45 (ddt, J = 8.3, 6.8, 0.9 Hz, 2H), 4.25 – 4.11 (m, 1H), 3.84 (ddd, J = 11.3, 8.9, 4.7 Hz, 1H), 3.70 (ddd, J = 15.4, 11.4, 7.3 Hz, 1H), 2.50 (ddd, J = 14.9, 10.2, 2.5 Hz, 1H), 2.36 – 2.26 (m, 1H), 2.00 – 1.88 (m, 1H), 1.43 (dd, J = 6.2, 2.9 Hz, 3H).

¹³C-NMR (75 MHz, CDCl₃, δ$_C$) 165.9 (C$_q$), 133.1 (+), 129.6 (C$_q$), 129.6 (+), 128.4 (+), 68.5 (+), 57.1 (+), 48.4 (-), 41.9 (-), 20.5 (+).

Yield: 31%, 0.016 g, 0.062 mmol, colourless oil.

3a
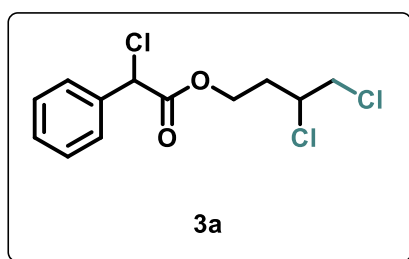
3,4-dichlorobutyl 2-chloro-2-phenylacetate (**3a**)

The dichlorinated product **3a** was isolated in moderate yields (33%) starting from the respective alkene aryl ester **3**.

¹H-NMR (300 MHz, CDCl₃, δ$_H$) 7.56 – 7.45 (m, 2H), 7.45 – 7.31 (m, 3H), 5.38 (s, 1H), 4.50 – 4.24 (m, 2H), 4.06 – 3.89 (m, 1H), 3.79 – 3.51 (m, 2H), 2.45 – 2.24 (m, 1H), 1.97 (ddtd, J = 14.6, 9.6, 4.8, 1.6 Hz, 1H).

¹³C-NMR (75 MHz, CDCl₃, δ$_C$) 168.1 (C$_q$), 135.6 (C$_q$), 129.5 (+), 129.0 (+), 127.9 (+), 62.7 (-), 59.2 (+), 57.1 (+), 48.1 (-), 34.0 (-).

HRMS (ESI) (m/z): [M-H]$^+$ (C$_{12}$H$_{13}$Cl$_3$O$_2$): calc.: 294.00, found: 293.998.

Yield: 33%, 0.0194 g. 0.066 mmol, off-yellow oil.

4a
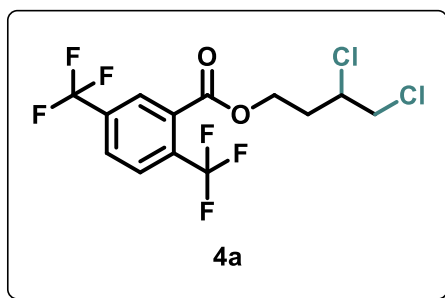
3,4-dichlorobutyl 2,5-bis(trifluoromethyl)benzoate (4a)

The dichlorination of starting material **4** worked successfully and compound **4a** was obtained in good yield (90%). The results are in good accordance to published work.[10]

^{1}H-NMR (300 MHz, CDCl$_3$, δ_H) 8.51 – 8.44 (m, 2H), 8.08 (tt, J = 1.8, 0.9 Hz, 1H), 4.71 – 4.53 (m, 2H), 4.24 (dddd, J = 9.5, 7.9, 4.7, 3.2 Hz, 1H), 3.87 (dd, J = 11.4, 4.7 Hz, 1H), 3.73 (dd, J = 11.4, 8.0 Hz, 1H), 2.59 (dddd, J = 15.0, 8.0, 6.2, 3.2 Hz, 1H), 2.21 (ddt, J = 14.8, 9.5, 5.2 Hz, 1H).

^{13}C-NMR (75 MHz, CDCl$_3$, δ_C) 163.7 (C$_q$), 133.0 (C$_q$), 132.5 (C$_q$), 132.1 (C$_q$), 131.6 (C$_q$), 129.8 (+), 126.6 (+), 124.6 (C$_q$), 121.0 (+), 62.7 (-), 57.1 (+), 47.8 (-), 34.0 (-).

^{19}F-NMR (377 MHz, CDCl$_3$, δ_F) -63.60 ppm.

Yield: 90%, 0.0689 g, 0.180 mmol, colourless oil.

5a
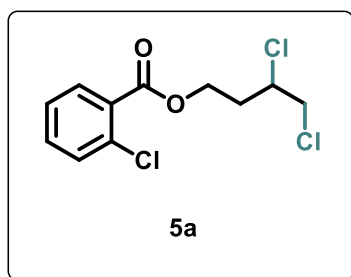
3,4-dichloro-butyl 2-chlorobenzoate (5a)

The dichlorinated product **5a** obtained in 22% yield from the photocatalytic dichlorination of starting material **5**. The experimental data are comparable to published literature about 3,4 dichloro-butyl 4-chloro benzoate.[10]

¹H-NMR (300 MHz, CDCl₃, δ_H) 7.81 (ddd, J = 7.7, 1.6, 0.6 Hz, 1H), 7.50 – 7.28 (m, 3H), 4.65 – 4.43 (m, 2H), 4.37 – 4.24 (m, 1H), 3.89 – 3.66 (m, 2H), 2.52 (dddd, J = 14.7, 8.9, 5.7, 3.3 Hz, 1H), 2.10 (ddt, J = 14.7, 9.6, 4.7 Hz, 1H).

¹³C-NMR (75 MHz, CDCl₃, δ_C) 165.5 (C_q), 133.7 (C_q), 132.8 (+), 131.5 (+), 131.2 (+), 129.9 (C_q), 126.7 (+), 61.9 (-), 57.5 (+), 48.2 (-), 34.2 (-).

HRMS (ESI) (m/z): [M+H]⁺ ($C_{11}H_{11}Cl_3O_2$): calc.: 279.98, found: 279.9825.

Yield: 22%, 0.012 g, 0.0426 mmol, colourless oil.
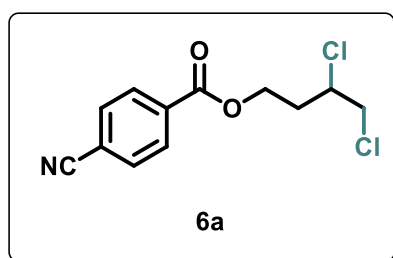
3,4-dichlorobutyl 4-cyanobenzoate (6a)

Product **6a** was obtained in 87% yield from starting material **6**. The spectroscopic data are in good accordance to the results from the published literature of regio-isomer 3,4-dichlorobutyl-3-cyanobenzoate.[10]

¹H-NMR (300 MHz, CDCl₃, δ_H) 8.16 – 8.08 (m, 2H), 7.78 – 7.69 (m, 2H), 4.67 – 4.46 (m, 2H), 4.24 (dddd, J = 9.7, 8.0, 4.8, 3.2 Hz, 1H), 3.85 (dd, J = 11.4, 4.8 Hz, 1H), 3.72 (dd, J = 11.4, 7.8 Hz, 1H), 2.55 (dddd, J = 15.0, 8.4, 5.9, 3.2 Hz, 1H), 2.23 – 2.07 (m, 1H).

¹³C-NMR (75 MHz, CDCl₃, δ_C) 164.7 (C_q), 133.7 (C_q), 132.3 (+), 130.2 (+), 117.9 (C_q), 116.6 (C_q), 62.2 (-), 57.3 (+), 48.0 (-), 34.1 (-).

HRMS (ESI) (m/z): [M+NH₄]⁺ ($C_{12}H_{11}Cl_2NO_2$): calc.: 271.020, found: 271.017.

Yield: 87%. 0.047 g, 0.173 mmol, pale yellow oil.
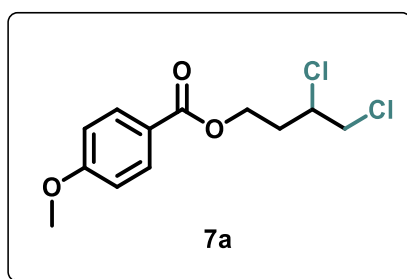
3,4-dichlorobutyl 4-methoxybenzoate (**7a**)

Starting from alkene aryl ester **7** the dichlorinated product **7a** could be isolated in excellent yields (94%). The results are in good according with published literature.[10]

^{1}H-NMR (300 MHz, CDCl₃, δ_H) 8.02 – 7.92 (m, 2H), 6.97 – 6.86 (m, 2H), 4.59 – 4.40 (m, 2H), 4.26 (dddd, *J* = 9.5, 7.4, 5.0, 3.4 Hz, 1H), 3.86 (s, 3H), 3.83 (d, *J* = 4.9 Hz, 1H), 3.73 (dd, *J* = 11.4, 7.4 Hz, 1H), 2.51 (dddd, *J* = 14.9, 8.4, 5.7, 3.5 Hz, 1H), 2.19 – 2.05 (m, 1H).

^{13}C-NMR (75 MHz, CDCl₃, δ_C) 166.1 (C_q), 163.5 (C_q), 131.7 (+), 122.3 (C_q), 113.7 (+), 61.0 (-), 57.6 (+), 55.5 (+), 48.2 (-), 34.4 (-).

Yield: 94%, 0.0521 g, 0.188 mmol, colourless oil.
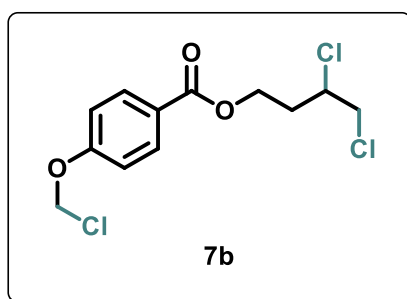
3,4-dichlorobutyl 4-(chloro-methoxy) benzoate (**7b**)

Product **7b** could be isolated in 25% yield starting from alkene aryl ester **7**. The ^{1}H- and ^{13}C-NMR spectra show residues from acetic acid that could not be removed. The product was isolated as minor product in the photoreaction from compound **7** to product **7a** and **7b**.

¹H-NMR (300 MHz, CDCl₃, δ_H) 8.05 – 7.96 (m, 2H), 7.11 – 7.02 (m, 2H), 5.81 (s, 2H), 4.61 – 4.41 (m, 2H), 4.31 – 4.20 (m, 1H), 3.91 – 3.81 (m, 1H), 3.73 (dd, J = 11.4, 7.6 Hz, 1H), 2.52 (dddd, J = 14.9, 8.5, 5.7, 3.4 Hz, 1H), 2.16 (dd, J = 9.7, 4.9 Hz, 1H).

¹³C-NMR (75 MHz, CDCl₃, δ_C) 165.8 (C_q), 160.5 (C_q), 131.7 (+), 124.2 (C_q), 115.5 (+), 84.6 (-), 61.2 (-), 57.5 (+), 48.1 (-), 34.3 (-).

Yield: 25%, 0.024 g, 0.077 mmol, pale yellow oil.

8a
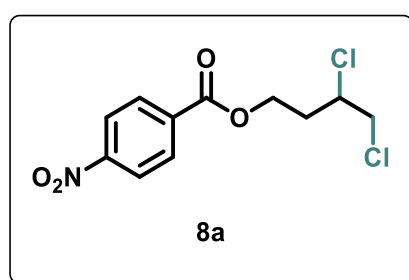
3,4-dichlorobutyl 4-nitrobenzoate (**8a**)

The dichlorinated compound **8a** was isolated in 91% starting from alkene aryl ester **8**. The results are in good accordance to published work.[10]

¹H-NMR (300 MHz, CDCl₃, δ_H) 8.35 – 8.25 (m, 2H), 8.24 – 8.15 (m, 2H), 4.70 – 4.50 (m, 2H), 4.25 (dddd, J = 9.6, 7.9, 4.8, 3.2 Hz, 1H), 3.93 – 3.67 (m, 2H), 2.57 (dddd, J = 14.9, 8.3, 5.9, 3.2 Hz, 1H), 2.27 – 2.11 (m, 1H).

¹³C-NMR (75 MHz, CDCl₃, δ_C) 164.5 (C_q), 150.7 (C_q), 135.2 (C_q), 130.8 (+), 123.7 (+), 62.4 (-), 57.2 (+), 47.9 (-), 34.1 (-).

HRMS (ESI+) [M+H]⁺ (m/z) (C₁₁H₁₁Cl₂NO₄): calc.: 291.01, found: 291.0066.

Yield: 91%, 0.053 g, 0.181 mmol, colourless solid.

9a
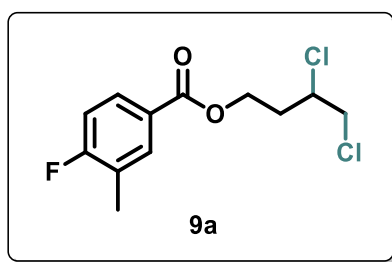
3,4-dichlorobutyl 4-fluoro-3-methylbenzoate (9a)

The dichlorinated product **9a** was isolated in 29% based on the photocatalytic transformation of starting material **9**.[10]

¹H-NMR (300 MHz, CDCl₃) δ 7.92 – 7.76 (m, 2H), 7.11 – 6.98 (m, 1H), 4.68 – 4.58 (m, 2H), 4.25 (dddd, J = 9.3, 7.5, 4.7, 3.1 Hz, 1H), 3.91 – 3.80 (m, 1H), 3.73 (dd, J = 11.4, 7.7 Hz, 1H), 2.53 (dtdd, J = 9.3, 7.8, 6.0, 4.5 Hz, 1H), 2.30 (t, J = 2.2 Hz, 3H), 2.21 – 2.06 (m, 1H).

No **¹³C-NMR** could be performed.

Yield: 29%, 0.016 g, 0.057 mmol, pale-yellow oil.

10a
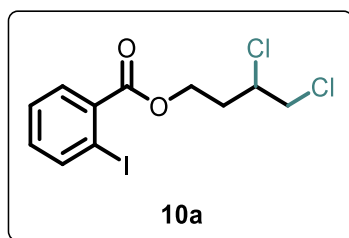
3,4-dichlorobutyl 2-iodobenzoate (10a)

Compound **10a** was isolated in 43% yield starting from the respective aryl alkene ester **10**.

The analytic data are in good accordance to the published literature.[10]

¹H-NMR (400 MHz, CDCl₃, δ_H) 7.93 (dd, J = 8.0, 1.1 Hz, 1H), 7.79 – 7.69 (m, 1H), 7.36 (qd, J = 7.8, 1.5 Hz, 1H), 7.10 (td, J = 7.7, 1.7 Hz, 1H), 4.54 (ddd, J = 10.8, 5.7, 4.9 Hz, 1H), 4.44 (ddd, J = 11.4, 8.8, 4.8 Hz, 1H), 4.36 – 4.20 (m, 1H), 3.79 (dd, J = 11.4, 4.9 Hz, 1H), 3.66 (dd, J = 11.4, 7.4 Hz, 1H), 2.49 (dddd, J = 14.7, 8.9, 5.7, 3.3 Hz, 1H), 2.06 (ddt, J = 14.7, 9.7, 4.8 Hz, 1H).

¹³C-NMR (101 MHz, CDCl₃, δ_C) 166.3 (C_q), 141.3 (+), 135.1 (C_q), 132.8 (+), 131.0 (+), 128.0 (+), 94.0 (C_q), 62.1 (-), 57.4 (+), 48.2 (-), 34.2.

Yield: 43%, 0.032 g, 0.086 mmol, pale yellow oil.

3.20 ¹H- and ¹³C-NMR Data of the Dichlorinated Products
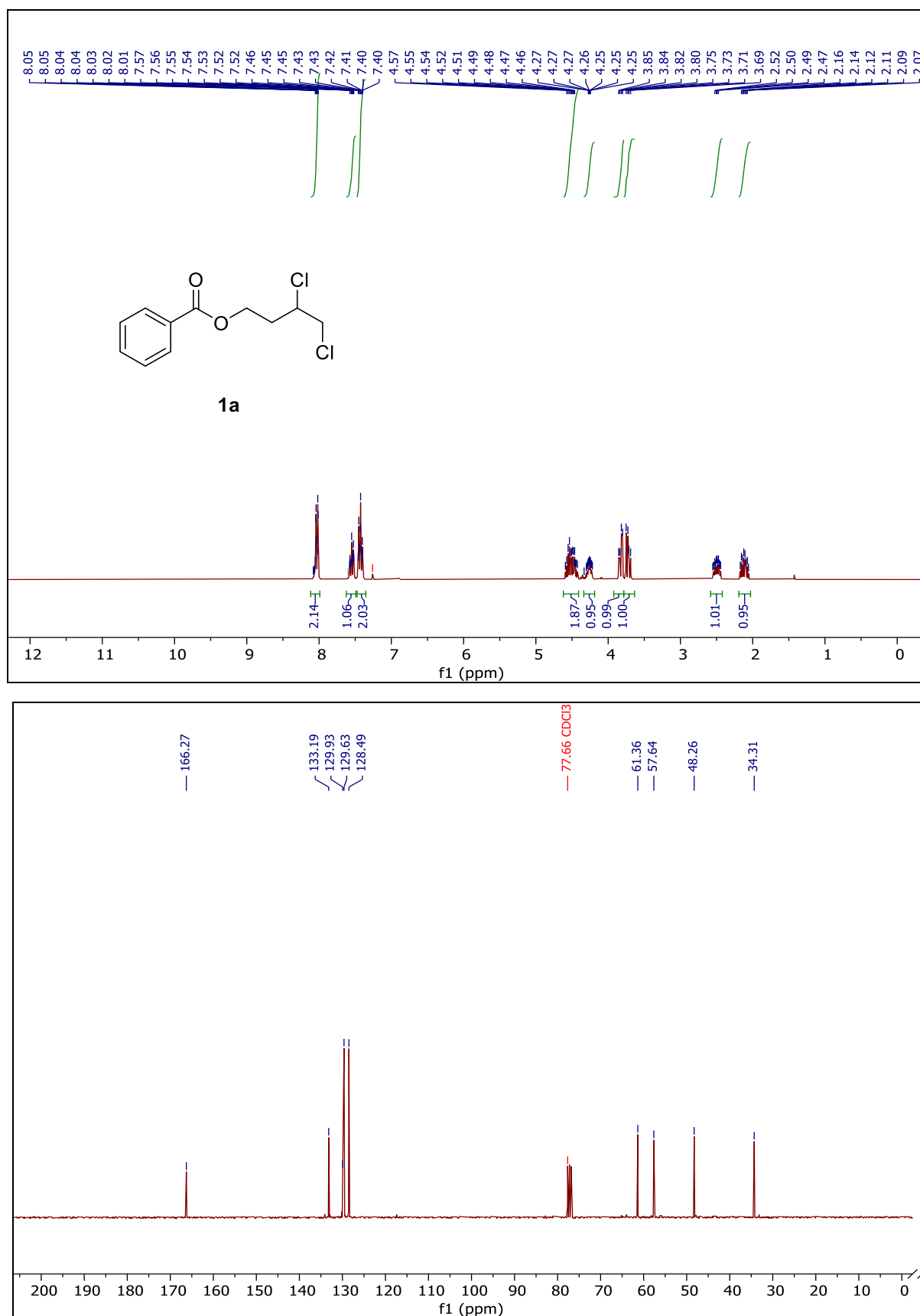
Spectrum S3.16. Compound **1a**, ¹H- and ¹³C-NMR (Chloroform-*d*).
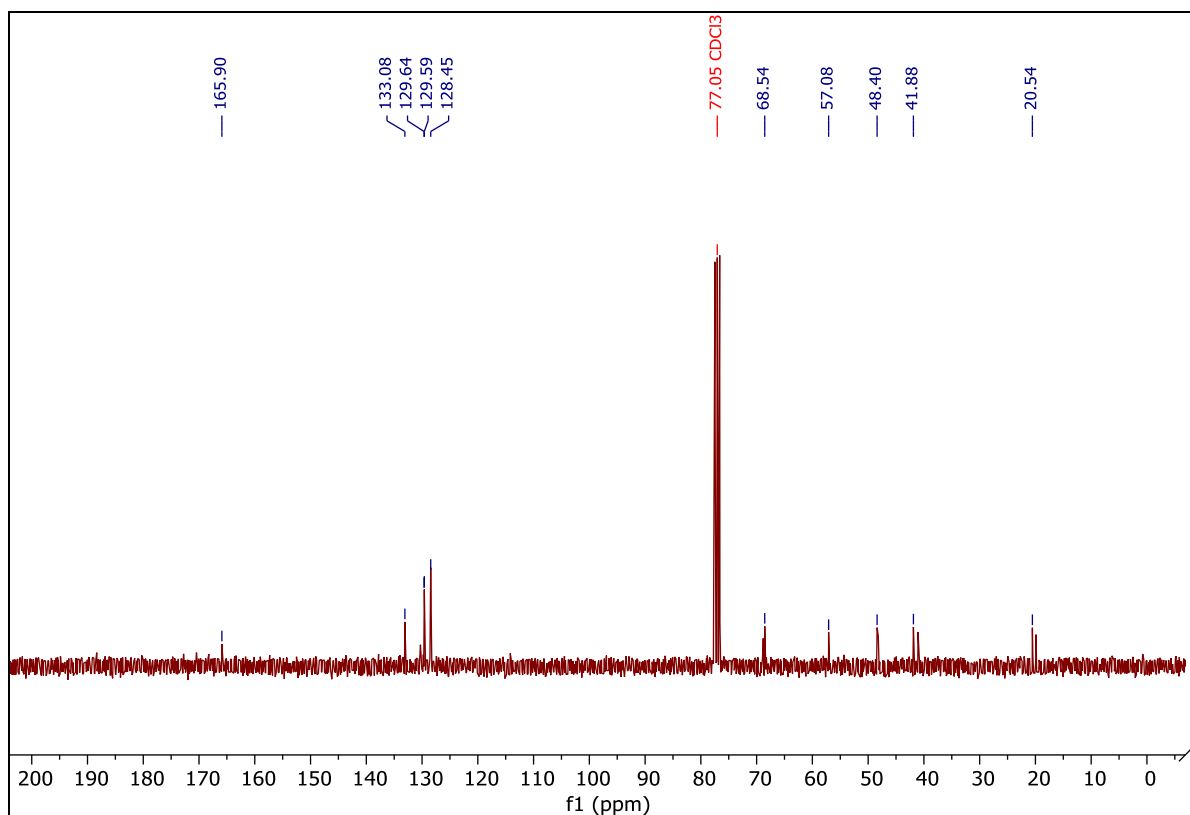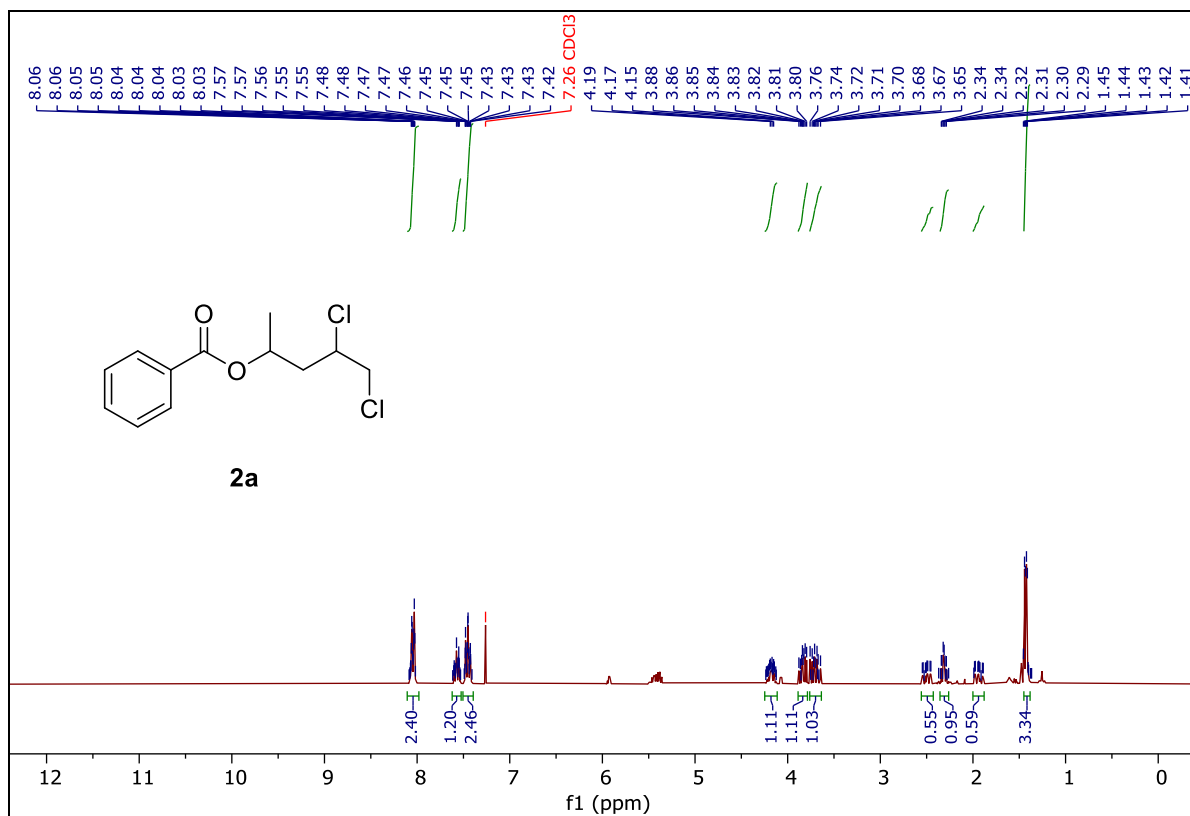
**Spectrum S3.17.** Compound **2a**, ^{1}H- and ^{13}C-NMR (Chloroform-*d*).
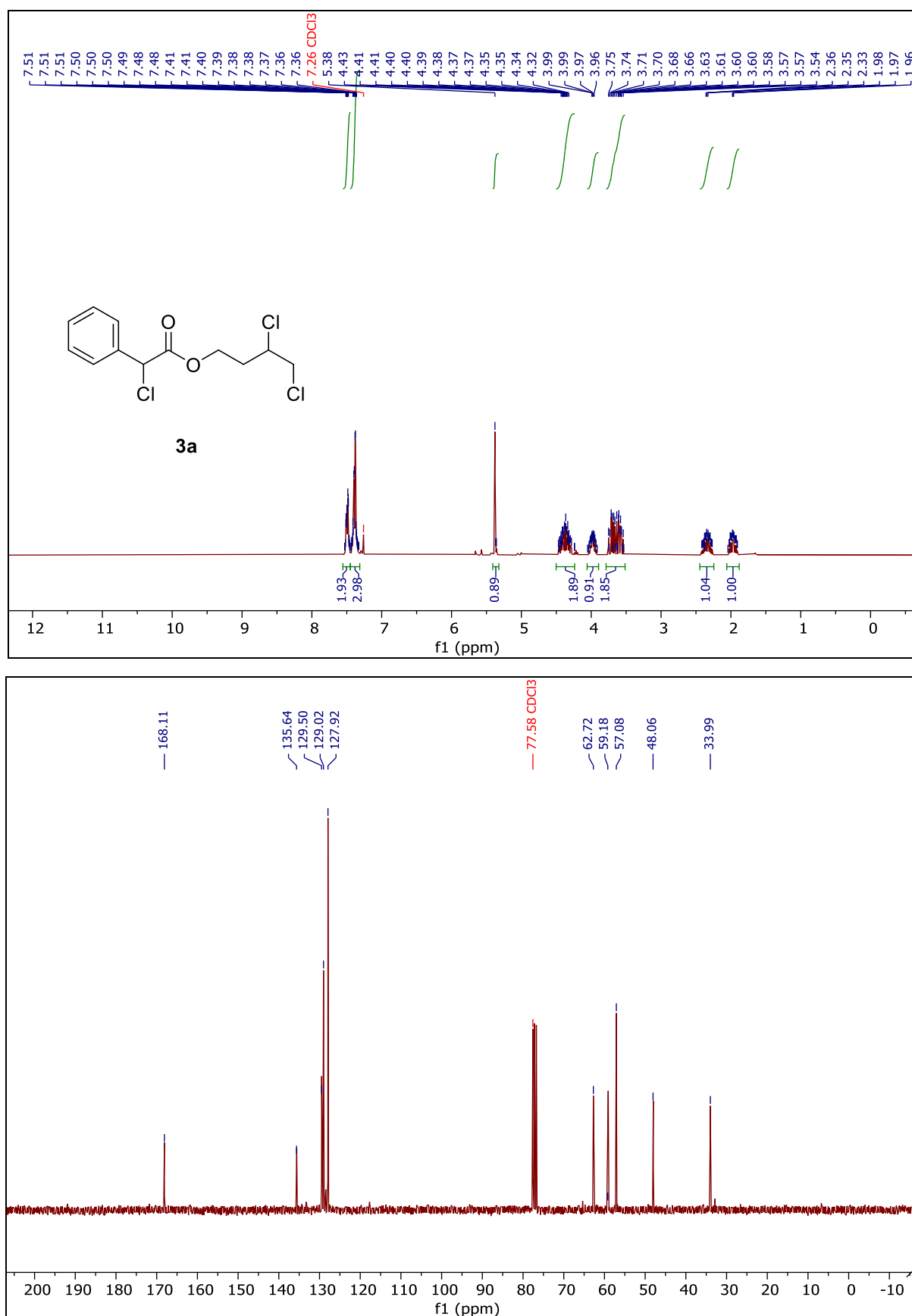
Spectrum S3.18. Compound **3a**, ^{1}H- and ^{13}C-NMR (Chloroform-*d*).
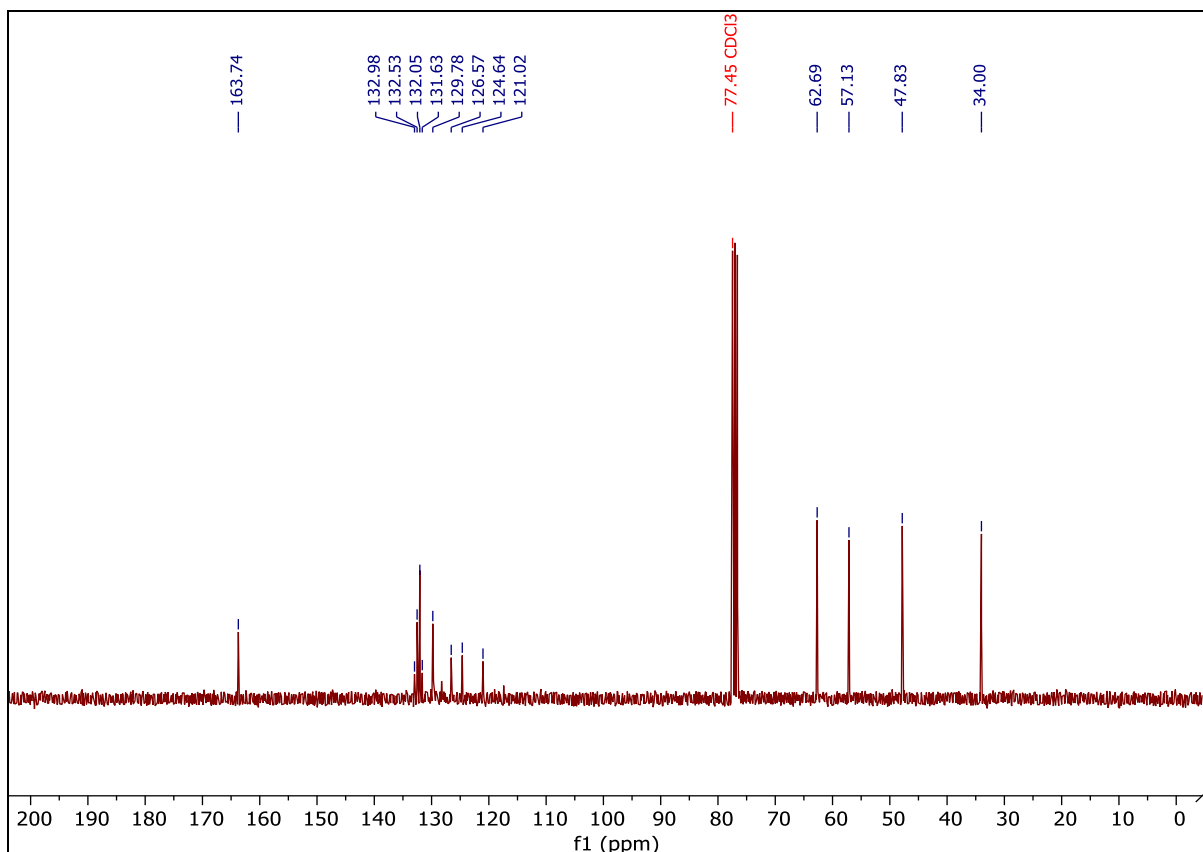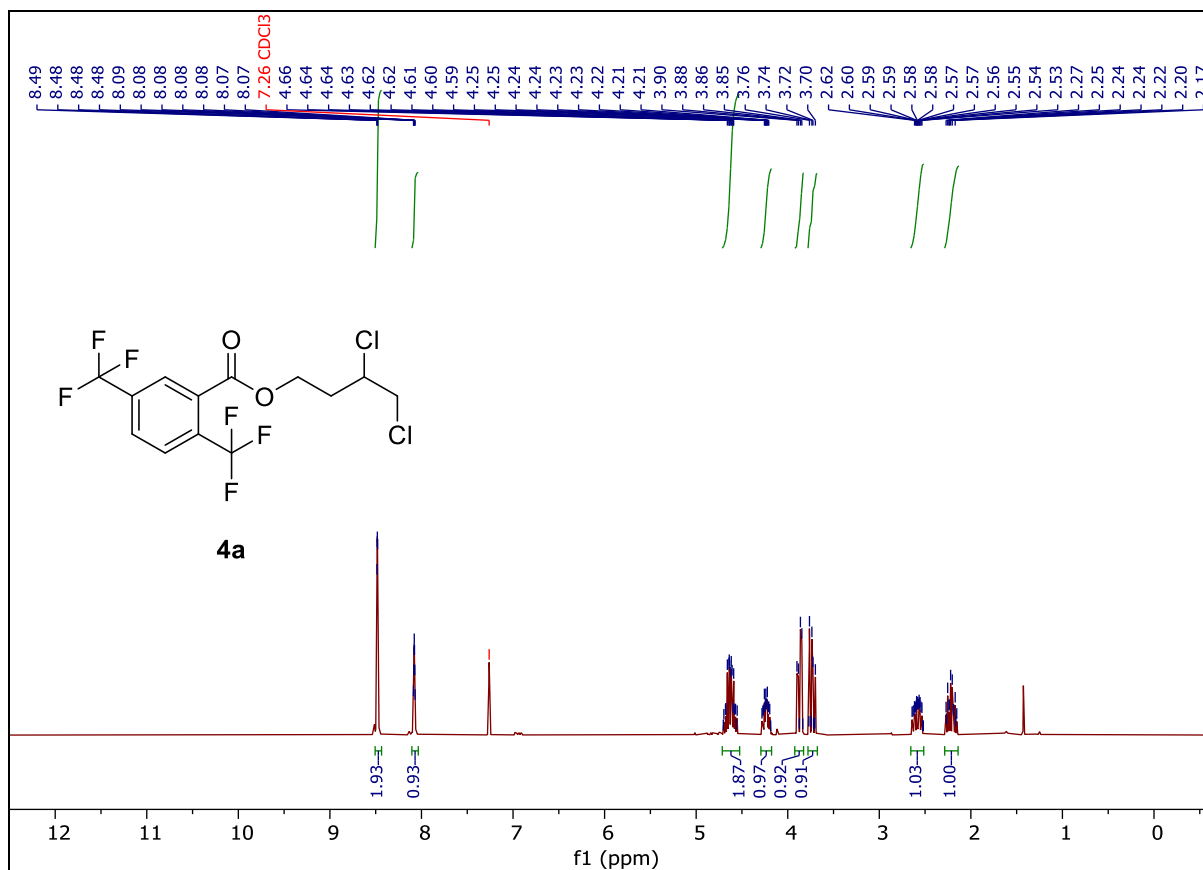
Spectrum S3.19. Compound **4a**, ^{1}H- and ^{13}C-NMR (Chloroform-*d*).
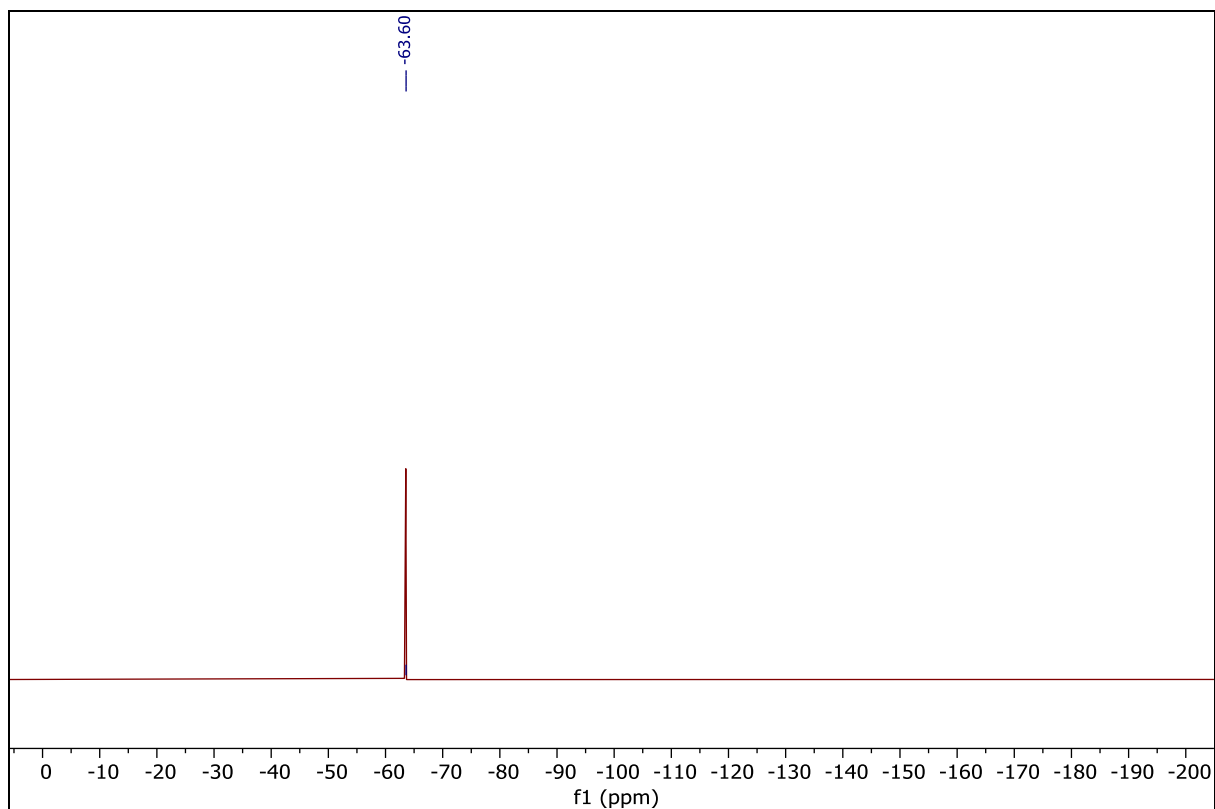
Spectrum S3.20. Compound **4a**, ^{19}F-NMR (Chloroform-*d*).
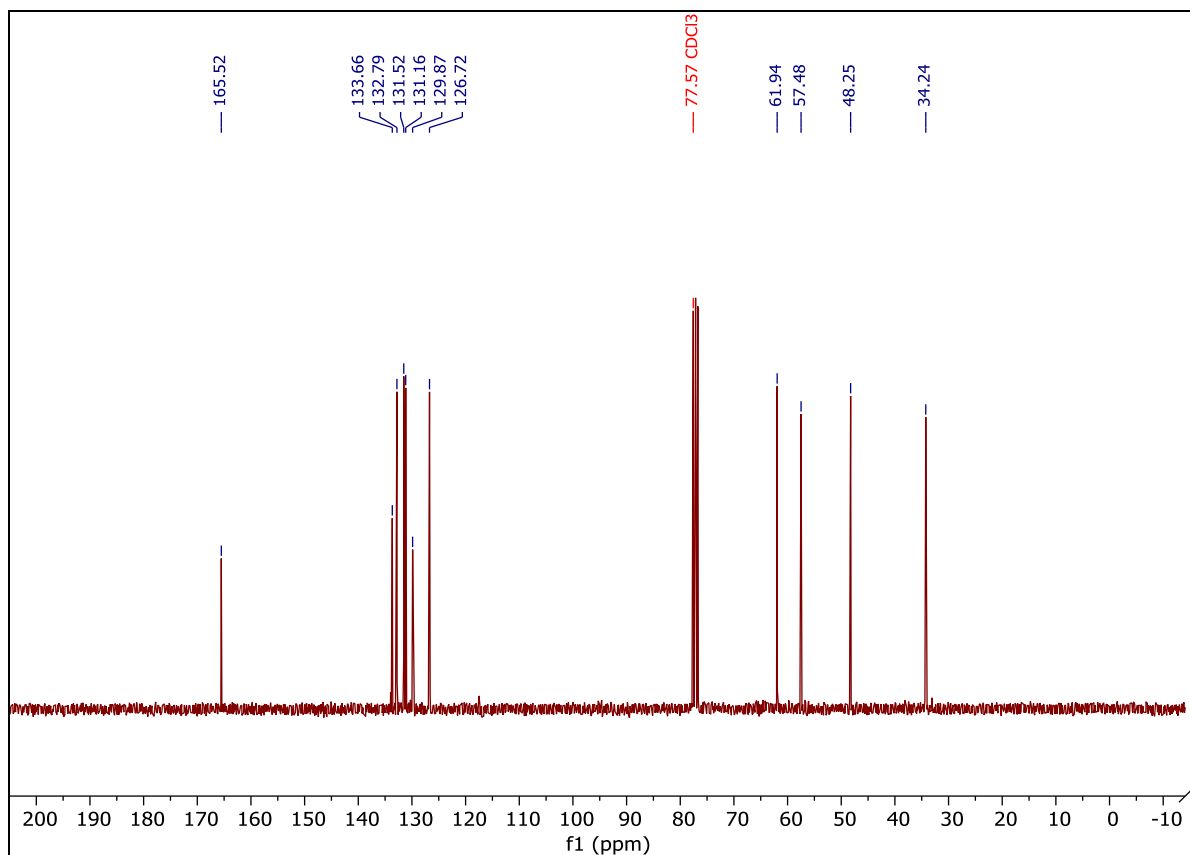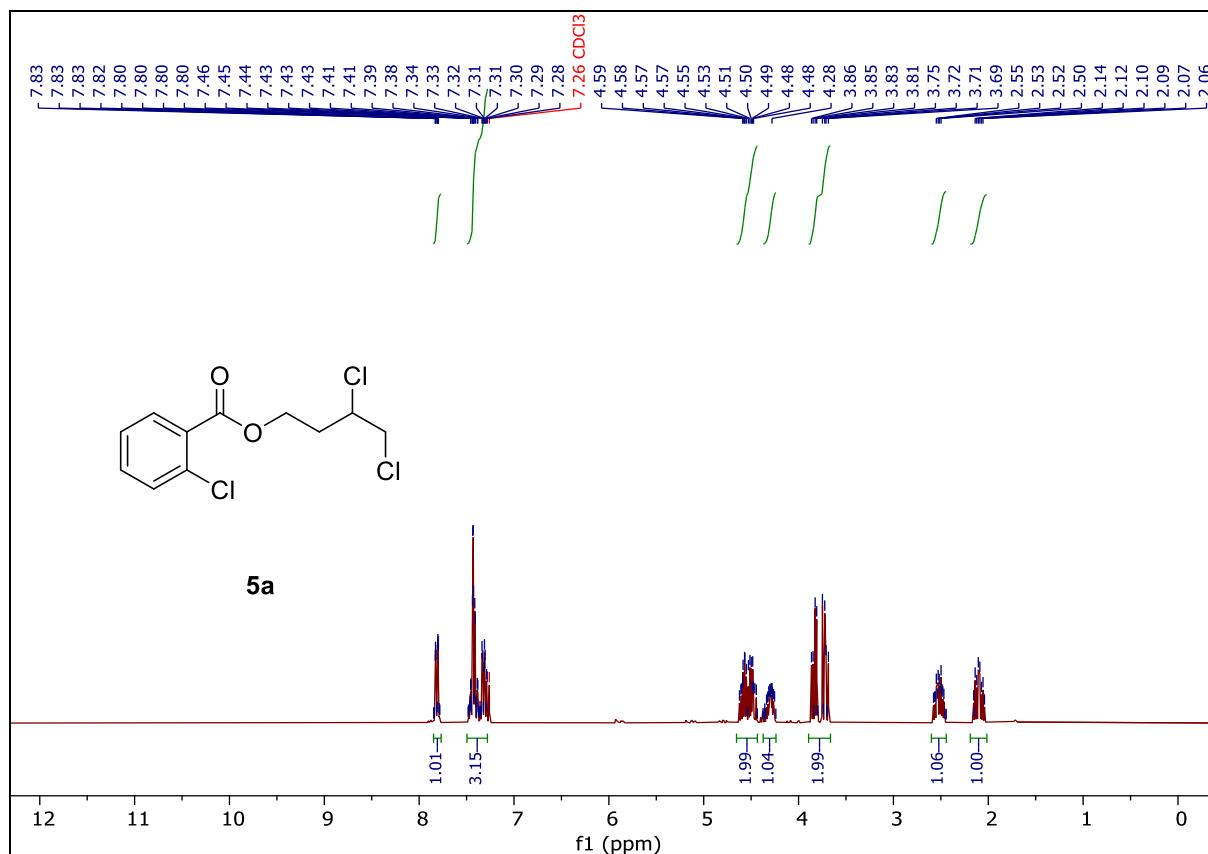
Spectrum S3.21. Compound **5a**, ^{1}H- and ^{13}C-NMR (Chloroform-*d*).
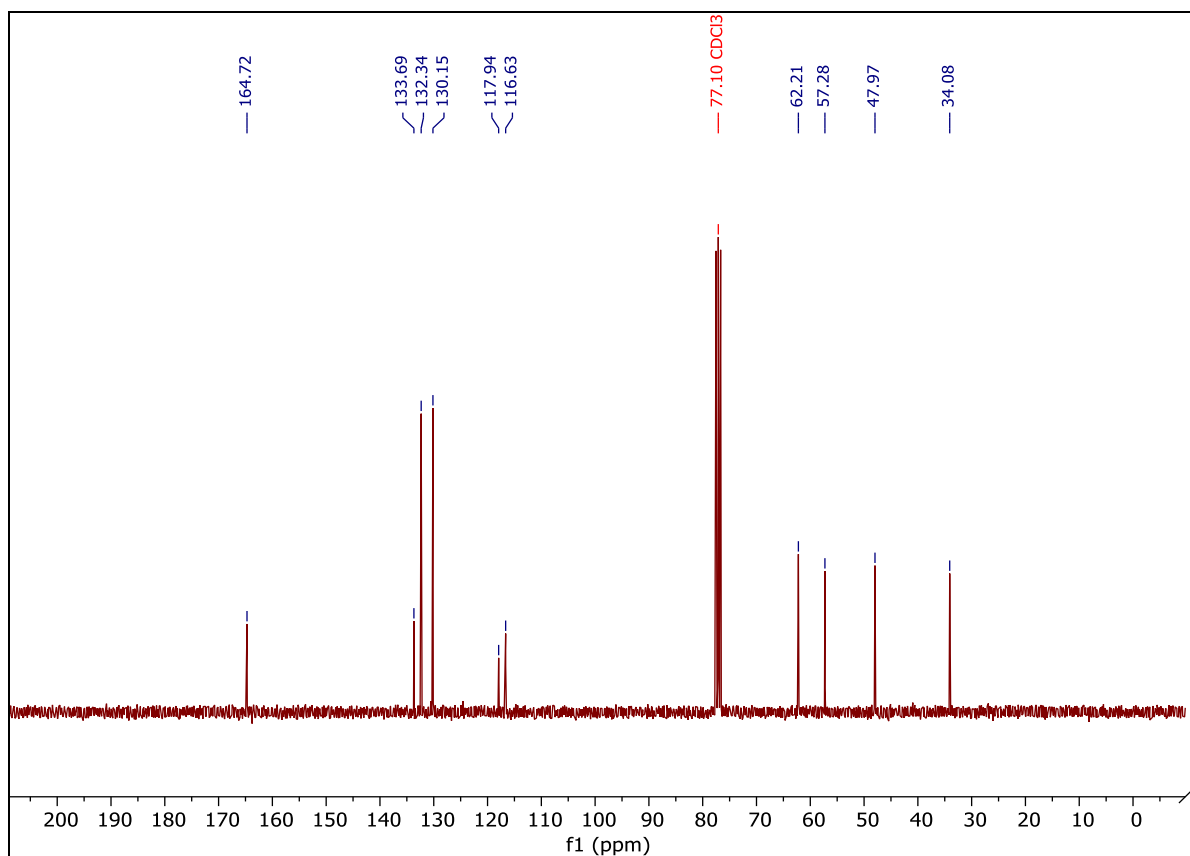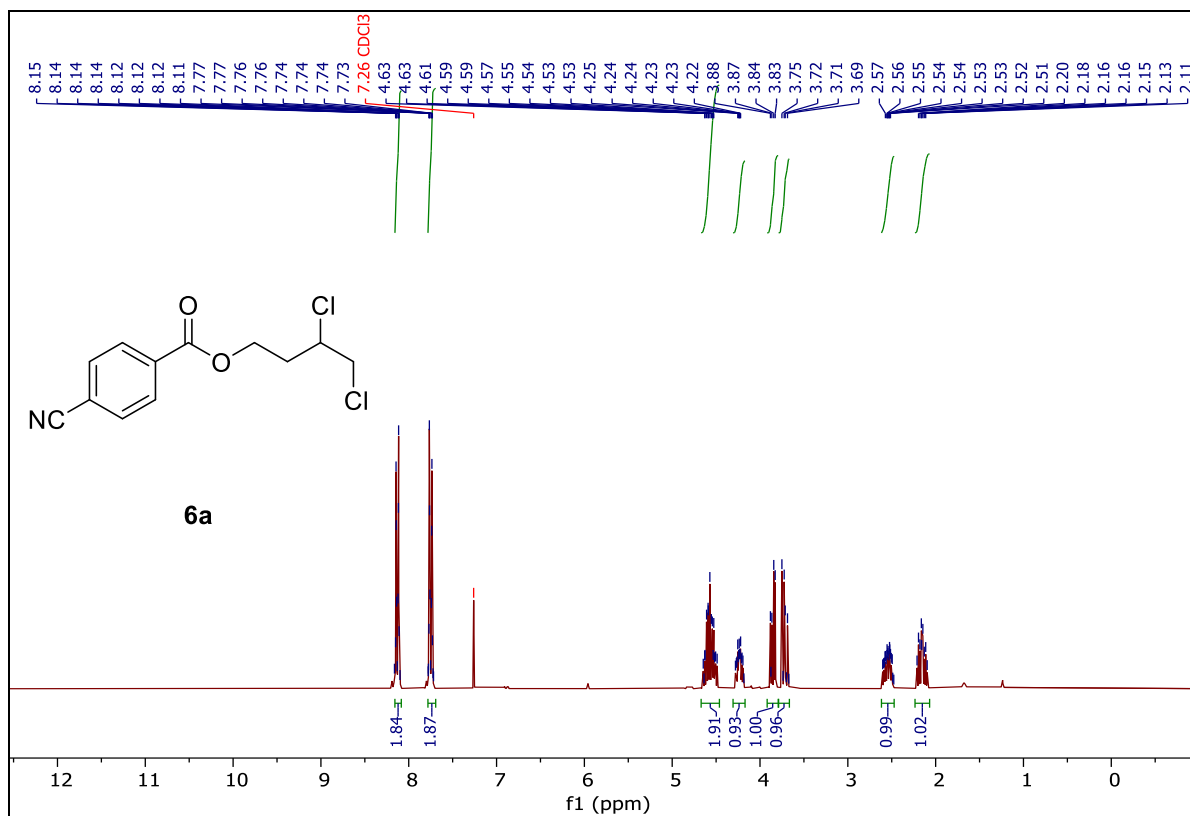
Spectrum S3.22. Compound **6a**, ^{1}H- and ^{13}C-NMR (Chloroform-*d*).
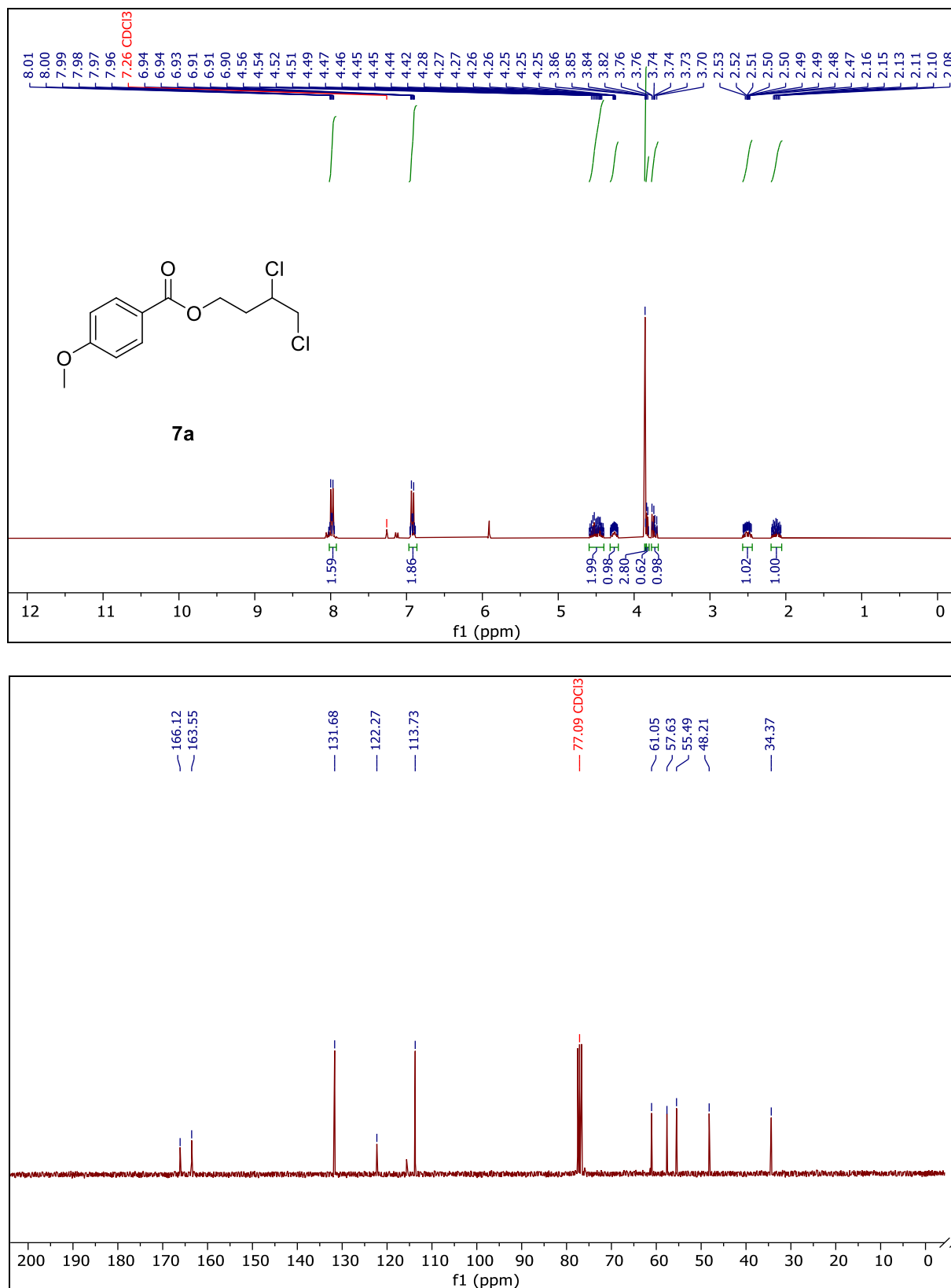
Spectrum S3.23. Compound **7a**, ¹H- and ¹³C-NMR (Chloroform-*d*).
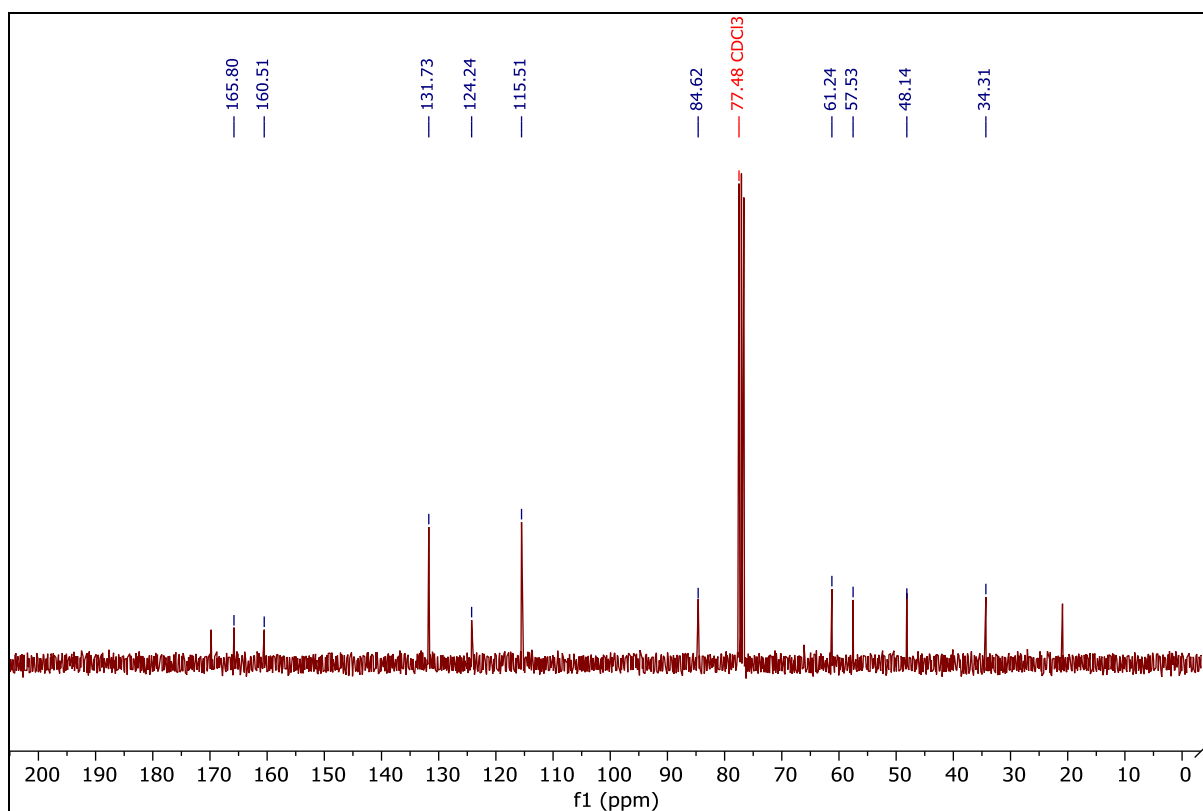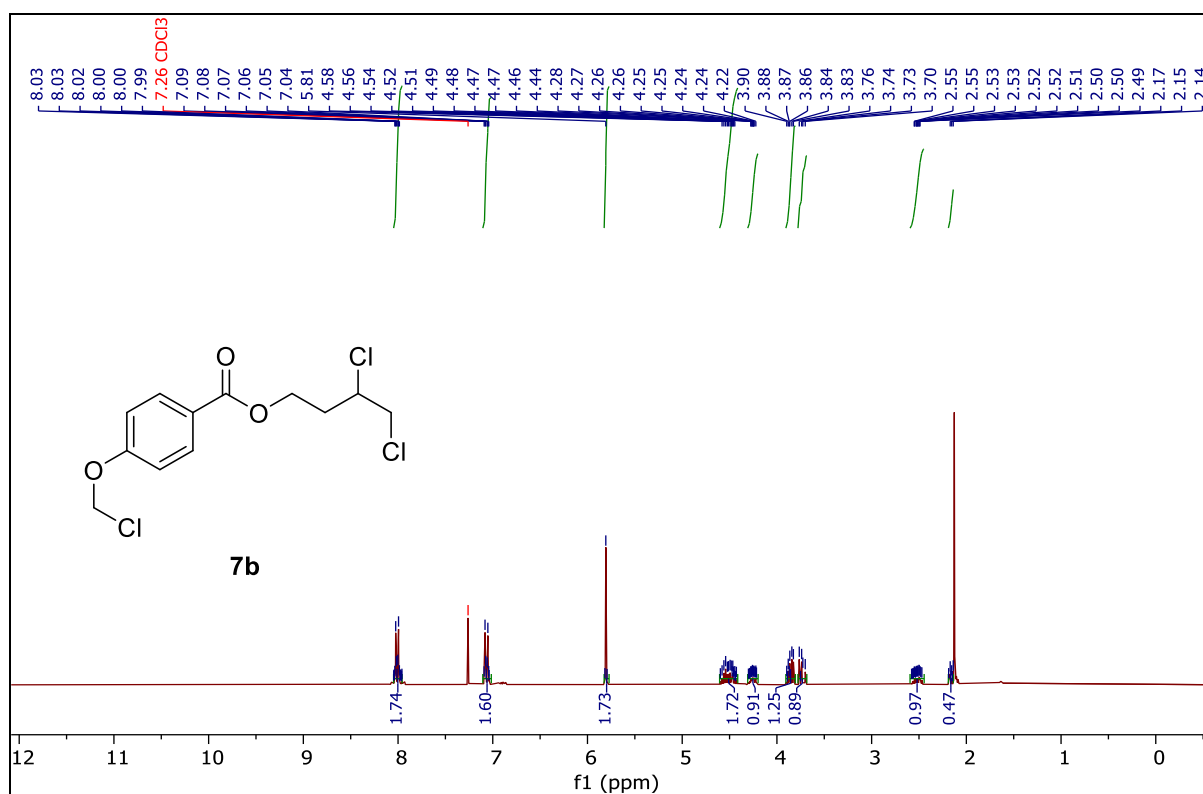
Spectrum S3.24. Compound **7b**, ^{1}H- and ^{13}C-NMR (Chloroform-*d*).
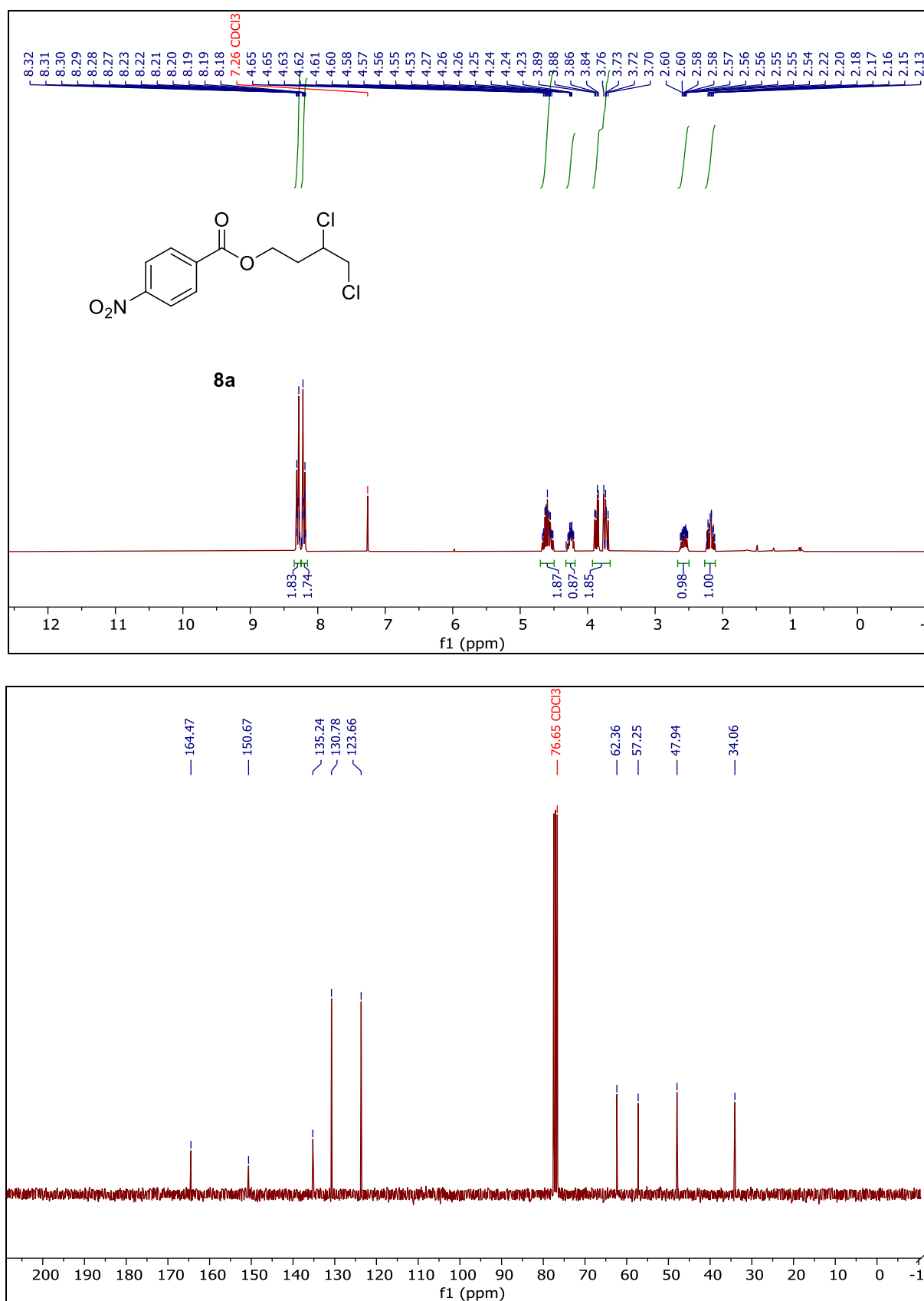
Spectrum S3.25. Compound **8a**, ^{1}H- and ^{13}C-NMR (Chloroform-*d*).
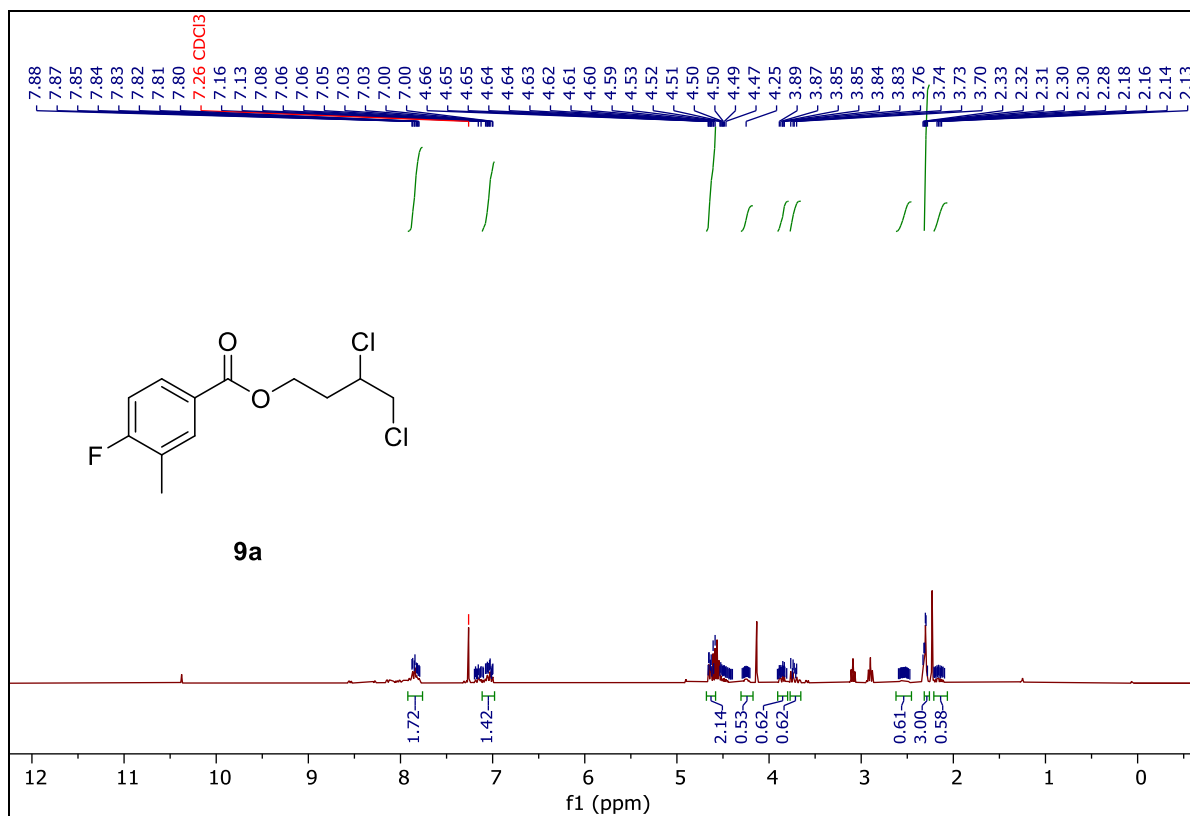
Spectrum S3.26. Compound **9a**, ^{1}H-NMR (Chloroform-*d*).
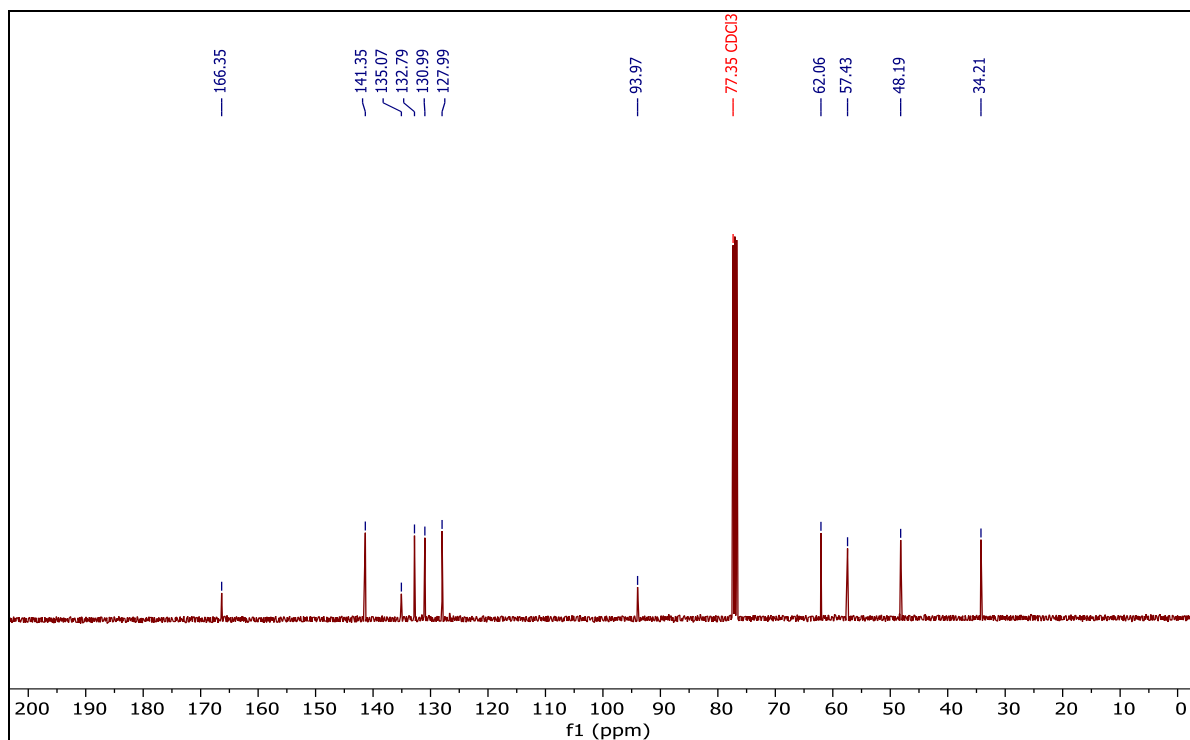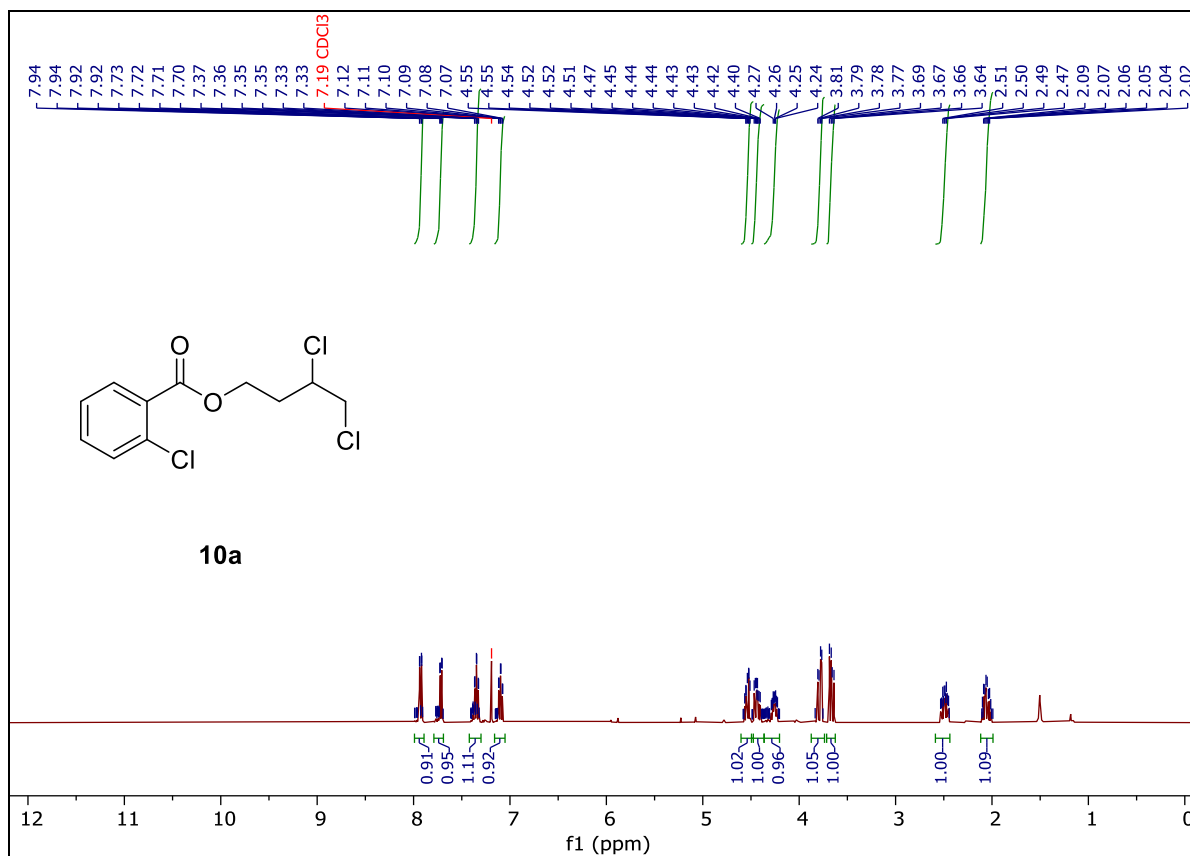
Spectrum S3.27. Compound **10a**, [^1]H- and [^13]C-NMR (Chloroform-*d*).

3.21 References

[1]   X. Wang, C. Shi, M. Yang, Y. Ma, Y. Chen, T. Lu, W. Tang, J. Feng, *Asian J. Org. Chem* **2023**, *6*, e202300077.

[2]   R.S. Drago, D.M. Hart, R.L. Carlson, *J. Am. Chem. Soc.* **1965**, *9*, 1900-1904.

[3]   M. Torras, C. Moya, G.A. Pasquevich, A. Roig, *Michrochim. Acta* **2020**, *9*, 488.

[4]   Y.C. Kang, S.M. Treacy, T. Rovis, *ACS Catal.* **2021**, *12*, 7442-7449.

[5]   G.N. Raut, S.B. Wagh, D.S. Reddy, *ARKIVOC* **2015**, *2*, 116-122.

[6]   H. Fuwa, H. Yamaguchi, M. Sasaki, *Tetrahedron* **2010**, *38*, 7492-7503.

[7]   J.M.R. Narayanam, J.W. Tucker, C.R.J. Stephenson, *J. Am. Chem. Soc.* **2009**, *25*, 8756-8757.

[8]   P.-W. Sun, Z. Zhang, X. Wang, L. Li, Y. Li, Z. Li, *Chin. J. Chem.* **2022**, *9*, 1066-1072.

[9]   S.M. Hell, C.F. Meyer, A. Misale, J.B.I. Sap, K.E. Christensen, M.C. Willis, A.A. Trabanco, V. Gouverneur, *Angew. Chem. Int. Ed.* **2020**, *28*, 11620-11626.

[10]   P. Lian, W. Long, J. Li, Y. Zheng, X. Wan, *Angew. Chem. Int. Ed.* **2020**, *52*, 23603-23608.

[11]   X.-L. Luo, D. Ge, Z.-L. Yu, X.-Q. Chu, P. Xu, *RSC Adv.* **2021**, *49*, 30937-30942.

[12]   F. Sun, H. Feng, L. Huang, J. Huang, *Synlett* **2021**, *7*, 713-717.

[13]   Y. Tan, S. Luo, D. Li, N. Zhang, S. Jia, Y. Liu, W. Qin, C.E. Song, H. Yan, *J. Am. Chem. Soc.* **2017**, *18*, 6431-6436.

4 Application of New Ligands for the Cerium-Catalysed Ligand-to-Metal Charge Transfer
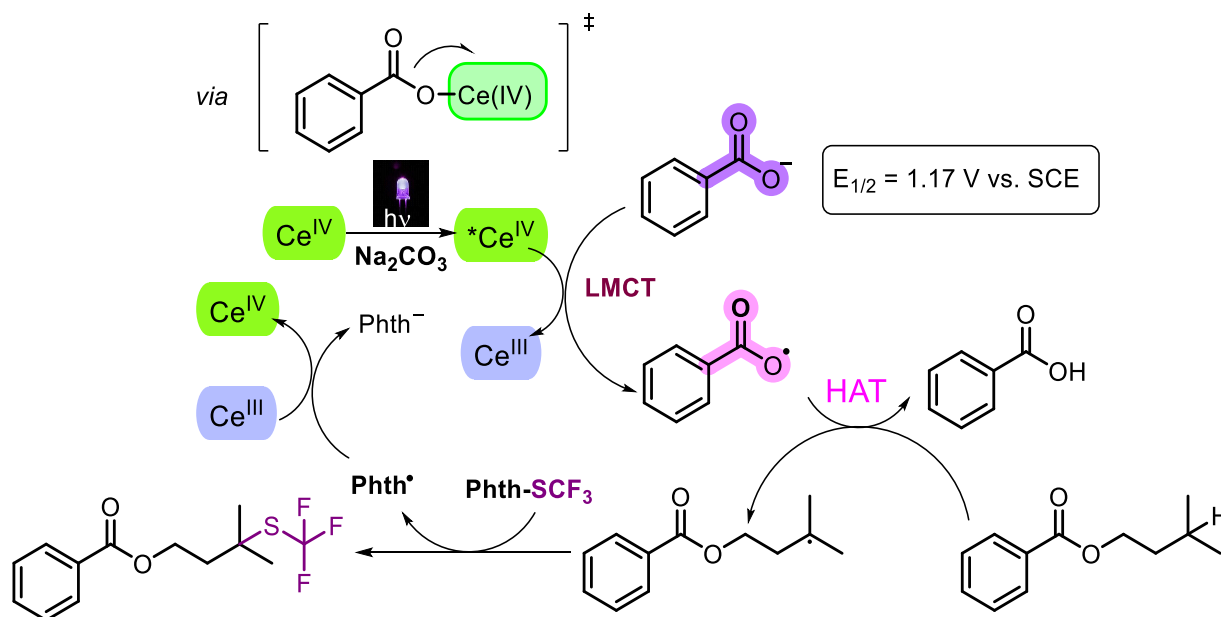
Jessica Stahl performed the synthetic and analytical reactions as well as reaction optimisation and screening attempts, Burkhard König supervised the project. Jessica Stahl wrote the manuscript. Marcel Fischer contributed to the reaction calculations as well as the UV/Vis measurements listed in the Supporting Information.

Chapter 4

Abstract

Benzoate anions coordinate to cerium ions. Excitation of such complexes by light leads to homolytic oxygen-cerium bond cleavage through ligand-to-metal charge transfer (LMCT). This process results in the reduction of the metal ion and the oxidation of the ligand *via* a single-electron transfer event. The resulting benzoic acid radical can serve as a potent hydrogen atom abstractor, facilitating the activation of carbon atoms *via* C-H activation. In this study, we investigated the scope of other oxo-anions and other ligands on cerium(IV) ions that undergo synthetically useful LMCT processes. As a model reaction, the nucleophilic carbon-centred radical arising from C-H abstraction in alkyl esters was reacted with phthalimide derivatives.

4.1 Introduction

The selective functionalisation of short alkanes such as methane, available in natural gases, is a topic of current interest.[1-4] Processes have been developed to convert gaseous hydrocarbons into highly valuable chemicals that serve as platform substrates for further applications.[2] However, due to their non-polar and volatile nature, the specific activation of C-H bonds remains a challenging task. To address this challenge, hydrogen atom transfer (HAT) processes have emerged as a powerful tool.[3-5] Small molecules such as chlorine radicals or oxygen-centred alcoholate radicals act as electrophilic open-shell species with a high propensity for abstraction of hydrogen atoms from electron-rich C-H bonds within the range of their bond-dissociation energy.[6-10] The resulting carbon-centred radicals undergo subsequent transformations and functionalisation reactions.

One of the most efficient strategies for generating reactive radical species is ligand-to-metal charge transfer (LMCT).[11, 12] Among the various metals capable of undergoing charge-transfer chemistry, cerium stands out as an appealing option due to its abundance in the Earth's crust and suitable redox window, featuring oxidation states of +3 and +4.[9, 13-16] Recently, the groups of Schelter and Zuo have developed impressive methodologies involving the formation of coloured Ce^{4+}-ligand complexes through the reaction of $CeCl_3$ and chloride salts or alcoholate ligands, respectively. Upon excitation by visible or near UV light, these complexes undergo oxidative accumulation, yielding chlorine or alkoxy radicals.[17, 18] These electrophilic species selectively abstract hydrogen atoms from complex molecules, and the resulting nucleophilic carbon-centred radicals are successfully trapped by derivatives of di-*tert*-butyl (azodicarboxylate), hypothesized to close the catalytic cycle of Ce^{3+}/Ce^{4+}.[19] However, in some conditions where both $CeCl_3$ and short alcohols were used as the catalytic system, the nature of the eventual active hydrogen atom transfer (HAT) species remains unresolved and is still under discussion despite numerous mechanistic investigations conducted by both groups (Scheme 4.1).[10, 15, 18]

reactive species for HAT process:

Scheler group: **Zhuo group:**
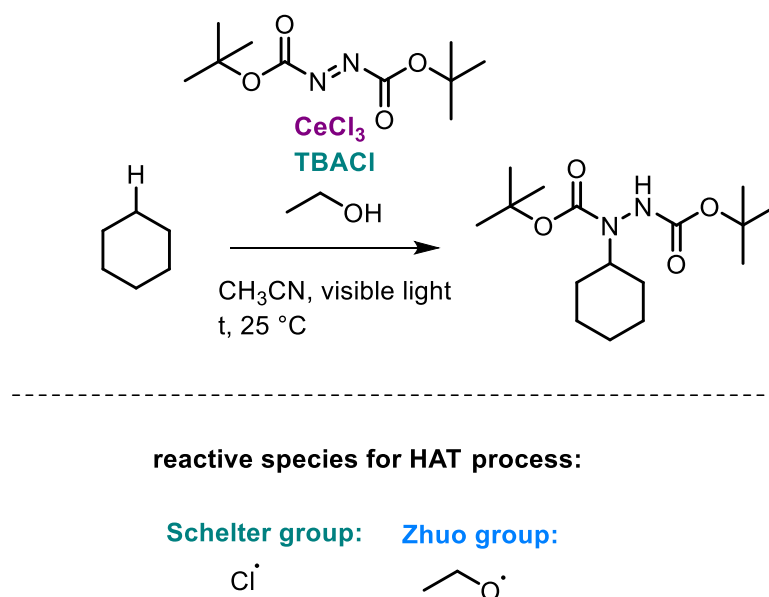
Scheme 4.1. Different opinions on the reactive species in cerium LMCT chemistry.[10, 18]

Jeevarajan *et al.* demonstrated that benzoic acids can function as hydrogen-atom acceptors in the presence of a hydrogen atom donor such as alcohols. Upon transfer of a hydrogen atom radical hexa-dienyl radicals are formed, which are detectable by electron paramagnetic resonance (EPR) spectroscopy.[20] Frank Glorius and colleagues developed a strategy for the selective transformations of tertiary C-H bonds using benzoic acid or appropriate salts thereof as precursors for highly reactive electrophilic hydrogen atom transfer reagents. Through single electron transfer processes, the benzoic acid anion is oxidised by an Ir^{4+} photocatalyst, which undergoes reductive quenching. Instead of the decarboxylative degradation observed in copper chemistry, the resulting radical can effectively abstract hydrogen atoms from nucleophilic C-H bonds, exhibiting high reaction rates (Scheme 4.2, **A**).[21-23]

To expand our understanding of HAT-active ligands, we conducted screenings across various compound classes in search of additional potential ligands capable of LMCT activation with Ce^{4+}, aiming to gain deeper insights into the nature of charge transfer processes. Drawing inspiration from the single-electron transformation achieved by an excited-state redox couple of Ir^{4+} and tetrabutylammonium benzoate for the selective trifluoromethyl-thiolation of complex C-H precursors, we selected this established system from the Glorius group as a benchmark reaction for cerium-catalysed transformations *via* hydrogen atom transfer (Scheme 4.2, **B**).[22]
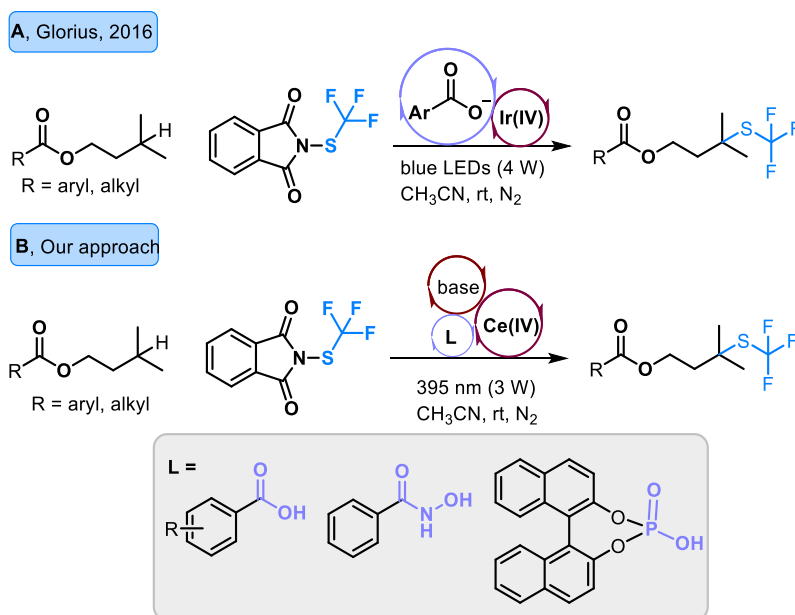
Scheme 4.2. Selective C-H functionalisation of tertiary C-H bonds using benzoic acid salts as HAT catalysts. **A)** Approach from the Glorius group: applying single-electron transfer chemistry with an Ir(IV) catalyst, **B)** our approach: extending the scope for LMCT-active ligands forming complexes with Ce(IV).[22]

4.2 Results and Discussion

We initiated our investigations by conducting the test transformation outlined in Scheme 4.3. Isopentyl benzoate (**1**) underwent a reaction with *N*-(trifluoromethyl) thio-phthalimide (**2**) using a catalytic system comprising of CeF$_4$ (5 mol%) and tetrabutylammonium benzoate (**3**) (5 mol%) in 1 mL of dry acetonitrile, under irradiation with 395 nm light (2.6 W) for 24 h at 25 °C. Evaluation of the reaction *via* ^{19}F-NMR spectroscopy revealed the formation of 26% of the desired product, accompanied by the fading of the initial yellow colour of the reaction mixture upon exposure to the high-power LED. Notably, the reaction failed to proceed in the absence of light, without the cerium salt or when both conditions were lacking (Table 4.1, entries **b**-**d**). Additionally, in the absence of benzoic acid derivatives, product **4** was not formed (Table 4.1, entry **e**). CeF$_4$ was selected due to its low likelihood of generating fluorine radicals upon irradiation with near UV or visible light and consequently, this choice helped to prevent competition between two potential hydrogen atom abstraction agents, as demonstrated by the work of Zhiwei Zuo.[15, 24, 25]
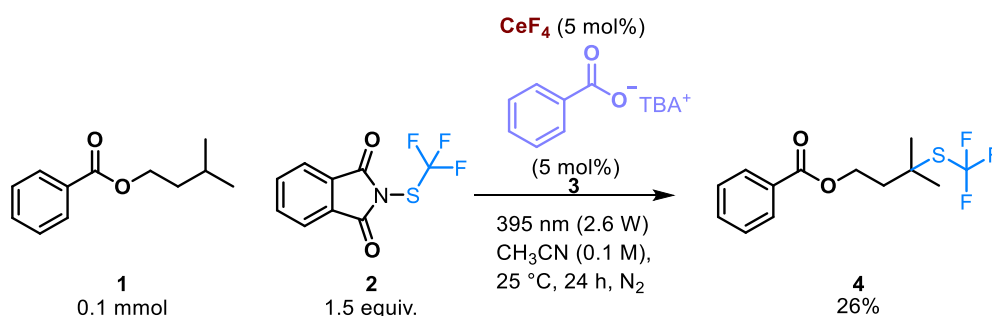
Scheme 4.3. Benchmark reaction for the regio-selective trifluoromethyl-thiolation of branched esters.

Table 4.1. Optimisation of the reaction conditions.

Entry	Deviation from standard conditions	Wavelength [nm]	[a] Yield of 4 [%] from ^{19}F-NMR
a	none	395, high power (~ 2.6 W)	26
b	no cerium salt	395, high power	0
c	no light	395, high power	0
d	no cerium salt, no light	395, high power	0
e	no benzoate salt	395, high power	0
f	Ce(SO$_4$)$_2$	395, high power	3
g	-	385, normal power (~0.2 W)	4
h	-	455, normal power (~0.2 W)	0
i	Benzoic acid (5 mol%), Cs$_2$CO$_3$ (5 mol%)	395, high power	33
j	CeF$_4$ (2 mol%), benzoic acid (2 mol%), Cs$_2$CO$_3$ (5 mol%)	395, high power	86

[a] Yields were determined by ^{19}F-NMR spectroscopy using trifluoro toluene (0.1 mmol) as internal standard in CD$_3$CN.

The combination of a Ce(IV) salt and benzoate derivatives is essential for product formation. Notably, the yield could be enhanced by *in-situ* deprotonation of benzoic acid using Cs$_2$CO$_3$ (Table 4.1, entry **i**) instead of tetrabutylammonium benzoate (Table 4.1, entry **a**). Interestingly, the photo-transformation necessitates high light intensity rather than high light energy, as evidenced by the fact that LEDs emitting at 385 or 455 nm (~200-300 mW) with medium light

intensity failed to induce the photon-induced bond homolysis of the cerium-oxygen bond in the respective benzoate complex (entries **g** and **h**). Similar observations were reported by Zuo's group, who utilised high-intensity LEDs with in their cerium photocatalysis reactions.[26] A maximum yield of 86% was obtained using 2 mol% of CeF_4 and benzoic acid, respectively as well as 5 mol% of Cs_2CO_3, along with a starting material ratio of 1:1.5 for ester **1** (0.1 mmol) and phthalimide **2** (0.15 mmol) in 1 mL of dry acetonitrile under irradiation with a 395 nm LED (~2.6 W) for 24 h at 25 °C (Table 4.1, entry **j**). Subsequent experiments were performed with 5 mol% of the cerium salt, ligand, and caesium carbonate, respectively, for better preparative handling (Supporting Information Table T4.2 for detailed information).

To obtain a general understanding of ligand classes that, upon complexation with CeF_4, facilitate a productive ligand-to-metal charge transfer (LMCT) reaction cascade, we conducted a screening (Scheme 4.4, Table 4.2).
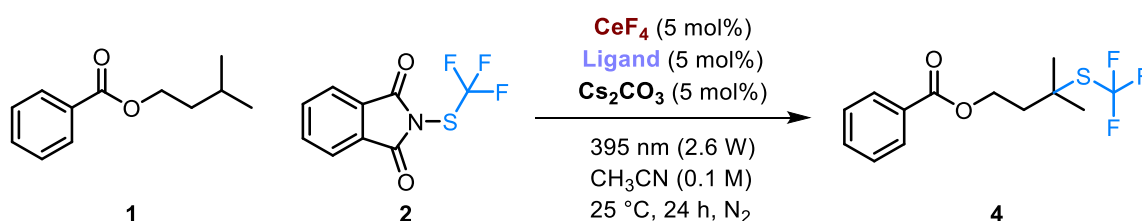
Scheme 4.4. Initial screening for LMCT-active ligands.

Table 4.2. Impact on yield formation upon deviation of ligands for Ce^{4+}.

Entry	Ligand class (5 mol%)	Colour change	[a] Yield of 4 [%] from ^{19}F-NMR
a	phenols	prominent	0
b	Schiff Base Salen ligand	no	0
c	aliphatic thiols	no	0
d	aromatic thiols	slight	0
e	phosphates	slight	9 - 50, see Table 4.3
f	phosphine amides	no	0
g	phosphinic acids	no	0
h	sulfonic acids	no	0

extension of Table T4.2
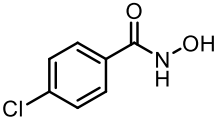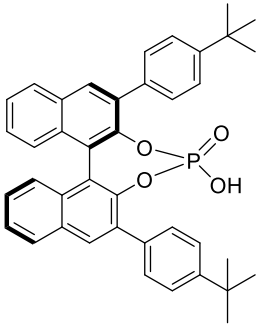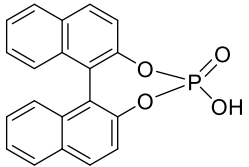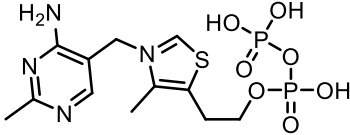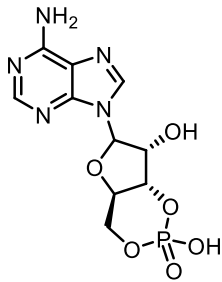
Entry	Ligand class (5 mol%)	Colour change	[a] Yield of 4 [%] from ^{19}F-NMR
i	sulfonamides	no	0
j	hydroxamic acids	prominent	44
k	dihydroxy binaphthyl derivatives	no	0
l	bi (naphthyl amines)	no	2
m	bromine anion	slight	32
n	thiocyanates	prominent	0
o	amino acids	slight	0
p	pyridines	no	0
q	benzoic acid derivatives	slight	49 - 83, see Table 4.3
r	amines	no	0
s	amides	no	0

[a] Yields were determined by ^{19}F-NMR spectroscopy using trifluoro toluene (0.1 mmol) as internal standard in CD$_3$CN.
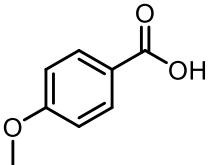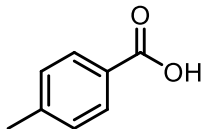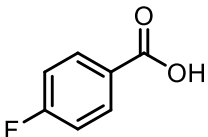
The proposed LMCT activation proved synthetically applicable only for phosphate ligands (Table 4.2, entry **e**), hydroxamic acids (entry **j**), bromide anions (entry **m**) and benzoic acid derivatives (entry **q**). In cases involving other ligand classes, either no charge transfer band arose upon complexation, or a LMCT process did not lead to product formation, e.g., because radical recombination after LMCT outpaced diffusion rates. Consequently, the observation of a colour change upon complexation of the ligands with CeF$_4$ did not enable the prediction of the transformation efficiency.

Specific ligands that efficiently participated in both LMCT and HAT reactions with CeF$_4$, resulting in the formation of product **4**, are outlined in Table 4.3.

Table 4.3. Successful ligands for the complexation with CeF$_4$.

Entry	Ligand (5 mol%)	[a] **Yield of 4 [%] from ^{19}F-NMR**
a	**5**	44
b	**6**	47
c	**7**	44
d	Tetrabutylammonium bromide	32
e	**8**	50
f	**9**	9

next page: extension of
Table 4.3

Entry	Ligand (5 mol%)	[a] Yield of 4 [%] from ^{19}F-NMR
g	**10**	83
h	**11**	64
i	**12**	49

[a] Yields were determined by ^{19}F-NMR spectroscopy using trifluoro toluene (0.1 mmol) as internal standard in CD$_3$CN.

The coordination to CeF$_4$ and subsequent reaction steps demonstrated optimal performance for hydroxamic acid **5** (Table 4.3 entry **a**) and phosphates (Table 4.3, entries **b, c, e, f**). Interestingly, the electron density and the resulting pK_a change of the tested *para*-substituted benzoic acid core structures had only little impact on the efficiency of LMCT-derived oxygen-centred radical formation and the overall photoreaction (entries **g, h, i**).[27]

Next, 1,1´-binaphthyl-2,2´-diyl hydrogen phosphate (**7**) was further investigated as ligand in the light-induced bond-homolysis with Ce^{4+} (Scheme 4.5) and the results were compared to those obtained using benzoic acid as a catalyst for hydrogen atom abstraction.

Phosphate esters attached to 2,2´-dihydroxy-1,1´-binaphthyl (BINOL) backbones have been extensively used for their capacity to engage in hydrogen bonding and Brønsted acid/base catalysis, leveraging the reactivity of their carbonyl- and hydroxy groups.[28, 29] The research conducted by the Kanai group has demonstrated that thiol-derivatives of BINOL possess the ability to abstract hydrogen atoms following single-electron oxidation to form a sulphur-centred radical, facilitated by an organic photocatalyst.[30, 31] To confirm our mechanistic hypothesis

involving cerium binding to phosphate derivatives, we employed commercially available racemic 1,1´-binaphthyl-2,2´-diyl hydrogen phosphate (**7**) at 5 mol% in the benchmark reaction illustrated in Scheme 4.5. Analysis using ^{19}F-NMR spectroscopy revealed that 44% of product **4** was generated, providing support for our proposed mechanistic hypothesis regarding cerium binding to phosphate derivatives.
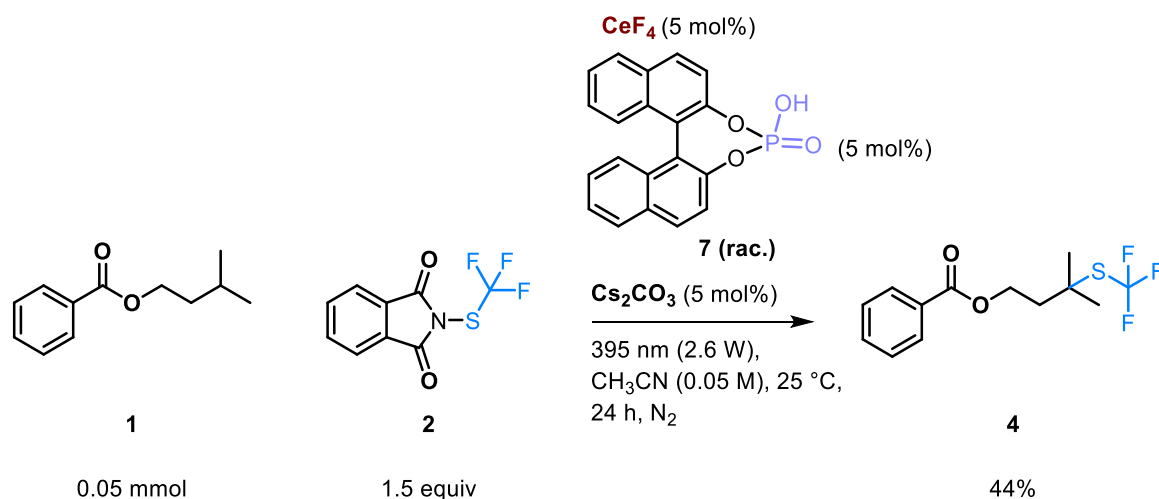
Scheme 4.5. 1,1´-binaphthyl-2,2´-diyl hydrogen phosphate as HAT catalyst for C-H functionalisation.

To eliminate the possibility of a ground-state reactivity of the BINOL phosphate, control reactions were conducted.[28]

Table 4.4. Control experiments and reaction optimisation for the HAT transformations using 1,1´-binaphthyl-2,2´-diyl hydrogen phosphate (**7**).

Entry	Deviation from standard conditions	Wavelength [nm]	[a]Yield of compound 4 [%] from ^{19}F-NMR
a	none	395, high power (~2.6 W)	44
b	no cerium salt	395, high power	0
c	no light	-	0
d	no cerium salt, no light	-	0
e	no BINOL-phosphate	-	0
f	CeO$_2$ (5 mol%) instead of CeF$_4$	395, high power	33
g	CeCl$_3$ (5 mol%) and 9,10 diphenyl anthracene (5 mol%)	395, high power	26
h	Na$_2$CO$_3$ (5 mol%) instead of Cs$_2$CO$_3$ (5 mol%)	395, high power	46
i	1:3 stoichiometry of starting material **1** (0.05 mmol) and **2**	395, high power	59
j	0.017 M instead of 0.05 M based on substrate **1**	395, high power	54

[a] Yields were determined using trifluoro toluene as ^{19}F-NMR standard. All measurements were performed in CD$_3$CN.

Further optimisation reactions are summarised in the Supporting Information. Similar to the reactions with benzoic acid as HAT reagent (Table 4.1), the transformation fails to proceed in the absence of light, cerium salt or both (Table 4.4, entries **b-d**). The addition of the aromatic phosphate reagent as the HAT catalyst is essential for product formation (entry **e**). CeF$_4$ as a cerium salt, proved most successfully for generating product **4** (entry **a**), however using CeO$_2$ as heterogenous lanthanoid catalyst gave 33% of the C-S coupled product (entry **f**). The yield could be further increased by replacing Cs$_2$CO$_3$ with Na$_2$CO$_3$ as the base (entry **h**).

Adjusting the ratio of starting materials **1** and **2** resulted in a 59% yield of the trifluoromethyl-thiolated product (entry **i**), while dilution of the reaction mixture had a slight positive impact on the formation of compound **4** (entry **j**) compared to the conditions in entry **a**. This phenomenon could be elucidated by the decreased likelihood of BINOL phosphate dimer formation in the diluted system, thereby preventing complexation with the cerium salt.[32]

4.3 Mechanistic Investigations

To validate our mechanistic hypothesis regarding the cerium-ligand LMCT and the observed reactivity trends among different ligands in the benchmark reaction, mechanistic investigations were conducted.

Initially, control experiments demonstrated that benzoic acid can serve as an active hydrogen-atom transfer catalyst in the system (Scheme 4.6, Table 4.5). The formation of an oxygen-centred radical was confirmed, triggered by visible-light induced bond homolysis of the cerium-oxygen bond in the complex (Scheme 4.8, Table 4.6).
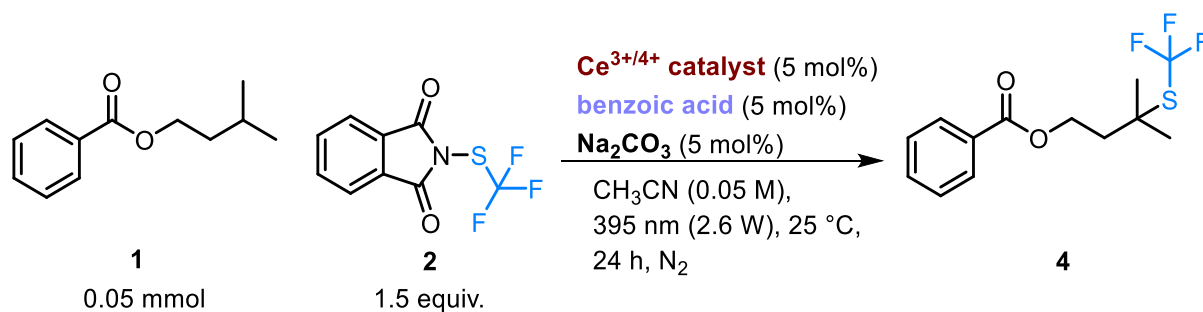
Scheme 4.6. Chlorine radial and benzoate radical competition for hydrogen atom abstraction.

Table 4.5. Comparison of different Ce-Cl and Ce-benzoate systems.

Entry	Catalytic system	Wavelength [nm]	[a] Yield of 4 [%] from ^{19}F-NMR
a	$CeCl_3$ (5 mol%), - base, + benzoic acid	395, high power (~2.6 W)	17
b	$CeCl_3$ (5 mol%), + base, + benzoic acid	395, high power	33
c	$CeCl_6^{2-}$ (5 mol%), - base, + benzoic acid	395, high power	10
d	$CeCl_6^{2-}$ (5 mol%), + base, + benzoic acid	395, high power	13
e	$CeCl_3$ (5 mol%), - base, - benzoic acid	395, high power	2
f	$CeCl_3$ (5 mol%), + base, - benzoic acid	395, high power	5
g	$CeCl_6^{2-}$ (5 mol%), - base, - benzoic acid	395, high power	27
h	$CeCl_6^{2-}$ (5 mol%), + base, - benzoic acid	395, high power	47
i	CeF_4 (5 mol%), + base (5 mol%), - benzoic acid	395, high power	0
j	CeF_4 (5 mol%), + base (10 mol%), - benzoic acid	395, high power	0

[a] Yields were determined using trifluoro toluene (0.1 mmol) as ^{19}F-NMR standard. All measurements were performed in CD_3CN.

The experimental findings indicate that benzoic acid can act as HAT catalyst for the reaction to progress, with higher yields of product **4** observed in the presence of a base (Table 4.5, entry **b** and **d**). In entries **a-d**, both benzoic acid radicals and chlorine radicals, which are generated during a LMCT reaction with cerium, may act as HAT reagents, but the overall product formation is less efficient given by their competitive coordination to cerium. While the reaction gave decent yields in presence of benzoic acid as hydrogen atom transfer reagent (entries **a-d**), utilising exclusively ceriumate-complexes was most efficient in the presence of an additional base (entry **h**). Activation of the Ce-Cl bond through LMCT leads to the generation of chlorine radicals.[18] Product **4** was formed in good yields using the reactive $CeCl_6^{2-}$ species (entries **g** and **h**). and only in traces with $CeCl_3$ as the metal salt (entries **e** and **f**). The performance of $CeCl_3$ can be improved by introducing additional halide or alcoholate ligands, whereas $CeCl_6^{2-}$

exhibits fast photo-degradation once exposed to irradiation in polar aprotic solvents.[33][1] This experimental findings resonate with the outcomes obtained from mechanistic investigations on the $CeCl_6^{2-}$ and $CeCl_3$ photoactivation by the Schelter and Zuo group (Scheme 4.7).[10, 18]
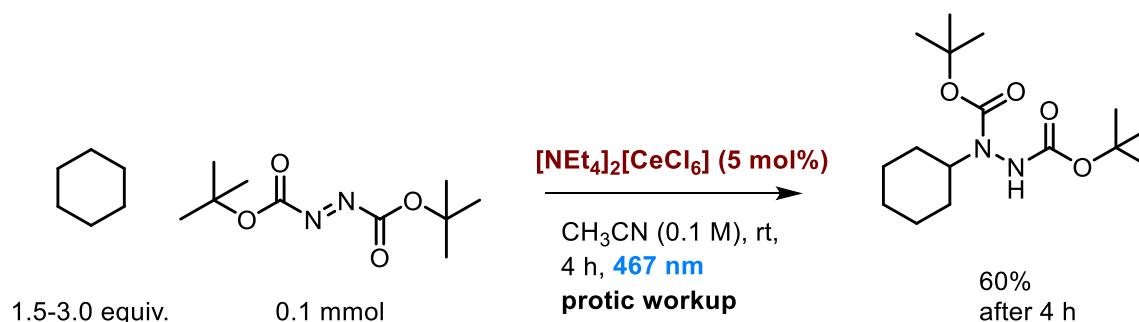
Scheme 4.7. C-H activation of cyclohexane by $CeCl_6^{2-}$ ligand-to-metal charge transfer.[18]

Herein, di-*tert*-butyl-(azodicarboxylate) (DBAD) was employed as a trapping reagent for the nucleophilic carbon-centred radical generated through chlorine-radical induced C-H abstraction on cyclohexane in slight excess. The research group indicated that the reagent served the dual function of a radical trapping agent and an effective photocatalyst. It was anticipated to facilitate the closure of the photocatalytic cycle of Ce^{3+} to Ce^{4+} through a suitable redox potential for single electron transfer.[18, 34]. In the benchmark reaction outlined in Scheme 4.6, phthalimide **2** was utilised instead of DBAD as a single electron transfer reagent in 1.5 equivalents. Unlike DBAD, the phthalimide reagent could not be excited directly upon irradiation.[26] Hence, no product formation was observed when irradiating the phthalimide species with the starting material **1** in the absence of either the cerium salt or the benzoic acid catalyst, indicating that phthalimide **2** did not function as a photocatalyst (Table 4.1 entries **b** and **e**).[19] The reaction from Table 4.5 worked upon Ce-Cl LMCT of $CeCl_6^{2-}$ yielding compound **4** in good yields in the presence of an additional base (entry **h**). LMCT reactions typically achieve higher yields when the corresponding C-H precursor is used in excess such as shown in Scheme 4.7.[8, 18, 35]

To investigate the effect of varying amounts of inorganic base on the CeF_4 benzoate LMCT reaction and simultaneously prove the formation of oxygen-centred radicals on carboxylates, compound **13** was reacted in 0.1 mmol scale with Na_2CO_3 and Cs_2CO_3 (Scheme 4.8, Table 4.6), resulting in the formation of the respective γ-lactone **14** exclusively.[36]
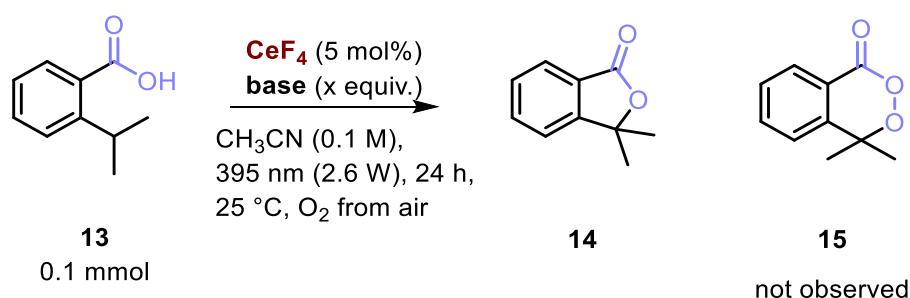
Scheme 4.8. Formation of γ-lactone **14** and peroxy-lactone **15** by cerium LMCT.

Table 4.6. Different bases and base loadings for the effective deprotonation of substrate **13**.

Entry	Base	[a] **Yield of 14 [%] from GC-MS**
a	Na_2CO_3 (5 mol%)	80
b	Na_2CO_3 (0.1 mmol, 1.0 equiv.)	37
c	Cs_2CO_3 (5 mol%)	63
d	Cs_2CO_3 (0.1 mmol, 1.0 equiv.)	traces

[a] Yields were determined by GC-MS using isopropyl benzene (Cumol) as internal standard in 0.1 mmol.

Using Na_2CO_3 at 5 mol% yielded compound **14** in 80% (Table 4.6, entry **a**), whereas only 63% of the γ-lactone product was formed with the same amount of Cs_2CO_3 (entry **c**). Stoichiometric amounts of Na_2CO_3 decreased the yield of **14** to 37%, while the reaction stopped with 1 equivalent of Cs_2CO_3. Either the water content of the bases (entries **b** and **d**) or the carbonate competition for cerium complexation of benzoate inhibits the reaction. The formation of peroxy-lactone **15,** reported by Shirase *et al.* as the main product, upon the reaction of molecular oxygen from air with the carbon-centred radical resulting from a 1,5-hydrogen atom transfer (HAT) of the oxygen-centred radical on benzoic acid, was not observed under our conditions.[36] The investigation about the influence of water introduced into the reaction *via* the carbonate base on the reaction outcome is detailed in the Supporting Information.

Due to the low solubility of CeF_4 in acetonitrile, synthesis approaches were initiated with the aim of forming of soluble anionic lanthanoid complexes by incorporating additional bromide ligands. Bromide anion ligands were successful in ligand-to-metal charge transfer processes with cerium and therefore introduction of bromide ligands was envisaged to facilitate the spectroscopic investigation of the reaction mechanism.

We treated CeF_4 with HBr as the acidic reaction medium.[37] Tetrabutylammonium bromide served as the source of bromide ligands. Stirring the reaction mixture ratios of 1:1 and 1:2 for lanthanoid and ligand, respectively, in an ice bath resulted in the formation of a bright-orange precipitate. Analysis using UV/Vis spectroscopy revealed the unexpected formation of Br_3^- instead of the anticipated CeF_4Br^- or $CeF_4Br_2^{2-}$.[38] The accumulation of Br_3^- appears to outperform the formation of the lanthanoid complex. The possibility of generating bromine radicals from this species is discussed in the Supporting Information.
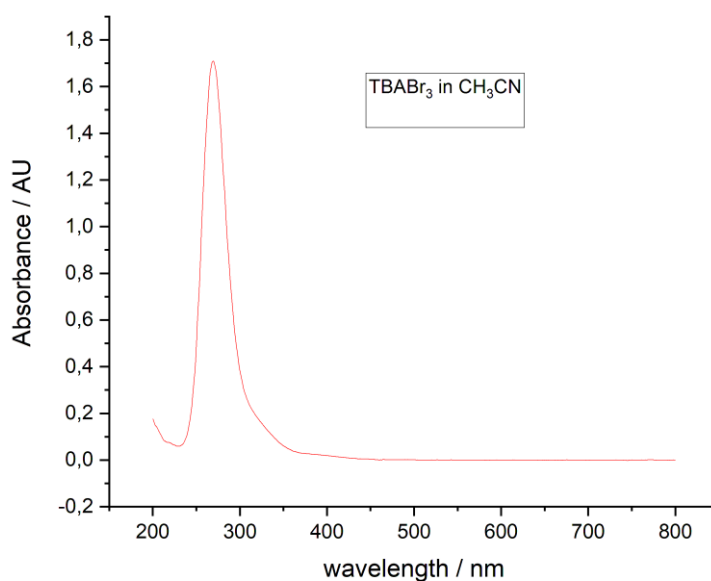
Spectrum 4.1. Tetrabutylammonium tribromide in acetonitrile (qualitative measurement).

The spectral data are in good accordance with literature reports about the tribromide salt.[39]

It has been documented in literature that an excess coordination of (halide) ligands leads to an absorption shift of the resulting (anionic) metal-complex (e.g. $FeCl_4^-$ or $BiCl_5^-$) towards longer wavelengths.[35, 40] However, the attempt to coordinate different kind of ligands simultaneously to the lanthanoid cation, aiming to shift the complex absorption to longer wavelengths and improving its solubility in acetonitrile, resulted in the complete loss of the ligand-to-metal charge transfer (LMCT) activity of the lanthanoid (Table 4.7). We hypothesised that the added ligand in excess displaces benzoic acid.
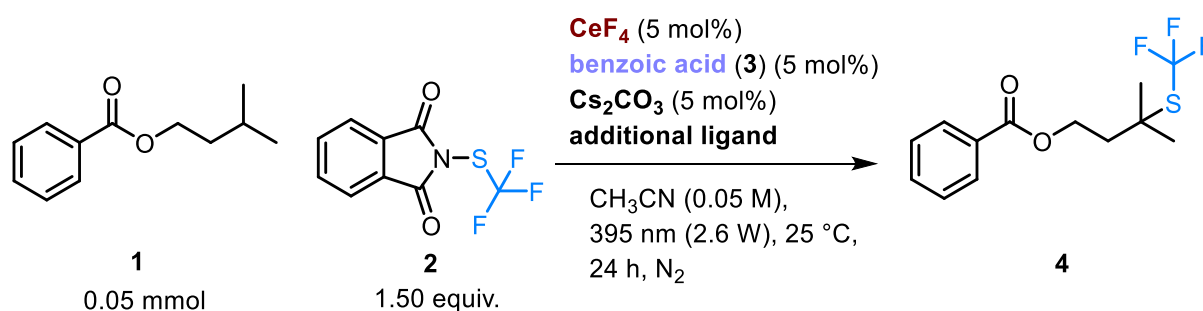
Scheme 4.9. Impact on LMCT-activity of CeF_4 in case of two competing ligand for metal complexation.

Table 4.7. Dual ligand system for the complexation with CeF_4.

Entry	Additional ligand	[a] Yield of compound 4 [%] from ^{19}F-NMR
a	TBAF (10 mol%)	0
b	TBAF (20 mol%)	0
c	TBAF (50 mol%)	0
d	Na_2SO_4 (10 mol%)	0
e	K_2HPO_4 (10 mol%)	0
f	Salen-type ligand[41] (10 mol%)	0
g	DMSO[42] (1 mL)	0
h	KSCN[43] (10 mol%)	0

extension of Table 4.7

Entry	Additional ligand	Yield of compound 4 [%] from ^{19}F-NMR
i	LiNO$_3$ (10 mol%)	0
j	TBAI (10 mol%)	0
k	Na$_2$S (10 mol%)	0

[a] Yields were determined by ^{19}F-NMR spectroscopy using trifluoro toluene as internal (0.1 mmol) standard in CD$_3$CN.

The addition of supplementary ligands may prevent the binding of the benzoate anion. Consequently, no benzoate radical could be formed *via* the desired light-induced bond-homolysis, resulting in the absence of product formation. The pseudohalide or oxoanionic ligands did not exhibit any synthetically productive LMCT activity when combined with CeF$_4$ [10, 44, 45].

As previously noted in Table 4.1, upon mixing CeF$_4$ with a ligand and a base in acetonitrile, the colour of the acetonitrile solution turned from colourless (for the individual components) to various shades depending on the ligand species. However, due to the low solubility of CeF$_4$ in acetonitrile and the high extinction coefficient of benzoic acid or aromatic phosphate **7** itself, it was not possible to isolate and analyse *in-situ* formed lanthanoid-ligand complexes using UV/Vis spectroscopy.[46]
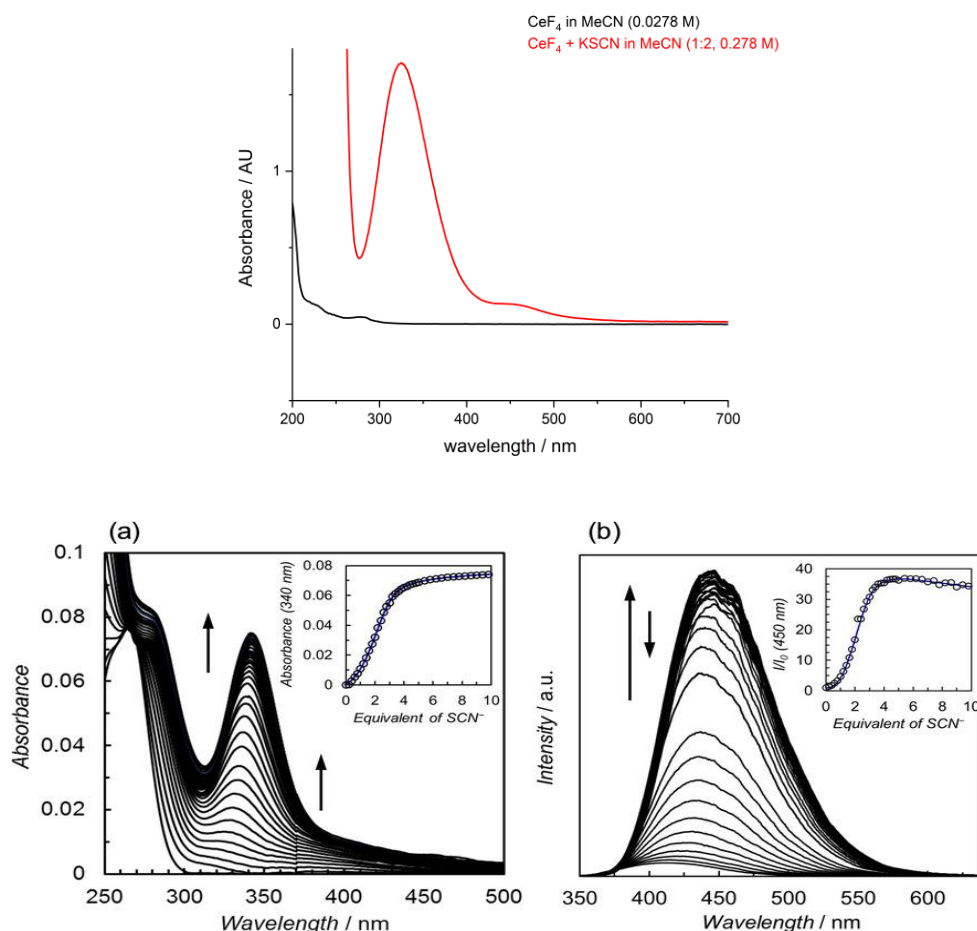
Spectrum 4.2. top: CeF$_4$ (0.0278 M) in acetonitrile and CeF$_4$ and KSCN in a 1:2 mixture in 3 mL acetonitrile (c = 0.278 M). bottom: UV/Vis spectrum (left) and emission spectrum (right) of Ce(SCN)$_3$ as reported in ref [47]. Reprint permission from John Wiley and Sons.

Combing CeF$_4$ and KSCN results in the formation of a highly orange-coloured solution immediately upon mixing in acetonitrile. Spectrum 4.2, top, reveals the appearance of a broad absorption band in the visible region, specifically at 380 and 480 nm, the latter tailing into the 500 nm region. However, in the reference reaction depicted in Scheme 4.9, thiocyanate failed to undergo oxidative activation followed by hydrogen atom abstraction on substrate **1** by cerium-LMCT (Table 4.7). This observation may be attributed to ground-state redox complexation, wherein Ce^{4+} is reduced to Ce^{3+}. [43, 47] A comparison of the observed UV/Vis absorption upon reaction of CeF$_4$ with KSCN with the literature reported spectrum of a titration with isothiocyanate supports the hypothesis (Spectrum 4.2, bottom part).

For the proposed photocatalytic transformation, we suggest the following mechanism (Scheme 4.10). A complex comprising CeF$_4$, benzoic acid and a base is excited by 395 nm light, leading to the single electron oxidation of the deprotonated form of benzoic acid (**3.1**) to yield the respective radical species **3.2**.[48] This radical compound can then abstract a hydrogen atom from the starting material **1,** wherein the resulting carbon-centred radical (**1.1**) is stabilised in the tertiary position within the carbon chain of ester **1**. The nucleophilic radical is subsequently trapped by the phthalimide derivative **2,** and upon transfer of a trifluoromethyl thio-radical, product **4** is formed. The remaining nitrogen-centred phthalimide radical can re-oxidise Ce^{3+} to the Ce^{4+} species, completing the cycle as it converts into the phthalimide anion **2.2**. Alternatively, instead of benzoic acid, BINOL phosphate, hydroxamic acids or bromide ligands can be considered as an active hydrogen atom transfer (HAT) catalyst in combination with Ce^{4+}.[22, 49]
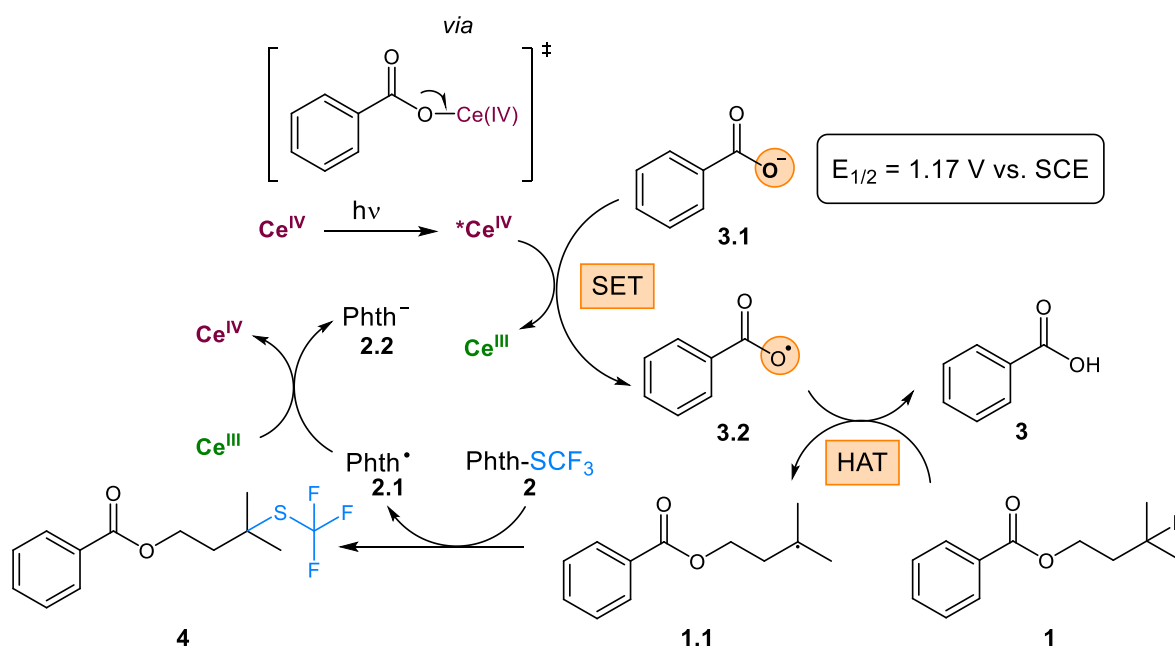
Scheme 4.10. Proposed mechanism for the C-H activation of tertiary carbon atoms *via* cerium-benzoic acid radical.[22]

4.4 Conclusion

In this project, we explored the range of LMCT-active ligands capable of forming complexes with CeF_4 and other cerium compounds, such as CeO_2. Benzoic acid, phosphates, hydroxamic acids and halides such as bromides were successfully employed as ligands for the selective photocatalytic C-H functionalisation, resulting in tertiary carbon-centred radicals. Other ligands did not promote the photoreaction. Complex formation attempts between CeF_4 and tetrabutylammonium bromide yielded Br_3^- quantitively. Mixing CeF_4, a base and KSCN, gave a coloured complex, possibly resulting from a ground-state redox reaction between cerium and the ligand, which was not active in C-H photoactivation. In general, the formation of coloured coordination compounds upon ligand addition to CeF_4 does not correlate with productive LMCT C-H activation. Many parameters define LMCT-active cerium complexes, including the mostly unknown structure and dynamic of the coordination compounds, the specific photophysical processes induced upon irradiation and the lifetimes of generated reactive intermediates in the context of the kinetic parameters of the C-H activation reaction.

4.5 References

[1]   A. Hu, J.-J. Guo, H. Pan, Z. Zuo, *Science* **2018**, *6403*, 668-672.

[2]   G. Zichittella, V. Paunović, J. Pérez-Ramírez, *CHIMIA* **2019**, *4*, 288.

[3]   H. Cao, X. Tang, H. Tang, Y. Yuan, J. Wu, *Chem. Catal.* **2021**, *3*, 523-598.

[4]   L. Capaldo, D. Ravelli, M. Fagnoni, *Chem. Rev.* **2022**, *2*, 1875-1924.

[5]   D. Ravelli, M. Fagnoni, T. Fukuyama, T. Nishikawa, I. Ryu, *ACS Catal.* **2018**, *1*, 701-713.

[6]   M.I. Gonzalez, D. Gygi, Y. Qin, Q. Zhu, E.J. Johnson, Y.-S. Chen, D.G. Nocera, *J. Am. Chem. Soc.* **2022**, *3*, 1464-1472.

[7]   L. Feray, N. Kuznetsov, P. Renaud, *Hydrogen Atom Abstraction*, in *Radicals in Organic Synthesis* 2001. p. 246-278.

[8]   Y.C. Kang, S.M. Treacy, T. Rovis, *ACS Catal.* **2021**, *12*, 7442-7449.

[9]   L. Chang, S. Wang, Q. An, L. Liu, H. Wang, Y. Li, K. Feng, Z. Zuo, *Chem. Sci.* **2023**, *25*, 6841-6859.

[10]   Q. An, Y.-Y. Xing, R. Pu, M. Jia, Y. Chen, A. Hu, S.-Q. Zhang, N. Yu, J. Du, Y. Zhang, J. Chen, W. Liu, X. Hong, Z. Zuo, *J. Am. Chem. Soc.* **2023**, *1*, 359-376.

[11]   Y. Abderrazak, A. Bhattacharyya, O. Reiser, *Angew. Chem. Int. Ed.* **2021**, *39*, 21100-21115.

[12]   F. Juliá, *ChemCatChem* **2022**, *19*, e202200916.

[13]   Y. Chen, X. Wang, X. He, Q. An, Z. Zuo, *J. Am. Chem. Soc.* **2021**, *13*, 4896-4902.

[14]   J. Du, X. Yang, X. Wang, Q. An, X. He, H. Pan, Z. Zuo, *Angew. Chem. Int. Ed.* **2021**, *10*, 5370-5376.

[15]   Q. An, Z. Wang, Y. Chen, X. Wang, K. Zhang, H. Pan, W. Liu, Z. Zuo, *J. Am. Chem. Soc.* **2020**, *13*, 6216-6226.

[16]   Y. Chen, J. Du, Z. Zuo, *Chem* **2020**, *1*, 266-279.

[17]   Y.-H. Wang, Q. Yang, P.J. Walsh, E.J. Schelter, *Org, Chem. Front.* **2022**, *10*, 2612-2620.

[18]   Q. Yang, Y.-H. Wang, Y. Qiao, M. Gau, P.J. Carroll, P.J. Walsh, E.J. Schelter, *Science* **2021**, *6544*, 847-852.

[19]   V.R. Yatham, P. Bellotti, B. König, *Chem. Commun.* **2019**, *24*, 3489-3492.

[20]   A.S. Jeevarajan, R.W. Fessenden, *J. Am. Chem. Soc.* **1992**, *26*, 10461-10470.

[21]   X.-Q. Hu, Z.-K. Liu, Y.-X. Hou, Y. Gao, *iScience* **2020**, *7*, 101266.

[22]   S. Mukherjee, B. Maji, A. Tlahuext-Aca, F. Glorius, *J. Am. Chem. Soc.* **2016**, *50*, 16200-16203.

[23]   A. Reichle, H. Sterzel, P. Kreitmeier, R. Fayad, F.N. Castellano, J. Rehbein, O. Reiser, *Chem. Commun.* **2022**, *28*, 4456-4459.

[24]   T. Liang, C.N. Neumann, T. Ritter, *Angew. Chem. Int. Ed.* **2013**, *32*, 8214-8264.

[25]   K. Zhang, L. Chang, Q. An, X. Wang, Z. Zuo, *J. Am. Chem. Soc.* **2019**, *26*, 10556-10564.

[26]   A. Hu, J.-J. Guo, H. Pan, H. Tang, Z. Gao, Z. Zuo, *J. Am. Chem. Soc.* **2018**, *5*, 1612-1616.

[27]   J. Jover, R. Bosque, J. Sales, *QSAR & Combinatorial Science* **2008**, *5*, 563-581.

[28]   D. Parmar, E. Sugiono, S. Raja, M. Rueping, *Chem. Rev.* **2014**, *18*, 9047-9153.

[29]   A. Zamfir, S. Schenker, M. Freund, S.B. Tsogoeva, *Org. Biomol. Chem.* **2010**, *23*, 5262-5276.

[30]   H. Fuse, H. Mitsunuma, M. Kanai, *J. Am. Chem. Soc.* **2020**, *9*, 4493-4499.

[31]   S. Tanabe, H. Mitsunuma, M. Kanai, *J. Am. Chem. Soc.* **2020**, *28*, 12374-12381.

[32]   M. Franta, J. Gramüller, P. Dullinger, S. Kaltenberger, D. Horinek, R.M. Gschwind, *Angew. Chem. Int. Ed.* **2023**, *27*, e202301183.

[33]   L.L. Costanzo, S. Pistarà, G. Condorelli, *J. Photochem.* **1983**, *1*, 45-51.

[34]   A. Hu, J.-J. Guo, H. Pan, Z. Zuo, *Science* **2018**, *6403*, 668.

[35]   D. Birnthaler, R. Narobe, E. Lopez-Berguno, C. Haag, B. König, *ACS Catal.* **2023**, *2*, 1125-1132.

[36]   S. Shirase, S. Tamaki, K. Shinohara, K. Hirosawa, H. Tsurugi, T. Satoh, K. Mashima, *J. Am. Chem. Soc.* **2020**, *12*, 5668-5675.

[37]   J. Zhao, S. Meng, D. Li, *Solvent Extr. Ion Exch.* **2004**, *5*, 813-831.

[38]   S. Kajigaeshi, T. Kakinami, T. Okamoto, S. Fujisaki, *Bull. Chem. Soc. Jpn.* **2006**, *3*, 1159-1160.

[39]   R.E. Buckles, A.I. Popov, W.F. Zelezny, R.J. Smith, *J. Am. Chem. Soc.* **1951**, *10*, 4525-4528.

[40]   J.-L. Tu, A.-M. Hu, L. Guo, W. Xia, *J. Am. Chem. Soc.* **2023**, *13*, 7600-7611.

[41]   C. Chen, H. Chen, P. Yan, G. Hou, G. Li, *Inorg. Chim. Acta* **2013**, *405*, 182-187.

[42]   E.G. Il'in, A.S. Parshakov, V.G. Yarzhemsky, E.A. Ugolkova, L.V. Goyeva, V.I. Privalov, *Dokl. Phys. Chem.* **2019**, *1*, 120-124.

[43]   Y. Kuramochi, S. Sayama, A. Satake, *Chem. Eur. J.* **2019**, *52*, 12042-12045.

[44] T. Kawakami, S. Tamaki, S. Shirase, H. Tsurugi, K. Mashima, *Inorg. Chem.* **2022**, *50*, 20461-20471.

[45] H. Yin, P.J. Carroll, B.C. Manor, J.M. Anna, E.J. Schelter, *J. Am. Chem. Soc.* **2016**, *18*, 5984-5993.

[46] I. Carmichael, W.P. Helman, G.L. Hug, *J. Phys. Chem. Ref. Data* **1987**, *2*, 239-260.

[47] Y. Kuramochi, K. Ohminato, S. Sayama, A. Satake, *Eur. J. Inorg. Chem.* **2021**, *41*, 4273-4279.

[48] S. Gavelle, M. Innocent, T. Aubineau, A. Guérinot, *Adv. Synth. Catal.* **2022**, *24*, 4189-4230.

[49] T. Franck, A. Mouithys-Mickalad, T. Robert, G. Ghitti, G. Deby-Dupont, P. Neven, D. Serteyn, *Chem. Biol. Interact.* **2013**, *2*, 194-203.

4.6　General Considerations

Starting materials and reagents were purchased from commercial suppliers (Sigma Aldrich, Alfa Aesar, Acros or Fluka) and were used without further purification. Solvents were used as p.a. grade. Reactions were monitored by analytic thin-layer chromatography (TLC) using Fluka silica gel plates with a fluorescent indicator. Visualisation of the developed TLC chromatogram was performed using 254 nm UV light source or potassium permanganate stain. Organic solutions were concentrated using Büchi rotary evaporator. Flash column chromatography was performed either on an automated column machine (Biotage® IsoleraTM Spektra) or manually for non-UV absorbing products. In both cases we used columns filled with silica gel (60-200 μm).

NMR spectroscopy

NMR spectra were recorded at room temperature using a Bruker Advance 300 (300 MHz for ^{1}H, 75 MHz for ^{13}C, 282 MHz for ^{19}F) or a Bruker Advance 400 (400 MHz for ^{1}H, 101 MHz for ^{13}C, 376 MHz for ^{19}F) NMR spectrometer. All chemical shifts are reported in δ-scale as parts per million [ppm], relative to the solvent residual peaks. Coupling constants J are given in Hertz [Hz]. Abbreviations used for signal multiplicity: ^{1}H-NMR: br = broad, s = singlet, d = doublet, t = triplet, q = quartet, dd = doublet of doublets, dt = doublet of triplets, and m = multiplet. The NMR solvent and trifluoro toluene (0.05 or 0.1 mmol, respectively) as internal standard were added to the crude reaction mixtures, the samples were filtered and ^{1}H and ^{19}F-NMR measurements were performed.

Mass spectrometry

High resolution mass spectrometry (HRMS) was performed at the Central Analytical Laboratory of the University of Regensburg. Mass spectra were either measured on a Finnigan MAT 95, ThermoQuest Finnigan TSQ 7000, Finnigan MAT SSQ 710 A or Agilent Q-TOF 6540 UHD instrument together with a Waters Acquity UPLC system equipped with Waters PDA, sample manager, sample organiser, column oven and Waters Xevo QTOF mass spectrometer.

UV/Vis

Absorption spectra were measured on an Agilent Cary 100 UV/Vis spectrometer in a 10 mm × 10 mm quartz cuvette at 25.0 °C under air. Solvents were used from commercial suppliers in HPLC or spectroscopy grade and without further purification. Prior to every measurement, the samples were filtered through a CHROMAFIL®/PTFE-20/15 MS one-way filter (pore size 0.2 µm, membrane diameter: 15 mm) that is usually used for GC sample preparation.

Gas chromatography

GC measurements were performed on a GC 7890 system from Agilent Technologies coupled to a flame-ionisation detector (FID). The system was equipped with a capillary column (HP-5ms UI, length 30 m, diam. 0.25 mm, film 0.25 µm) and worked with H_2 as carrier gas. GC program: The initial temperature of the GC was set to 40 °C and kept for 1.5 minutes. Subsequently, the oven temperature was increased at a rate of 25 °C/min. until reaching 280 °C, which was maintained for 3 min. Then, the temperature was further increased (42 °C/min) until reaching 300 °C and the final temperature was held for 5 minutes. The injector temperature was set to 280 °C and the temperature of the detecting unit to 310 °C. A split ratio of 30:1 (split flow 42 mL/min) was applied, and the column flow was set to 1.4 mL/min. Data acquisition and evaluation were done with Agilent ChemStation Rev.C.01.04.

4.6.1 Photochemical Setup

The photoreactions were performed in 5 mL crimp neck vials that were equipped with a magnetic stir bar. Before placing them into the cooling block on top of the LED (**Figure S4.1**), with six available sample positions, they were crimped. The cooling blocks for photoreactions were fabricated on demand by the mechanical workshop at the University of Regensburg. The samples were placed approximately 2 cm above a 395 nm high power LED (2580 mW) (**Figure S4.2.**, LED-Modul 6-fold, 6x 8.9 V, 0.7 A, Ser. Number: 192-22-3). The reaction temperature was controlled by a thermostat (25 °C) that is connected to every individual metal cooling block.

Figure S4.1. Thermostated metal block for simultaneous irradiation of 6 reaction vials.
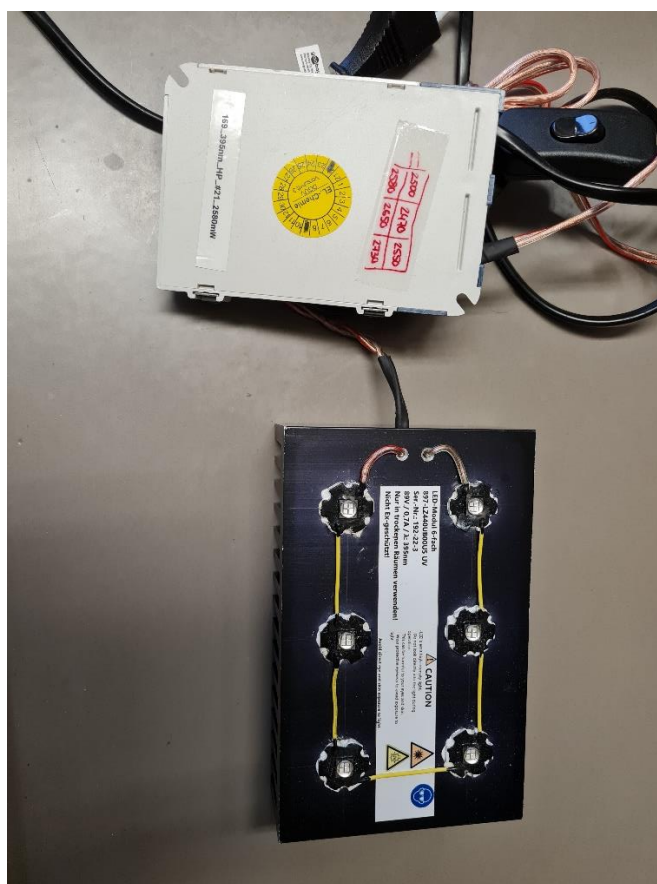
Figure S4.2. LED-plate with six individual single spot LEDs for irradiation at 395 nm.

4.7   General Experimental Procedures

4.7.1   General Procedure for Screening and Optimisation Studies

A 5 mL crimp neck vial was equipped with a magnetic stir bar, isobutyl benzoate (**1**) (0.10 mmol, 1.00 equiv., 20.6 mg, 19.9 mg, respectively), *N*-(trifluoro-methyl-thio) phthalimide (**2**) (0.15 mmol, 1.50 equiv., 37.0 mg), a Ce(III/IV) salt (5 mol%), a ligand (5 mol%) and a base (5 mol%) and 1 mL of dry acetonitrile was added to every vial. The samples were degassed by three cycles of pump freeze-pump-thaw and placed in a thermostated (25 °C) cooling block where they were irradiated at 395 nm (2168-2580 mW) for 24 h. After completion of the reaction, trifluoro toluene (0.10 mmol, 1.00 equiv., 12.2 µL) and CD$_3$CN (0.70 mL) were added to each reaction vial, and 0.7 mL of the resulting mixtures were filtered and subjected to quantitative ^{1}H- and ^{19}F-NMR analysis. For isolation attempts, the solvent of the crude reaction mixture was removed under reduced pressure and the C-H functionalised

product was purified by column chromatography on silica using a solvent mixture of petroleum ether/ethyl acetate (95:5) to obtain the trifluoromethyl-thiolated product in good yields.

4.7.2 General Procedure for the Cerium-Catalysed Selective Trifluoromethyl Thiolation of Tertiary Alkanes

A 4 mL crimp neck vial equipped with a magnetic stir bar was loaded with isobutyl benzoate (**1**) (0.05 mmol, 1.00 equiv.), Phth-SCF$_3$ (**2**) (1.50 mmol, 3.00 equiv.), CeF$_4$ (0.0001 mmol, 0.002 equiv.), benzoic acid or BINOL phosphate hydrogen atom transfer catalyst (0.0001 mmol, 0.002 equiv.) and a carbonate base (0.0001 mmol, 0.002 equiv.). Dry acetonitrile (1.00 mL) was added, and the reaction mixture was degassed three times by freeze-pump-thaw before irradiating the vials for 24 h at 25° C by a high-power LED setup (395 nm, ~2.6 W). After completion of the reaction, CDCl$_3$ (0.7 mL) and trifluoro toluene (6.14 µL) as internal standard for NMR yield determination were added. Purification of the respective products was performed by column chromatography on silica gel (petroleum ether/ethyl acetate, 100:0 – 95:5). The data of the isolated products are in good accordance with the results of Mukherjee *et al.*[1]

4
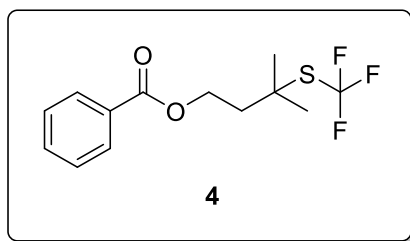
3-methyl-3-((trifluoro-methyl)thio) butyl benzoate (4)

The compound was synthesised and isolated based on the procedure described in **1.2.1**[1] using iso-pentyl benzoate (**1**) (0.20 mmol, 1.00 equiv., 41.3 mg) and *N*-(trifluoro-methyl)thio phthalimide (**2**) (0.30 mmol, 1.50 equiv., 78.7 mg) as well as CeF$_4$ (0.01 mmol, 0.02 equiv., 2.20 mg), benzoic acid (0.01 mmol, 0.02 equiv., 1.22 mg) and Cs$_2$CO$_3$ (0.01 mmol, 0.02 equiv., 3.30 mg) in 1 mL of dry acetonitrile irradiated with a 395 nm (2.6 W) LED for 24 h at 25 °C.

^{1}H-NMR (400 MHz, CDCl$_3$, δ$_H$) 8.06 – 8.00 (m, 2H), 7.60 – 7.54 (m, 1H), 7.48 – 7.42 (m, 2H), 4.52 (t, *J* = 6.7 Hz, 2H), 2.21 (t, *J* = 6.7 Hz, 2H), 1.56 (d, *J* = 0.9 Hz, 7H).

^{19}F-NMR (377 MHz, CDCl$_3$, δ$_F$): -36.24.

HRMS (ESI) (m/z): [M + H]$^+$ (C$_{13}$H$_{15}$F$_3$O$_2$S): cal.: 292.0818, found: 292.0818.

Yield: 15%, 0.01 g, 0.034 mmol, colourless oil.

17
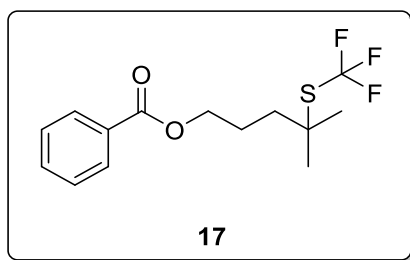
4-methyl-4-((trifluoro-methyl)thio) pentyl benzoate (17)

The compound was synthesized and isolated based on the procedure described in **1.2.1**[1] using iso-pentyl benzoate (**16**) (0.20 mmol, 1.00 equiv., 41.3 mg) and *N*-(trifluoro-rmethyl)thio phthalimide (**2**) (0.30 mmol, 1.50 equiv., 78.7 mg) as well as CeF$_4$ (0.01 mmol, 0.02 equiv.,

2.20 mg), benzoic acid (0.01 mmol, 0.02 equiv., 1.22 mg) and Cs_2CO_3 (0.01 mmol, 0.02 equiv., 3.30 mg) in 1 mL of dry acetonitrile irradiated with a 395 nm (2.6 W) LED for 24 h at 25 °C.

^{1}H-NMR (400 MHz, CDCl$_3$, δ_H) 7.88 – 7.82 (m, 2H), 7.41 – 7.34 (m, 1H), 7.29 – 7.22 (m, 2H), 4.15 (t, J = 6.3 Hz, 2H), 1.82 – 1.71 (m, 2H), 1.68 – 1.60 (m, 2H), 1.30 (d, J = 1.0 Hz, 6H).

^{19}F-NMR (377 MHz, CDCl$_3$, δ_F) -36.3 ppm.

HRMS (ESI) (m/z): [M + H]$^+$ (C$_{14}$H$_{17}$F$_3$O$_2$S) cal.: 306.0974, found: 306.0975.

Yield: 65%, 0.041 g, 0.13 mmol, colourless solid.

4.7.3   General Procedure for the Synthesis of Tertiary Esters

The synthesis of the starting material compounds was performed according to published procedures.[1]

A solution of the branched alcohol (10.0 mmol, 1.00 equiv.), dimethyl amino pyridine (2.00 mmol, 0.20 equiv.) and NEt$_3$ (15.0 mmol, 1.50 equiv.) in chloroform (50.0 mL) was stirred and cooled to 0 °C in an ice bath. Benzoyl chloride (12.0 mmol, 1.20 equiv.) was added and stirring was continued at 0 °C for another hour. The reaction mixture was warmed to room temperature and stirred for further 5 h before being quenched with water (10.0 mL) and extracted with dichloromethane (3 x 20.0 mL). The combined organic phases were dried over Na$_2$SO$_4$ and the solvent was removed under reduced pressure. Purification of the crude product was performed by column chromatography on silica gel with an eluent of petroleum ether/ethyl acetate (98:2) to afford the branched ester in good yields.

1
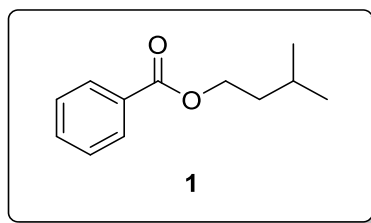
Isobutyl benzoate (1)

Compound **1** was synthesised according to the published procedure from 3-methylbutan-1-ol (10.0 mmol, 1.00 equiv., 1.09 mL), dimethyl aminopyridine (2.00 mmol, 0.20 equiv., 0.24 g), triethylamine (15.0 mmol, 1.50 equiv., 2.09 mL) and benzoyl chloride (12.0 mmol, 1.20 equiv., 1.38 mL) in 30.0 mL of dichloromethane. Isopentyl benzoate (**1**) could be isolated as colourless liquid in 57% yield (5.72 mmol, 1.10 g).[1]

^{1}H-NMR (300 MHz, CDCl$_3$, δ_H) 8.08 – 7.99 (m, 2H), 7.57 – 7.49 (m, 1H), 7.47 – 7.36 (m, 2H), 4.35 (t, J = 6.7 Hz, 2H), 1.80 (ddq, J = 12.8, 7.7, 6.5 Hz, 1H), 1.71 – 1.59 (m, 2H), 0.97 (d, J = 6.6 Hz, 6H).

^{13}C-NMR (75 MHz, CDCl$_3$, δ_C) 166.7 (C$_q$), 132.8 (C$_q$), 130.5 (+), 129.5 (+), 128.3 (+), 63.6 (-), 37.5 (-), 25.2 (+), 22.7 (+).

Yield: 57%, 1.01 g, 5.72 mmol, colourless liquid.

4.8 Reaction Optimisations
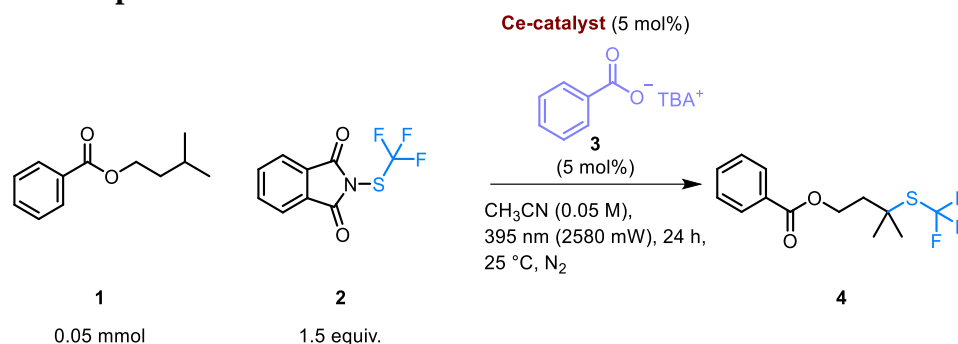
Scheme S4.1. Optimisation reaction for the C-H functionalisation *via* cerium LMCT.

Table T4.1. Screening for different cerium catalysts.

Entry	Ce-catalyst (5 mol%)	Wavelength [nm]	[a] Yield of 4 [%] from ^{19}F-NMR
a	Ce(III)$_2$(CO$_3$)$_3$ · H$_2$O instead of CeCl$_3$	395, high power (~2.6 W)	traces
b	Ce(III)$_2$(CO$_3$)$_3$ · H$_2$O, - benzoate catalyst	395, high power	0
c	Ce(III)(NO$_3$)$_3$ · 6 H$_2$O instead of CeCl$_3$	395, high power	0
d	Ce(III)(NO$_3$)$_3$ · 6 H$_2$O, - benzoate catalyst	395, high power	0
e	C$_3$CeF$_9$O$_9$S$_3$ instead of CeCl$_3$	395, high power	0
f	C$_3$CeF$_9$O$_9$S$_3$, - benzoate catalyst	395, high power	0
g	CeF$_4$ instead of CeCl$_3$	395, high power	26
h	CeF$_4$, - benzoate catalyst	395, high power	0
i	C$_4$CeF$_{12}$O$_{12}$S$_4$ instead of CeCl$_3$	395, high power	0
j	C$_4$CeF$_{12}$O$_{12}$S$_4$, - benzoate catalyst	395, high power	0
i	Ce(IV)(SO$_4$)$_2$ instead of CeCl$_3$	395, high power	3
j	Ce(IV)(SO$_4$)$_2$, - benzoate catalyst	395, high power	0

[a] Yields were determined by ^{19}F-NMR analysis using trifluoro toluene (12.2 μL, 0.1 mmol) as internal standard. CD$_3$CN (0.7 mL) was added to every entry and the reactions were filtered before NMR measurements were performed.
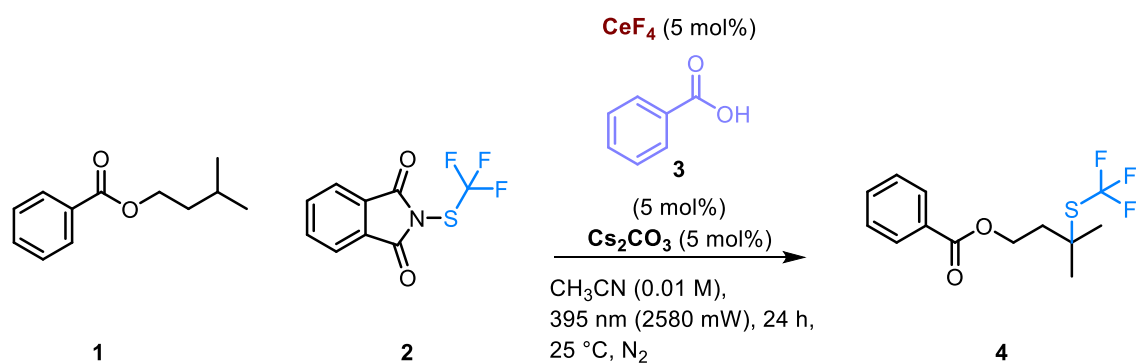
Scheme S4.2. Optimisation of the starting material ratio and the catalyst loading.

Table T4.2. Optimisation of the reaction conditions towards stoichiometry of the reagents.

Entry	CeF$_4$ [mol%]	Benzoic acid [mol%]	Iso-butyl benzoate (1) [mmol]	NPhth-SCF$_3$ (2) [mmol]	Ratio of (1):(2)	c [M]	[a] Yield of 4 [%] from ^{19}F-NMR
a	1.0	1.0	0.10	0.15	1:1.5	0.1	74
b	1.5	1.5	0.10	0.15	1:1.5	0.1	21
c	2.0	2.0	0.10	0.15	1:1.5	0.1	86
d	2.5	2.5	0.10	0.15	1:1.5	0.1	43
e	5.0	5.0	0.10	0.15	1:1.5	0.1	58
f	1.0	1.0	0.15	0.10	1.5:1	0.1	44
g	1.5	1.5	0.15	0.10	1.5:1	0.1	5
h	2.0	2.0	0.15	0.10	1.5:1	0.1	59
i	2.5	2.5	0.15	0.10	1.5:1	0.1	12
j	5.0	5.0	0.15	0.10	1.5:1	0.1	63

[a] Yields were determined using trifluoro toluene (12.2 µL, 0.1 mmol) as internal standard for ^{19}F-NMR analysis in CD$_3$CN. The signal of desired product **4** was observed at -35.2 ppm.

Although entry c gave the highest yield of product **4**, an equimolar amount of CeF$_4$, benzoic acid and Cs$_2$CO$_3$ (5 mol%, respectively) was used due to easier handling while experimental execution.
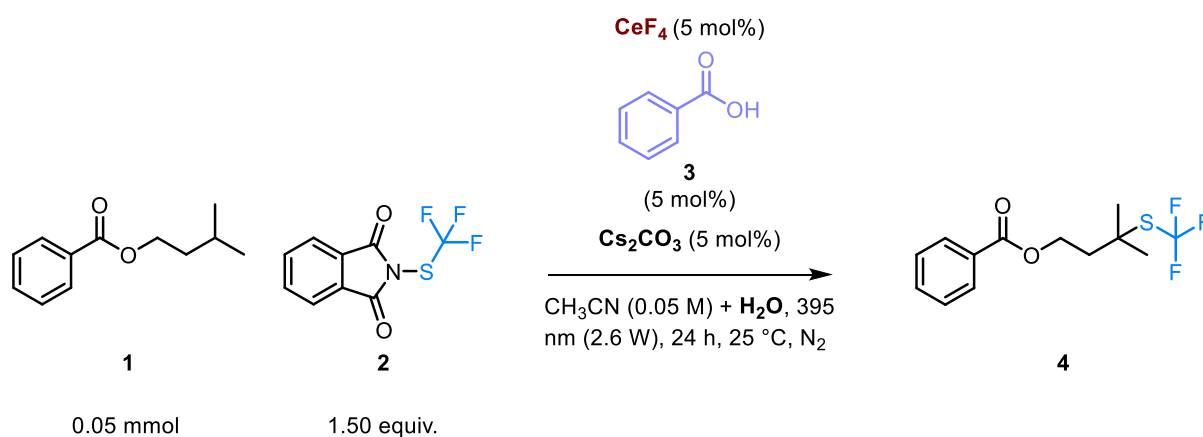
Scheme S4.3. Impact of water content on the reaction outcome.

Table T4.3. Screening for water loading in the photo-transformation.

Entry	Volume of water [μL]	[a] Yield of 4 [%] from ^{19}F-NMR
a	20	0
b	50	0
c	100	0
d	150	0
e	200	0
f	250	0

[a] Yields were determined using trifluoro toluene (6.1 μL, 0.05 mmol) as internal standard for ^{19}F-NMR analysis in CD$_3$CN. The signal of desired product **4** was observed at -35.2 ppm.

In Table T4.3., it is demonstrated that the photoreaction ceases with the addition of just 20 μL of water. Our hypothesis suggests that this cessation of the reaction could be attributed to either the competitive coordination of water molecules with the cerium catalyst or the hydrolysis of phthalimide trapping reagents **2**.[2,3]
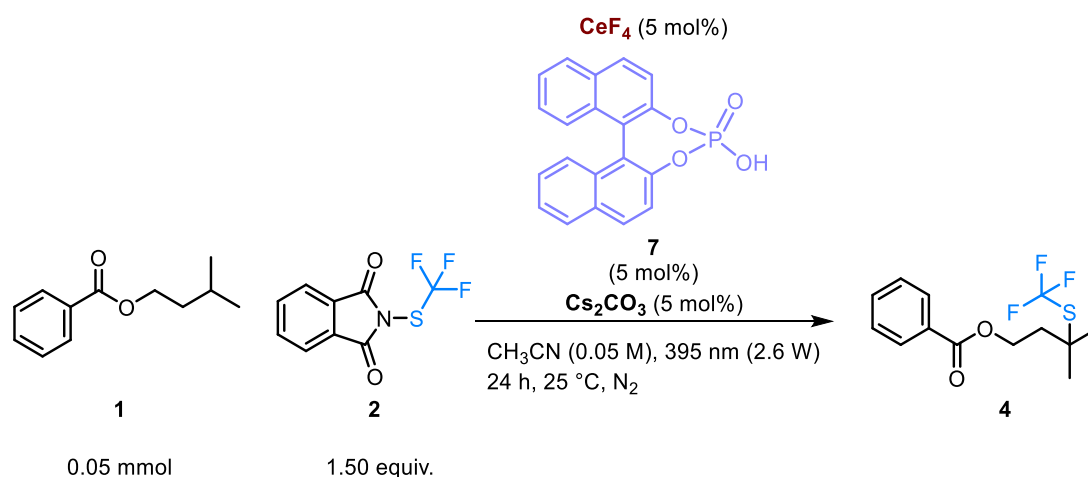
Scheme S4.4. BINOL Phosphate as HAT catalyst in cerium LMCT catalysis.

Table T4.4. Control reaction with the phosphate HAT catalyst **7**.

Entry	Deviation from standard conditions	Wavelength [nm]	[a] Yield of 4 [%] from ^{19}F-NMR
a	no cerium	395, high power (~2.6 W)	0
b	no base	395, high power	0
c	no phosphoric acid HAT	395, high power	0
d	no light	395, high power	0
e	no cerium catalyst, no light	395, high power	0

[a] Yields were determined using trifluoro toluene as internal standard (6.1 µL, 0.05 mmol) for ^{19}F-NMR analysis in CD$_3$CN. The signal of desired product **4** was observed at -35.2 ppm.
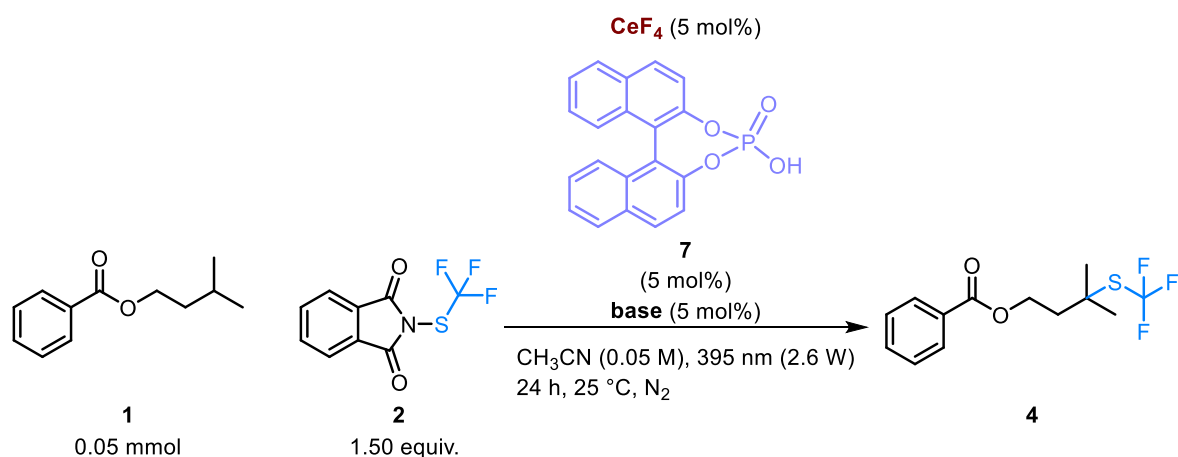
Scheme S4.5. Base screening for the cerium-catalysed C-H functionalisation with BINOL phosphate **7** as HAT catalyst.

Table T4.5. Base screening.

Entry	Base (5 mol%)	[a] Yield of 4 [%] from ^{19}F-NMR
a	Cs$_2$CO$_3$	34
b	Na$_2$CO$_3$	46
c	K$_2$CO$_3$	37
d	Rb$_2$CO$_3$	35
e	Li$_2$CO$_3$	37
f	Ca(OH)$_2$	35
g	NaHCO$_3$	36
h	pyridine	3
i	triethylamine	3
j	DIPEA	9
k	DABCO	37
l	DMAP	14

[a] Yields were determined using trifluoro toluene as internal standard for ^{19}F-NMR analysis (6.1 µL, 0.05 mmol) in CD$_3$CN. The signal of desired product **4** was observed at -35.2 ppm.

The use of various carbonate bases had a negligible effect on product formation in the specific reaction with phosphate HAT catalyst **7** (Table T4.5., entries **a**-**g**) however, Na_2CO_3 gave the highest yield of C-S coupled product **4** (entry **b**), most likely given by its solubility in acetonitrile. However, the organic bases used in entries **h** to **j** resulted in a decrease in the formation of product **4**. 1,4-Diazabicyclo[2.2.2]octan (DABCO) (Table T4.5 entry **k**) allowed for the formation of 37% of the desired product.[4]
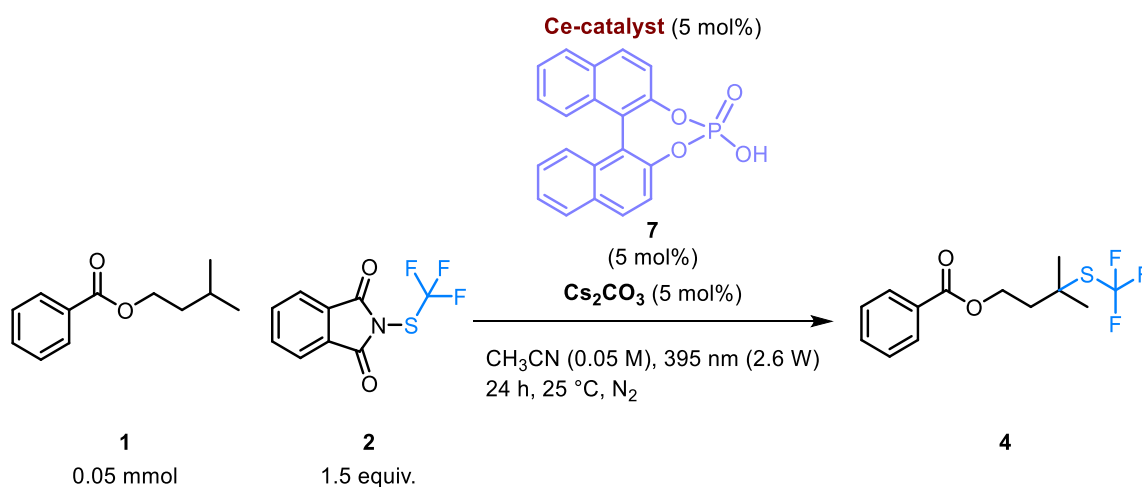
Scheme S4.6. Screening for cerium catalysts for the C-H functionalisation.

Table T4.6. Cerium catalyst screening.

Entry	Cerium catalyst (5 mol%)	[a] Yield of 4 [%] from ^{19}F-NMR
a	CeF_4	44
b	Ce(IV)(trifluoro methane sulfonate)	0
c	CeO_2	33
d	$CeCl_3$, air as oxidant[5]	1
e	Ce(III)trifluoro methane sulfonate, air as oxidant	0
f	$Ce(NO_3)_3 \cdot 6H_2O$, air as oxidant	0
g	$Ce_2(C_2O_4)_3 \cdot H_2O$, air as oxidant	0
h	$Ce_2(CO_3)_2 \cdot H_2O$, air as oxidant	0
i	$[Ce(NO_3)_6][NH_4]_2$	0
j[6]	$CeCl_3$ + 9,10 diphenyl anthracene (5 mol%) as oxidant[6]	26
k	$Ce(IV)(SO_4)_2$	16

[a] Yields were determined using trifluoro toluene as internal standard for ^{19}F-NMR analysis (0.05 mmol) in CD_3CN. The signal of desired product **4** was observed at -35.2 ppm.

Apart from CeF_4 (Table T4.6., entry **a**), CeO_2 (entry **c**), and $CeCl_3$ combined with 9,10 diphenyl anthracene acting as single electron oxidant for Ce^{3+} (entry **j**)[6], were effective in facilitating the formation of product **4**. However, the utilisation of oxygen from air as a terminal oxidant (entries **e**-**h**) failed to complete the catalytic cycle of the metal catalyst. Additionally, cerium ammonium nitrate, functioning as strong oxidant (entry **i**) could not initiate a self-oxidation mechanism for product formation.[7]

CeF$_4$ (5 mol%)

7
(5 mol%)

Cs$_2$CO$_3$ (5 mol%)

CH$_3$CN, 395 nm (2.6 W)
24 h, 25 °C, N$_2$
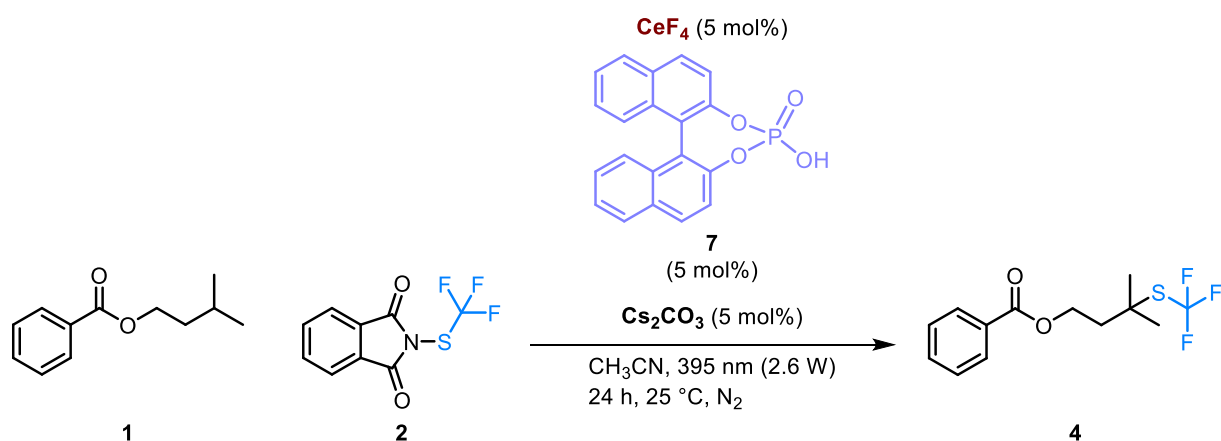
Scheme S4.7. Optimisation of the starting material ratio.

Table T4.7. Reaction optimisation for the starting material ratio.

Entry	Iso-butyl benzoate (1) [mmol]	NPhth-SCF$_3$ (2) [mmol]	Ratio of (1):(2)	c [M]	Yield of 4 [%] from ^{19}F-NMR [a]
a	0.05	0.05	1:1	0.05	28
b	0.05	0.075	1:1.5	0.05	36
c	0.05	0.10	1:2	0.05	39
d	0.05	0.15	1:3	0.05	59
e	0.075	0.05	1.5:1	0.05	28
f	0.10	0.05	2:1	0.05	26
g	0.15	0.05	3:1	0.05	30

[a] Yields were determined using trifluoro toluene as internal standard (0.05 mmol) for ^{19}F-NMR analysis in CD$_3$CN. The signal of desired product **4** was observed at -35.2 ppm.
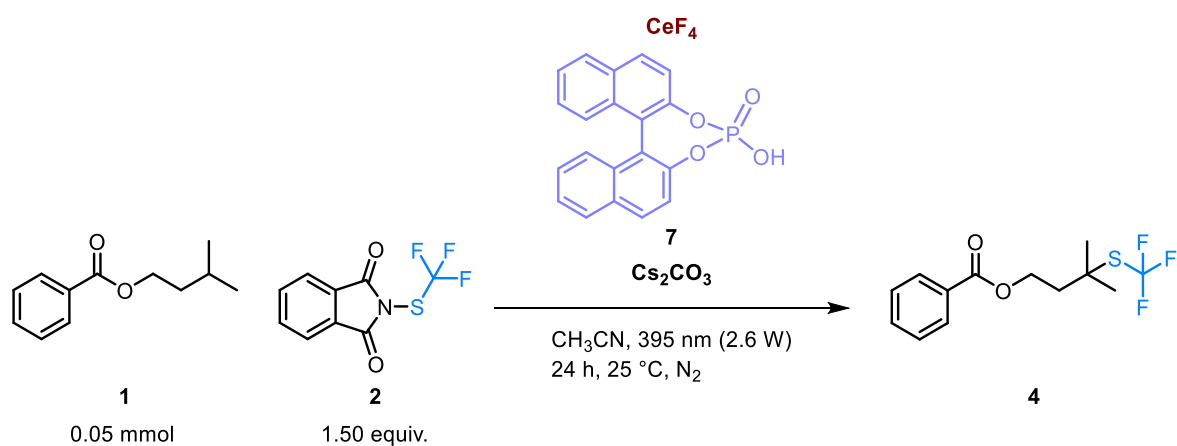
Scheme S4.8. Optimisation of the catalytic system.

Table T4.8. Optimisation of the catalytic system.

Entry	CeF$_4$ [mol%]	BINOL-phosphate HAT 7 [mol%]	Cs$_2$CO$_3$ [mol%]	Ratio Ce:phosphate:base	c [mM]	[a] Yield of 4 [%] from ^{19}F-NMR
a	1.0	1.0	1.0	1:1:1	0.05	56
b	1.5	1.5	1.5	1:1:1	0.05	38
c	2.0	2.0	2.0	1:1:1	0.05	31
d	5.0	5.0	5.0	1:1:1	0.05	25
e	10	10	10	1:1:1	0.05	31
f	5.0	10	10	1:2:2	0.05	34
g	10	5.0	10	2:1:2	0.05	34
h	10	10	5.0	2:2:1	0.05	37
i	5.0	5.0	15	1:1:3	0.05	29
j	5.0	5.0	100	1:1:20	0.05	0

[a] Yields were determined using trifluoro toluene as internal standard (0.05 mmol) for ^{19}F-NMR analysis in CD$_3$CN. The signal of desired product **4** was observed at -35.2 ppm.

The reaction outcome observed in entry **j** (with one equivalent of base, 0.05 mmol) aligns well with the observation detailed in Table 4.6 in the main manuscript, where an excess of caesium carbonate leads to the cessation of the photoreaction. This correlation could be attributed to an elevation in water content upon the introduction of a hygroscopic salt into the reaction mixture. Additionally, the reduced effectiveness of light penetration from scattering effects caused by the presence of inorganic particles in acetonitrile could lead to a reduced yield.
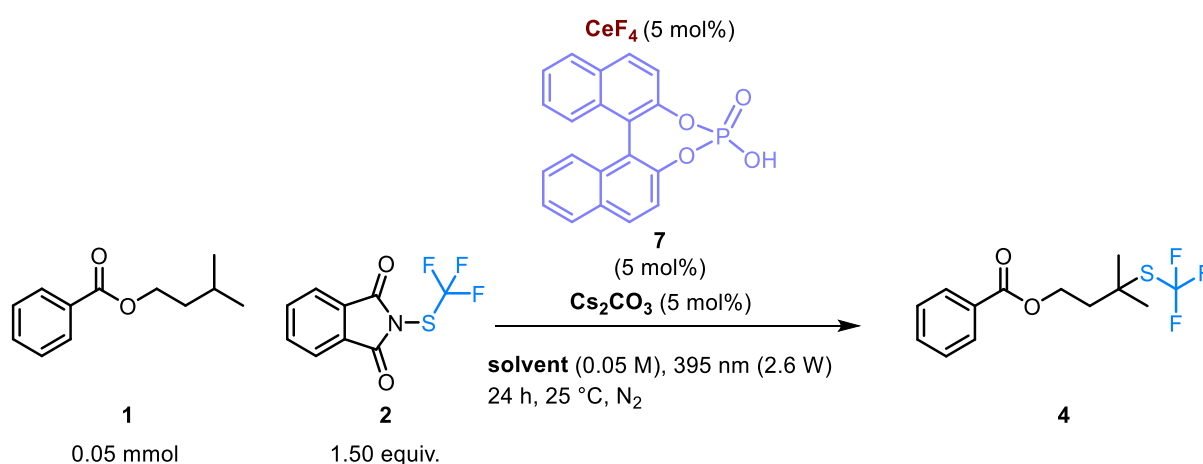
Scheme S4.9. Solvent screening.

Table T4.9. Solvent screening results.

| Entry	Solvent (0.05 M)	[a] **Yield of 4 [%] from ^{19}F-NMR**
a	Acetonitrile	37
b	Dichloromethane	0
c	Chloroform	0
d	Dichloroethane	0
e	Benzene	0
f	Acetone	31
g	Benzonitrile	27

[a] Yields were determined using trifluoro toluene as internal standard for ^{19}F-NMR analysis (0.05 mmol) in CD$_3$CN. The signal of desired product **4** was observed at -35.2 ppm.
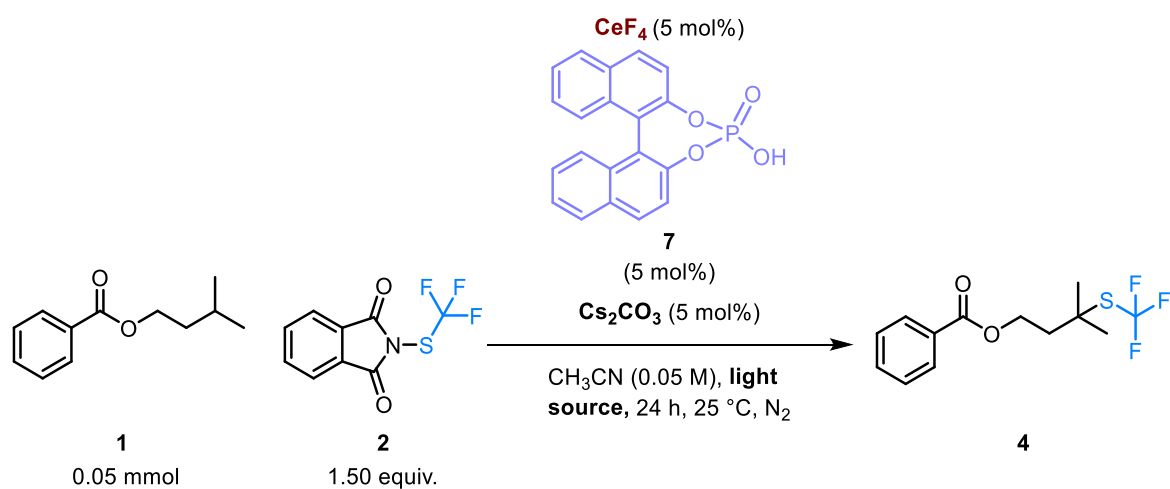
Scheme S4.10. Screening for the reaction wavelength.

Table T4.10. LED wavelength and intensity screening.

Entry	Light source	[a] Yield of 4 [%] from ^{19}F-NMR
a	395 nm (2.6 W)	44
b	451 nm (0.4 W)	0
c	365 nm (2.5 W)	21

[a] Yields were determined using trifluoro toluene as internal standard for ^{19}F-NMR analysis (0.05 mmol) in CD₃CN. The signal of desired product **4** was observed at -35.2 ppm.

4.8.1 Synthesis of CeF₄ Complexes with Base and Benzoic Acid

CeF₄-benzoate complexes were synthesised according to a published procedure[8] using the lanthanoid salt, a respective first row-metal carbonate base and benzoic acid in equimolar amounts. A solution of CeF₄ (1.00 mmol, 1.00 equiv., 0.216 g) in water (5.00 mL) was added to a stirred solution of the carbonate base (1.00 mmol, 1.00 equiv.) and benzoic acid (1.00 mmol, 1.00 equiv., 0.122 g) in water (5.00 mL). Stirring was continued for 12-18 h at room temperature, then the heterogenous mixture was filtered. The remaining solid was washed with cold water and dried under reduced pressure. Table T4.11. shows the reaction condition as well as the experimental outcome of the respective complex formation.

Table T4.11. Synthesis of cerium-benzoate complexes.

Entry	Carbonate base [g]	Expected mass of complex [g/mol]	[a] Yield of isolated solid [g]
a	Li₂CO₃, 0.074	412.12	0.130, pale yellow solid, **32%**
b	Na₂CO₃, 0.106	444.22	0.135, pale yellow solid, **30%**
c	K₂CO₃, 0.138	476.43	0.099, pale yellow solid, **21%**
d	Cs₂CO₃, 0.326	664.05	0.090, pale yellow solid, **14%**

[a] Yields were determined after careful washing and drying of the respective off-yellow solids.

Due to the limited solubility of CeF₄, the yields of the corresponding complexes ranged from 14 to 32% of the dry product. A noticeable colour change from colourless to pale yellow was observed for the three-component complexes when comparing the individual starting materials and the products. However, due to the strong self-absorption characteristic of benzoic acid, a comparison of the complexes by UV/Vis spectroscopy was not feasible.

4.8.2 Synthesis of Anionic CeF$_4$Br$_x^{n-}$ Complexes

HBr (47%) or HClO$_4$ (70%) (5.00 mL) was cooled in an ice bath before the addition of CeF$_4$ (1.00 equiv.) and tetrabutylammonium bromide (1.00 – 10.0 equiv.). A yellow precipitate formed, and the mixture was stirred for 30 min. before being filtered and dried under reduced pressure. For purification purposes the following conditions were tested:

(a) Filtering the reaction mixture; residual solvent was removed under reduced pressure; purification by column chromatography on silica with a solvent mixture of DCM/CH$_3$CN (4:1), R$_f$-value of the orange product band: 0.9.; 3 individually coloured fractions were collected, and the solvent was removed under reduced pressure.

(b) preparative DC (HPTLC silica 60 F$_{254}$ plates for Nano-DC), 10 x 10 cm) on with DCM/CH$_3$CN (4:1), R$_f$-value of the orange product band: 0.9.

(c) centrifugation of the crude reaction mixture, removal of the supernatant. The isolated solid was analysed *via* UV/Vis spectroscopy and identified as (TBA)Br$_3$ (Spectrum 4.1.)[9]

4.8.3 Analysis of the Synthesis Products

The following UV/Vis measurements were performed in collaboration with Marcel Fischer and data were plotted by latter. Calculations were performed by him using the given parameters:

Functional: CAM-B3LYP
Basis set: def2-TZVPD
Solvent code: COSMO

The absorption of tetrabutylammonium tribromide in acetonitrile, generated synthetically upon stirring CeF$_4$ and tetrabutylammonium bromide in HBr (Supporting Information chapter **4.8.2**), is depicted in Spectrum S4.1. In presence of tetrabutylammonium benzoate as potential coordination partner in solution, Br$_3^-$ is stable once handled in absence of light (Spectrum S4.2) When subjected to 309 nm LED irradiation for 120 seconds in acetonitrile, the complex remains stable without undergoing degradation *via* bromine-radical formation.
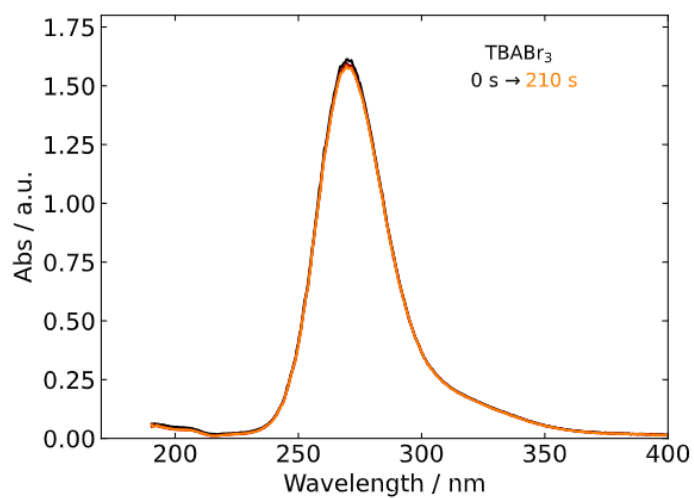
Spectrum S4.1. Photo-stability of TBABr$_3$ (0.11 mM) upon irradiation in acetonitrile over a period of 120 seconds.
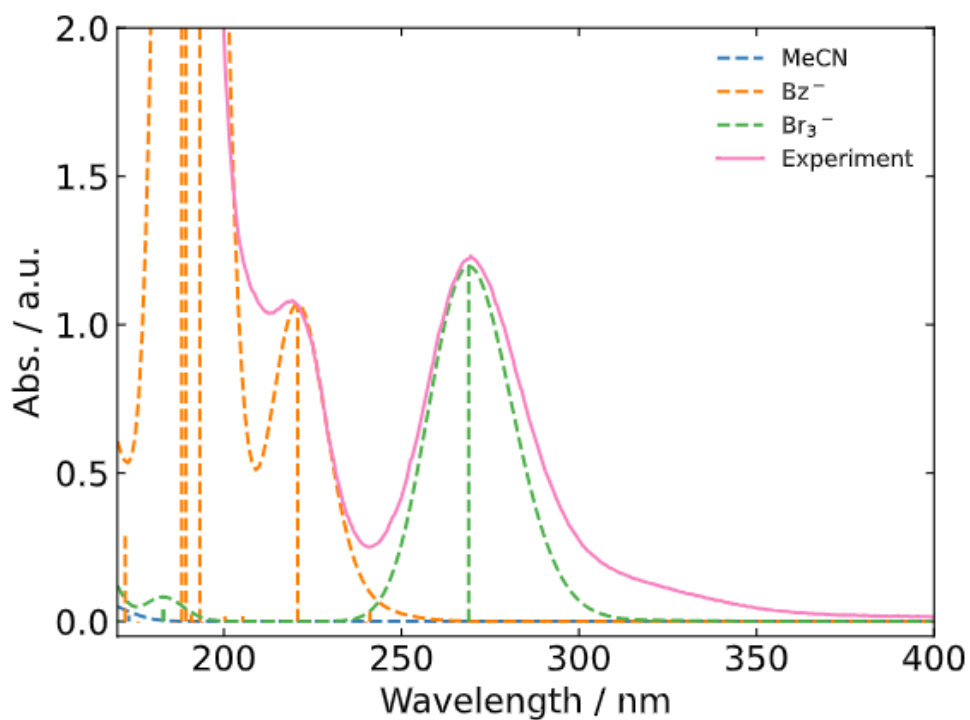
Spectrum S4.2. Interaction of TBABr$_3$ (0.11 mM) and tetrabutylammonium benzoate anion (0.26 mM) in acetonitrile. Conditions are recorded before irradiation upon 309 nm light and proved by calculations using the basis set mentioned in abstract **4.8.3** of the Supporting Information.

Upon irradiation in the presence of the benzoate anion, bromine radicals originating from TBABr$_3$ trigger an oxidative transformation of the benzoic acid anion (Spectrum S4.3). Additionally, when a cerium metal and 395 nm light are present, bromine radicals can be generated (Table 4.2, entry **m**). As a result, the concentration of the Br$_3^-$ species is diminished after the irradiation process (Spectrum S4.3).
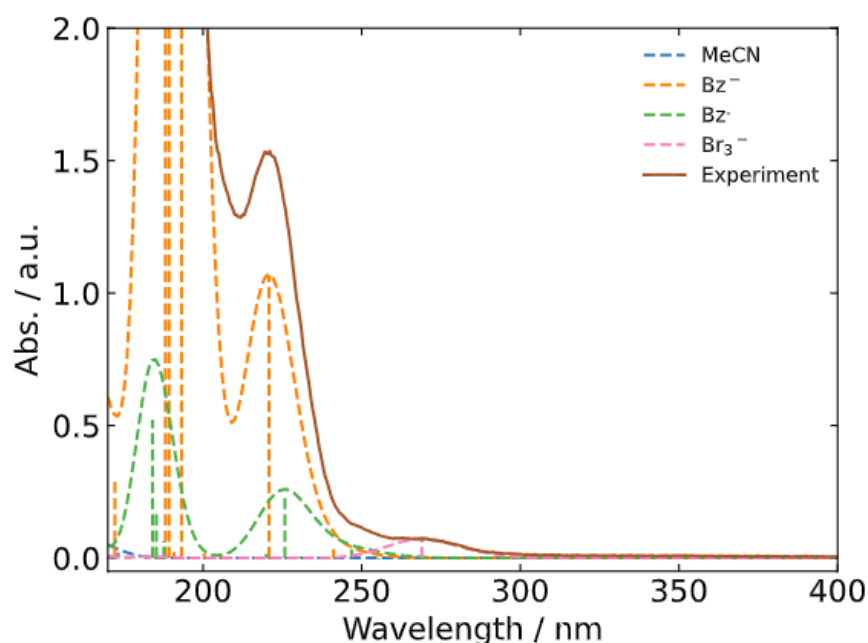
Spectrum S4.3. Interaction of Br$_3^-$ (0.11 mM) and tetrabutylammonium benzoate anion (0.26 mM), orange dotted curve) under irradiation. Benzoate radicals are generated (illustrated by the green dotted line) and the concentration of Br$_3^-$ (pink dotted line) decreases.

4.9 NMR-Data of Products and Starting Materials
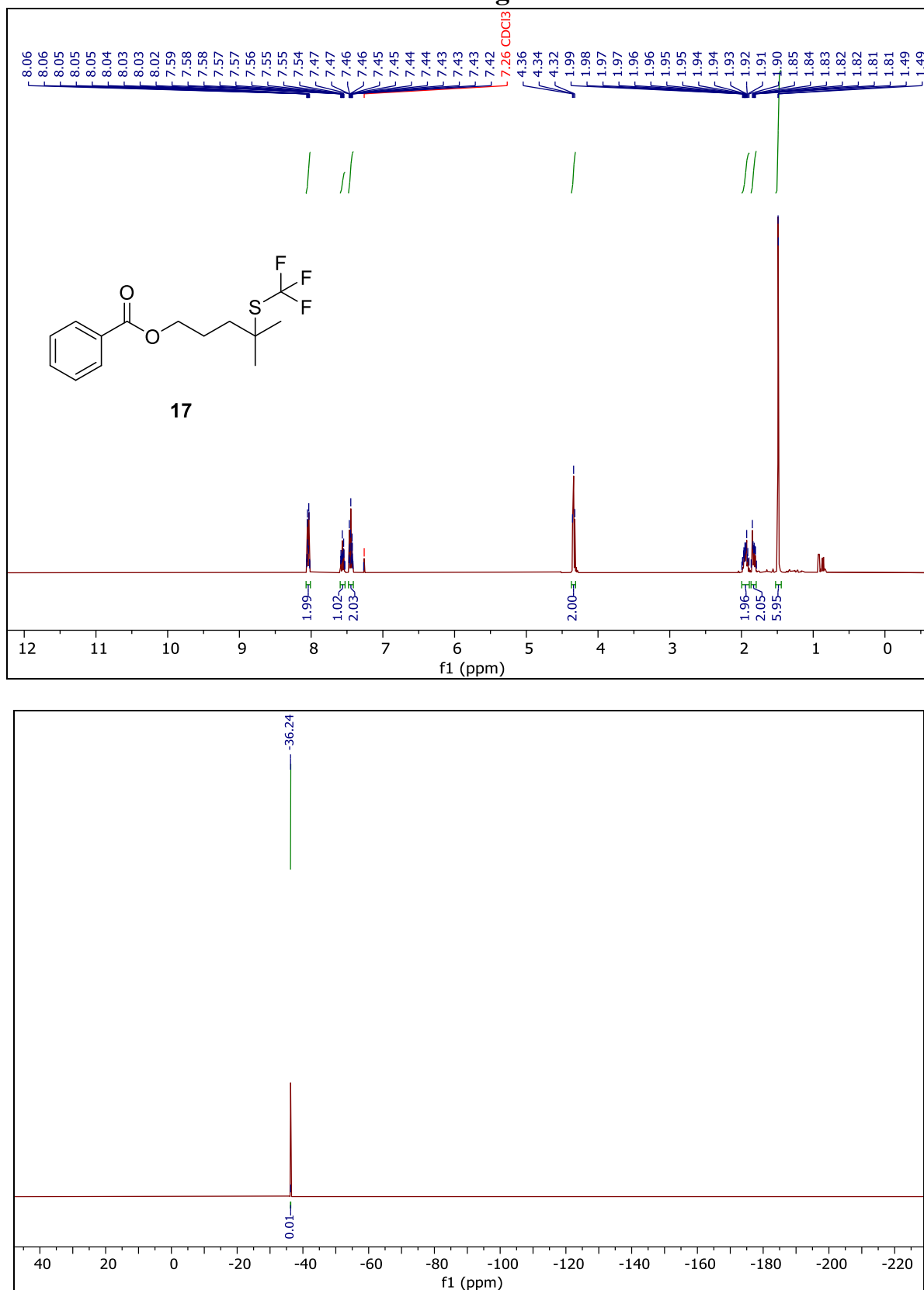
Spectrum S4.4. Compound **17**, ¹H- and ¹⁹F-NMR (Chloroform-*d*).
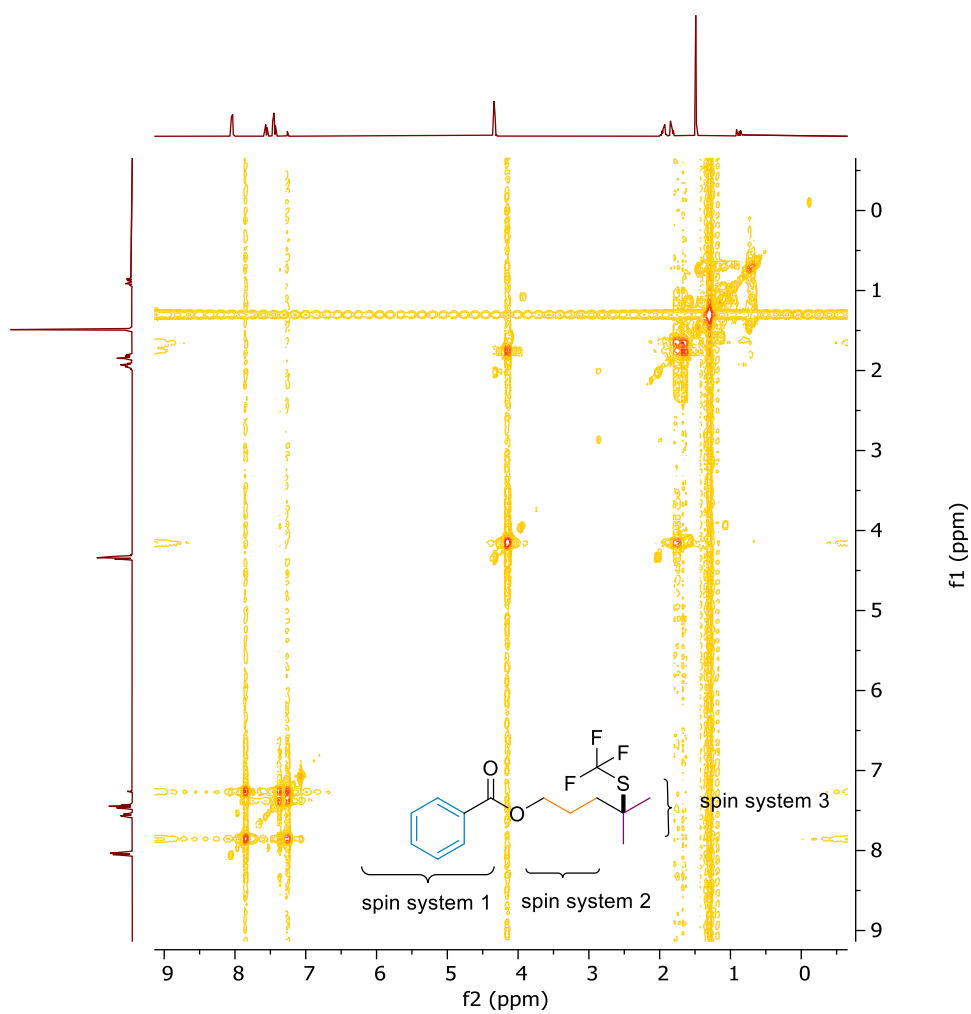
Spectrum S4.5. Compound **17**, ^{1}H-COSY (Chloroform-*d*).
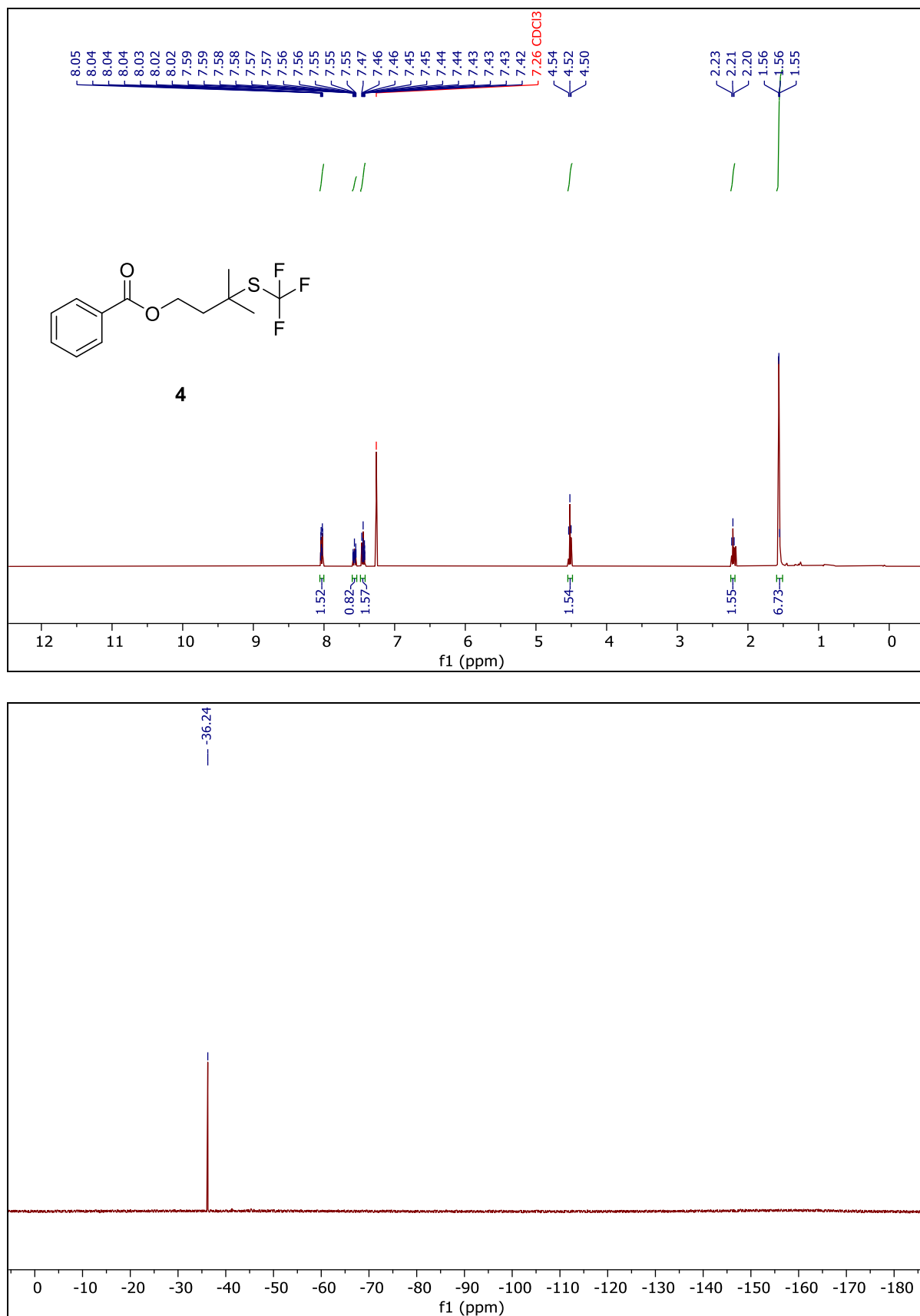
Spectrum S4.6. Compound **4**, ^{1}H- and ^{19}F-NMR (Chloroform-*d*).
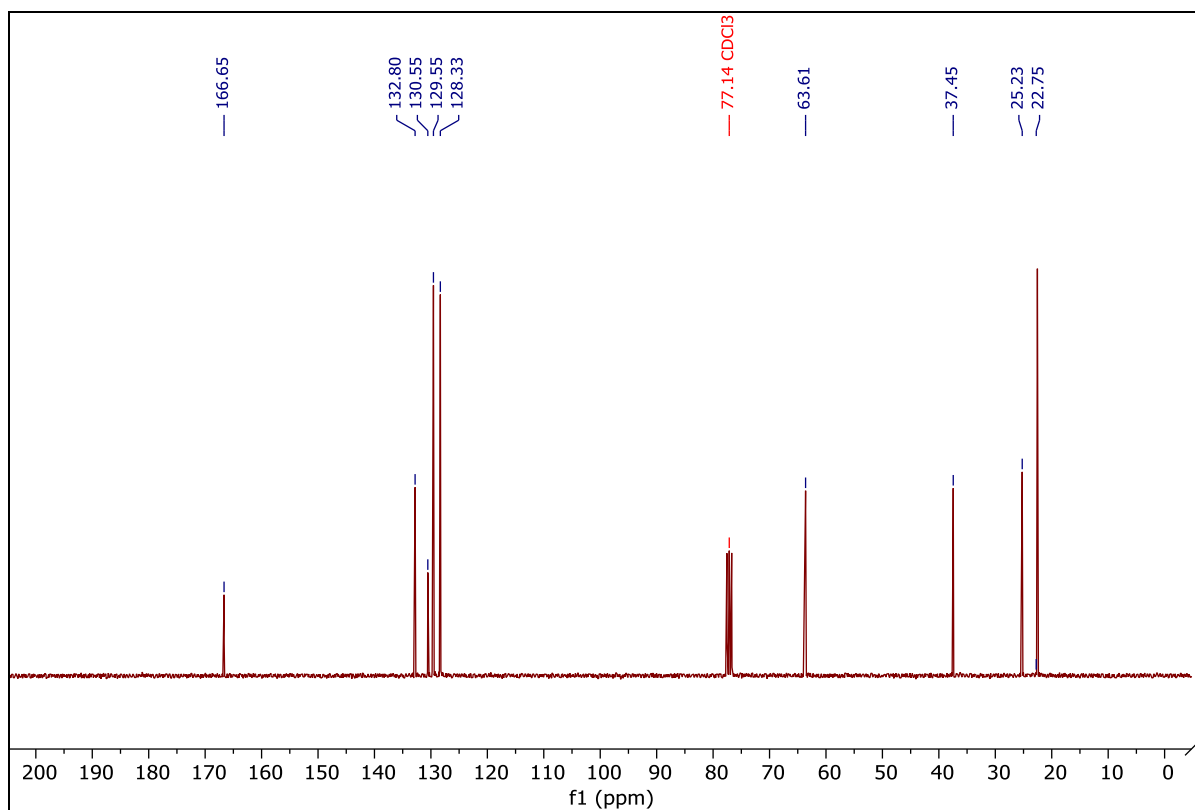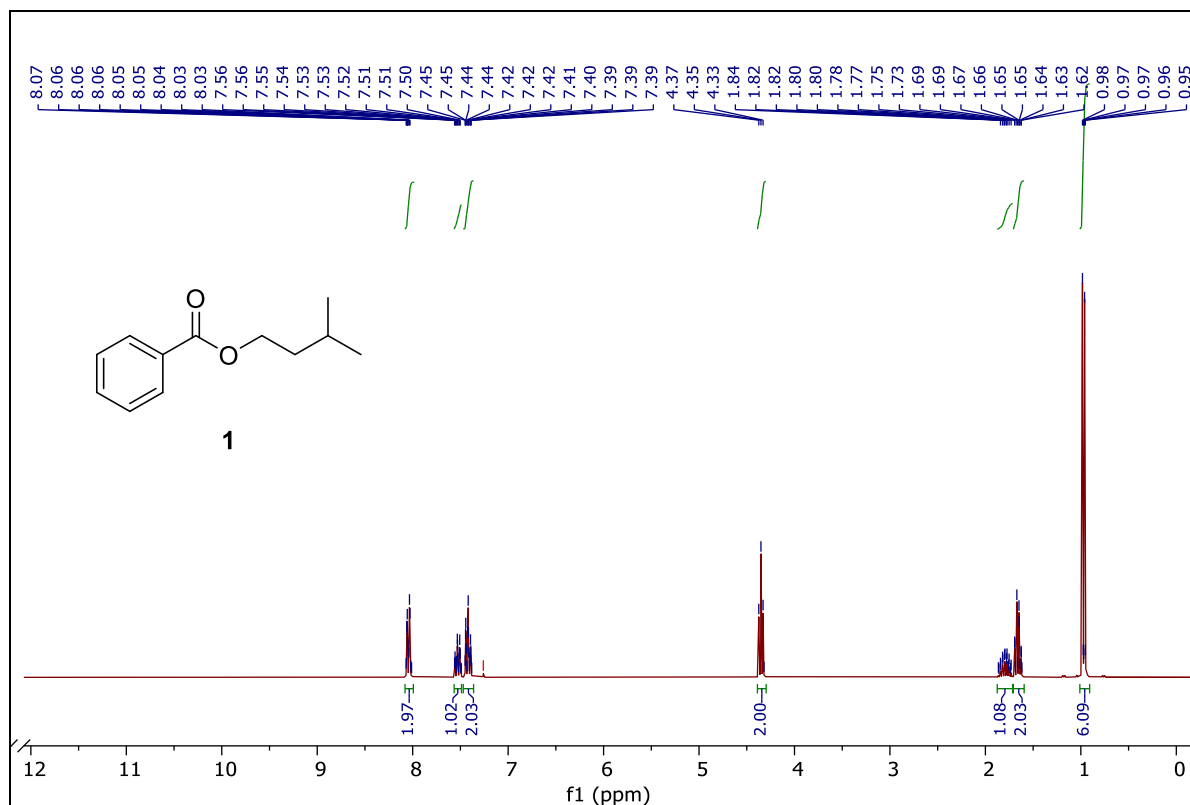
Spectrum S4.7. Compound **1**, ¹H- and ¹³C-NMR (Chloroform-*d*).

4.10 References

[1]   S. Mukherjee, B. Maji, A. Tlahuext-Aca, F. Glorius, *J. Am. Chem. Soc.* **2016**, *50*, 16200-16203.

[2]   W. Gong, K. Zheng, P. Ji, *RSC Adv.* **2017**, *55*, 34776-34782.

[3]   M.N. Khan, A.A. Khan, *J. Chem. Soc., Perkin trans.2* **1979**, *6*, 796-798.

[4]   N. Chakraborty, A.K. Mitra, *Org. Biomol. Chem.* **2023**, *34*, 6830-6880.

[5]   G.S. Yedase, S. Kumar, J. Stahl, B. König, V.R. Yatham, *Beilstein J. Org. Chem.* **2021**, *17*, 1727-1732.

[6]   A. Hu, Y. Chen, J.-J. Guo, N. Yu, Q. An, Z. Zuo, *J. Am. Chem. Soc.* **2018**, *42*, 13580-13585.

[7]   V. Nair, A. Deepthi, *Chem. Rev.* **2007**, *5*, 1862-1891.

[8]   Y. Chen, X. Wang, X. He, Q. An, Z. Zuo, *J. Am. Chem. Soc.* **2021**, *13*, 4896-4902.

[9]   R.E. Buckles, A.I. Popov, W.F. Zelezny, R.J. Smith, *J. Am. Chem. Soc.* **1951**, *10*, 4525-4528.

5 C-H Functionalisation by Iron Ligand-to-Metal Charge Transfer in Water
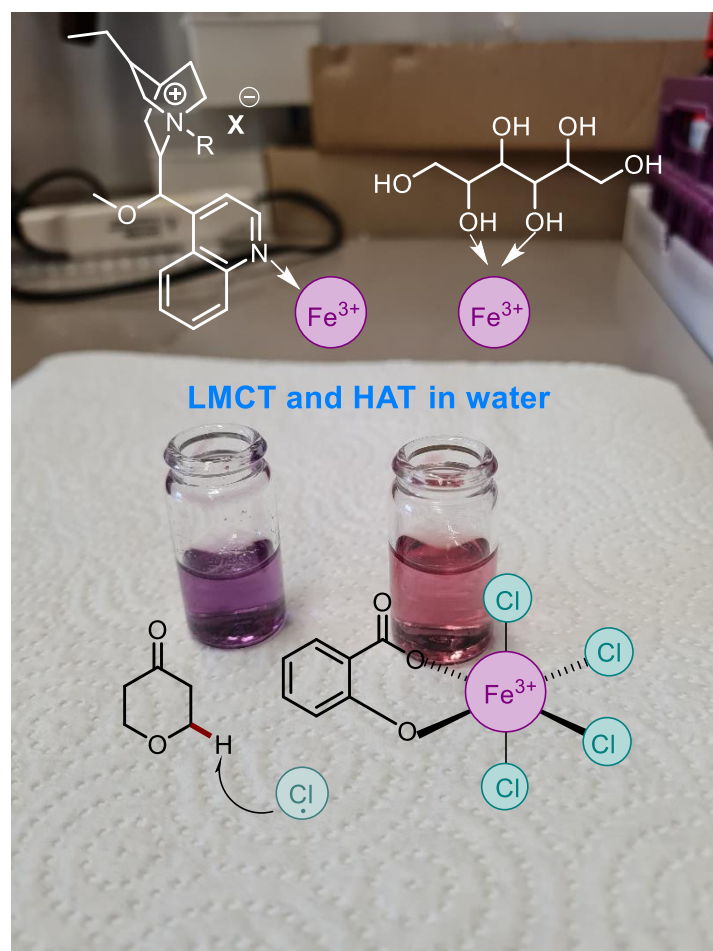
Jessica Stahl performed the synthetic work for this chapter and wrote the manuscript, Burkhard König supervised this project. Elina Taskinen synthesised alkaloid species **19**, **20** and **21** that were used without further deviation or purification.

Chapter 5

Abstract

Functionalisation of partially water-soluble C-H precursors through $Fe(III)Cl_3$ Ligand-to-Metal charge transfer catalysis in aqueous solution is achieved under near UV light irradiation. The light-driven bond-homolysis of the Fe-Cl bond within the iron complex results in the generation of highly reactive chlorine radicals, facilitating hydrogen atom abstraction from a furane-derived starting material. Assistance from sugars or cinchonidin-derivatives promotes effective interaction between the metal salt and organic substrates, crucial for successful reaction execution in the aqueous milieu. Lowering the reaction temperature to 4 °C, can modulate the reaction kinetics, resulting in an acceleration of the induction period of the photoreaction.

5.1 Introduction

Until recently, water as a solvent was often considered unsuitable for organic synthesis due to the sensitivity of substrates to moisture and oxygen.[1] However, recent literature highlights that conducting synthetic and catalytic transformations *in* and *on* water offers numerous advantages compared to traditional organic solvents.[1-9] The high bond dissociation energies of the O-H bonds in water preclude the alternative abstraction of hydrogen atoms from H_2O to produce reactive hydroxy radicals.[10] Consequently, this characteristic enables selective transformations in aqueous media without side reactions arising from radical interactions with the solvent.

In an aqueous environment, iron(III) salts, like $FeCl_3$ and $Fe(ClO_4)_3$ undergo hydrolysis, with the number of water molecules surrounding the cationic metal varying depending on the solution's pH.[11] $Fe(H_2O)_6^{3+}$ exhibits a pale colour, necessitating excitation of the complex's LMCT transition by highly energetic light.[12, 13] Substituting the aqua ligands with excess additional ligands can prevent the hydrolysis event of $FeCl_3$. The additional ligands coordinate with Fe(III) to stabilise the transition metal while simultaneously shifting the complex' absorption towards longer wavelengths. [14-16]

Only a limited number of reports are known where a LMCT photo transformation has been exclusively conducted in water. In 2023, Can Jin's research group accomplished the decarboxylative halogenation of aliphatic carboxylic acids *via* cerium LMCT in an aqueous medium.[17] In the presence of molecular oxygen from air, Ce(III) is oxidised to the +4 species, which forms complexes with the carboxylic acid starting material, and the cleavage of the O-Ce bond is achieved upon excitation with 100 W blue LEDs (Scheme 5.1, **a**). The resulting electron rich radicals are trapped with electrophilic bromine or chlorine radicals.[17] In a similar project, Li *et al.* conducted the ligand-accelerated decarboxylative alkylation of heteroarenes using iron LMCT at 456 nm.[15] The rate constant of irreversible decarboxylation and formation of nucleophilic carbon-centred radicals could be increased by employing pyridine-2-carboxylic acid (picolinic acid) as a ligand for Fe(III) and $NaBrO_3$ as oxidant. The photoreactions were carried out in a solvent mixture of 9:1 v/v water and DMSO, and the alkylated products were obtained in moderate to good yields. However, the research group mentioned in the supporting information that the reaction fails in the absence of the additional pyridine carboxylic acid ligand (Scheme 5.1, **b**).

The objective of the here reported project is to explore the feasibility of an effective ligand-to-metal charge transfer in pure water as the reaction solvent. We use Fe(III)Cl$_3$·6H$_2$O in aqueous solution. Upon exposure to near UV light, homolysis of the Fe-Cl bond is induced in the complex. The resulting electrophilic chlorine radical abstracts hydrogen atoms from aliphatic C-H reactants, generating nucleophilic carbon-centred radicals that subsequently react with various electron-poor alkenes (Scheme 5.1, **c**). To enhance yields, simple sugar alcohols and cinchonidin derivatives were employed to increase the water solubility of the organic starting materials. Additionally, lowering the reaction temperature resulted in a positive impact on the reaction kinetics, leading to accelerated rates.
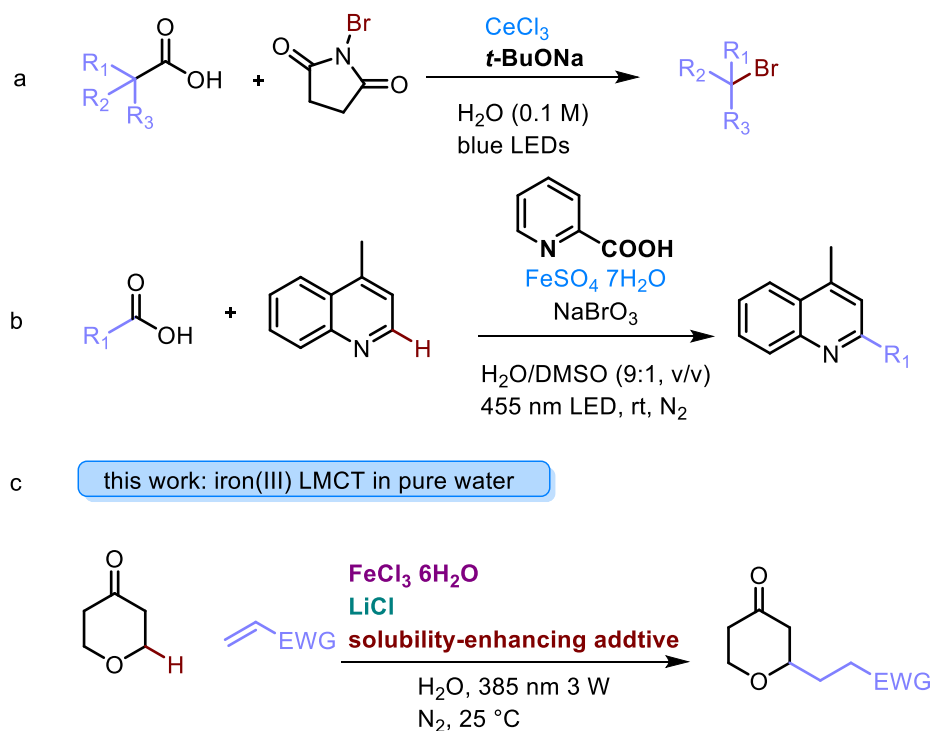
Scheme 5.1. Literature reports about LMCT in water (**a** and **b**) and our approach (**c**).

5.2 Results and Discussion

Inspired by the spectroscopic work on iron(III)-salicylic acid complexes in water, we started our investigations with the photoreaction between tetrahydro-4H-pyran-4-on (**1**) and trifluoromethyl acrylonitrile (**2**) with a catalytic system of Fe(ClO$_4$)$_3$ H$_2$O (20 mol%), LiCl (20 mol%) and salicylic acid (20 mol%) at 385 nm in de-ionised water under N$_2$ atmosphere. After irradiating the reaction solution for 24 h the purple colour of the mixture faded and 38% of two diastereomers could be observed in ^{19}F-NMR spectroscopy.[18] Starting material **1** was chosen due to the reactive α-oxygen C-H bond and compound **2** allowed for the ^{19}F-spectroscopic monitoring of product formation. The results from a reaction condition screening are summarized in Table 5.1.
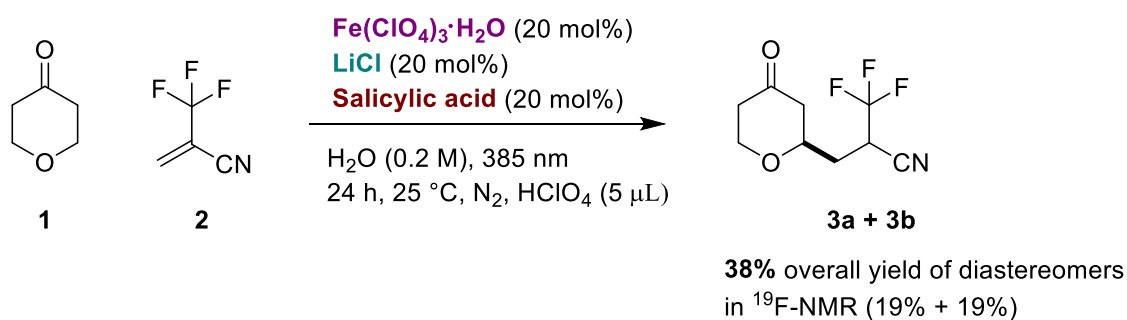
Scheme 5.2. Benchmark reaction for iron LMCT in water.

Table 5.1. Control reactions and optimisation attempts.

Entry	Fe-source	Cl-source	λ [nm]	Additives	[a] Yield of 3a and 3b [%] from ^{19}F- NMR
a	Fe(ClO$_4$)$_3$ · H$_2$O (20 mol%)	LiCl (20 mol%)	385	salicylic acid (20 mol%)	38
b	-	LiCl (20 mol%)	385	salicylic acid (20 mol%)	0
c	Fe(ClO$_4$)$_3$ · H$_2$O (20 mol%)	-	385	salicylic acid (20 mol%)	0
d	-	LiCl (20 mol%)	385	-	0
e	Fe(ClO$_4$)$_3$ · H$_2$O (20 mol%)	LiCl (20 mol%)	-	N$_2$ atmosphere, salicylic acid (20 mol%)	0
f	Fe(ClO$_4$)$_3$ · H$_2$O (20 mol%)	LiCl (20 mol%)	385	O$_2$ from air, salicylic acid (20 mol%)	traces of oxidation products
g	-	LiCl (20 mol%)	-	N$_2$, salicylic acid (20 mol%)	0
h	FeCl$_3$ · 6H$_2$O (20 mol%)	LiCl (20 mol%)	385	N$_2$, no salicylic acid	95
i	FeCl$_3$ · 6H$_2$O (20 mol%)	LiCl (20 mol%)	385	N$_2$, salicylic acid (20 mol%)	51
j	FeCl$_3$ · 6H$_2$O (20 mol%)	LiCl (20 mol%)	385	N$_2$, 5-sulfosalicyclic acid dihydrate (20 mol%)	80
k	FeCl$_3$ · 6H$_2$O (20 mol%)	LiCl (20 mol%)	400	N$_2$, salicylic acid (20 mol%)	20
l	FeCl$_3$ · 6H$_2$O (20 mol%)	LiCl (20 mol%)	452	N$_2$, salicylic acid (20 mol%)	0
m	FeCl$_3$ · 6H$_2$O (20 mol%)	LiCl (20 mol%)	528	N$_2$, salicylic acid (20 mol%)	0
n	FeCl$_3$ · 6H$_2$O (20 mol%)	-	385	N$_2,$ no salicylic acid	46

extension of Table
5.1

Entry	Fe-source	Cl-source	λ [nm]	Additives	[a] Yield of 3a and 3b [%] from ^{19}F-NMR
o	FeCl$_3$·6H$_2$O (20 mol%)	LiCl (20 mol%)	385	O$_2$ from air, no salicylic acid	16
p	FeCl$_3$·6H$_2$O (20 mol%)	LiCl (20 mol%)	-	O$_2$ from air, no salicylic acid	0
q	FeCl$_3$·6H$_2$O (20 mol%)	LiCl (20 mol%)	385	N$_2$, neat conditions, no salicylic acid	66
r	FeCl$_3$·6H$_2$O (20 mol%)	-	365	N$_2$, no salicylic acid	55
s	-	LiCl (20 mol%)	365	N$_2$, no salicylic acid	0

[a] Yields of the photoreaction were determined using trifluoro toluene as ^{19}F-NMR standard in 0.1 mmol. CD$_3$CN was used as NMR solvent.

The iron-catalysed photoreaction gave 38% of the desired C-H functionalised products **3a** and **3b** under the conditions mentioned in Table 5.1 (entry **a**). FeCl$_3$ 6H$_2$O proved to be the most efficient metal salt for the photo-transformation (entry **h**). Interestingly, in the absence of additional chloride anions, there was a significant decrease in product formation, particularly evident for FeCl$_3$·6H$_2$O as the catalyst (entry **n**) and complete absence of product with Fe(ClO$_4$)$_3$·H$_2$O as the metal salt (entry **c**). Moreover, the yield of products **3a** and **3b**, as observed in ^{19}F-NMR, decreased in presence of additional ligands such as salicylic acid or 5-sulfosalicylic acid dihydrate (entries **e-g**, **i-m**). The reaction does not proceed in the absence of light, with Fe(III) present (entries **e** and **p**), or without the presence of an iron salt at 365 nm or 385 nm (entries **b, d, g,** and **s**). The presence of oxygen from air should be avoided as it leads to the formation of side products upon irradiation of the reaction (entries **o** and **p**). Despite the bathochromic shift observed in the absorption of the metal-salicylic acid complex (Supporting Information, **Spectra S5.1** and **S5.2**) the reaction worked most efficiently at 385 nm. At 400 nm, the yield with FeCl$_3$·6H$_2$O as the catalyst (entries **k**) significantly decreased, and beyond 450 nm, no photo-transformation was observed (entries **l** and **m**). Further reaction optimisation attempts are listed in **Table T5.1** in the Supporting Information.

Additional information about the interaction of salicylic acid derivatives and Fe(III)Cl$_3$·6H$_2$O is described in the Supporting Information (chapter **5.6.5**).
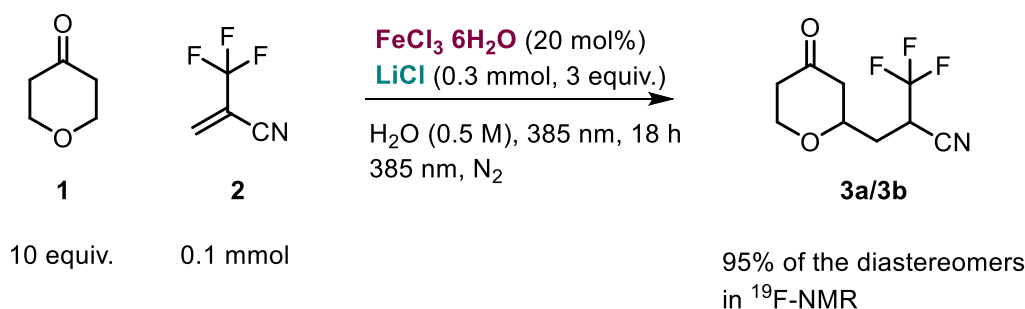
Scheme 5.3. Summary of the optimised reaction conditions.
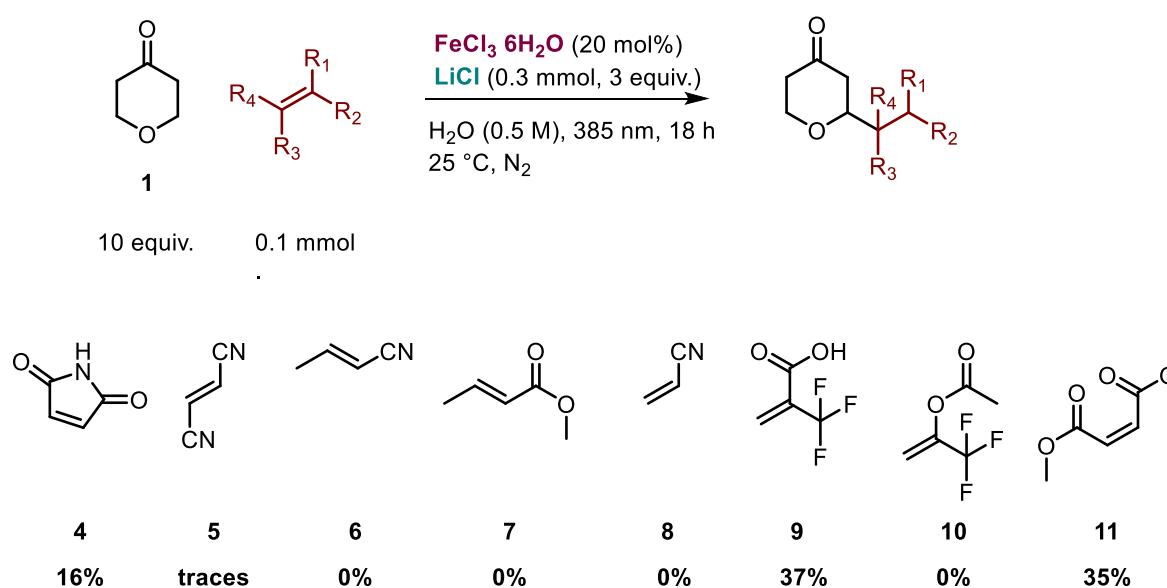
Scheme 5.4. Screening for radical trapping reagents.

With the optimised conditions in hands, we started to investigate the product scope of the iron LMCT induced C-H abstraction in water. Trapping reagents **4**, **9** and **11** gave moderate yields of the respective C-H functionalised product whereas acrylonitrile derivatives **5** and **6** and **8** as well as arylates **7** and **10** led to polymerisation of the respective double bond, indicated by the formation of a white viscous precipitate (Scheme 5.4). From ^{1}H-NMR spectroscopic evaluation, tarting material **1** was not converted.

To potentially improve the scope of the reaction, solubilising agents were introduced. Inspired by the work of Tian *et al.* sugar alcohols were considered as helpful tool to achieve an effective interplay between the catalyst and the organic coupling partners in the photoreaction.[19] Additionally, cinchonidin-derivatives were screened as literature-known inter-face active species that realise asymmetric transformations applied in industry.[20] Sugar alcohols were used as reported by Tian *et al.*[19] Elina Taskinen synthesised the alkaloid catalysts highlighted in Scheme 5.6. Compound **11** was chosen as the radical trapping reagent (Scheme 5.5).[21]

Interestingly, amino alcohols such as meglumine (**13**), N-ethyl D-glucamine (**14**) or miglitol (**15**) did not result in any product formation in the optimised reaction with dimethyl maleate (**11**). This fact may be given by a competitive coordination to Fe^{3+} or the facile photo-oxidation of amines to their radical cation as competing reaction.[22] D-sorbit (**16**), dulcitol (**17**) and D-fructose (**18**) allowed for the formation of products **12a** and **12b** in good yields (Figure 5.1). Among the test sugar alcohols dulcitol (**17**) showed the lowest solubility in water.
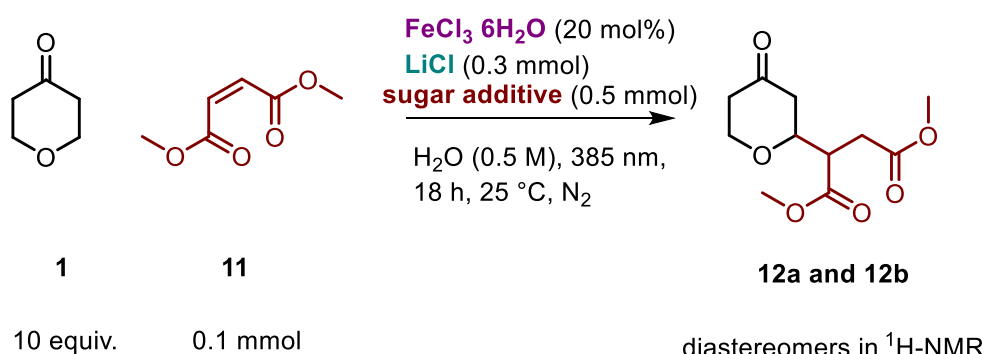
Scheme 5.5. Iron LMCT in water with sugar alcohol additives.

Meglumin

13

0% of **12a/b**

N-ethyl-D-glucamin

14

0%

Miglitol

15

0%

D-Sorbit

16

44%

Dulcitol

17

34%

D-Fructose

18

50%
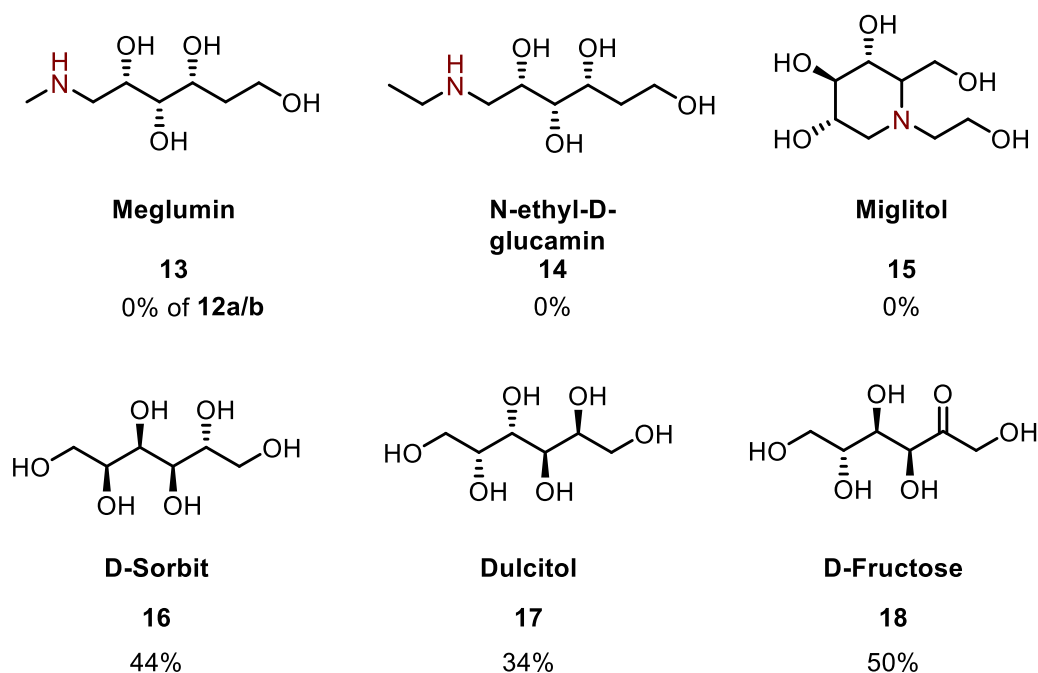
Figure 5.1. Tested sugar alcohols and respective yields of product **12a** and **12b**.

Table 5.2. Optimisation of the iron LMCT in water using sugar additives.

Entry	Sugar alcohol derivative (0.25 mmol)	Deviation from standard condition	[a] Yield of 12a/b [%] from ^{1}H-NMR
a	**13**	0.5 mL instead of 0.2 mL	0
b	**14**	0.5 mL instead of 0.2 mL	0
c	**15**	0.5 mL instead of 0.2 mL	0
d	**16**	0.5 mL instead of 0.2 mL	12
e	**17**	0.5 mL instead of 0.2 mL	10
f	**18**	0.5 mL instead of 0.2 mL	17
g	**17**	50 °C instead of 25 °C	36
h	**18**	50 °C instead of 25 °C	16
i	**17**	30 °C instead of 25 °C	29

extension of Table 5.2

Entry	Sugar alcohol derivative (0.25 mmol)	Deviation from standard condition	[a] Yield of 12a/b [%] from ¹H-NMR
j	**18**	30 °C instead of 25 °C	42
k	**16**	5 equiv. LiCl	12
l	**17**	5 equiv. LiCl	38
m	**18**	5 equiv. LiCl	48
n	**16**	5 equiv. LiCl, 400 nm	46
o	**17**	5 equiv. LiCl, 400 nm	41
p	**18**	5 equiv. LiCl, 400 nm	30

[a] Yields were determined by ¹H-NMR analysis using methyl iso-butyrate (11.2 µL) as internal standard.

Several test reactions were performed. Increasing the volume of water, did not lead to product formation in case of amino sugars **13**, **14** and **15** and decreased the formation of product **12a/b** in case of sugar alcohol **16**, **17** and **18** (Table 5.2 entries **a-f**). For 50 °C the yield became lower for D-fructose and improved for dulcitol, that showed a poor water-solubility at room temperature (entries **g** and **h**). At 30 °C D-fructose as additive leads to 42% of **12a/b** (entries **i** and **j**). Once 5 equivalents of LiCl were added to the reaction mixture D-fructose worked most efficiently (entries **k-l**) whereat the change to 400 nm did not lead to an improved catalyst performance (entries **n-p**). In general, the yield of products **12a** and **b** could be slightly increased for entries **j**, **m**, **n**, and **o** compared to the reaction without additive (Scheme 5.5).

A slight change in colour towards deep yellow was noted upon the addition of D-fructose or LiCl to $FeCl_3 \cdot 6H_2O$. However, changes in the absorption spectra of $FeCl_3 \cdot 6H_2O$ upon the additive addition are not pronounced (Spectrum 5.1).
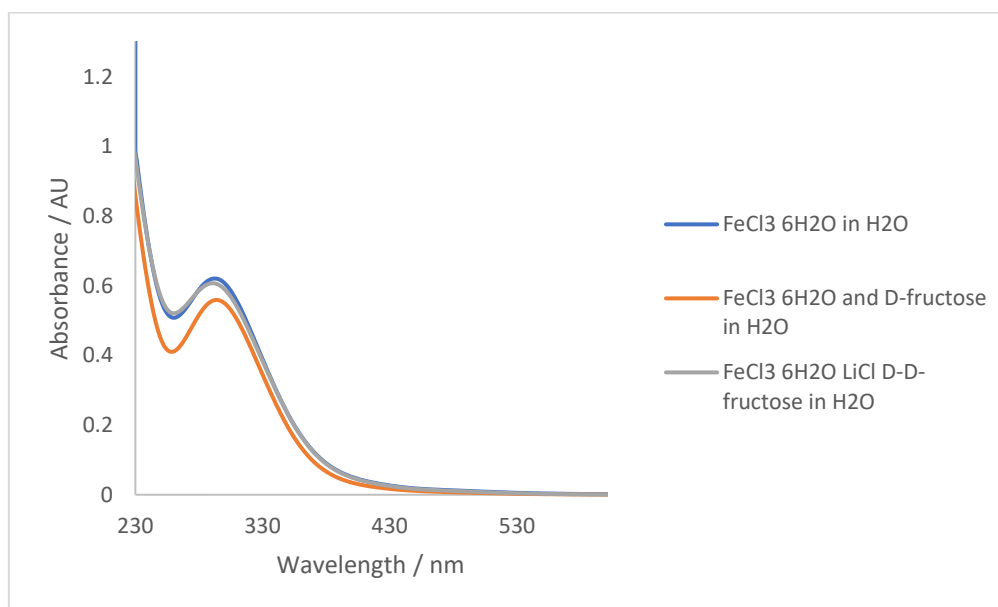
Spectrum 5.1. Absorption spectra of FeCl$_3$·6H$_2$O (blue curve) in 3 mL of water (0.33 mM). Only small changes upon the addition of D-fructose (4.17 mM) and both, D-fructose and LiCl (grey curve; 0.33 mM for FeCl$_3$·6H$_2$O, 4.17 mM for D-fructose and 8.33 mM for LiCl).

Subsequently, cinchonidin catalysts **19**, **20** and **21**, synthesised by Elina Taskinen, were evaluated as solubilising agent in the iron-catalysed photo-transformation (Scheme 5.6). Due to their poor solubility in water, only 5 mol% of each catalyst was employed.
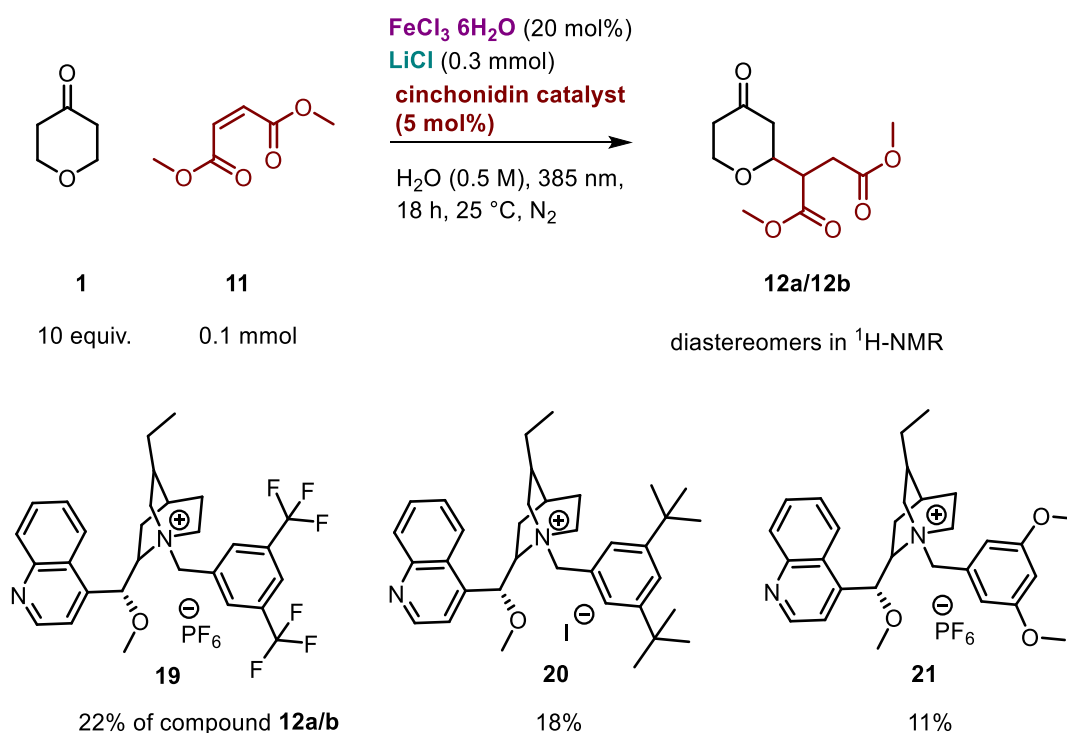
Scheme 5.6. Alkaloid-derivatives used as phase transfer catalysts.

Addition of catalyst **19** resulted in a 22% yield of compound **12a/b** under standard conditions, compound **20** gave 18% of product **12a/b** as determined by ^{1}H-NMR. The solubility of alkaloid derivative **21** was the highest in water in the series of the salts, though being the less efficient catalyst. Table 5.3 shows further optimisation attempts for yield improvement.

Table 5.3. Optimisation of the reaction conditions using alkaloids as solubilising catalysts.

Entry	Alkaloid catalyst	Deviation from standard conditions	[a] Yield of 12a/b [%] from ^{1}H-NMR
a	**19**	0.5 mL instead of 0.2 mL	14
b	**20**	0.5 mL instead of 0.2 mL	10
c	**21**	0.5 mL instead of 0.2 mL	12
d	**19**	50 °C instead of 25 °C	18
e	**20**	50 °C instead of 25 °C	20
f	**21**	50 °C instead of 25 °C	5
g	**19**	30 °C instead of 25 °C	16
h	**20**	30 °C instead of 25 °C	9
i	**21**	30 °C instead of 25 °C	18
j	**19**	5 equiv. LiCl	24
k	**20**	5 equiv. LiCl	26
l	**21**	5 equiv. LiCl	27
m	**19**	5 equiv. LiCl, 400 nm	20
n	**20**	5 equiv. LiCl, 400 nm	20
o	**21**	5 equiv. LiCl, 400 nm	19

[a] Yields were determined by ^{1}H-NMR using methyl iso-butyrate (11.2 μL) as internal standard.

Yields dropped upon increasing the water content to 0.5 mL (Table 5.3, entries **a-c**). Raising the temperature from 25 °C to 50 °C had a positive impact on the performance of catalyst **20**, probably given by a higher solubility (entries **d-f**). This temperature dependency reflects for entries **g-I**, because once the reaction temperature was set to 30 °C the yield for catalyst **20** decreased again while staying relatively constant for alkaloid **19** and **21** in direct comparison to the room temperature runs (entries **a-c**). Overall, the effect of the reaction temperature on product formation was small. Increasing the amount of LiCl from 3 equivalents to 5 equivalents increased the product yield for all phase transfer catalysts (entries **j-l**). Switching to 400 nm with the same LiCl loading did not improve the reaction compared to the 25 °C entries (entries **m-o**). Summing up, catalyst **19** performed best in the photoreaction but the yields were lower than for the sugar alcohol screening highlighted in Table 5.2.

5.3 Mechanistic Investigations

According to literature, the viscosity of water exhibit temperature dependency, notably increasing for temperatures below 10 °C.[23] This effect can be further amplified in sugar-water mixtures with varying molar fractions.[24-27] To assess whether additives influence the efficiency of iron LMCT in water at different temperatures, the kinetics of the reaction's induction period were examined. Starting material conversion with and without D-fructose were monitored using ^{1}H-NMR spectroscopy over a 3 h-period at reaction temperatures of 4 °C and 25 °C, with samples drawn every 30 min, respectively (Scheme 5.7 and 5.8).[28] Additional experimental details can be found in the Supporting Information (chapter **5.6.3**).
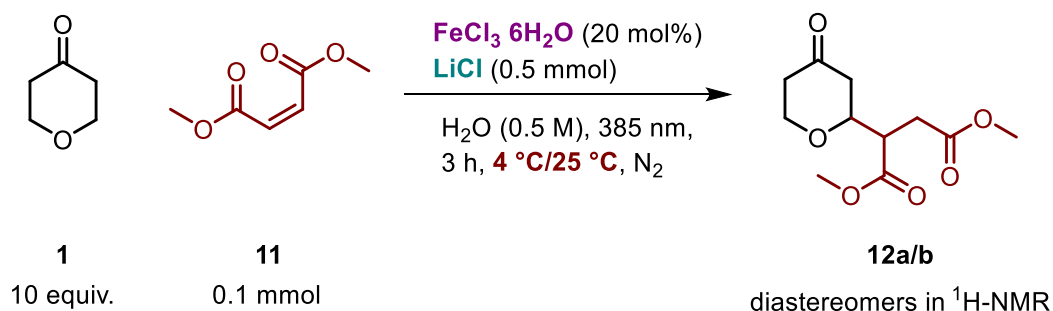
Scheme 5.7. Reaction monitoring of product formation for the iron LMCT in water at 4 °C and 25 °C.
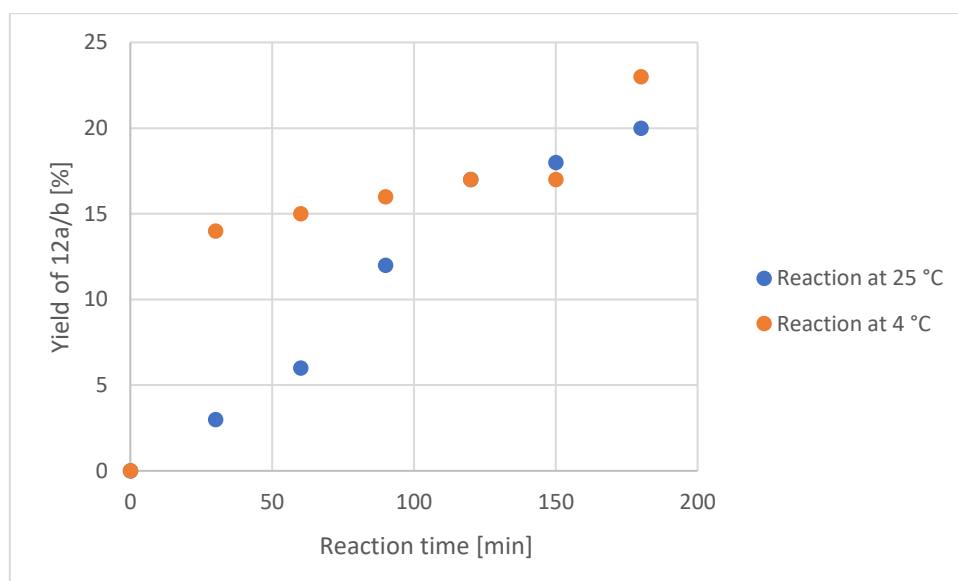
Diagram 5.1. Product formation at 4 °C (orange data points) and 25 °C (blue data points).

1   **11**   **12a/b**

10 equiv.   0.1 mmol   diastereomers in ^{1}H-NMR
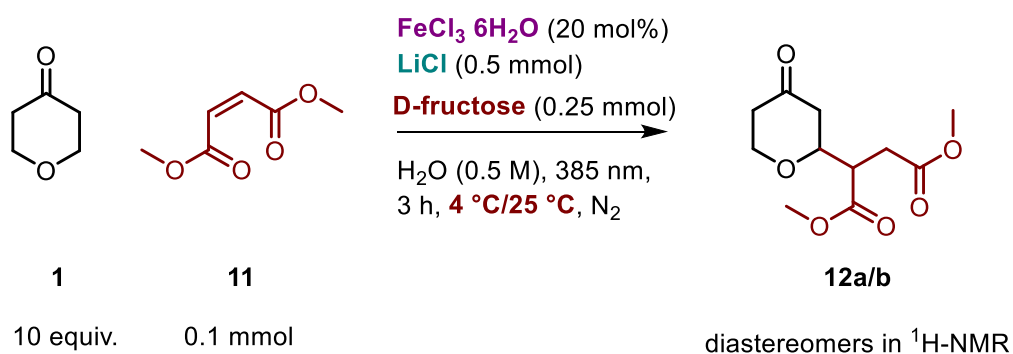
Scheme 5.8. Radical addition reaction of the iron LMCT in water with D-fructose at 4 °C and 25 °C.
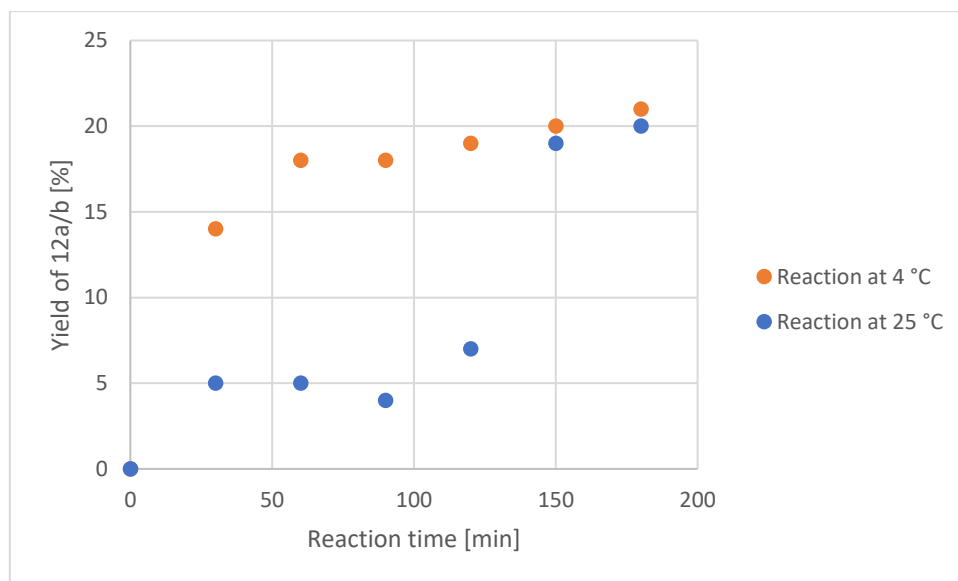
Diagram 5.2. Product formation with D-fructose at 4 °C (orange data points) and 25 °C (blue data points).

Interestingly, the initial product formation rate was faster for both cases with and without the sugar additive at 4 °C, respectively. We hypothesise that the increase in water's viscosity due to the lower temperature of the reaction medium, as well as the presence of D-fructose, may lead to a more effective reaction.[25] Comparable yields are achieved after 150 min without sugar additive (Diagram 5.1) and after 120 min in the presence of D-fructose (Diagram 5.2).

We propose the following mechanism for the photocatalytic transformation (Scheme 5.9). FeCl$_3$·6H$_2$O (**I**) and LiCl react to form [FeCl$_4$]$^-$ (**II**) whose Fe-Cl LMCT band is excited by 385 nm light. Chlorine radicals as well as [Fe(II)Cl$_3$]$^-$ (**III**) are generated and the former abstracts a hydrogen atom of substrate **1**. The carbon-centred radical **1'** adds to Michael acceptor **11** resulting in the formation of radical intermediate **11'**. Reduction to derivative **11''** takes places, leading to the re-oxidation of Fe(II) to Fe(III) to close the overall catalytic cycle. After protonation of the anionic product derivative, final compound **12** is formed.[29]
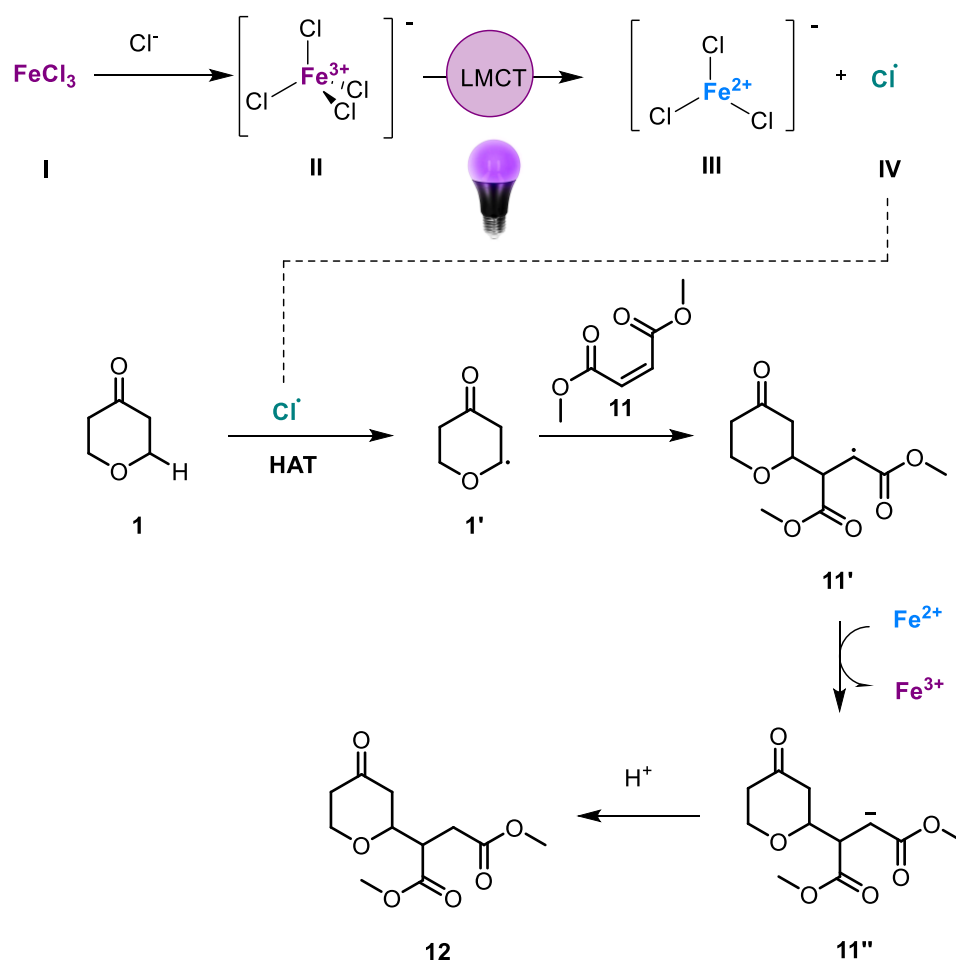
Scheme 5.9. Proposed reaction mechanism.

5.4 Conclusion

We have developed a method enabling the C-H functionalisation of cyclic ethers in water using iron LMCT. Chlorine radicals act as hydrogen atom abstractors, facilitating the formation of highly nucleophilic carbon-centred radicals on the pyran-derived starting material. The addition of solubilising agents, such as sugar alcohols or cinchonidinium salts slightly improved product yields. Lower reaction temperatures resulted in a faster initial product formation.

5.5 References

[1]   M. Cortes-Clerget, J. Yu, J.R.A. Kincaid, P. Walde, F. Gallou, B.H. Lipshutz, *Chem. Sci.* **2021**, *12*, 4237-4266.

[2]   R. Schulte, M. Löcker, H. Ihmels, M. Heide, C. Engelhard, *Chem. Eur. J.* **2023**, *9*, e202203203.

[3]   B. Pfund, D.M. Steffen, M.R. Schreier, M.-S. Bertrams, C. Ye, K. Börjesson, O.S. Wenger, C. Kerzig, *J. Am. Chem. Soc.* **2020**, *23*, 10468-10476.

[4]   F. Gao, H. Chang, J. Li, R. Wang, Y. Gu, *Curr. Opin. Green. Sustain. Chem.* **2023**, *40* 100774.

[5]   T. Seki, K.-Y. Chiang, C.-C. Yu, X. Yu, M. Okuno, J. Hunger, Y. Nagata, M. Bonn, *J. Phys. Chem. Lett.* **2020**, *19*, 8459-8469.

[6]   A. Rakshit, T. Yamaguchi, T. Asada, P. Bandyopadhyay, *RSC Adv.* **2017**, *30*, 18401-18417.

[7]   R. Kumar, T. Keyes, *Theor. Chem. Acc.* **2012**, *3*, 1197.

[8]   C.-W. Cho, T.P.T. Pham, S. Kim, Y.-R. Kim, Y.-C. Jeon, Y.-S. Yun, *J. Appl. Phycol.* **2009**, *6*, 683-689.

[9]   Q. Sun, *Molecules* **2022**, *20*, 7009.

[10]   O.V. Boyarkin, M.A. Koshelev, O. Aseev, P. Maksyutenko, T.R. Rizzo, N.F. Zobov, L. Lodi, J. Tennyson, O.L. Polyansky, *Chem. Phys. Lett.* **2013**, *568-569*, 14-20.

[11]   I. Persson, *J. Solution Chem.* **2018**, *5*, 797-805.

[12]   F. David, P.G. David, *J. Phys. Chem.* **1976**, *6*, 579-583.

[13]   U. Lueder, B.B. Jørgensen, A. Kappler, C. Schmidt, *Envir. Sci. Process Impact* **2020**, *1*, 12-24.

[14]   J. Šima, J. Makáňová, *Coord. Chem. Rev.* **1997**, *160*, 161-189.

[15]   Z. Li, X. Wang, S. Xia, J. Jin, *Org. Lett.* **2019**, *11*, 4259-4265.

[16]   E.L. Rue, K.W. Bruland, *Mar. Chem.* **1995**, *1*, 117-138.

[17]   Y. Xu, P. Huang, Y. Jiang, C. Lv, P. Li, J. Wang, B. Sun, C. Jin, *Green Chem.* **2023**, *21*, 8741-8747.

[18]   I.P. Pozdnyakov, V.F. Plyusnin, V.P. Grivin, E. Oliveros, *J. Photochem. Photobiol. A* **2015**, *307-308*, 9-15.

[19]   Y.-M. Tian, E. Hofmann, W. Silva, X. Pu, D. Touraud, R.M. Gschwind, W. Kunz, B. König, *Angew. Chem. Int. Ed.* **2023**, *17*, e202218775.

[20]   S.-s. Jew, H.-g. Park, *Chem. Commun.* **2009**, *46*, 7090-7103.

[21]   S. Rohe, A.O. Morris, T. McCallum, L. Barriault, *Angew. Chem. Int. Ed.* **2018**, *48*, 15664-15669.

[22]   J.W. Beatty, C.R.J. Stephenson, *Acc. Chem. Res.* **2015**, *5*, 1474-1484.

[23]   J. Kestin, M. Sokolov, W.A. Wakeham, *J. Phys. Chem. Ref. Data* **1978**, *3*, 941-948.

[24]   E.I. Benítez, D.B. Genovese, J.E. Lozano, *Food Hydrocoll.* **2009**, *2*, 519-525.

[25]   A.V. Minakov, M.I. Pryazhnikov, E.I. Mikhienkova, Y.O. Voronenkova, *Petroleum* **2023**, *4*, 534-544.

[26]   V.R.N. Telis, J. Telis-Romero, H.B. Mazzotti, A.L. Gabas, *Int. J. Food Prop.* **2007**, *1*, 185-195.

[27]   K.R. Harris, L.A. Woolf, *J. Chem. Eng. Data* **2004**, *4*, 1064-1069.

[28]   S.D. Naik, L.K. Doraiswamy, *AIChE Journal* **1998**, *3*, 612-646.

[29]   Z. Zhang, X. Li, D. Zhou, S. Ding, M. Wang, R. Zeng, *J. Am. Chem. Soc.* **2023**, *13*, 7612-7620.

[30]   A. Hu, Y. Chen, J.-J. Guo, N. Yu, Q. An, Z. Zuo, *J. Am. Chem. Soc.* **2018**, *42*, 13580-13585.

5.6   General Considerations

Starting materials and reagents were purchased from commercial suppliers (Sigma Aldrich, Alfa Aesar, Acros or Fluka) and were used without further purification. Solvents were used as p.a. grade. Reactions were monitored by analytic thin-layer chromatography (TLC) using Fluka silica gel plates with a fluorescent indicator. Visualisation of the developed TLC chromatogram was performed using 254 nm UV light source or potassium permanganate stain. Organic solutions were concentrated using Büchi rotary evaporator. Flash column chromatography was performed either on an automated column machine (Biotage® IsoleraTM Spektra) or manually for non-UV absorbing products. In both cases we used columns filled with silica gel (60-200 µm).

NMR spectroscopy

NMR spectra were recorded at room temperature using a Bruker Advance 300 (300 MHz for ^{1}H, 75 MHz for ^{13}C, 282 MHz for ^{19}F) or a Bruker Advance 400 (400 MHz for ^{1}H, 101 MHz for ^{13}C, 376 MHz for ^{19}F) NMR spectrometer. All chemical shifts are reported in δ-scale as parts per million [ppm], relative to the solvent residual peaks as the internal standard. Coupling constants J are given in Hertz [Hz]. Abbreviations used for signal multiplicity: ^{1}H-NMR: br = broad, s = singlet, d = doublet, t = triplet, q = quartet, dd = doublet of doublets, dt = doublet of triplets, and m = multiplet. NMR solvent and trifluoro toluene (0.05 or 0.1 mmol, respectively) were added to the crude reaction mixtures, the samples were filtered, and ^{1}H- and ^{19}F-NMR measurements were performed.

Mass spectrometry

High resolution mass spectrometry (HRMS) was performed at the Central Analytical Laboratory of the University of Regensburg. Mass spectra were measured on a Finnigan MAT 95, ThermoQuest Finnigan TSQ 7000, Finnigan MAT SSQ 710 A or Agilent Q-TOF 6540 UHD instrument and a Waters Acquity UPLC system equipped with Waters PDA, sample manager, sample organizer, column oven and Waters Xevo QTOF mass spectrometer.

UV/Vis

Absorption spectra were measured on an Agilent Cary 100 UV/Vis spectrometer in a $10 \text{ mm} \times 10$ mm quartz cuvette at $25.0 \, °C$ under air atmosphere. Solvents were used as Millipore® standard and without further purification.

5.6.1 Photochemical setup

The photoreactions were performed in 5 mL crimp cap vials that were equipped with a magnetic stirring rod. Before placing them into the cooling block with 15 available spots for sample positioning on top of the LED (**Figure F5.1.**), every crimp cap vial was closed. The cooling blocks were fabricated on demand by the mechanical workshop at the University of Regensburg. The crimp cap vials were placed approximately 2 cm above a 385 nm LED (1015 mW, Series number: Opulent LST1-01G01-UV02-00 380-390 nm, peak at 385 nm). The reaction temperature was controlled by a thermostat (25 °C) that is connected to every individual metal cooling block.
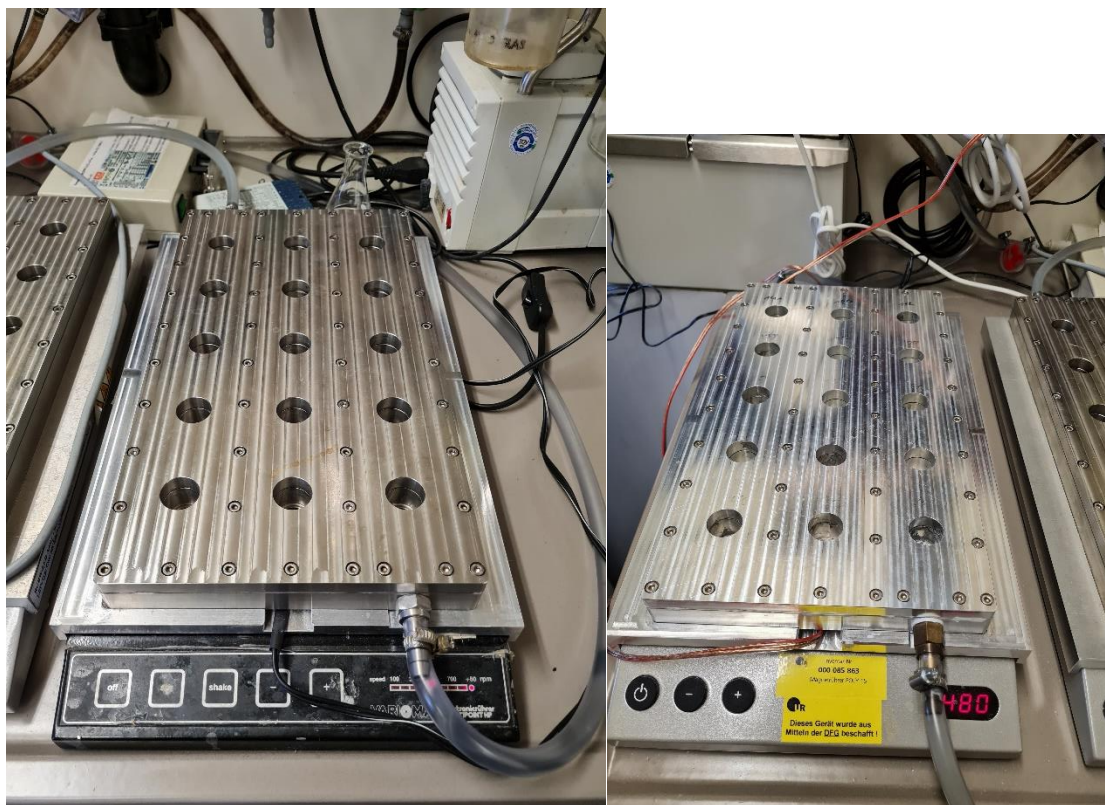
Figure F5.1 Photo-setup including metal cooling blocks and 385 nm LEDs.

For the kinetic studies, a six-spot 385 nm high power LED (640 mW, LED-Modul 6-fold, LST1-01G01-UV02-00 UV, Ser.-Nr.: 244-19) was used in combination with a thermostated (25 C) six-spot metal cooling block fabricated in the mechanical workshop at the University of Regensburg. For the reactions at 4 °C the 385 nm LED (640 mW, LED-Modul 6-fold, LST1-01G01-UV02-00 UV, Ser.-Nr.: 244-19) was placed in a six-spot metal cooling block (**Figure F5.2**, left picture) connected to a Julabo 200F cryostat (**Figure F5.2**, right picture) and the samples were allowed to stir overnight at 4 °C.

Figure F5.2. Cooling block and cryostat for the photoreactions at 4 °C.

5.6.2   General Procedure for the Iron-catalysed C-H Activation *via* LMCT in Water

To a 5 mL crimp cap vial, equipped with tetrahydro-4H-pyran-4-on (**1**) (1.0 mmol, 10 equiv., 52 µL), a radical trapping agent (0.1 mmol, 1.0 equiv., 10.5 µL), an iron(III) salt (0.05 equiv., 20 mol%), LiCl (0.3 – 0.5 mmol, 3.0 – 5.0 equiv.), an additional ligand (0,05 equiv., 20 mol%) and a magnetic stir bar were added 0.2 – 0.5 mL of de-ionised water and the glass vial was crimped. The reactions were degassed by three cycles of freeze-pump-thaw and irradiated by a 385 nm LED at 25 °C for 24 h. For trifluoromethyl acrylonitrile (**2**) as reagent, CD$_3$CN (0.7 mL) as well as trifluoro toluene (0.10 mmol, 1.00 equiv., 12.2 µL) as internal standard for

^{19}F-NMR yield determination were added to every sample and the reaction outcome was analysed using ^{19}F-NMR spectroscopy.

For maleic acid dimethyl ester (**11**) or other non-fluoride containing substrates as radical trapping reagents the procedure was following: After completion of the reaction, ethyl acetate (2 x 1 mL) was added to the individual entries and the reactions were extracted two times. The combined organic phases were dried over anhydrous Na_2SO_4 and the residual organic solvent was removed under reduced pressure. Methyl iso-butyrate (0.10 mmol, 1.00 equiv., 11.2 µL) was added for yield determination *via* ^{1}H-NMR spectroscopy. Herein, CDCl$_3$ (0.70 mL) was used as NMR solvent.

5.6.3 Reaction Monitoring in Presence and Absence of D-fructose

The reaction monitoring followed the general reaction setup procedure described in chapter **1.6.2**. Additionally, D-fructose (0.25 mmol, 2.50 equiv., 45.0 mg) was added to entries **c** and **d** (**Table T5.1.**). Kinetic investigations were performed setting four batches (**Table T5.1.**, **a** to **d**) of 6 reaction with 0.1 mmol scale each (**Table T5.1.**, entries **a-d**). As no entire reaction kinetics were performed previously, a reaction time of 3 h was chosen.

After pump freeze thaw, irradiation at 385 nm (640 mW) was started, and after every 30 minutes of irradiation one sample was removed from the photo setup. Opening the samples to air, workup by extraction with ethyl acetate (2 x 1 mL), drying over anhydrous salt, removal of the residual organic solvent and addition of methyl iso-butyrate (0.10 mmol, 1.00 equiv., 11.2 µL) was performed for the individual entries. For yield determination, the entries were submitted to ^{1}H-NMR spectroscopy in CDCl$_3$.

Table T5.1. Overview on kinetic studies w/o D-fructose as solubilising agent.

entry	reaction temperature	D-fructose additive	number of individual reactions
a	25 °C	no	6, one removed from light source after 30 min, respectively
b	4 °C	no	6, one removed from light source after 30 min, respectively
c	25 °C	yes	6, one removed from light source after 30 min, respectively
d	4 °C	yes	6, one removed from light source after 30 min, respectively.

5.6.4   Reaction Optimisation

Further optimisation reactions were performed and are highlighted in **Table T5.2**.
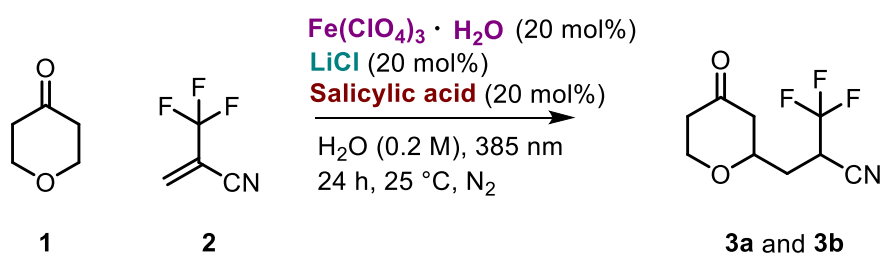
Scheme S5.1. Benchmark reaction for the C-H activation *via* iron LMCT in water.

Table T.5.2. Reaction optimisation attempts.

Entry	Deviation from standard condition	λ [nm]	[a] Yield of 3a and 3b determined by ^{19}F-NMR [%]
a	Fe(SO$_4$)$_3$ (20 mol%)	385	81
b		385	
	Fe(NO$_3$)$_3$ · 9H$_2$O (20 mol%)		78
c	Fe(acac)$_3$ (20 mol%)	385	26
d	FeF$_3$ · 3H$_2$O (20 mol%)	385	62
f	0.5 M based on substrate **2**	385	92
g	NaCl (20 mol%)	385	93
h	NaBr (20 mol%)	385	95
i	FeBr$_3$ (20 mol%) and NaCl (20 mol%)	385	86
j	FeBr$_3$ (20 mol%) and NaBr (20 mol%)	385	7
k	FeBr$_3$ (20 mol%)	385	80
l	Fe(ClO$_4$)$_3$ · H$_2$O (20 mol%), - LiCl	385	traces
m	Fe(ClO$_4$)$_3$ · H$_2$O (20 mol%), pyridine *N*-oxide (20 mol%)	385	19
n	Fe(ClO$_4$)$_3$ · H$_2$O (20 mol%), potassium benzoate (20 mol%)	385	4
o	Fe(ClO$_4$)$_3$ · H$_2$O (20 mol%), + Bis(4-methoxyphenyl) disulfide (20 mol%) as ligand	385	6
p	Maltol (20 mol%) as ligand	385	2
q	1:1 ratio of **1** and **2**, Fe(ClO$_4$)$_3$ · H$_2$O (20 mol%)	385	27
r	1:5 ratio of **1** and **2**, Fe(ClO$_4$)$_3$ · H$_2$O (20 mol%)	385	32
s	1:10 ratio of **1** and **2**, Fe(ClO$_4$)$_3$ · H$_2$O (20 mol%)	385	57
t	10:1 ratio of **1** and **2**, Fe(ClO$_4$)$_3$ · H$_2$O (20 mol%)	385	82

extension of
Table T5.2.

Entry	Deviation from standard condition	λ [nm]	[a] Yield of 3a and 3b [%] determined by ^{19}F-NMR
u	5:1 ratio of **1** and **2**, Fe(ClO$_4$)$_3$ · H$_2$O (20 mol%)	385	76
v	Fe(ClO$_4$)$_3$ · H$_2$O (20 mol%)	365	49
w	(FeClO$_4$)$_3$ · H$_2$O (20 mol%)	400	34
x	Fe(ClO$_4$)$_3$ · H$_2$O (20 mol%)	451	0
y	Fe(ClO$_4$)$_3$ · H$_2$O (20 mol%)	528	0
z	FeCl$_3$ · 6H$_2$O (20 mol%), LiCl (0.3 mmol, 3.0 equiv.)	385	94
za	FeCl$_3$ · 6H$_2$O (20 mol%), LiCl (0.5 mmol, 5.0 equiv.)	385	39

[a]Yields were determined by ^{19}F-NMR using trifluoro toluene (0.1 mmol) as internal standard.

Inspired by the work of Zuo and his group, who utilized diphenyl anthracene as a support-catalyst to facilitate the oxidation of Ce(III) back to Ce(IV), we aimed to incorporate a similar organic dye catalyst to close the catalytic cycle of Fe(II) to Fe(III).[30] **Table T5.3**. presents the results of the catalyst screening. In the case of 9-cyano anthracene (entry **i**), the yield remained constant, while for the other redox-active dyes, the formation of the diastereomers **3a** and **3b** decreased significantly. The organic dyes exhibited poor water solubility.
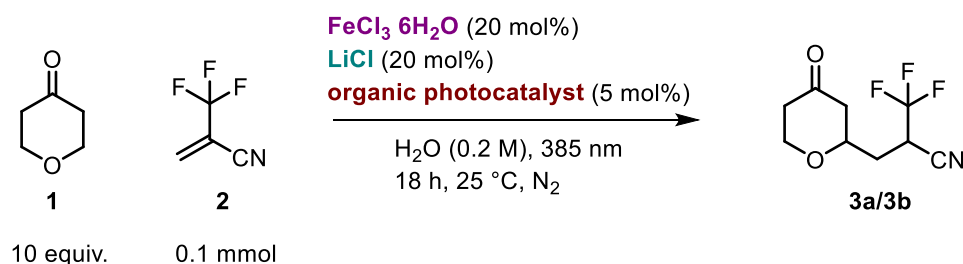
Scheme S5.2. Screening for different organic dyes for dual catalysis.

Table T5.3. Results from the screening of different organic photocatalysts.

Entry	Photocatalyst (5 mol%)	Excitation wavelength [nm]	[a] Yield of 3a and 3b from ^{19}F- NMR [%]
a	1,8-dihydroxy anthraquinone	455	0
b	9,10-dicyano anthracene	455	0
c	Riboflavin tetraacetate	455	0
d	9,10-dibromo anthracene	385	traces
e	9-phenyl phenothiazine	365	0
f	3DPAIFPN	400	0
g	4CzIPN	400	0
h	Riboflavin	455	0
i	9-cyano anthracene	385	94
j	9,10-dicyano anthracene	385	74
k	Alizarin Red	385	17
l	9-cyano anthracene, FeCl2 · 4H2O	385	41

[a] Yields of the photoreaction were determined using trifluoro toluene as ^{19}F-NMR standard in 0.1 mmol. CD$_3$CN was used as NMR solvent.

4CzIPN   **3DPAIFPN**   **Alizarin Red**
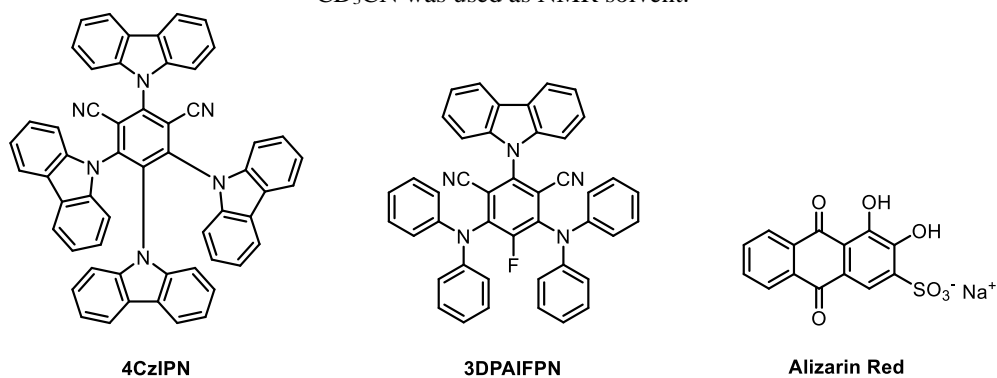
Figure F5.3. Chemical structures of 4CzIPN, 3DPAIFPN and Alizarin Red.

Among the organic dyes tested and presented in **Table T5.3**, only 9-cyano anthracene and 9,10-diphenyl anthracene showed promising results (entries **i** and **j**). For the other catalysts, solubility even in the organic part of the reaction mixture, was poor, and no product formation was observed. Alizarin Red, a sulfonated organic dye with slight water solubility, provided low yields of 17% (entry **k**). Upon addition of the dyes, both 9-cyano anthracene and 9,10-diphenyl anthracene resulted in a turbid yellow solution. An attempt to *in-situ* oxidise Fe(II) to Fe(III) using 9-cyano anthracene yielded 41% of the diastereomers **3a** and **3b** in ^{19}F-NMR (entry **l**). However, as the yields of the photoreaction slightly decreased and the efficiency of light penetration within the sample vial diminished, we decided to proceed without additional photocatalyst.

5.6.5 UV/Vis Spectroscopy

The interaction between FeCl$_3$·6H$_2$O and salicylic acid or 5-sulfosalicyclic acid dihydrate in water is illustrated in the UV/Vis spectra **S5.1** and **S5.2**. Upon the addition of these salicylic acid derivatives, new broad absorption bands form, causing a change in colour from yellow to purple for salicylic acid and red for 5-sulfosalicylic acid dihydrate. This experimental observation is displayed in the absorption spectra, with graphs extending into the 700- and 600 nm regions (**Spectra S5.1**. and **S5.2**.). Despite the noticeable shift in absorbance, complexation of the transition metal with salicylic acid ligands had an adverse effect on the photoreaction, leading to a decrease in the yield of products **3a** and **3b** (Table 5.1). We postulated that the desired LMCT of the Fe-Cl bond was hindered by competing excited state reactions of Fe(III) and salicylic acid.[18]
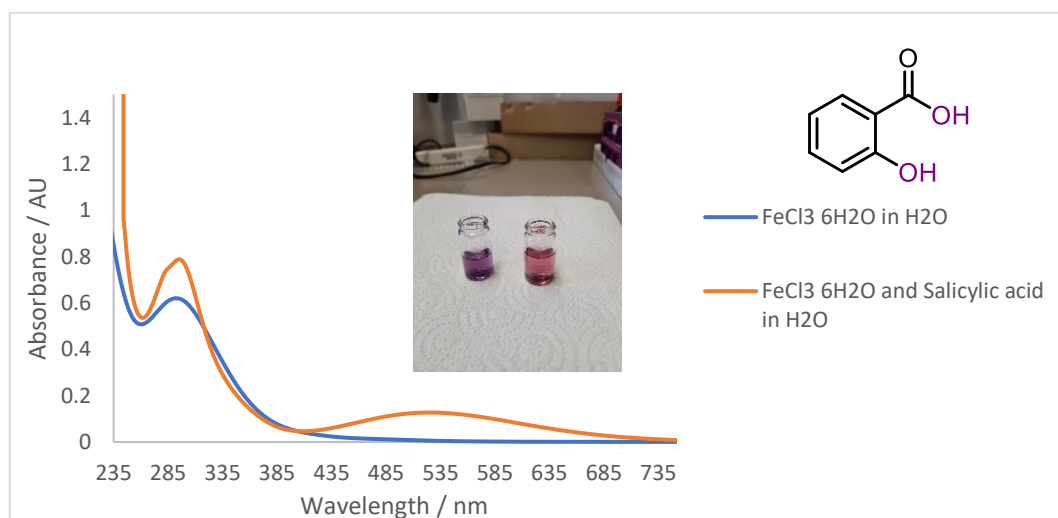
Spectrum S5.1. FeCl$_3$ · 6H$_2$O (0.33 mM, blue curve), FeCl$_3$ · 6H$_2$O (0.33 mM) and salicylic acid (0.083 mM), orange curve. Formation of a broad absorption band at 535 nm tailing into the 700 nm region.
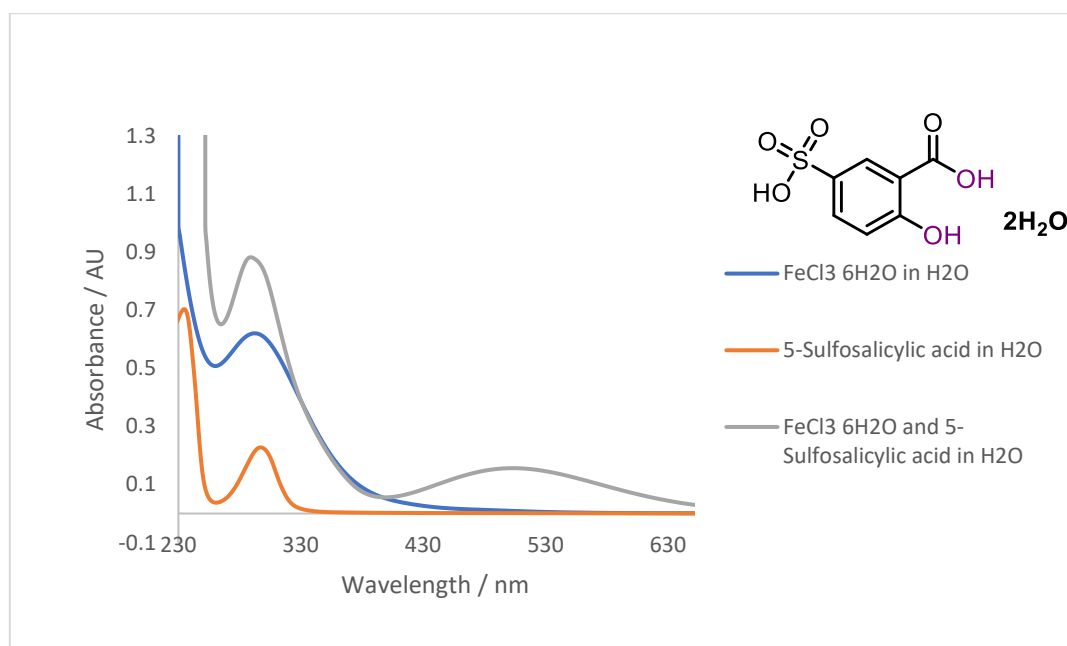
Spectrum S5.2. FeCl$_3$ · 6H$_2$O in water (0.33 mM, blue curve) and 5-sulfosalicyclic acid dihydrate in water (0.087 mM, orange curve). Formation of a broad absorption for the combination of both substrates at 525 nm (grey curve), tailing into the 600 nm region.

6 Summary

Summary

Selective functionalisation of one specific carbon atom by removing hydrogen atoms within complex molecule structures remains a challenging task in Organic Chemistry. Considering the absence of any heteroatom, the polarity difference within homogenous carbon chains does not show a prominent deviation and therefore, selective transformations become even more challenging.

Metal-complexes with tuneable coordination sphere can be used for selective C-H functionalisation. Upon the addition of sterically demanding ligands of different polarity, intermolecular interactions between substrates and the catalyst change. Iron- and cerium-salts investigated in this work exist in high oxidation states and when coordinated to ligands that can be oxidised, ligand-to-metal charge transfer interactions are observed. As a consequence of this light-driven bond-homolysis event, highly reactive radicals are generated that allow for hydrogen atom abstraction or radical addition to alkenes.

Chapter 1 summarises the principles of iron-LMCT in water. The behaviour of different iron-salts in aqueous medium is discussed and the main reactivity pathways (ligand-to-metal charge transfer within the Fe-OH bond or the Fenton process with Fe(II) are highlighted. Based on several examples the applicability and peculiarity of the light-driven bond homolysis and the reactivity of radicals generated under these conditions are underlined.

Chapter 2 summarises the results of the caesium carbonate catalysed O-alkylation of oximes. The possibility to control the *E/Z* isomerisation of several oximes upon addition of Ce(III) complexes as coordination compounds and diphenyl anthracene as sensitiser is explained. Besides the short lifetime of *Z*-isomers of the respective O-alkylated products attempts were made to isolated both, the *E* and *Z* isomers of the respective addition product. Caesium carbonate is considered as crucial base that, known for its "caesium effect" has a huge impact on the isomerisation behaviour and reactivity of oximes in organic solvents.

Chapter 3 presents the vicinal dichlorination of alkenes by iron ligand-to-metal charge transfer. Applying a simple catalytic system consisting of $FeCl_3 \cdot 6H_2O$ and LiCl in a solvent mixture of acetic acid and acetonitrile (9:1) terminal alkene aryl esters could be equipped with two chlorine radicals leading to the dichlorination of the double bond. The reaction proceeds upon visible light-induced bond homolysis of Fe-Cl in $[FeCl_4]^-$ and after the first addition of chlorine radicals to the double bond we hypothesised that upon Radical Ligand Transfer the catalytic cycle of the iron-salt is closed and a closed-shell dichloro-species is formed. The high viscosity of the reaction mixture is discussed and considered important for the formation of acetate-iron clusters that have an impact on the selectivity of the reaction.

Chapter 4 summarises the effort in screening for several ligands that can undergo reactive LMCT-transformations in combination with CeF_4. For this purpose, the trifluoromethyl thiolation of tertiary C-H bonds is introduced as benchmark reaction. Numerous ligands are tested and a tendency towards the most efficient transformation is discovered for halides, benzoates, phosphates and hydroxamic acids. A colour change of the reaction solution induced upon mixing the cerium salt, a base, and the respective ligand, does not allow for clear predictions of a successful LMCT transformation. Many parameters must be considered describing the complexation and charge-transfer reaction behaviour of cerium in ground and excited state. As CeF_4 shows poor solubility in acetonitrile, approaches for the synthesis of highly soluble, anionic Ce(IV) complexes that can be investigated by spectroscopical techniques were attempted. However, the kinetics for the formation of tetrabutylammonium tribromide outcompete the generation of the desired cerium-ate complexes.

Chapter 5 demonstrates the utilisation of iron LMCT for C-H functionalisation of organic molecules in water. Irradiation of $FeCl_3$ in aqueous environment by near UV or visible light leads to the excitation of the Fe-Cl charge transfer band and the generation of highly reactive chlorine radicals that abstract hydrogen atoms from cyclic ethers. The nucleophilic carbon-centred radicals were trapped with various Michael acceptors. Solubilising agents like sugar alcohols or cinchonidin derivatives are introduced and contribute to a slight increase in product formation. Reaction monitoring reveals that lowering the temperature to 4 °C positively impacts the initial period of the photo transformation, likely due to changes in the solvent's viscosity.

7 Zusammenfassung

Zusammenfassung

Die selektive Funktionalisierung eines spezifischen Kohlenstoffatoms durch das Entfernen eines Wasserstoffatoms innerhalb einer komplexen Molekülstruktur bleibt eine große Herausforderung in der Organischen Chemie. Ohne Heteroatome im Molekül sind die Polaritätsunterschiede in einer homogenen Kohlenstoffkette klein, was selektive Transformationen schwierig macht.

Metallkomplexe, deren Koordinationssphäre verändert werden kann, gelten als vielversprechende Werkzeuge zur selektiven C-H Funktionalisierung. Durch Zugabe von sterisch anspruchsvollen Liganden unterschiedlicher Polaritäten können intermolekulare Wechselwirkungen zwischen Substrat und Katalysator beeinflusst werden. Cer- und Eisensalze, die in dieser Arbeit untersucht wurden, besitzen leicht zu oxidierende Liganden, aus diesem Grund können Ligand-zu-Metall Ladungstransfer Reaktionen beobachtet werden. Als Folge dieser lichtinduzierten Bindungs-Homolyse entstehen hoch reaktive Radikale, die selektive Transformationen, wie z.B. Wasserstoffatom Abstraktionen oder Additionen an Doppelbindungen eingehen können.

Kapitel 1 fasst das Prinzip des LMCT in Wasser zusammen. Das Verhalten verschiedener Metallsalze in wässriger Umgebung sowie die wichtigsten Reaktionspfade (Ligand-zu-Metall Ladungstransfer innerhalb der Fe-OH Bindung bzw. der Fenton Prozess mit Fe(II)) werden aufgeführt. Anhand verschiedener Beispiele werden die Anwendbarkeit und die Besonderheit dieser lichtgesteuerten Bindungs-Homolyse sowie die Reaktivität der generierten Radikal-Spezies erläutert.

Kapitel 2 stellt die Ergebnisse aus der Studie über die Cäsiumcarbonat katalysierte O-Alkylierung von Oximen vor. Das *E*/*Z* Isomerisierungsverhalten von Oximen wird durch Zugabe von Cer(III)-Komplexen als Koordinationspartner sowie 9,10-Diphenyl Anthracen als Photo-Sensibilisator beeinflusst. Trotz der Kurzlebigkeit des *Z*-Isomers des jeweiligen O-alkylierten Produkts werden Ansätze zur Isolierung des *E*- und *Z*-Isomers des Additionsprodukts aufgezeigt. Cäsiumcarbonat spielt hierbei die Rolle einer speziellen Base,

die einen großen Einfluss auf das Isomerisierungsverhalten sowie die Reaktivität von Oximen in organischen Lösungsmitteln aufweist.

Kapitel 3 gibt Einblicke in die vicinale Dichlorierung von Alkenen mittels Eisen-Ligand-zu-Metall Ladungstransfer. Unter Anwendung eines einfachen Katalyse Systems bestehend aus $FeCl_3 \cdot 6H_2O$ und LiCl in einem Lösungsmittelgemisch aus Essigsäure und Acetonitril (9:1) wurden durch die schrittweise Addition von Chlor-Radikalen an die terminale Doppelbindung von Alken-Arylestern dihalogenierte Produkte zugänglich. Die Reaktion basiert auf der Bindungs-Homolyse von Eisen-Chlorid in $[FeCl_4]^-$ mittels Licht. Nach der ersten Addition eines Chlor-Radikals an die Doppelbindung erfolgt die Vervollständigung des Eisen-Katalysezyklus und die Bildung einer closed-shell Spezies vermutlich durch einen sogenannten Radikal Liganden Transfer. Die hohe Viskosität der Reaktionsmischung ist von Bedeutung in Bezug auf die Bildung von Acetat-Eisen Netzstrukturen, die einen Einfluss auf die Selektivität der Reaktion haben.

Kapitel 4 zeigt ein Liganden Screening für die reaktive LMCT-Aktivierung zusammen mit CeF_4. Für diesen Zweck wird die Trifluormethyl-Thiolierung von tertiären C-H Bindungen als Modelreaktion genutzt. Zahlreiche Liganden werden untersucht und Halogen- und Benzoesäure-Anionen sowie Phosphate und Hydroxamsäuren katalysieren die Reaktion. Die mit einer Verfärbung der Reaktionslösung einhergehende Komplexierung des Cer-Salzes mit der Base und dem entsprechenden Liganden lässt keinen Rückschluss auf eine effizient ablaufende LMCT-Reaktion zu, da viele Parameter für die Ladungstransfer Reaktionen mit Cer im Grundzustand und im angeregten Zustand einbezogen werden müssen. Da CeF_4 in Acetonitril schlecht löslich ist, wurden Versuche unternommen, anionische Cer-Komplexe zu synthetisieren, allerdings ist die Kinetik für die Bildung von Tetrabutylammonium Tribromid schneller als die der anionischen Cer-Komplexe.

In **Kapitel 5** werden C-H Aktivierungen von organischen Verbindungen durch Eisen-LMCT in Wasser beschrieben. Durch Beleuchtung von $FeCl_3$ in Wasser mit nahem UV oder sichtbarem Licht wird die Fe-Cl Ladungstransfer Bande angeregt, wodurch hoch reaktive Chlor-Radikale gebildet werden, die zur Wasserstoffatom Abstraktion an zyklischen Ethern führen. Die nukleophilen Kohlenstoff-zentrierten Radikale werden durch Michael Akzeptoren abgefangen. Lösevermittler, wie Zucker Alkohole und Cinchonidin Derivate werden hinzugegeben und die Reaktionsausbeute kann leicht erhöht werden. Die zeitliche Verfolgung der Reaktion zeigt, dass die Verringerung der Reaktionstemperatur die Produktbildung in der Anfangsphase der Umsetzung positiv beeinflusst, was möglicherweise auf Veränderungen der Viskosität des Reaktionsgemisches zurückzuführen ist.

8 List of Abbreviations

Abbreviation	Full expression
°C	Degree Celsius
3DPAIFPN	2,4,6-Tris (diphenyl amino)-5-fluorisophthalonitril
4CzIPN	1,2,3,5-Tetrakis(carbazole-9-yl)-4,6-dicyanobenzene
As	Arsenic
b	broad
BINOL	2,2'-Dihydroxy-1,1'-Bi-2-naphthol
d	doublet
DABCO	1,4-Diazabicyclo (2.2.2)octan
DBAD	di-*tert*-butyl-(azodicarboxylate)
dd	double of doublets
DFT	Discrete Fourier-Transformation
DIPEA	*N,N* diisopropylethylamine
DMAP	Dimethyl aminopyridine
DMF	dimethyl formamide
DMSO	dimethyl sulfoxide
DOTA	2,2',2'',2'''-(1,4,7,10-tetraazacyclododecane-1,4,7,10-tetrayl) tetraacetic acid
DPA	diphenyl anthracene
dt	doublet of triplets
e.g	example given
EtOAc	ethyl acetate
EXAFS	Extended X-ray Absorption Fine Structure
Fe	Iron
FID	flame ionization detector
g	gram
GC	Gas Chromatography
GC-MS	Gas chromatography coupled to Mass spectrometry
h	hour
h	heptet
H	hydrogen atom
HAT	Hydrogen Atom Transfer
HMBC	Heteronuclear Multiple Bond Correlation
HOAc	acetic acid
HPLC	high pressure liquid chromatography
HSQC	Heteronuclear Single Quantum Correlation
Hz	Hertz
i-PrOH	isopropanol
K_D	dissociation constant
LED	light emitting diode
LMCT	Ligand-to-metal charge transfer
M	molar
m	multiplet

278

extension of the List of Abbreviations

Abbreviation	Full Expression
MeOH	methanol
mg	milli gram
min	minute
mL	milli Liter
M-L	metal-ligand bond
mM	milli Mole
mmol	milli Mol
n.d.	not detected
n-Bu	*n*-butyl ($CH_2CH_2CH_2CH_3$-group)
nm	nano meter
NMR	Nuclear Magnetic Resonance
p	para
PE	petrol ether
ppm	parts per million
PTC	phase transfer catalyst
q	quartet
R_f	
RLT	Radical Ligand Transfer
s	singlet
sat	saturated
$S_N1/2$	nucleophilic substitution type 1/2
stoic.	stoichiometric
t	triplet
TA	Transient Absorption
TBA	tetrabutylammonium cation
TBABr	tetrabutylammonium bromide
TBADT	tetrabutylammonium decatungstate
t-butanol	*tert*-butanol
TFA	trifluoro acetic acid
TLC	thin layer chromatography
UV	ultra-violet
UV-Vis	ultra-violet/visible range of the solar spectrum
W	Watt
Xe	Xenon
μm	micro meter

9 Curriculum Vitae

Personal data

Name	Jessica Stahl
Day of Birth	09/19/1994
Place of Birth	Straubing, Germany
Nationality	German

Education

October 2019 – March 2024	**PhD in Organic Chemistry**
	Institute of Organic Chemistry and Pharmacy, University of Regensburg, **"Selective Ligand-to-Metal Charge Transfer Photocatalysis using Cerium and Iron Complexes with Defined Ligands"**
	Supervisor Prof. Dr. Burkhard König
October 2017 – September 2019	**Master of Science in Chemistry**
	Institute of Chemistry and Pharmacy, University of Regensburg
	Master thesis: **"Cerium-catalysed Photo-Beckmann Rearrangement"**
	Supervisor Prof. Dr. Burkhard König
October 2014 – July 2019	**Bachelor of Science**
	Institute of Organic Chemistry and Pharmacy, University of Regensburg
	Bachelor thesis**: "Photocatalytic Organometallic Reactions using _In Situ_ Generated Zerovalent Metals".**
	Supervisor Prof. Dr. Burkhard König

September 2011 – July 2014	**Allgemeine Hochschulreife**
	Gymnasium der Ursulinen Schulstiftung, Straubing
September 2004 – July 2011	**Mittlere Reife**
	Mädchenrealschule der Ursulinen Schulstiftung, Straubing

Memberships

July 2022 – March 2024	Associated member of the DFG-funded Collaborative Research Centre CRC 325 **"Assembly-Controlled Chemical Photocatalysis"**
September 2020 – September 2023	Scholarship of the *Studienstiftung des Deutschen Volkes*
2015 – 2019	Student Organisation „Fachschaft Chemie", University of Regensburg

International Experiences

20th – 22nd February 2024	Conference of Sustainable Chemistry, Goa, India, Poster Contribution, title of the poster: "Vinal Dichlorination of Alkenes by Iron Ligand-to-Metal Charge Transfer"

Conferences

20th – 22nd February 2024	**Conference of Sustainable Chemistry, Goa, India**, poster contribution, title of the poster: "Vicinal Dichlorination of Alkenes by Iron Ligand-to-Metal Charge Transfer"

5th – 7th October 2023	**Conference on Light-induced Transformations (CLIT), Regensburg, Germany**, poster contribution, title of poster: "Vicinal Dichlorination of Alkenes by Iron Ligand-to-Metal Charge Transfer"
8th – 9th October 2021	**Exploratory Chemistry – Light Creates Structure, Halle a. d. Saale, Germany**, poster contribution, title of the poster: "Visible Light Photocatalysis with Cerium in Complexes with high Coordination Number"
July 2021 – January 2024	**Seminar days and retreats of the DFG-funded Collaborative Research Centre (325) "Assembly Controlled Chemical Photocatalysis"**, oral contributions and presentations of ongoing research projects

Publications

- **J. Stahl**, V. R. Yatham, S. Crespi, B. König, *ChemistrySelect* **2021**, *6*, 4107.
- **J. Stahl**, T. Reiter, B. König, *Synlett* **2024**, 35, A-E.
- **J. Stahl**, B. König, *Green Chemistry*, 2024, DOI: 10.1039/D3GC04595A
- Yedase, G. S., Kumar, S., **Stahl, J**., König, B., Yatham, V. R. *Beilstein J. Org. Chem.* **2021**, 17, 1727-1732.

10 Danksagung

Zunächst einmal möchte ich Burkhard danken, für die motivierende Art, die mich dazu gebracht hat, unbedingt in den AK König kommen zu wollen und zudem für das Vertrauen, das er in mich hatte, als ich mit dem Projekt meiner Doktorarbeit gestartet bin. Vielen Dank, dass ich meine Projektideen frei entfalten und selbstständig forschen durfte.

Diese aufregende Zeit mit all seinen Höhen und Tiefen konnte ich nur dadurch so gut bewältigen, weil meine Kollegen gleichzeitig zu engen Freunden, ja eigentlich Familie geworden sind. Ich danke Becky, Maksim und Sena für ihre unterstützenden und weisen Wort – ihr habt mich immer wieder aufgerichtet und bestärkt, besonders dann, wenn ich aufgehört habe an mich zu glauben. Besonderer Dank gilt auch Elina, meiner engsten Freundin in der Gruppe, so wie ich Fan von Taylor Swift und INFJ. Von ihr habe ich mich immer verstanden und umsorgt gefühlt und manchmal waren Worte gar nicht nötig, um eine gleiche Meinung zum Ausdruck zu bringen.

Ich bin froh, das Labor 32.1.22 als meinen Arbeitsplatz gewählt zu haben, denn ich hatte stets wahnsinnig liebe Laborkollegen. Vielen Dank an Anamitra, Kathiravan, Alex und Leon, mit euch war es stets lustig und unterhaltsam und oft hat man glaube ich, unsere laute Musik in den Gang hinaus gehört. Bis heute vermisse ich Rok als meinen Laborkollegen. Er war für mich wie ein großer Bruder und guter Freund (ich weiß ja nicht, wie es ist ältere Geschwister zu haben). Zu ihm habe ich immer aufgeschaut und war froh um seine Ratschläge, sei es in Bezug auf Chemie, sein Heimatland Slowenien zu besuchen oder gelassen zu bleiben. Mit meinen aktuellen Laborkollegen Armaz und Kousik ist es wunderbar harmonisch im Labor. Wir sind auf einer Wellenlänge und ich danke euch für die großartigen Gespräche und die einladende Atmosphäre, die immer im Labor geherrscht hat. Vielen, vielen Dank an den gesamten Arbeitskreis, ich werde euch nie vergessen und immer positiv an die Zeit mit euch zurückdenken.

Der AK König wäre nur halb so gut organisiert ohne unsere festangestellten Kollegen. Hierbei möchte ich zuerst Ernst danken – er war immer zur Stelle, wenn es Probleme im Labor gab. Ich spreche für alle, wenn ich sage, dass Ernst der heimliche Papa aller Lehrstuhlmitglieder ist. Des Weiteren möchte ich Regina, Simone, Britta, Julia und Rudi danken, ich habe oft meinen Kummer bei euch ausgeschüttet und bin immer liebevoll aufgefangen und getröstet worden.

Euere Ratschläge waren unbezahlbar und ich habe die Kaffeepausen mit euch sehr genossen. Vielen Dank selbstverständlich auch für die „chemische Hilfestellung" wie z.B. für die Bestellung von Chemikalien, die Unterstützung bei der Benutzung des Fluoreszenz- und Quantenausbeute Messgeräts sowie das Messen der zahlreichen Cyclovoltammogramme bzw. GC-Massen.

Eine wichtige Verbündete für mich war zudem Barbara. Mit konnte ich immer über alles reden und du hattest immer ein offenes Ohr für jegliche Anliegen und hat Unmögliches möglich gemacht. Vielen Dank für die schönen und angenehmen Kaffee-Pausen!

Danke an alle Freunde aus meinem Semester, die mich auf meinem Weg begleitet haben; ohne euch hätte ich es bestimmt nicht geschafft: Philipp, Chris, Alina, Kathi, Risi, Robin, Flo, Felix, Ela, Ufo, Kalti.

Zum Schluss möchte ich mich vor allem bei meiner Familie und der Schüler Familie bedanken. Ihr wart immer für mich da, habt zugehört, an mich geglaubt und wart stolz auf mich, wenn ich es nicht war. Danke an meine Eltern für die Hilfe bei den Umzügen während der Doktorarbeit, die vielen Telefonate, die schönen Wochenenden in Straubing, die Hilfe und die Ratschläge in allen Lebenslagen und eure bedingungslose Liebe. Danke auch an meine Geschwister Jenni und Chris, ich bin so froh, dass ich euere große Schwester sein darf, wir sind ein tolles Team und ich könnte mir nicht vorstellen, ein Einzelkind zu sein. Vielen Dank auch an Rosi Oma und Opa an dich, „Bauerhof-Oma" und an Tante Bärbel, ihr habt dazu beigetragen, dass ich der Mensch geworden bin, der heute vor euch steht. Ich bin froh, ein Mitglied der Stahl Familie zu sein. Und zu guter Letzt, danke an Lissi und Coopi, ihr seid die besten Haustiere, die man sich wünschen kann und immer (mehr oder weniger) bereit zum Kuscheln.

Ich hab euch so lieb.

Danke

11 Eidestattliche Erklärung

1) Ich erkläre hiermit an Eides statt, dass ich die vorliegende Arbeit ohne unzulässige Hilfe Dritter und ohne Benutzung anderer als der angegeben Hilfsmittel angefertigt habe; die aus anderen Quellen direkt oder indirekt übernommenen Daten und Konzepte sind unter Angabe des Literaturzitats gekennzeichnet.

2) Bei der Auswahl und Auswertung folgenden Materials haben mir die nachstehend aufgeführten Personen in der jeweils beschriebenen Weise unentgeltlich geholfen:

   1. Die Ergebnisse aus Kapitel 2 entstanden in wissenschaftlicher Zusammenarbeit mit Dr. Reddy Veera Yatham (Ideen und wissenschaftlicher Input) and Stefano Crespi (Berechnungen mittels aufgeführten mathematischen Rechenprogrammen). Gekennzeichnete Experimente wurden von den genannten Personen durchgeführt.

   2. In Kapitel 3 wurden sowohl Daten von Thilo Reiter, der das Projekt in seiner Masterarbeit gestartet hatte, sowie von Jessica Stahl, die die Arbeit zu Ende geführt hatte zusammengefasst. Unterstützung durch Thilo Reiter erfolgte über den gesamten Publikationsprozess hinweg. Gekennzeichnete Experimente wurden von der genannten Person durchgeführt.

   3. Das Projekt aus Kapitel 4 entstand aus der gleichberechtigen Zusammenarbeit mit Marcel Fischer. Gekennzeichnet Experimente und Messungen wurden von der genannten Person durchgeführt.

   4. Für das Projekt, zusammengefasst in Kapitel 5, wurden Phasentransfer Katalysatoren verwendet, die von Elina Taskinen synthetisiert und ohne vorherige Aufreinigung/Umwandlung/Funktionalisierung unentgeltlich verwendet wurden.

3) Weitere Personen waren an der inhaltlich-materiellen Herstellung der vorliegenden Arbeit nicht beteiligt- Insbesondere habe ich hierfür nicht die entgeltliche Hilfe eines Promotionsberaters oder anderer Personen in Anspruch genommen. Niemand hat von mir weder unmittelbar noch mittelbar geldwerte Leistungen für Arbeiten erhalten, die im Zusammenhang mit dem Inhalt der vorliegenden Dissertation stehen.

4) Die Arbeit wurde bisher weder im In- noch im Ausland in gleicher oder ähnlicher Form einer anderen Prüfstelle vorgelegt.

Regensburg, den, 17.04.2024

X _____